

TUOMO NIEMINEN

**Molecular Mechanisms of
Selected Disease-Linked
Proteins Studied through
Atomistic Molecular
Dynamics Simulations**

TUOMO NIEMINEN

Molecular Mechanisms of
Selected Disease-Linked
Proteins Studied through
Atomistic Molecular
Dynamics Simulations

ACADEMIC DISSERTATION

To be presented, with the permission of
the Faculty of Engineering and Natural Sciences
of Tampere University,
for public discussion in the auditorium S4
of the Sähköotalo, Korkeakoulunkatu 3, Tampere,
on 8 November 2019, at 12 o'clock.

ACADEMIC DISSERTATION

Tampere University, Faculty of Engineering and Natural Sciences
Finland

<i>Responsible supervisor and Custos</i>	Professor Ilpo Vattulainen Tampere University Finland	
<i>Pre-examiners</i>	Professor Adam Foster Aalto University Finland	Professor Alexander Lyubartsev Stockholm University Sweden
<i>Opponent</i>	Associate Professor Georg Pabst University of Graz Austria	

The originality of this thesis has been checked using the Turnitin OriginalityCheck service.

Copyright ©2019 Tuomo Nieminen

Cover design: Roihu Inc.

ISBN 978-952-03-1316-6 (print)
ISBN 978-952-03-1317-3 (pdf)
ISSN 2489-9860 (print)
ISSN 2490-0028 (pdf)
<http://urn.fi/URN:ISBN:978-952-03-1317-3>

PunaMusta Oy – Yliopistopaino
Tampere 2019

ABSTRACT

Membrane proteins are complexes formed of long chains of amino acids capable of carrying out various functions in cellular life. Correct folding of the protein structure is relevant for its function, the folding patterns arising from the amino acid sequence. Membrane proteins are also primary targets for many diseases, their function being inhibited by factors such as mutations in the gene encoding the protein sequence. As a result, certain amino acids in the sequence may be point mutated, often with unpleasant consequences to the protein function.

Due to the small scale of membrane proteins and their primary interaction partners, lipids and ions, observing the molecular mechanisms and dynamics of protein function can be impossible by traditional experimental measurements. Here, we are able to bypass the visual limit by employing atomistic molecular dynamics simulations in order to study the properties of these membrane proteins. Understanding the dynamics of proteins at the atomistic level can be beneficial for pharmaceutical development as drugs targeting membrane proteins are cures for many diseases. Our goal in this Thesis is to explore two different types of membrane proteins, to study the dynamics and molecular mechanisms of their native states at an atomistic level, and to employ various computational methods to establish potential links between their function and related diseases.

The first part of this Thesis focuses on P2, a major protein of the myelin sheath of the peripheral nervous system, active in stacking myelin leaflets together. Certain mutations in the gene encoding P2 have been connected with an inherited demyelinating disease, while other mutations have been found to affect P2 activity in other ways. We performed sets of simulations on the P2 wild type and a number of its point mutated variants in order to gain insight on its structural dynamics at an atomistic level, and found the point mutants to alter its properties. The results also provide clues on how the changed activity is related to the demyelinating diseases. We also discovered a mechanism for the opening of the P2 barrel structure, suggest-

ing a similar mechanism for other fatty acid binding proteins as well. The research was conducted alongside an experimental group allowing us to produce a wide and thorough study on the protein function.

The second part of this Thesis focuses on rhodopsin, a G protein-coupled receptor (GPCR) of the visual transduction cycle. Recent studies have found rhodopsin to be a possible scramblase – to rapidly facilitate lipid translocation between the two membrane leaflets, which is an essential element of cellular physiology. Scramblases are found in nearly every cellular membrane, yet the mechanisms behind their function have remained unknown at a molecular level. Their dysfunction has also been linked to a number of severe diseases. We extensively studied the molecular mechanisms with which rhodopsin is able to create an energetically favorable environment for scramblase-assisted lipid flip–flop and found its properties to be non-selective regarding the lipid headgroup. The mechanism functioned in a manner that could be generalized to other GPCRs as well.

TIIVISTELMÄ

Kalvoproteiinit ovat aminohappoketjuista muodostuvia monimutkaisia komplekseja, joilla on tärkeä rooli solujen ylläpidossa. Jotta proteiini pystyisi toteuttamaan tehtävänsä kalvossa, sen muodostaman aminohappoketjun täytyy ensin laskostua oikeanlaiseen muotoon. Kalvoproteiinien toiminta heikkenee usein monien sairauksien johdosta. Heikentävinä tekijöinä saattavat toimia muun muassa mutaatiot proteiinien geenissä. Tämän seurauksena tietyt aminohapot proteiinissa saattavat muuttua toisiksi, vaikuttaen siten proteiinin rakenteeseen ja dynamiikkaan.

Kalvoproteiinit ovat kooltaan pieniä, joten niiden toimintamekanismien ja dynamiikan tutkiminen molekyyllitasolla perinteisin menetelmin on vaikeaa. Perinteiset pienen kokoluokan tutkimusongelmat voidaan kiertää käyttämällä atomitason molekyyldynamiikkasimulaatioita, joissa kalvoproteiinisysteemejä tutkitaan laskennallisesti. Proteiinien rakenteellisen dynamiikan ymmärtäminen atomitasolla voi olla hyödyllistä esimerkiksi lääkekehityksessä, jolloin lääkkeillä voitaisiin pyrkiä korjaamaan vaurioituneita proteiineja. Tässä väitöskirjassa perehdymme kahteen hyvin erityyppiseen kalvoproteiiniin ja tutkimme niiden natiivitilojen dynamiikkaa sekä toimintamekanismeja atomitasolla. Tarkoituksenamme on löytää mahdollisia syy-seuraus-suhteita niiden toiminnan katkeamisen ja siitä aiheutuvien sairauksien välillä.

Väitöskirjan ensimmäinen osa koskee kalvoproteiinia P2, joka on yksi ääreishermoston myeliinitupen yleisimpiä proteiineja. Viimeaikaiset tutkimukset ovat yhdistäneet tietyt tämän proteiinin geenimutaatiot eräaseen periytyvään myeliiniä hajottavaan sairauteen. Muiden mutaatioiden on havaittu vaikuttavan proteiinin aktiivisuuteen toisilla tavoilla. Me tutkimme P2-proteiinia ja useita sen pistemutatoituja variantteja atomitasolla saadaksemme lisää tietoa sen dynaamisista ominaisuuksista ja nähdäksemme, miten pistemutaatiot vaikuttavat näihin ominaisuuksiin. Löysimme vihjeitä siitä, kuinka tämä muuttunut aktiivisuus saattaisi aiheuttaa myeliinikatoa heikentämällä proteiinin kalvonsitomisos ominaisuuksia. Löysimme myös mekanismin, jolla tämän proteiinin tynnyrimäinen rakenne pääsee aukeamaan tavalla,

jonka voi yleistää muihinkin samantyyppisiin proteiineihin. Tämä osa tutkimuksesta on tehty yhteistyössä kokeellisen ryhmän kanssa, joten pystyimme muodostamaan laajan ja kattavan kuvan kyseisen proteiinin toimintaperiaatteista.

Väitöskirjan toinen osa käsittelee rodopsiinia, silmässä sijaitsevaa G-proteiini-kytkentäistä reseptoria (GPCR). Rodopsiinin on viimeaikoina havaittu omaavan tiettyjä skramblaasiproteiinin ominaisuuksia – se kykenee nopeuttamaan lipidien siirtymistä solukalvon läpi, mikä on solun toiminnan kannalta elintärkeää. Skramblaasi-proteiineja löytyy lähes jokaisesta solun kalvorakenteesta, mutta niiden toimintamekanismit ovat siitä huolimatta edelleen hämärän peitossa. Väärin toimivien skramblaasien on myös havaittu aiheuttavan useita vaarallisia sairauksia. Tutkimme atomitasolla mekanisme, jolla tämä prosessi toimii. Havaitimme lipidien siirtymisen tapahtuvan spontaanisti rodopsiinin pinnalla tavalla, joka ei ole riippuvainen lipidin pääryhmästä. Mekanismin toimintaperiaate on sellainen, jonka voisi yleistää käsittelemään muitakin GPCR-tyypin proteiineja niiden tyypillisestä rakenteesta johtuen.

PREFACE

Well, this is it. The long journey towards becoming a Doctor of Science that began back when I joined the Biological Physics and Soft Matter group at Tampere University of Technology has finally culminated in this Thesis. The journey had many similarities to running a marathon – an excited start continued by steady progress that at some point hit a wall, followed up with a sprint to the finish line.

The major milestones of the journey are recorded within the pages of this book in the form of four publications. While performing the research presented in these publications, I have learned a lot about biology, physics and computer sciences. I have always been fond of teaching and therefore I have also tried to write this Thesis in such a way that the reader might also gain good understanding on its main subjects.

There are many people without whom this Thesis would not have been finished. The Biological Physics and Soft Matter group provided a supportive and a friendly environment to work in. Scientific discussions with our group members always proved to be fruitful, and the meetings outside of work were also great fun. Special mentions go to Matti and Sami for being a constant source of help and inspiration, and to Ilpo for providing interesting research projects and giving productive advice during their progress. Thanks also to Petri for collaboration in the myelin research.

Friends outside of work have also been extremely important in helping me take my mind off of science (and conversely in keeping reminding me to defend my Thesis already). Thanks to the Huhuilijat group and all my student friends from Hiukkainen for being around. I owe you all a pint or two.

Finally, I would like to thank my family for all the support and interest you have shown in my work. Special thanks go to Liisa for being there every step of the way and believing in the completion of this Thesis.

Tampere, September 30th, 2019

Tuomo Nieminen

There is nothing like looking, if you want to find something. You certainly usually find something, if you look, but it is not always quite the something you were after.

J.R.R. Tolkien

CONTENTS

Abstract	iii
Tiivistelmä	v
Preface	vii
List of symbols and abbreviations	xi
List of publications	xv
Author's contribution	xvii
1 Introduction	19
1.1 Research objectives and scope of the Thesis	21
1.2 Structure of the dissertation	23
2 Biological background	25
2.1 Cellular life	25
2.1.1 Lipids	26
2.1.2 Proteins	30
2.2 Point mutations – an issue in protein encoding	33
3 Myelin sheath and the P2 protein	39
3.1 The nervous system	39
3.2 The myelin sheath	44
3.3 The peripheral membrane protein P2	46
3.4 Diseases of the nervous system	48
4 Scramblases and lipid flip–flop	53

4.1	Transbilayer lipid motion	53
4.2	Scramblase proteins	56
4.3	Rhodopsin	59
4.4	Scramblase dysfunction in diseases	60
5	Molecular dynamics simulations and analysis	63
5.1	Building the model	63
5.2	Force fields and topologies	65
5.3	Analysis methods	71
5.3.1	Free energy and umbrella sampling	72
6	Overview of the simulated systems	77
7	Results and discussion	81
7.1	Point mutation in P2 lid hinge increases protein dynamics	81
7.2	CMT1-associated point mutations affect P2 dynamics	85
7.3	P2 barrel opening is regulated by a conserved residue in the portal region	88
7.4	Rhodopsin functions as a non-selective lipid scramblase	91
8	Conclusions	101
	Publications	125
I.	Dynamics of the peripheral membrane protein P2 from human myelin measured by neutron scattering – A comparison between wild-type protein and a hinge mutant	125
II.	Molecular mechanisms of Charcot-Marie-Tooth neuropathy linked to mutations in human myelin protein P2	147
III.	Structure and dynamics of a human myelin protein P2 portal region mutant indicate opening of the β barrel in fatty acid binding proteins	162
IV.	Understanding the role of lipids in signaling through atomistic and multiscale simulations of cell membranes	176

LIST OF SYMBOLS AND ABBREVIATIONS

β_2 AR	β_2 -adrenergic receptor
AD	Alzheimer's disease
ATP	adenosine triphosphate
CMT	Charcot-Marie-Tooth neuropathy
CNS	central nervous system
DCCM	dynamic cross-correlation map
DLPC	dilauroylphosphatidylcholine
DPPC	dipalmitoylphosphatidylcholine
DNA	deoxyribonucleic acid
FABP	fatty acid binding protein
GBS	Guillain-Barré syndrome
GPCR	G protein-coupled receptor
GTP	guanosine triphosphate
MBP	myelin basic protein
MD	molecular dynamics
MS	multiple sclerosis
MSD	mean square deviation
P2	peripheral myelin protein P2
PME	Particle Mesh Ewald
PNS	peripheral nervous system
POPC	1-palmitoyl-2-oleoylphosphatidylcholine
POPS	1-palmitoyl-2-oleoylphosphatidylserine
RMSD	root mean square deviation
RMSF	root mean square fluctuation
RNA	ribonucleic acid
SSM	stearolsphingomyelin
VMD	Visual Molecular Dynamics
WHAM	weighted histogram analysis method

β	inverse temperature
β_{ij}	isothermal compressibility
ϵ_0	permittivity of the vacuum
ϵ_{ij}	minimum energy of Lennard-Jones potential well
ϵ_r	relative permittivity of the medium
ξ_{ijkl}	improper dihedral angle
ξ_{ijkl}^0	reference improper dihedral angle
ϕ_{ijkl}	dihedral angle
ϕ_s	reference dihedral angle
σ_i	distance between atom i and reference
σ_{ij}	van der Waals distance
τ_p	time constant for pressure coupling
τ_T	time constant for temperature coupling
θ_{ijk}	bond angle
θ_{ijk}^0	reference bond angle
A	free energy of reaction path
\mathbf{b}	box vector
C_{ij}	cross-correlation coefficients
\vec{F}	force
F	Helmholz free energy
G	Gibbs free energy
H	enthalpy
h	Planck constant
k_ξ	force constant of improper dihedral angle
k_B	Boltzmann constant
k_f	rate constant of flip-flop
k_{ij}^r	force constant of bond length
k_{ijk}^θ	force constant of angle
L	largest simulation box element
m	mass
N	number of particles
n	integral defining periodicity
\mathbf{P}	pressure matrix
\mathbf{P}_{ref}	reference pressure matrix
P^b	biased probability distribution
p	pressure

q	charge
\vec{r}	position of atom
R	molar gas constant
r_{ij}	distance between two atoms
r_0	reference distance
S	entropy
T	temperature
T_0	reference temperature
t	time
U	internal energy
V	potential energy
V	volume
V_C	Coulombic potential
V_{LJ}	Lennard-Jones potential
v	velocity
W	matrix parameter defining pressure coupling strength
W	work
w	bias potential
x	position of protein residue

LIST OF PUBLICATIONS

This Thesis includes the following publications:

- I. Laulumaa, S., Nieminen, T., Lehtimäki, M., Aggarwal, S., Simons, M., Koza, M., Vattulainen, I., Kursula, P. and Natali, F. Dynamics of the peripheral membrane protein P2 from human myelin measured by neutron scattering – A comparison between wild-type protein and a hinge mutant. *PLoS One* 10(6), e0128954 (2015)
- II. Ruskamo, S., Nieminen, T., Kristiansen, C., Vatne, G., Baumann, A., Hallin, E., Raasakka, A., Joensuu, P., Bergmann, U., Vattulainen, I. and Kursula, P. Molecular mechanisms of Charcot-Marie-Tooth neuropathy linked to mutations in human myelin protein P2. *Scientific Reports* 7:6510 (2017)
- III. Laulumaa, S., Nieminen, T., Raasakka, A., Krokengen, O., Safaryan, A., Hallin, E., Brysbaert, G., Lensink, M., Ruskamo, S., Vattulainen, I. and Kursula, P. Structure and dynamics of a human myelin protein P2 portal region mutant indicate opening of the β barrel in fatty acid binding proteins. *BMC Structural Biology* 18:8 (2018)
- IV. Manna, M., Nieminen, T. and Vattulainen, I. Understanding the role of lipids in signaling through atomistic and multiscale simulations of cell membranes. *Annual Review of Biophysics* 48, pp. 421–439 (2019)

AUTHOR'S CONTRIBUTION

In Publication I, the Author was the sole person performing computational experiments. The project was led by the Kursula group and molecular dynamics simulations studies were utilized to support the primary findings of the experimental group. The first author of the publication (Saara Laulumaa) performed the majority of the wet lab experiments. As the Author had the main responsibility of conducting and analyzing the molecular dynamics simulations, the first author status in the publication was practically shared. The computational systems with the protein in the water box were designed with the help of Petri Kursula and Ilpo Vattulainen. The Author also participated in writing of the paper by providing the text and pictures related to the simulations and simulation results.

In Publication II, the Author had sole responsibility over the molecular dynamics simulations by creating the systems, and performing the simulations and the following analysis. The first author of the publication (Salla Ruskamo) designed and performed the wet lab experiments. As the Author was responsible of all the molecular dynamics simulations and the following analysis providing equal contribution to the results presented in the publication, the first author status was practically shared between Ruskamo and the Author. The Author participated in the writing process of the paper by contributing the methodology and results of the molecular dynamics simulations.

In Publication III, the Author set up and performed all the molecular dynamics simulations and conducted the analysis of the computational results. The main conceptualization of the research was conducted by the first author (Saara Laulumaa) who also carried out the crystallography and spectroscopy portions. Therefore, like in Publications I and II, the first author status was shared by Laulumaa and the Author in practise. The Author also participated in the writing of the manuscript by submitting the analysis of the computational results and the methodology section of the molecular dynamics simulations.

For Publication IV, the Author performed a large number of systematic molecular dynamics simulations investigating the mechanisms of lipid flip-flop in presence of rhodopsin. Majority of the results referenced in this publication are at the moment unpublished, but will be discussed in depth in Chapter 7.4 of this Thesis. The scramblase activities of β_2 -adrenergic receptor were further studied by Moutusi Manna. The majority of the writing process of the review article was conducted by Ilpo Vattulainen, but the Author contributed to the writing regarding lipid flip-flop with the main methods and results.

1 INTRODUCTION

Cells are the basic building blocks of every living organism. They are extremely complex structures containing multiple different organelles such as the nucleus, mitochondrion, endoplasmic reticulum and the Golgi device, each with their own specific function in cellular life. The cytoplasmic interior of a cell – as well as every cellular organelle – is surrounded by a membrane. This membrane, at its core, is a bilayer structure consisting mainly of lipids and proteins. It has numerous functions ranging from protecting the organelle from its surroundings to regulating the conditions within. Notable membrane structures relevant for this Thesis include the plasma membrane, which surrounds the entirety of a cell, and the myelin sheath, which is a special type of a membrane protecting the nerve fibers in the nervous system.

Each membrane type has its own specific composition of lipids and proteins. Even the lipid composition between the inner and outer leaflets of a bilayer is usually different within the same membrane. This lipid asymmetry within a bilayer is vital for many cellular functions, and sustaining it is the main function of many proteins [2]. In some cases, inducing a specific type of lipid asymmetry can be a key to create a signal from within a cell to extracellular enzymes. This can be achieved by transferring specific types of lipids, typically found only in the cytosolic leaflet of a bilayer, across the membrane interior into the extracellular leaflet. Appearance of these lipids on the cell surface acts as a signal resulting in, for instance, a controlled method for degrading a sick cell [3]. The translocation of lipids across the membrane interior is facilitated by certain types of proteins called flippases and scramblases [4]. Loss of function in these proteins – due to mutations or other issues – can have severe consequences as the signaling pathway calling for outside aid is disrupted.

Proteins have many different roles in membranes. Some act as signaling pathways, others as fatty acid transporters, and many proteins may even have multiple purposes. A group of signaling proteins of the G protein-coupled receptor (GPCR)

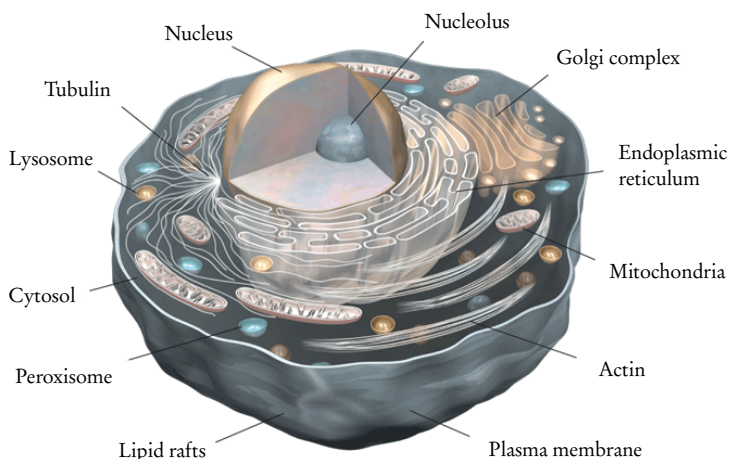


Figure 1.1 A schematic drawing of the interior of a cell. Figure modified from Ref. [1].

family have recently been found to have scramblase properties – they are able to act as lipid translocators in addition to their primary function [5]. In the myelin sheath, there are a number of fatty acid binding proteins, capable of transporting lipids, such as cholesterol, into the myelin [6]. These same proteins are also actively involved in binding the alternating layers of myelin together, ensuring a compact and insulating structure. Mutations targeting these proteins are involved in demyelinating diseases where the integrity of the myelin sheath is compromised resulting in interferences in the transmission of nerve signals [7].

Cell membranes and the function of membrane proteins have traditionally been studied experimentally in laboratory conditions. The downside of these traditional methods is the lack of information on events occurring on atomistic scale, such as lipid-lipid or lipid-protein interactions. Recent evolution in computing has brought molecular dynamics simulations up as an excellent alternative for the study of nano-scale biological systems. The atom-level resolution of the simulated systems allows for research on molecular mechanisms of membrane proteins, which would typically be invisible to human eye. Combining simulations with experimental results allows us to draw an extensive picture on events happening on a cellular surface.

1.1 Research objectives and scope of the Thesis

The research performed in this Thesis revolves around two proteins, both with very specific and important functions in their respective locations. Due to their roles in the cellular membrane, dysfunction of either protein can lead to severe health issues. In order to properly establish a link between the failure of protein function to the devastating effects arising as a result, one first has to understand the dynamics and the molecular mechanisms of the protein under native conditions at an atomistic level. Changes in protein function can be observed by altering the conditions under which they normally function. Our goal in this Thesis is to employ atomistic molecular dynamics simulations on these proteins in order to study the function of their native states and discover the potential root causes of their protein-related diseases through various computational methods.

Our first target is the protein P2 – a peripheral membrane protein found in the myelin sheath of the peripheral nervous system. The nervous system is a vital part of the human body that is in control of everyone’s actions. Whether it is conscious actions such as walking or talking, or subconscious actions such as breathing or heartbeats, actions such as these are controlled by neural impulses that travel through the human body. Damage to the nervous system, often caused by diseases or mutations targeting proteins of the myelin sheath, can affect the speed at which nerves are able to transmit these impulses and in severe cases block their passage completely. As a result, this may cause weakened motor functions, loss of memory and other devastating effects. In many cases, these diseases target membrane proteins in charge of sustaining the integrity of the nervous system [8]. Investigating these proteins at an atomistic level can provide deep insight on their function within the nervous system and show how the loss of that function due to a disease will ultimately lead to the aforementioned issues.

Myelin stacking in the central nervous system is known to be mainly performed by the myelin basic protein [9]. In the peripheral nervous system, myelin basic protein is not as prevalent, suggesting that adjacent myelin sheaths are held together by different proteins, such as P2. Therefore, diseases targeting P2 may change its properties, eventually resulting in demyelination. Recent advances have found implications of such effects in the Charcot-Marie-Tooth disease, facilitating demyelination in the peripheral nervous system (PNS) [10]. As a peripheral membrane protein,

the crystal structure of P2 has been relatively easy to resolve to an extremely high detail [11], making it a prime candidate for computational studies. By conducting molecular dynamics simulations at an atomistic detail, we are able to study the wild type P2 along with its carefully selected point mutants and compare their functional properties with each other in order to uncover how the dynamics of the protein change upon mutation. By collaborating with an experimental wet lab group, our goal was to create a wide and thorough picture on the dynamics of P2 and several of its point mutated variants in order to further the research on diseases of the peripheral nervous system.

Our second protein target discussed in this Thesis is rhodopsin, a well-studied G protein-coupled receptor found in the retina of the human eye. Our interest in rhodopsin does not involve its relevance in the visual sense, but in the fact that opsin, the apoprotein of rhodopsin, was recently revealed to greatly facilitate lipid translocation between two membrane leaflets – a property common with all scramblase proteins [12]. Lipid translocation is intrinsically a very slow process, therefore specific proteins are needed to increase the rate of lipid flip–flop to a high enough level to sustain essential cellular events.

Scramblase proteins are found in nearly every cellular component. They are an interesting group of proteins in a sense that their main function involves disrupting the natural lipid composition of a cellular membrane. They are relevant for sustaining cellular life in many cases such as helping cellular growth by transferring multiple types of lipids to the cellular surface, or apoptosis, where transfer of phosphatidylserine to the surface marks a sick cell to be degraded by phagocytes [13]. In other cases, the scrambling of the lipid composition of a membrane may, for instance, often hinder the function of many proteins that depend on the surrounding lipid environment [14]. One unanswered question regarding scramblase proteins is how their function (or dysfunction) eventually leads to diseases that have been linked to the protein group.

The existence of scramblase proteins has been known for a long time, but the identities of specific lipid translocators have remained unknown. Only in the past few years has progress been made in identifying potential scramblase candidates [15, 16], but the lack of available crystal structures on many transmembrane proteins have made their study extremely difficult. As a result, the molecular mechanisms behind protein-facilitated lipid scrambling has remained unknown. The crystal struc-

ture of rhodopsin has luckily been resolved to a highly accurate level, making it a prime target for molecular dynamics simulations [17]. By employing molecular dynamics on rhodopsin at an atomistic level, our goal was to uncover these elusive mechanisms to further our knowledge on these basic cellular functions. Understanding the mechanisms behind GPCR-facilitated lipid flip-flop may have benefits even as far as research on a cure for cancer, as debilitation of lipid scrambling pathways is prevalent in its initial stages, and as GPCRs are primary targets in drug research [18].

1.2 Structure of the dissertation

This Thesis is divided into eight chapters, beginning from the introduction to the research subjects in this first chapter. In the second chapter we discuss the basic biological background relevant to understanding the concepts in this Thesis. Cells and their building blocks – lipids and proteins – are introduced. One major subgroup of the transmembrane proteins – the G protein-coupled receptors are further discussed. Protein synthesis and mutations are also discussed at a basic level.

In the third chapter we focus on the background of Papers I-III of this Thesis. The nervous system and its main function is introduced. Further background is given on myelin sheath – the special membrane structure present in the nerve cells – and the myelin protein P2 is introduced. Several common diseases of the nervous system are also discussed.

In the fourth chapter we present background relevant to Paper IV of this Thesis. The concept of transbilayer lipid motion is introduced along with its difficulty due to the amphipathic properties of lipids. Proteins facilitating this process – flippases and scramblases – are introduced with special focus on rhodopsin, a G protein-coupled receptor. Diseases related to scramblase dysfunction are discussed with an example given in the loss of the ability to perform programmed cell death.

The fifth chapter introduces the computational mechanics behind molecular dynamics simulations. A basic introduction is given on different ways systems can be built for simulation along with the equations on which molecular dynamics are based on. The main analysis methods used in the Papers of this Thesis are presented. The concept of free energy is also discussed due to its relevance in lipid flip-flop.

The sixth chapter gives an overview on the simulated systems of all four Papers.

In the seventh chapter we discuss the results of all four Papers included in this Thesis. Sections 7.1 to 7.3 include Papers I-III and research conducted on myelin protein P2. Section 7.4 discusses Paper IV and research conducted on scramblase function. This section includes large quantities of unpublished data, which is referenced to in the review article that is the final Paper of this Thesis. These unpublished results are discussed in greater depth.

The final chapter summarizes the research conducted for this Thesis and presents ideas for future prospects.

2 BIOLOGICAL BACKGROUND

This chapter comprises an introduction to lipids and proteins, the main building blocks of every cell. Special focus is given to G protein-coupled receptors (GPCRs), the largest subgroup of transmembrane proteins relevant for Paper IV of this Thesis. A short introduction on protein synthesis, mutations and their roles in disease is also presented as point mutated proteins are the main targets of research in Papers I-III of this Thesis. The main reference on the basic knowledge given in this chapter is the book by Alberts et al. [19].

2.1 Cellular life

Cells are the basic structural units of every living organism. They are highly complex structures, containing all the biomolecules and organic machinery required for sustaining life, surrounded by a plasma membrane, which separates the cell from its surroundings. The plasma membrane is a lipid bilayer, built of two layers of amphipathic phospholipids – fatty acids with a hydrophilic head group and a hydrophobic tail group – and proteins embedded in the bilayer. Other primary constituents of a cell membrane are cholesterol – a small lipid essential for a number of biological processes – and carbohydrates, which generally attach to certain lipids and proteins on the extracellular side of the membrane.

Even in the cell membrane, each constituent has an important function in sustaining cellular life. Membrane proteins can work as transporters, transferring either lipids or ions across the hydrophobic interior of the membrane. They can also have a role in keeping the membrane structure intact, or give signals to other organelles, transporting information from one cell to another. Cholesterol can bind itself to various proteins, and even other lipids, giving it a major role in many cases as a stabilizer. By attaching itself between lipid tails, it both strengthens the membrane structure and helps keep the lipids and proteins in constant motion. As a result, the

cell membrane is a fluid, which is a prerequisite for many of its possible functions.

In addition to the plasma membrane of the cell, lipid bilayer structures can be found in many other places as well. Many cellular components such as the endoplasmic reticulum, the Golgi device and the mitochondria have a membrane separating them from their surroundings. An important membrane structure related to this Thesis is the myelin sheath, a multilamellar membrane structure found in the nervous system, consisting of alternating layers of lipids and proteins.

2.1.1 Lipids

Cells are protected from their environment by a membrane structure that encloses the cellular components (see Fig. 2.1). These membranes are mainly composed of lipids and proteins and their compositions are quite different in different cell types. Lipids are small biomolecules with varying chemical structures united by many common features such as amphiphilicity, insolubility in water and solubility in nonpolar organic solvents [20, 21]. Due to their amphiphilic nature, lipids spontaneously form membrane-like structures in water – their hydrophilic headgroups forming bonds with water molecules while their hydrophobic tails prefer to interact with each other. This results in either a spherical micelle consisting of a single layer of lipids with the tailgroups pointing towards the center, or more commonly a bilayer that surrounds a larger volume of fluid, typically an organelle or even a whole cell. The lipids found in cell membranes are often divided into three classes depending on their general structure: phospholipids, glycolipids and sterols [22].

Phospholipids are the most abundant lipid group found in biological membranes. They consist of a polar hydrophilic headgroup, a phosphate group, a glycerol backbone and two hydrocarbon tails formed out of fatty acids. The type of a phospholipid is defined by its headgroup and its hydrocarbon tails, and its structure can easily be derived from its name. For instance, POPC, or 1-palmitoyl-2-oleoylphosphatidylcholine, is a common component of all cell membranes (visualized in Fig. 2.2).

The first part of the name (PO) defines the tailgroup – the first hydrocarbon tail is a palmitic acid and the second an oleic acid. Palmitic acid is a saturated fatty acid consisting of 16 carbon atoms connected by single bonds, often denoted by a lipid number of 16:0, the latter number describing the number of double bonds in the carbon chain. Oleic acid is a monounsaturated acid, meaning it has a single

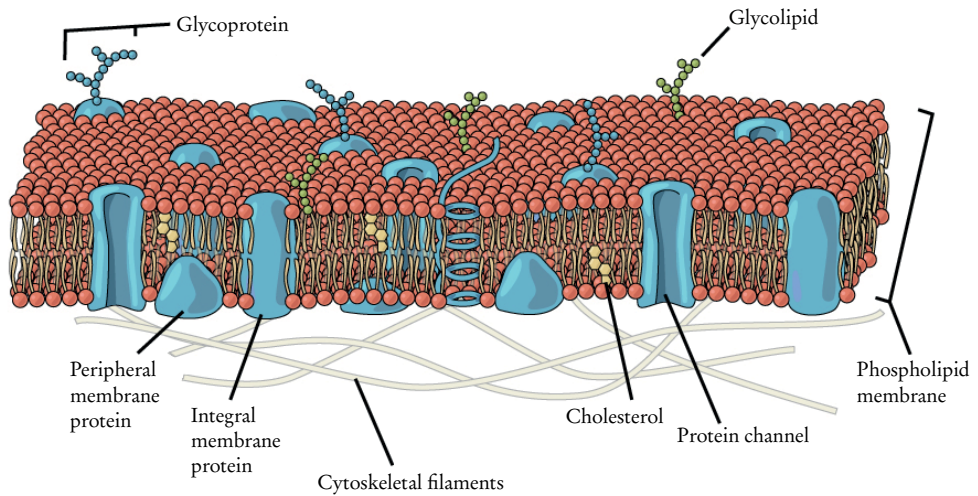


Figure 2.1 Schematic picture of a cellular membrane. Figure adapted from Ref. [23].

double bond in the carbon chain, consisting of 18 carbon atoms, and denoted by a lipid number of 18:1. Oleic acid is also classified as an omega-9 fatty acid due to the double bond located at the ninth bond from the end of the tail. The lengths of the hydrocarbon tails of membrane lipids are generally between 14 and 24 carbon atoms, meaning that a typical lipid bilayer has a thickness of 3 – 6 nanometres. The tail lengths and the number of double bonds also affect membrane fluidity.

The second part of the lipid name (PC) defines the headgroup – a charged choline at the end of the lipid connected to a phosphate group. There is a large variety of different headgroups ranging from a single hydrogen atom to extremely complex molecular chains, all giving the phospholipid specific properties at the membrane surface. The charge of the headgroup also has extreme importance in determining how the membrane surface behaves, creating repulsion between other similarly charged molecules and attracting specific parts of membrane proteins. The size and charge of the lipid headgroup also affect its ability to submerge into the hydrophobic membrane interior. This diversity allows lipids to partake in many vital cellular activities such as cellular signaling or substrate transport [24].

Glycolipids are a specific group of lipids found only on the outer monolayer of a membrane [25]. They are recognizable by long sugar chains attached to the lipid backbone protruding from the membrane surface. They have several main func-

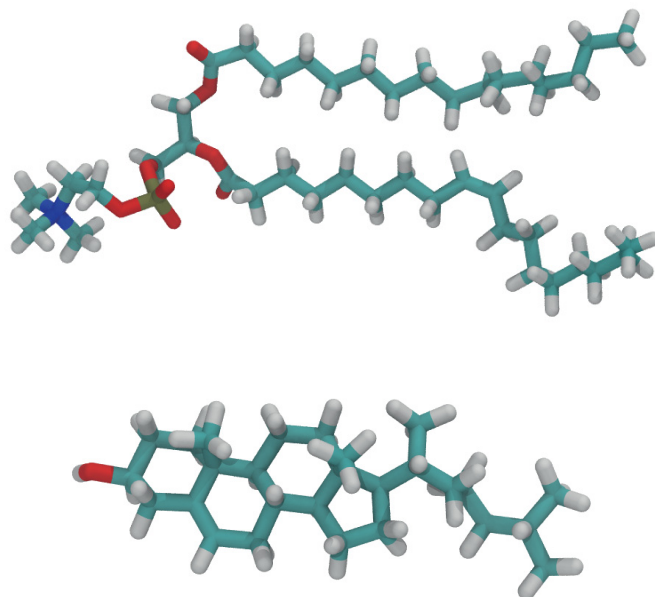


Figure 2.2 Molecular structures of POPC (above) and cholesterol (below). Structures visualized with Visual Molecular Dynamics (VMD) [26] and rendered using the Tachyon ray tracing library [27].

tions depending on their localization, all related to the saccharide chains. One main function is to serve as recognition sites for interactions between two cells, where the saccharides bind to carbohydrate-binding proteins or to the carbohydrates found on a neighboring cell. Glycolipids also have an important role in defining the blood group of a person. A specific glycolipid found on the surface of red blood cells is able to bind only one type of three different antigens. The O blood group is defined by binding of the basic form of the antigen. By addition of one of two different groups to the saccharide chain, the antigen is converted to a form found in people with blood groups A or B. An exception is found in the AB blood group where the antigen is able to bind either one of these two modified groups. As a consequence, glycolipids have important roles in the immune system, where the antigens of the red blood cells are able to identify whether an external cell with which they interact belongs to the body or not, and activate the immune system against invaders such as viruses or bacteria. Glycolipids serve as a prime example of lipids function in cellular signaling.

Sterols are a group of small lipids with rigid structures consisting of three cyclo-

hexane rings and a cyclopentane ring connected to a short functional group acting as the lipid tail. The headgroup is a small polar hydroxyl group found on the first ring. Due to the rigidity of the core structure and their small size, sterols of both animal and plant cells have general functions of supporting membrane structures, regulating membrane fluidity and modulating the activities of many membrane proteins [28].

The most common sterol found in animal cells is cholesterol (see Fig. 2.2). It is a well-studied molecule composing around 30 % of all biological membranes. Cholesterol inserts itself into a lipid bilayer with the hydroxyl group at the membrane surface along with the other lipid headgroups. The ring structure is in the membrane interior, interacting with nearby lipid tailgroups reducing their mobility. As a result, cholesterol concentration has a major effect on the relative fluidity of local areas of the bilayer, and whether these areas are in an ordered or disordered phase [29]. Areas with large cholesterol concentrations have more order and they become more tightly packed and less permeable to small water-soluble molecules. Conversely, the lack of cholesterol allows the lipid tails to move more freely, increasing the disorder. Even though the bilayer structure in certain areas can become quite solid, the lipid bilayer itself remains in a liquid state. Therefore, these two states are referred to as liquid-ordered (Lo) and liquid-disordered (Ld) states. The existence of these states has led to the hypothesis of lipid rafts – ordered membrane domains rich in cholesterol that are involved in transporting proteins and other large molecules by floating along the cell surface [30]. As the lipid rafts bind proteins and other enzymes, they have important roles as platforms for cellular signaling.

In addition to its effect on membrane structure, cholesterol also has an important role in stabilizing and activating many membrane proteins. For instance, many integral membrane proteins of the GPCR family have a cholesterol-binding interface with bound cholesterol molecules found after crystallization [31, 32]. Upon binding, cholesterol increases the packing of the protein structure, increasing its thermal stability and ability to form protein dimers.

Due to its small size, cholesterol is also able to flip-flop easily from one layer of a membrane to the other. For instance, in order to reduce membrane curvature in certain areas, cholesterol can readily transfer from the overcrowded side of the membrane to the other and help relax membrane stress [33].

2.1.2 Proteins

Proteins are masswise the most abundant group of molecules found in a cell. They act both as building blocks of the cellular structure and as executors of the main functions of the cell. Proteins have extremely complex structures, having developed over the years of evolution to perform specific tasks within the cell. They consist of a chain of amino acids, the length of which defines the size of the protein. There are a total of 20 different types of natural amino acids, each with the same backbone consisting of an amino group, a carbonyl group and a hydrogen atom, and a side-chain group different for each amino acid. The side-chains can be large or small in size, acidic or basic, polar or nonpolar, all depending on the amino acid in question.

The amino acid sequence, which defines a protein, is called the primary structure of the protein. It has an important role in both intermolecular and intramolecular interactions. The intramolecular interactions define the final three-dimensional form of the protein – due to the electrostatic and van der Waals forces between each amino acid, the protein will fold over time to a conformation where it has the lowest possible free energy. The aforementioned forces along with the forming hydrogen bonds and a hydrophobic clustering force then stabilize the final form of the folded protein. The final three-dimensional structure of the protein is referred to as its tertiary structure.

When observing partial segments of the protein, it can be seen that groups of amino acids located near each other form specific types of structures. These structures are referred to as the secondary structure of a protein. They are well-known spontaneously forming structures that are found in different proteins. The two most common secondary structures are the alpha-helix and the beta-sheet. When the backbone of an amino acid chain rotates itself around the main axis in a certain fashion, it forms a so-called alpha-helical structure. A certain amount of rotation allows the side-chains of the amino acids in the same polypeptide chain to support each other, creating a stable molecular structure common in the majority of proteins bound inside a lipid bilayer. Another example can be seen when a protein folds in such a way that amino acid groups run parallel to each other. Often in such situations, an extensive hydrogen bond network forms between two groups of laterally adjacent amino acids, creating a sheet-like structure. This type of a structure is called a beta-sheet, common in many barrel-like proteins that are capable of transporting a molecule.

Membrane proteins can be divided into two main subgroups depending on how they interact with the membrane: peripheral membrane proteins and integral membrane proteins. Peripheral membrane proteins are a group of proteins that have only temporary interactions with the surface of the membrane as they perform their biological functions. Upon making contact with the membrane surface, the tertiary structure of a peripheral membrane protein may change as it interacts with the lipids and other membrane-bound proteins. This usually involves conformational changes around the binding region exposing the nonpolar regions of the protein with which the binding is made possible. These conformational changes depend on the biological function of the protein and may include, for instance, the opening of a ligand-binding channel, unfolding of an anchor region, or dissociation of a transported molecule. The ability to bind to a membrane typically requires the peripheral membrane protein to be in a specific orientation near the binding site, and a certain lipid composition or the presence of a binding protein at the target location. Many peripheral membrane proteins are typically associated with transporting of molecules from one cell to another – they are able to bind a molecule at the surface of a membrane, and transport it to another membrane where the molecule in question is dropped off. These types of interactions also have a large significance in cellular signaling [34].

Integral membrane proteins are mainly bound to the interior of the membrane with parts of the protein protruding from the membrane surface. Transmembrane proteins are a major subgroup of integral membrane proteins. They cross the whole membrane, often multiple times, thus making contact with both the intra- and the extracellular sides of the membrane. The polypeptide chain that crosses the membrane is generally in an alpha-helical conformation, but many transmembrane proteins with a beta-barrel structure also exist. Multi-pass transmembrane proteins often act as channels for ions and other substances as they are able to create an energetically favorable environment for these substances to traverse in their interior and vicinity when compared to a pure lipid bilayer.

The function of many transmembrane proteins also involve a change in their conformation. Ion channel proteins among others use mechanic gating to control the flux of molecules between the membrane interior and exterior. Certain potassium channels, for instance, are activated when intracellular calcium interacts with an intracellular part of the channel protein, triggering a change in the conformation of

the protein [35, 36]. The gate controlling entry from the extracellular side into the channel, surrounded by many transmembrane alpha-helices, opens for a short while and potassium ions are able to enter the protein interior. After a time, the protein conformation changes again in a way that the extracellular side closes and the intracellular side opens, releasing the ions into the cell interior. This mechanism is vital for the function of many different cell types, especially prominent during conduction of signals in nerve cells.

Another major group of transmembrane proteins are the G protein-coupled receptors (GPCRs). They have a similar overall architecture consisting of seven transmembrane alpha-helices spanning the membrane, creating a cylindrical structure [37]. The main differences in their overall structures lie in their extracellular parts which are able to interact with various protein-specific ligands. These interactions in turn activate the protein. Instead of acting as transporters, their main function lies in signal transduction. Upon binding of an extracellular signal molecule, the GPCR undergoes a conformational transformation enabling it to activate a G protein – a trimeric GTP-binding protein – which couples the GPCR to enzymes or other proteins, triggering protein-specific functions.

There are nearly a thousand different GPCR proteins, all with a specific duty in cellular life [38]. Many GPCRs are involved with the function of the senses. Opsin, for instance, is able to bind a retinal-ligand inside its transmembrane structure, thus converting itself to rhodopsin. By changing the isomerization of the retinal by absorbing light, the protein changes its conformation initiating the visual transduction process [39].

GPCRs are also prevalent in the nervous system. These receptors are able to bind neurotransmitters – chemicals created at the synapses of the nervous system – which activate the protein. The GPCR then is able to control nearby ion channels, thus regulating the charge of the cell [40]. This kind of GPCR activation controls the function of the sympathetic and parasympathetic parts of the nervous system. Some GPCRs in the brain control the behavior and the mood of a person. Dopamine, for instance, is a neurotransmitter created in the synapses of the central nervous system. Dopamine receptors are GPCRs found in the brain able to bind dopamine as an external ligand, which then triggers a typical GPCR signaling pathway resulting in control over memory, motivation and other executive functions [41, 42].

Due to their large variety and importance in life, GPCRs are major drug targets.

Currently approximately 34 % of all approved clinical drugs in the US are targeting over a hundred different GPCRs [18] while ten years earlier the number was 27 % [43]. GPCR drug discovery is the most intensively studied area in drug research with significant progress constantly made in order to identify new targets.

It is worth noting that proteins can function in more ways than their designated group indicates. For instance, recent studies have shown that many proteins of the GPCR family have secondary functions as lipid scramblases – they actively induce lipid translocation across the bilayer, thus scrambling the lipid composition of the two opposing leaflets [12, 44]. One such GPCR is rhodopsin, the protein mainly involved in visual transduction. The transmembrane alpha-helices provide a favorable environment for the hydrophilic lipid head groups giving them easier entry to the membrane interior. There are also indications that the peripheral myelin protein P2, a member of the fatty acid binding (FABP) family, acts as a lipid transporter as is typical for fatty acid binding proteins, but also has an important role in holding the myelin sheath – a membrane complex vital for the nervous system – together [6]. These secondary functions of both rhodopsin and P2 are further explored in the following chapters of this Thesis.

2.2 Point mutations – an issue in protein encoding

For proteins to function in their intended manner, they have to fold into a very specific tertiary structure. The folding process is mainly spontaneous, led by the sequence of amino acids that form the primary structure of the protein. The hydrophobic residues are buried within the protein core while the active parts participating in protein–substrate interplay are generally located on the protein surface. In some cases, the amino acid sequence of a known protein can be disrupted, resulting in a mutation in the protein. This can have major effects on both protein folding and function.

Protein synthesis

Protein synthesis occurs in the ribosomes of a cell, but the process originates all the way from the genetic sequence. Human DNA is a long double-helical molecule built of four different types of nucleotides, containing all the genetic material required to

create proteins. The genetic information is transported from the DNA chain to ribosomes via messenger RNA (mRNA), which makes a copy of a certain part of the DNA chain into its single-stranded structure. With the help of transfer RNA (tRNA), which acts as a transporter for the required amino acids, and ribosomal RNA (rRNA) located at the ribosomes, protein synthesis is able to take place.

During the RNA translation process, the ribosomes read the genetic chain encoded in the nucleotides of the mRNA chain three nucleotides at a time. These nucleotide triplets are referred to as codons, which specify a certain amino acid, or the beginning and the end of the translation process. Since there are 64 possible nucleotide triplets, but only 20 different amino acids, a specific amino acid can be obtained from multiple nucleotide combinations.

Protein synthesis is initiated at the N-terminus of the amino acid chain, always containing methionine, from a specific start codon found in the mRNA. The ribosome then reads the following nucleotide triplet and the tRNA attaches the corresponding amino acid to the previous one by a peptide bond. This continues until the ribosome reads a nucleotide triplet containing a stop codon, upon which the finished protein is released from the ribosome. The proteins are then folded and transported to their final destinations. Misfolded proteins are either captured by molecular chaperones which attempt to refold them, or degraded back to amino acids in order to prevent them from causing harm.

Mutations

Mutations in protein structure occur mainly due to altered nucleotide base sequences in the DNA. The DNA replication process involves unwinding the double helix until new nucleotide pairs are generated for both divided halves. In rare cases, wrong types of nucleotides or additional nucleotide pairs are inserted into the newly generated DNA, which modifies the genetic code. Enzymes performing verification of these new chains are able to correct most of these errors, but some mismatched nucleotide base pairs inevitably remain, resulting in a mutated DNA chain after the next cell division. If the mutation is located in the part of the DNA encoding the structure of a certain protein, the protein synthesis process produces a mutated protein if the codons read from the mRNA make sense. Errors may also occur in a similar fashion when reading a correct mRNA sequence. The ribosomes operate in

a rapid fashion, so the tRNA molecules may occasionally attach wrong amino acids into the polypeptide chain. Additional proofreading mechanisms along the translation process, so most mutated proteins are rapidly identified and discarded.

Several different types of mutations of the polypeptide chain may occur as a result. Most common mutation types are substitutions – mutations of the nucleotide sequence where one nucleotide base is replaced with another. A silent mutation occurs when a change in one nucleotide base in a codon does not affect the generated amino acid. This is possible because certain amino acids can be obtained from several different nucleotide triplet combinations. Silent mutations are generally harmless as they do not affect the protein structure, but they can slow down the protein synthesis process.

Another common substitution is a missense mutation. This occurs when a nucleotide base of a codon is replaced with another in such a way that the resulting amino acid differs from the protein wild type. This is the main cause of point mutations found in proteins and can have significant effects in the protein function. As the initial effect of the mutation is quite small – the protein essentially retains its size and often folds properly – point mutated proteins are the most likely ones to pass post-translational inspection and find their way into the target cells.

The third type of substitution is called a nonsense mutation. It occurs when replacing a nucleotide base in a codon changes the meaning of the codon from inserting a new amino acid to signal termination of translation. There are three different stop codons identified by the ribosome that signal the end of the protein. Missense mutations usually result in a truncated protein structure easily recognized by enzymes and dissolved back into amino acids.

Another common way the nucleotide base sequence can be altered is via frameshift mutation. It happens when additional nucleotide base pairs are inserted (or some are removed) into the replicated DNA. This in turn causes the nucleotides to be shifted in either direction. As the nucleotides in the mRNA are read in triplets, each triplet beginning from the insertion point is different from the wild type, resulting in every codon changing its original meaning. If three additional nucleotide base pairs are inserted, it merely corresponds to the addition of a single amino acid. Due to its nature, frameshift mutations usually involve the change of multiple amino acids and an early stop codon, resulting in an unusable protein.

The effects of mutations

While protein mutations generally have negative effects on the function of the cell, there are also many examples of beneficial mutations with positive effects. One well-known example is the ability to digest lactose contained in milk [45]. Human infants generate the enzyme lactase which breaks down the lactose sugar chains contained in milk. In most mammals, the activity of the enzyme greatly subsides with time when other food replaces milk as the main source of nutrition. However, many human populations have a point mutation in the gene encoding the enzyme, keeping the enzyme active throughout their lives. The lack of this mutation is known as lactose intolerance.

One example of a well-known mutation with both beneficial and negative effects is sickle-cell anemia [46]. A single point mutation in the haemoglobin gene changes the shape of the red blood cells from their typical fluid round shape into a rigid sickle shape. The sickle shaped cells are prone to clumping together at junctions of the blood vessels, thus blocking blood flow and resulting in many health problems such as swelling and stroke. On the other hand, the unnatural shape of the red blood cells makes them more resistant to several blood diseases such as malaria [47]. Geographically, high representation of the sickle-cell gene in the population is generally found in areas where malaria has a high transmission intensity [48].

Most of the occurring mutations do not have such highly visible effects, but instead are seen only at a cellular level, facilitating or hindering cellular functions. For instance, a point mutation at a ligand-binding site of a protein may either accelerate the binding process or prevent the binding altogether [49]. A GPCR with the ability to facilitate lipid flip-flop across the lipid bilayer could become even more effective if additional polar amino acids appear along the lipid translocation path [50]. A fatty-acid binding protein found in the myelin sheath of the nervous system becomes more flexible when a point mutation occurs near the lid region of its barrel-like structure, which in turn increases its lipid stacking ability [51].

With recent advances in gene therapy, point mutated proteins can also be artificially generated in laboratory conditions. Generating point mutated proteins can be an interesting alleyway into further studying the structure and function of many proteins and protein complexes. Many signaling proteins, among others, naturally form dimer structures – two identical proteins attached to each other by an interface

in the side of the protein [52]. One often asked question regarding protein function is whether these types of proteins are able to function alone or if they need to dimerize in order to perform in their designated role. This is usually the case when the functional site is located at the dimerization interface. A way to separate two normally dimerized proteins is to generate point mutations at the dimerization interface which in turn reduces the ability of the two proteins to attach to each other. These point mutated proteins can then be reconstituted into vesicles as monomers and their function studied. If the protein still works as intended in its monomeric form, it can be deduced that dimerization or the dimerization interface is not essential for its function.

One such example can be found in opsin, a GPCR acting as a phospholipid scramblase transporting lipids from one membrane leaflet to the other. Several different lipid translocation pathways have been suggested, one of them at the dimerization interface of two opsin proteins. A recent study conducted by using the aforementioned method showed that the point mutated dimerization interface (transmembrane helix IV) is not the main location of the scrambling activity and monomeric opsin was able to facilitate lipid flip-flop at a sufficient level [53]. In a nutshell, performing point mutations on specific amino acids at putative functional interfaces can generally be used as a method of researching whether the interface in question is relevant for the studied function of the protein.

Artificially created proteins and targeting of mutated genes can also be used to treat certain protein-altering diseases. For instance, proteins facilitating programmed cell death are often disabled upon the onset of cancer. Gene therapy applied to proteins involved in the apoptotic pathway, such as p53, are used to heal the lost ability of the protein to aid in the controlled degradation of the sick cancer cell [54].

3 MYELIN SHEATH AND THE P2 PROTEIN

In this part of the Thesis we focus on a central part of the nervous system. The myelin sheath is the membrane layer that surrounds the axons transmitting neural signals across the body. A major component of this specific type of membrane is the peripheral membrane protein P2, which is a member of the fatty-acid binding protein (FABP) group. The Papers I-III presented in this Thesis, conducted in collaboration with an experimental group, have provided new insight on the dynamics of the P2 protein, its function in the myelin sheath and how certain point mutations can be the root of many nervous diseases. In this chapter, we present an overview on the structure and function of the nervous system and the myelin sheath surrounding its axons, introduce the P2 protein, and discuss the many different diseases affecting the nervous system.

3.1 The nervous system

The human body operates through signals sent from the brain. These signals are transmitted to all parts of the body through nerve cells interconnected by long bundles of branching fibers called axons. Sensations obtained through sight, touch, hearing, smell or taste are also transferred to the brain by the same route. The function of all organs, or the ability to move our limbs is due to functional transmission of nerve signals. Loss of this function may lead to paralysis, forgetfulness or loss of other senses, highlighting the importance of the nervous system. The main sources of reference in this chapter are the books on neuroanatomy by Patestas et al. [55] and Amerman et al. [56].

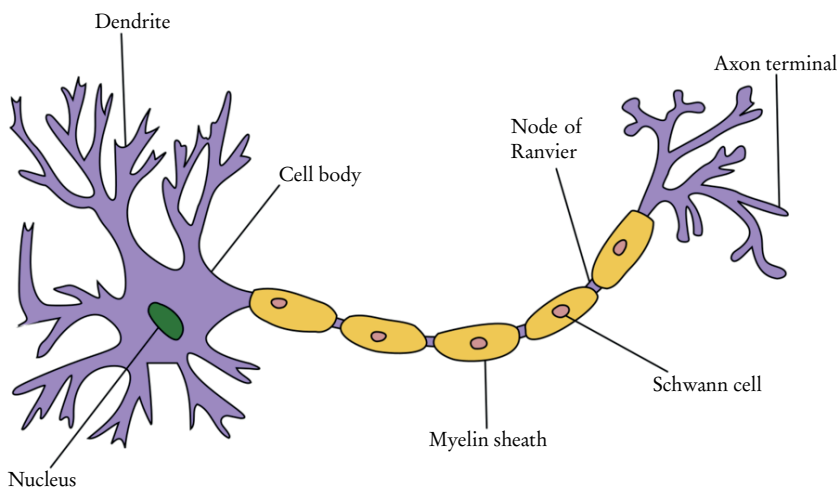


Figure 3.1 A schematic drawing of the structure of a neuron. The axon emerging from the cell body is segmentally covered by the myelin sheath. The axon termini generally connect to the dendrites of another neuron or muscle cells. Figure modified from Ref. [57].

Cellular structure

The basic elements of the nervous system are the nerve cells or neurons (see Fig. 3.1). They can be divided into two regions: the cellular body (soma) and branching neuronal processes called dendrites and axons. The soma contains the basic elements of any cell, but its size and form vary depending on its location inside the nervous system. The nucleus is the source of the RNA produced in neurons required for the protein translation process. The cytoplasm contains a large number of ribosomes and the endoplasmic reticulum required for protein synthesis. The large number of mitochondria ensure that the energy requirements for the neuron are met. The Golgi complex is also present, its function being to modify and package the various proteins and enzymes that are used by the cellular body.

Branching from the cellular body are the dendrites and axons. Dendrites are short, branching extensions protruding from the cell surface. Their main function is to receive the impulses coming from other neurons and transmit them forward to their host cell body. One of the dendritic branches will be connected to an axon at an area called the axon hillock. The axon, or nerve fiber, is a long projection of a nerve cell responsible for conducting the electrical impulses known as nerve signals from one neuron to another. The length of axons may vary from millimeters to over

a meter within the spinal cord. Axons typically branch both at right angles at their length as axon collaterals, and at their termini forming numerous axon terminals which permit a single axon to make contact with multiple neurons or other cells such as muscle cells. These contact points are called synapses and are the locations of ion or ligand exchange between neurons, electrical or chemical in nature.

Each nerve cell can contain multiple dendrites, but only one axon, highlighting its importance in proper function of the nervous system. Most axons are surrounded by a thick, multilamellar membrane structure called the myelin sheath. The myelin sheath begins from the axon hillock and ends at the axon terminal, with small gaps here and there called nodes of Ranvier. The main functions of the myelin sheath are to both protect the axons from outside damage and to insulate them from their surroundings in order for faster nerve signal propagation. A thicker myelin sheath often results in better insulation and therefore a faster signal. Axon thickness is also directly related to the conduction velocity of the signal. As a result, the thickness of an axon varies depending on its location while remaining constant along its length excepting the nodes of Ranvier.

In addition to the nerve cells, the nervous system is also a host to multiple other cell types with their own functions. The glial cells are a group of several different cell classes that mainly glue the nervous system together providing them support, insulation and protection. In addition, they also support the neurons with other functions such as regulating the chemical content of the fluid outside the neurons, providing nutrients to neurons, or aiding in sustaining the integrity of the myelin sheath. [58]

Nerve signals

Information is transferred between nerve cells through electrical signals. The inside of a nerve cell has a slight negative charge due to the proteins and ions located in the cytoplasm. The charge is sustained by a number of membrane proteins located in the outer membrane of the cell acting as ion channels allowing sodium and potassium ions to enter and exit the cell interior at a controlled rate. The charge difference between the cytoplasm and the extracellular area causes a potential difference across the membrane of the neuron. The typical resting potential in a neuron is around -70 millivolts.

A nerve signal is generated when a sudden disturbance changes the resting potential across the neuron membrane. This happens when the ion channels on the neuron surface open and allow a large amount of positively charged ions to pass into the cytoplasm. As a result, the cell interior becomes less negatively charged. Once the potential difference across the membrane reaches the threshold potential of around -55 millivolts, a radical change in the voltage difference can be seen. For a short period of time, the charge of the neuron interior becomes positive compared to the extracellular area with a potential difference of about $+40$ millivolts. This abrupt change is called the action potential. After the sudden change, which lasts for about a millisecond, the potential quickly reverses back to even higher negative values than the resting potential. After a short refractory period, during which a nerve cell can not be excited to generate another action potential, the potential difference swiftly returns to its resting state. As a result, action potentials are only very short pulses often referred to as all-or-nothing electrical outputs of a neuron.

The potential differences happen only at small parts of the membrane of the nerve cell at a time, but the generation of an action potential at one location changes membrane permeability around that part of the membrane. This change allows the action potential pulse to rapidly propagate along the membrane surface of an axon towards another nerve cell. The propagation of the action potential is basically the nerve signal as we know it. This active method preserves the strength of the nerve signal making it a very effective way of transmitting information. If the signal would only be generated at one location, it would progressively weaken as a function of distance. Upon reaching the target synapse, the action potential passes through to the next nerve cell either through a rapid, but simple electrical transmission or by a slower, but more intricate chemical transmission.

Regions of the nervous system

The human nervous system can be anatomically divided into two main regions: the central nervous system (CNS) and the peripheral nervous system (PNS). The CNS consists of the brain and the spinal cord, and the PNS are all the nerves connected to the CNS. There are significant differences between the two regions, including their functions and composition.

The CNS is primarily responsible for processing and coordinating most of the

functions of the human body. The brain consists mainly of nervous tissue, with about 100 billion nerve cells, and can be thought of as the control center of all both voluntary and involuntary human actions. The brain is directly connected with the spinal cord, which enables the brain to communicate with other parts of the body. The CNS has basically two kinds of nervous tissue: grey matter and white matter. Grey matter consists of the unmyelinated parts of neurons including cell bodies, dendrites, axon terminals and some unmyelinated axons. White matter is almost completely made of axons, the color arising from the thick myelin layers. As such, both white and grey matter have different roles in the central nervous system.

The PNS consists of all the parts of the nervous system that connect to the CNS. It is made up primarily of nerves – enclosed bundles of axons coupled with blood vessels and protective tissue. Nerves can be categorized according to their origin or destination. Cranial and spinal nerves act as links between the CNS and the rest of the body and are in charge of performing sensory and motor functions of the body. The sensory division carries signals beginning from the internal or external environments of the body to the CNS. Such signals may come externally from sight, touch or hearing, or internally from the feel of hunger or tiredness. Conversely, the motor division transmits signals coming from the CNS to the muscles, essentially generating a reply to previously received signals.

A more general way to divide the PNS is to decompose it to the somatic and autonomic nervous system. The somatic nervous system comprises the sensory and motor divisions excluding the autonomic parts. It is the consciously controlled part of the PNS responsible for the conduction of nerve impulses to skeletal muscles, thus enabling interaction with the external environment. The autonomic nervous system, on the other hand, is responsible for the subconscious or involuntary impulses such as blood flow or breathing. The autonomic nervous system itself can be divided into two categories: the sympathetic and parasympathetic nervous systems that essentially work in opposite fashion to each other. The sympathetic division is activated during situations of high stress, basically preparing the body for emergency action. It is responsible for increasing heart rate, releasing adrenaline or other stress hormones, and increasing sweating. The parasympathetic division acts as its counterpart, trying to inhibit its effects by decreasing heart rate, conserving energy and generating other calming effects. The bodily state of a person is essentially the balance between these divisions.

3.2 The myelin sheath

Axons are surrounded by a special type of a membrane structure known as the myelin sheath. It is a multilamellar membrane structure, consisting of proteins and lipids, that enwraps the axon core in a spiral-like fashion thus insulating it from its surroundings. The insulation enables fast and uninterrupted propagation of nerve signals along the axon core. Damage to the myelin sheath or incorrect stacking of myelin membranes are root causes of many myelin-related diseases. These are often caused by reduced nerve conduction velocities due to weakened insulation around the axon.

The composition of the myelin sheath is different in the central and peripheral nervous systems. The dry weight of CNS myelin is typically 70% lipid and 30% protein. The lipids are mainly cholesterol and various types of fatty acids. The main proteins include the proteolipid protein PLP and the positively charged myelin basic protein MBP, which is considered a major constituent in the stacking of myelin membranes, holding two opposing membranes together. The dry weight of PNS myelin is even more lipid-favored, consisting of 80% lipid and 20% protein. The major proteins of the PNS myelin include P0, accounting for over half of the total PNS protein, MBP, PMP22, and another positively charged protein, P2 [59]. MBP is not as prominent in the peripheral nervous system suggesting the possibility that P2 plays an active role in the myelin membrane stacking process.

Myelination process

The myelination process is also different in the CNS and the PNS. In the CNS, myelin is constructed by oligodendrocytes, which are able to myelinate parts of multiple separate axons at once. As a consequence, the myelin sheaths on the opposite sides of a node of Ranvier in a single axon are generated by a different oligodendrocyte [60]. After making contact with the axon, the arms of an oligodendrocyte begin to wrap themselves inwards toward the axon in order to form a tight sheath of alternating layers of lipids and proteins surrounding the axon. This process is facilitated by lipid–lipid and lipid–protein interactions and is highly dependent on the protein composition of the cell [61]. For instance, in the CNS, the cytoplasmic leaflets are held together very tightly by the highly positively charged protein MBP, which is

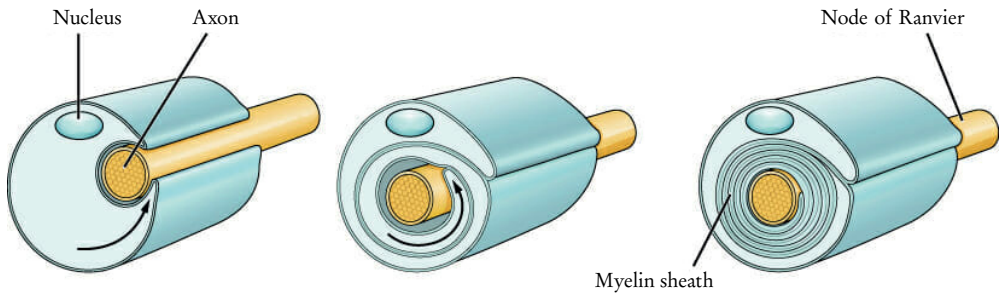


Figure 3.2 Illustration of the formation of the myelin sheath in the peripheral nervous system. The Schwann cell wraps itself around a single axon and rotates itself around it forming alternating layers of lipids and proteins. The myelin sheath is tight enough to squeeze the cytoplasm completely to the outer edges of the cell. Figure modified from Ref. [63].

likely synthesized in the oligodendrocytes themselves for this purpose [9]. Other myelin proteins, such as CNP, have an opposite effect, hindering myelin formation [62]. Thus, proper interplay and correct positioning and function of myelin proteins is essential to ensure healthy and functional myelin formation.

In the PNS, the myelin sheath is made by Schwann cells, which interact with only a single axon. Once the Schwann cells have attached themselves around an axon, they slowly begin to rotate outwards away from the axon forming the myelin sheath in a fashion similar to the process in the CNS. The main difference is that the myelin compacts itself in the opposite direction. The structure is tight enough to squeeze the cytoplasm completely to the outer edges of the cell (see Fig. 3.2). The nodes of Ranvier appear between two separate Schwann cells.

It is worth noting that not all axons are myelinated in this fashion. Some shorter axons both in the CNS and the PNS do not have a myelin sheath surrounding them. However, in the PNS, even these axons are surrounded by a Schwann cell, though in an unmyelinated form. Short unmyelinated axons are typically found in areas where proper insulation is not required to protect the axon or if rapid nerve signal propagation is not mandatory. Another important factor regarding whether an axon is myelinated is the axon thickness. In the PNS, a minimum diameter of $1.0 \mu\text{m}$ is required for myelination. In the CNS, no such limit has been observed, but oligodendrocytes are able to myelinate axons thicker than $0.2 \mu\text{m}$ [64].

The differences between PNS and CNS myelination processes can also be seen when trying to repair possible myelin damage. Schwann cells are incredibly flexible

in their abilities to convert to cells with regenerative abilities [65]. As a result, damage to peripheral nerves is repaired within a few weeks. The process involves clearing the damaged myelin sheath with aid of macrophages after which a new myelin sheath is built around the cleared sections [66]. If the axon itself is severed, it is able to create new growth processes that along with newly created myelin is able to reconnect with the target cell [56]. Conversely, the oligodendrocytes of the central nervous system do not seem to have the same regenerative abilities. The inability to break down damaged myelin seems to be due to the lack of autophagy activation in the CNS [67]. Other factors hindering nerve healing in the CNS are due to the oligodendrocytes inhibiting neuronal growth and the absence of growth factor chemicals [56]. As a result, both axon and myelin sheath damage in the CNS is much slower to heal.

3.3 The peripheral membrane protein P2

One major protein in the human peripheral nervous system is myelin protein P2, comprising up to 15% of the total protein composition [68]. It is a member of the fatty acid binding protein (FABP) group and mainly expressed by the Schwann cells of the PNS [69]. Due to its fatty acid binding properties, it is able to transport lipids to the myelin membranes through a collision transfer mechanism giving it an important role in conserving lipid homeostasis in myelin [70]. The bound ligands may include myelin-specific phospholipids or cholesterol.

The structure of P2 has been solved using x-ray crystallography to a 0.93 Å resolution [11]. The crystal structure consists of a total of 132 amino acids, forming a beta-barrel of 10 anti-parallel beta-strands ($\beta 1-\beta 10$) connected to each other via loops on both sides of the protein. The top of the protein is covered by a lid consisting of two short alpha-helices and a loop. The N- and C- termini can both be found near the open bottom of the protein. The high resolution of the crystal structure allows for pinpointing the exact location of every atom of the protein. This in turn makes the protein a prime candidate for atomistic molecular dynamics studies. A visualization of the crystal structure of P2 is shown in Figure 3.3.

Traces of a bound ligand were found in the crystal structure further supporting the fatty acid binding properties of P2. The ligand obtained from the crystallization process was a palmitate chain, belonging to a bound fatty acid. It is worth noting that

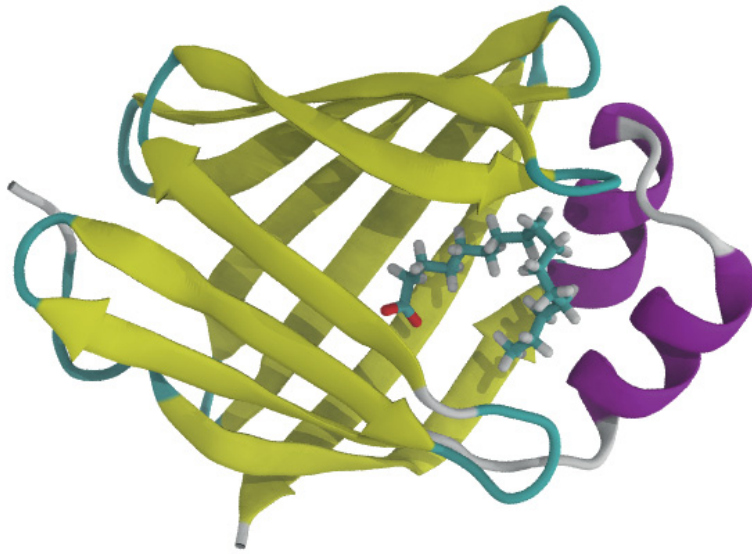


Figure 3.3 Visualization of the crystal structure of P2. The yellow coloring represents the β -barrel and the purple helices the alpha-helical lid. The bound palmitate ligand is visible inside the barrel structure.

the size of the barrel is large enough for a cholesterol molecule. The so-called portal region of P2, consisting of the helix $\alpha 2$ and its nearby loops between beta strands $\beta 3$ - $\beta 4$ and $\beta 5$ - $\beta 6$, has been identified as a key area of conformational changes during ligand transfer [71].

In addition to its lipid-binding properties, P2 also has an important role in stacking membrane leaflets together in the myelin sheath [72, 73]. The effect is pronounced in the PNS where MBP is not as prominent. As a result, P2 dysfunction can be a root cause of myelin deformation affecting the rates at which the enclosed axons are able to transmit nerve signals. Connections between certain neural diseases and mutations of the P2 protein have recently been uncovered [74, 75, 76]. One such case is the Charcot-Marie-Tooth neuropathy (CMT), which is among the most common inherited neuropathies, affecting both motor and sensory nerve conduction in the PNS [10]. CMT is commonly triggered by abnormal myelin structure, which reduces both motor and sensory nerve conduction velocities, leading to muscle weakness.

Point mutations associated with CMT and their effect on P2 dynamics are studied in Paper II of this Thesis. Papers I and III of this Thesis include studies on several

other point mutants related to increased activity in the lid area and barrel opening.

3.4 Diseases of the nervous system

A properly functioning nervous system is necessary for life. If the propagation of nerve signals to parts of the human body is hindered or blocked altogether, that part of the body is unable to follow the commands given by the brain in a reasonable reaction time. In addition to physical damage that cuts the nerves, such effects can also happen by many types of neural diseases that target the myelin sheath. Rapid nerve conduction velocity is reliant of the insulative nature of myelin. Therefore, damage to the myelin sheath that reveals parts of the axons to the extracellular side can significantly slow down the nerve signals or prevent them from reaching their targets altogether. Repeated enough along a specific pathway, this can result in, for instance, slow reaction times in limbs.

Diseases that target the myelin sheath structure without damaging the axon itself are referred to as demyelinating diseases [77]. Generally, the most dangerous of these diseases are those targeting the central nervous system due to its reduced regenerative capabilities, but some diseases of the peripheral nervous system may also be extremely dangerous. Not all neural diseases are caused directly by demyelination, but many are involved in reducing nerve conduction velocity in some way. This can also be achieved by deformation of the myelin sheath. If the myelin sheath is not folded properly, resulting in bulges or loose contacts, the insulation around the axon is weakened. This is often due to dysfunction of the proteins involved in the myelin contraction process. Therefore, myelin proteins are also potential targets for myelin-related diseases. Other main types of diseases found in the nervous system are neurodegenerative diseases, where the nerve cells disintegrate over time for some reason [78]. Neurodegenerative diseases are often incurable. They are usually caused by genetic mutations, protein misfolding or incorrectly activated programmed cell death, mainly targeting the central nervous system.

The most common demyelinating disease in the central nervous system is multiple sclerosis (MS), targeting the myelin sheaths of the nerve cells in the brain and the spinal cord [8]. The demyelination process is visualized in Figure 3.4. The effects of MS vary greatly between patients, making it difficult to diagnose without performing biopsy. Generally, the symptoms include muscle weakness, coordina-

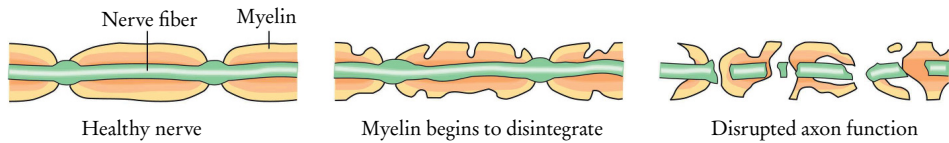


Figure 3.4 Illustration of the progress of demyelination in the MS disease. Damage to the myelin sheath reveals the nerve fiber and weakens nerve signal transduction. Eventually signals are unable to be transmitted when the axon is damaged enough. Figure modified from Ref. [79].

tion trouble, double vision or blindness. The main mechanisms initiating MS are thought to be the failure of the immune system or the inability to produce myelinating cells in the CNS. The common factor between MS patients is the destruction of the myelin sheath and the loss of oligodendrocytes [80]. However, the root cause still remains unknown [81]. The first symptoms are typically observed as early as between ages 20 and 40 and it remains the leading cause for neural non-traumatic disabilities in young adults [82]. No known cures for MS yet exist, but patients are being treated both with physical treatment and different types of medication.

One example of a neurodegenerative disease in the CNS is the Alzheimer’s disease (AD) [83]. It is a slowly progressing disease mainly targeting people over the age of 65. The main symptoms revolve around memory loss, beginning from occasionally forgetting small details, evolving to greater difficulties in remembering words, places and names, and finally resulting in loss of thinking and speaking abilities. The main cause behind AD is relatively unknown, but several theories exist revolving around CNS protein abnormalities initiating cell death in the neurons of the brain [84, 85]. No cures or definitive ways to prevent AD currently exist, but intellectual activities and a healthy diet have been shown to reduce the risk of the onset of the Alzheimer’s disease [86, 87].

In the peripheral nervous system there are two major demyelinating diseases. The Guillain–Barré syndrome (GBS) is a rapidly progressing neurological disorder where the peripheral nervous system is attacked by the immune system [88]. The myelin sheath around the axon, and in some cases the axon itself, can be damaged as a result, resulting in reduced nerve conduction velocity [89]. The Schwann cells of the PNS are able to rapidly repair the myelin damage, but by creating shorted internodes, that leaves the newly created myelin vulnerable for further damage. The symptoms typically include muscle weakness in the hands and the feet and can intensify signif-

icantly in a period of a few weeks to both sides of the body. In the most severe cases of GBS, the nerves of the respiratory system are damaged leading to extreme difficulties in breathing. There are no actual treatments for GBS, but the majority of people who experience the disease recover fully after intensive supportive care during the most dangerous period of the disease.

One of the most common inherited diseases of the nervous system is the Charcot-Marie-Tooth neuropathy (CMT) [90]. It is primarily a demyelinating disease of the peripheral nervous system which onsets when mutations in the proteins facilitating myelin sheath formation cause misfolding of the myelin sheath [91]. This results in reduced nerve conduction velocity in both motor and sensory nerves presenting itself as a loss of functional muscle tissue, touch sensitivity and slower reflexes in separate parts of the body. CMT usually presents itself at quite a young age, mainly varying from childhood to early adulthood [92]. The symptoms are usually visible on the patient, usually initially observed in the foot, where it is characterized with a loss of muscle, high arch and curved toes. At later stages the disease may spread to other peripheral parts of the body causing neuropathic pain and severely hindering day-to-day life. As with many other nervous diseases, there is currently no existing drug treatments available, and the main suggested therapy is exercise which maintains muscle strength in the afflicted regions [93].

CMT has been quite well studied. The root causes behind the disease have been identified as mutations in the genes (e.g. *pmp22*, *mpz*, *pmp2*) encoding the main proteins of the myelin sheath [10, 75, 94, 95]. The types of the Charcot-Marie-Tooth disease are named differently depending on the gene from which it originates and whether it targets the myelin sheath or the axons (e.g. CMT1A-F, CMT2, CMT3). CMT1 variants target the myelin sheath proteins and recent studies have associated certain mutations in the *pmp2*-gene with the CMT1A-variant of the disease, typically associated with the protein PMP22 [7]. The *pmp2*-gene encodes the peripheral myelin protein P2, which has been a main point of focus in this Thesis. The point mutants related to CMT1A are further discussed in Section 7.2 of this Thesis along with the research published in Paper II.

Most of the CMT variants cause demyelination in the myelin sheath, but some can also cause damage to the axon itself. The regenerative capabilities of Schwann cells help the myelin sheath rapidly reconstruct around the axon, but the mutations in the myelin proteins reduce the effectiveness of the protein-lipid interplay, essen-

tially resulting in a looser structure. This in turn results in a deformed myelin structure, or in some cases, a so-called onion bulb structure caused by repeating episodes of demyelination and remyelination, eventually causing thinning of the total functional myelin sheath. This in turn leads to a loss of functional nerve fibers in parts of the PNS [96].

4 SCRAMBLASES AND LIPID FLIP–FLOP

The second part of this Thesis focuses on another type of signaling where dysfunctioning proteins are also at the root of several serious diseases. Cellular signaling is often dependent on a certain lipid composition on the outer side of a cellular bilayer. This lipid composition is regulated by specific types of proteins known as flippases and scramblases. Their function is to facilitate lipid translocation across the membrane interior, which is intrinsically a rare event. In addition to cellular signaling, rapid lipid translocation is necessary for other cellular activities as well. Failure to transport lipids from one side of the bilayer to the other, or transport of the wrong types of lipids, usually has severe consequences for the cell. In Paper IV of this Thesis we present extensive discussion on the roles lipids have in cellular signaling. The author contributed to the publication by studying the scramblase properties of rhodopsin and the mechanisms with which it transports lipids across the bilayer. In this chapter, we discuss transbilayer lipid motion, the roles of scramblase proteins and the potential diseases that occur if this process is somehow hindered.

4.1 Transbilayer lipid motion

One important factor in controlling cellular life are the signaling processes that occur between cells. Information is gathered from the surface of a cell, on the extracellular side of a lipid bilayer, and transported to other cells via specific transporter molecules. Errors in the signaling process can have severe consequences in cellular function possibly resulting in diseases or other health problems in the long term.

As the information used in signaling is typically closely related to the configuration of lipids on the cellular surface, it is of great interest to understand the mechanisms with which these configurations are achieved. The lipid compositions of different types of bilayers are typically fixed in a specific manner, so in order to change these compositions, lipids must migrate from one part of a cell to the other.

Lipid transfer between cellular components (from one bilayer to the other) is generally achieved with the help of transporter proteins or by exocytosis and endocytosis – mechanisms by which lipids can exit and enter a bilayer surface. One example emphasizing the importance of lipid transfer is the sustainability of the plasma membrane surrounding the cell. The majority of all cellular lipids are synthesized in two sites within a cell: the endoplasmic reticulum and the Golgi apparatus [97]. In order to preserve cellular integrity, lipids synthesized in these two locations must be transferred to the plasma membrane, which is unable to create new lipids by itself. This is achieved by transporting lipids across the cytoplasm of the cell to the cytosolic side of the plasma membrane. From there, half of the transported lipids must transfer across the bilayer onto the cell surface in order to balance the number of lipids on both leaflets. This transbilayer lipid motion is often referred to as lipid flip–flop.

Lipid flip–flop has major importance in cellular physiology. It is vital for sustaining the asymmetric nature of many biological membranes. As mentioned before, phospholipid synthesis occurs only on the cytoplasmic side of the endoplasmic reticulum. For the ER to grow in a proper manner, half of the synthesized lipids must flip–flop across the ER bilayer to the luminal side [98]. Flip–flops are also necessary to sustain the asymmetrical lipid compositions of various cellular organelles [99, 100]. For instance, the curvature of a membrane increases when lipids with smaller headgroups on the inner leaflet oppose lipids with larger headgroups on the outer leaflet, signaling a target for scaffolding proteins to attach to, resulting in exocytosis [101]. Programmed cell death, or apoptosis, also occurs due to lipid asymmetry. When a high concentration of phosphatidylserine appears at the surface of a cell, it serves as a signal for phagocytes to destroy the sick cell in a controlled fashion [3, 102].

The mechanisms behind lipid flip–flop are very different from lateral lipid motion occurring in a bilayer due to the amphipathic nature of lipids. The amphipathic nature is also the reason why cellular membranes take their form with the hydrophilic headgroups of the lipids forming bonds with water molecules on the outside of a lipid bilayer and the hydrophobic tails facing the inside of the bilayer where they are not in contact with water [103]. In physiological temperatures, the structure of a lipid bilayer can be considered a fluid where lipids and embedded proteins are able to traverse laterally with relative ease. Lateral diffusion is energetically very easy as the polar headgroups of the lipids are able to remain in constant contact

with water and there are no clear energetic barriers blocking the motion.

Transverse diffusion, or lipid flip–flop, is another matter entirely. For a lipid to cross the membrane interior, its polar headgroup must first deattach itself from the surrounding water molecules and other lipid headgroups, and enter the hydrophobic core of the membrane, from where it will eventually reach the water located on the other side of the membrane. The lipid tails must also turn around in the process, moving against the lateral flow of the structure. All this effort creates a high energetic barrier the lipid undergoing flip–flop has to overcome, resulting in a slow and rare process when undertaken by a lone lipid.

The height of the energy barrier is dependent on both the properties of the translocating lipid and the surrounding lipid bilayer. The thickness of the bilayer affects the free energy profile of the flip–flopping lipid, the height of the energy barrier increasing along with the bilayer thickness. For instance, bilayers constituted of pure DLPC and DPPC were shown to have a fivefold difference in the height of the free energy barriers for flip–flops of their respective lipids (16 kJ/mol for DLPC and 80 kJ/mol for DPPC), even though the lengths of the lipid tails differ only by four carbon atoms [104]. Lipid size also affects the rate of the flip–flop process, as shown by the ease with which cholesterol molecules are able to cross a lipid membrane, with free energy barrier heights generally below 30 kJ/mol [105]. The size and charge of the lipid headgroup are also important factors, with larger and more polar headgroups having greater difficulties penetrating the membrane surface [106]. Other relevant factors include the phase behavior of the bilayer [107] and the concentration of membrane packing elements such as cholesterol [108].

There are several ways of reducing the free energy requirements of lipid flip–flop. Defects in the bilayer may induce the formation of a small water pore, which creates a hydrophilic environment inside the bilayer for the translocating lipid to use. For protein-free membranes, thinner bilayers in particular have been shown to allow a water pore to form across the bilayer with relative ease, providing a convenient hydrophilic path for the lipid headgroup to traverse [109]. These types of pore formations have been shown to occur spontaneously without any external stimuli, albeit at a slow rate [110]. As spontaneous pore formation is the rate-limiting step when considering lipid flip–flops in a defect-free membrane system, high enough rates of lipid flip–flop required for cellular sustainability are not possible to maintain by spontaneous effects alone.

In the presence of external influences such as transmembrane peptides or various types of proteins, when the surface of the membrane is disturbed, these types of membrane defects occur more often, increasing the rate of pore formation [111]. Mechanical or electrical stress applied on the membrane surface also influences the rate with which water pores appear [112].

The energy requirements for lipid flip-flops can also be reduced by other means. The following example is related to the modification of the membrane lipids. Oxidative stress is a chemical disturbance in the body where toxic reactive oxygen species are generated in excess resulting in extensive oxidative damage to lipids and proteins in a cellular environment [113]. This oxidative damage includes lipid peroxidation, often truncating the tail of a lipid with a double bond, fundamentally changing the characteristics of the lipid within the bilayer. Its effect on the free energy of lipid translocation has been studied, and the free energy barrier of POPS flip-flop in a pure POPC bilayer was found to reduce by 20 kJ/mol when 20 mol-% of the POPC molecules were substituted with oxidized variants [114]. Such an energy reduction meant a $10^3 - 10^4$ -fold increase in the flip-flop rates of POPS. Another recent study revealed a correlation between the decrease in the free energy of POPS flip-flop with increased concentrations of peroxidized POPC molecules in a similar system [115]. Oxidative stress has implications in many neurodegenerative diseases [116], or apoptosis, where rapid PS translocation to the cellular surface is the trigger [117].

4.2 Scramblase proteins

A more common way for cellular structures to improve the rate of lipid flip-flops is through specific types of proteins known as flippases or scramblases (see Fig. 4.1). Flippases are specialized transporter proteins generally activated by external energy obtained from ATP [118]. They are able to translocate phospholipids with selected headgroup types unidirectionally from one membrane leaflet to the other. They function in a controlled manner with the goal of preserving lipid asymmetry between the two leaflets.

Flippases can be divided into several subcategories, depending on the direction of lipid translocation and the lipid selectivity. P-type flippases have an important role in transferring lipids from the cellular surface back to the cytosolic side [119]. The most extensively studied subfamily of P-type flippases are the P4 ATPases, lipid flippases

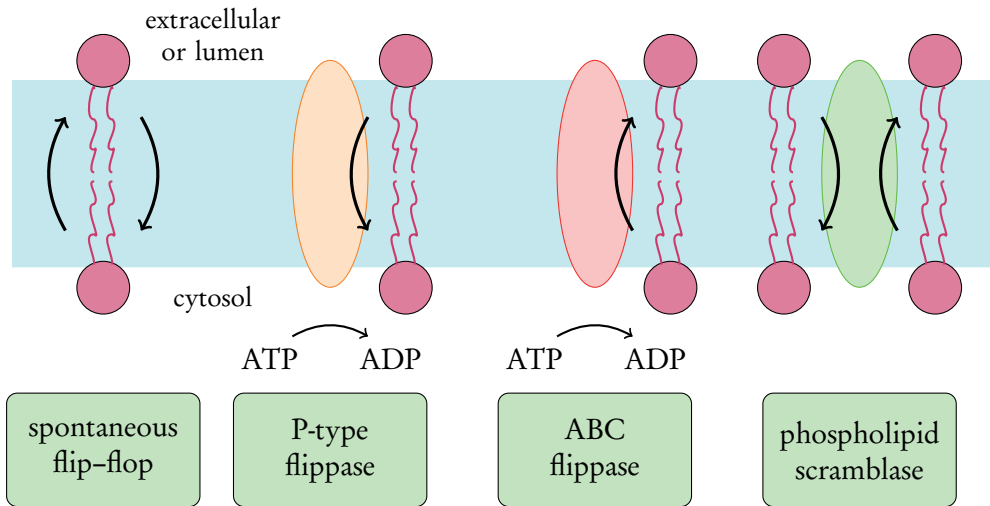


Figure 4.1 Four different types of transbilayer lipid motion. Spontaneous flip–flop is slow, bidirectional and requires no external energy. P-type flippases facilitate inward movement of phospholipids with external energy obtained from ATP. Likewise, ABC flippases facilitate outward movement of phospholipids by the use of ATP. Scramblase proteins are bidirectional and require no external energy sources, but can be activated by calcium binding. Figure adapted from [123].

involved in transferring excessive PS away from the cellular side of the membrane in order to prevent unwanted apoptosis [120, 121]. ABC transporters function in the opposite direction, transferring a large variety of lipids from the inner leaflet to the extracellular side [122].

The third subgroup of flip–flop-inducing proteins are referred to as scramblases, due to their role of non-selectively scrambling the lipid composition between the two membrane leaflets. They are a group of elusive membrane proteins mainly located in the plasma membrane surrounding the cell, where they participate in various cellular activities, or in the endoplasmic reticulum, where they ensure that lipids synthesized on the luminal leaflet are efficiently transferred to the cytosolic side. They are able to function without external energy from ATP and are able to flip lipids of all types in both directions [13].

Scramblase activity is mainly initiated as a response from external signals that call for cell activation, blood coagulation or apoptosis [124]. It may involve a mass influx of Ca^{2+} -ions into the cell through the many ion channel proteins on the cellular surface, which in turn switches the scramblase proteins on and subsequently destroys the lipid asymmetry of the plasma membrane [125]. Binding of calcium-ions to a

protein interface is proposed to change the conformation of the scramblase protein in a way that the surrounding lipids are able to access a translocation pathway with greater ease. However, a number of scramblase proteins, especially in the ER, are proposed to function without calcium [126].

Despite the fact that the existence of scramblase proteins have been known for a few decades, their structures and mechanisms are still relatively unknown. The first x-ray structure of a known scramblase protein, TMEM16, was only reported several years ago [16]. A significant breakthrough was also achieved in the last decade when opsin, a protein of the GPCR family, was reported to exhibit scramblase activities in reconstituted vesicles along with its holo-form rhodopsin [12]. With no clear calcium-binding motifs, it was proposed that the scramblase activities of opsin were due to its intrinsic properties. This led to the suggestion that all GPCRs, having very similar central structures, could have scramblase properties in addition to their main roles as signaling proteins. Later, three other GPCRs, β_1 -adrenergic receptor, β_2 -adrenergic receptor, and adenosine A_{2A} receptors were shown to scramble phospholipids, supporting the suggestion [44].

A major point of interest regarding scramblase activity is the mechanism with which they translocate lipids from one leaflet to the other. As of now, these mechanisms are relatively unknown, but significant progress has been made by studying GPCR-mediated lipid flip-flop [5]. Over the years, several different mechanisms have been suggested on how lipids might cross the hydrophobic membrane interior with the aid of transmembrane proteins. The first involves the lipid headgroup gliding across the membrane along the protein surface with the transmembrane helices and a transient water pore reducing the free energy barrier to an acceptable level [4]. The second is a so-called credit card model where the lipid headgroup enters the hydrophilic transmembrane channel of the scramblase, possibly via a conformational change in the protein, and exits on the other leaflet [127]. A third option involves the lipid fully submerging into the transmembrane channel and emerging out on the other side [4], though unlikely as a general mechanism due to the non-selectivity of scramblase proteins. It has also been suggested that transient disturbances caused by transmembrane helices may cause the lipid headgroup to slip into the bilayer interior in a hydrated state near the lipid-helix interface, from where it will eventually pop out onto the other side [128].

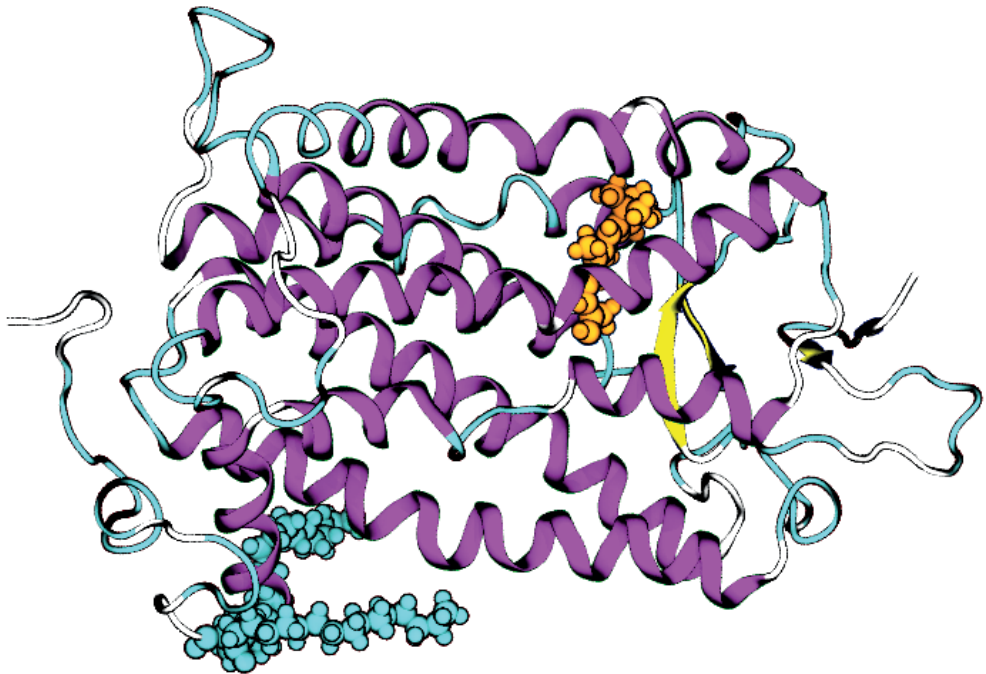


Figure 4.2 Visualization of the crystal structure of rhodopsin. The seven transmembrane alpha-helices are colored in purple. The retinal ligand is colored orange. The two palmitate chains attached to the cytosolic cysteine residues are also pictured in cyan.

4.3 Rhodopsin

Among the most studied proteins in the human body is rhodopsin, a key protein of the visual sense. It is a light-sensitive protein belonging to the GPCR superfamily, constituting around 90 % of all known GPCR proteins [129]. It is a derivative of opsin, differing from its apo-form by an additional 11-*cis*-retinal covalently bound inside its transmembrane channel. An absorption of a single photon by the retinal ligand changes the isomerization of the retinal to an all-*trans*-configuration, which activates the signaling pathway of the protein and leads to sight. The crystal structure of rhodopsin is visualized in Figure 4.2.

Due to its abundance in the retina, the crystal structure of rhodopsin has been solved to a 2.2 Å resolution [17]. It comprises a total of 348 amino acids that form a typical GPCR structure consisting of seven transmembrane alpha-helices (I-VII) connected to each other by short loops on both sides of the protein. The retinal

ligand is covalently bound to the lysine residue 296 within the transmembrane channel, and surrounded by a number of conserved water molecules. The extracellular side is home to the N-terminal along with a few short interhelical loops and beta sheets. The cytosolic side hosts the C-terminal and three interhelical loops. Notable amino acid residues include two cysteines 322 and 323 on the cytosolic side, which are able to bind palmitate chains acting as membrane anchors or targeting sites for other membrane proteins controlling the localization of rhodopsin [130].

Due to the high resolution with which the crystal structure of rhodopsin has been obtained, a complete model of the protein can be built with knowledge of the exact location of every single atom. This is extremely helpful for molecular dynamics simulations where rhodopsin can be simulated at an atomistic level for increased accuracy and deeper insight. We conducted simulations on rhodopsin embedded in a lipid bilayer in order to gain knowledge on its lipid scrambling mechanisms. These mechanisms are discussed in Paper IV of this Thesis.

4.4 Scramblase dysfunction in diseases

Due to their roles in sustaining lipid asymmetry and ensuring cellular growth, efficient function of flippase and scramblase proteins is essential for life. Changes in the activity of these proteins, through mutations or signals received from diseased cells, can often have severe consequences. Scramblase dysfunction is most visible in the loss of the apoptotic abilities of a sick cell, preventing their removal at the onset of a disease.

Apoptosis is the programmed mechanism with which the human body disassembles diseased or dysfunctional cells. In a healthy functional cell, there are only minimal amounts of phosphatidylserine located on the cellular surface due to the activity of P4 ATPases that flip any scrambled PS lipids back to the cytosolic side of the plasma membrane [121]. When a cell becomes ill or dangerous due to viruses or gene mutations, internal mechanisms of the cell deactivate the inward flippases and activate new scramblases in order to express high amounts of PS on the cellular surface. This in turn acts as a signal for phagocytes – large external cells capable of attaching to and subsequently devouring the sick cell and decomposing it back to its cellular components, nucleotides and amino acids [131]. By destroying a cell in a controlled manner, the release of potentially harmful cellular components to the extracellular

space can be prevented. As radical as it sounds, apoptosis is in fact a very common cellular phenomenon with 50 to 70 billion cells both dying and born each day in a healthy adult [132].

Problems occur when apoptosis can not be triggered on demand. In case of mutations or other hindering factors acting on the scramblase proteins, sufficient amounts of PS can not be translocated to the cellular surface for the cell to be recognized by the passing phagocytes. Left alone, a sick cell will die on its own and subsequently release its noxious cellular components to the extracellular space where it will cause inflammation in the nearby tissue [125]. Especially dangerous is the lack of apoptotic response in cancerous cells. Cancer occurs due to genetic mutations resulting in abnormal rate of growth in dysfunctional cells due to rapid cell division. Cancerous cells are unresponsive to external signals, will eventually form solid tumors and may spread to other parts of the body. The suppression of apoptotic signals in the early stages of cancer due to mutations in scramblase or other tumor-preventing genes is often the reason cancerous cells are able to survive [133]. By inhibiting the expression of apoptotic proteins, controlled degradation of cells is impossible to achieve. As a result, many anti-cancer drugs and radiation treatments target the apoptotic pathway in order to restore the ability to remove cancerous cells [54]. Further knowledge on scramblase function could be a helpful factor in improving the treatment of cancer patients in the long term.

Uncontrolled apoptosis can be dangerous as well as can be seen in many neurodegenerative diseases such as Alzheimer's disease, where nerve cells of the brain are rapidly destroyed by apoptotic responses [134]. Despite the fact that the main causes behind AD are unknown and the cells do not express typical apoptotic signs, it is treated with anti-apoptotic drugs [135]. However, there are many reasons excessive apoptosis may occur, including overexpression of proteins with scramblase characteristics in the nerve cells. Some links have already been established between neuronal GPCRs and the pathology of AD, and many of these GPCRs are targeted by drugs attempting to prevent the effects of the disease [136]. It might be interesting to see whether the recently discovered scramblase properties of the GPCR core structure could play a role in the excessive apoptotic response.

5 MOLECULAR DYNAMICS SIMULATIONS AND ANALYSIS

In recent years, computing facilities have evolved rapidly allowing us to perform higher numbers of calculations in a shorter time period than before. This in turn has enabled us to perform simulations on larger and more highly detailed models of molecular systems. These developments have made molecular dynamics simulations a viable and dependable method for studying cellular events at an atomistic level. When complemented by wet lab studies such as studying a cell membrane system at a larger scale, they can provide very insightful information on biological processes occurring in the system.

The basic ideas behind molecular dynamics simulations are quite simple to understand. First, we create a model of the system under study, then we let it run in environmental conditions of our choice for a set time. After some time has passed, we can analyze the results found in the simulation through a large variety of analysis programs. This chapter discusses these methods in more detail.

5.1 Building the model

The starting point for any MD simulation is the structure of the system under study. Whether it is a fully solvated lipid bilayer or a simple protein in a box, we have to know how all the atoms are initially positioned and which atoms are coupled together and how. High-resolution crystal structures of proteins obtained through x-ray crystallography, nuclear magnetic resonance or other similar methods, that are deposited into external data banks such as the RCSB Protein Data Bank [137], are generally used as initial structures. Similar methods are also used for obtaining structures of lipids and other cellular components.

There are several types of simulation approaches we can take, all depending on the

size of the system under study, the desired detail of the results and the computational resources we have available. Depending on all those factors, we can either choose a coarse-grained model, an atomistic model or a sub-atomic quantum level model.

Probably the easiest model to understand is the classical atomistic model, where every single atom of the system is assigned a value for their mass and electric charge. They are also given initial coordinates, which when put together, represent the system under study. Classical atomistic models are often referred to as ball-and-stick-models due to the simple nature of their appearance: the balls describe the atoms and the sticks holding the balls together are the elastic bonds between the atoms.

A more approximate model suitable for larger systems and longer timescales is a coarse-grained model. A coarse-grained model typically has several atoms of a single molecule combined into a larger bead, which in turn reduces the total number of units in the system. For instance, a hundred-atom lipid can be typically described by about ten beads. The properties of these united atoms are averaged as a single value for the bead. The reduction in system size results in less inter-atom interactions that have to be calculated thus requiring less computing power than an all-atom model of the same system. As a result, however, there is the loss of atomistic detail in the simulation results.

The most detailed description of a system is the quantum mechanical representation, in which the molecular structures and energy states of atoms are derived through quantum mechanical calculations. As a result, the electronic behavior of atoms can be accounted for. The calculations required in these types of structures are extremely heavy and thus are rarely used in larger systems. A typical target for a quantum mechanical approach could, for example, be the computation of the exact partial charges of a single lipid molecule.

It can be very time consuming to build a coordinate file of a system from scratch especially if it includes many types of lipids and proteins. However, there are many reliable repositories for coordinate and force field files of known substructures (proteins, lipids, etc.) where these basic building blocks can be downloaded and used for system creation. With the existing coordinate files, the construction of a model can be done quite easily. One can also use CHARMM-GUI, an interactive web-based platform for creating membrane systems and preparing simulation inputs for many widely used simulation packages [138]. A simple way to examine these models in a three-dimensional format is through a visualization program (such as VMD) [26].

All of the studies included in this Thesis have been built in a classical all-atom model. Therefore, from now on all further discussion will be related to a classical model. The coarse-grained approach has many similarities, but there the atoms are replaced by larger beads.

5.2 Force fields and topologies

In addition to the coordinate file, which describes the positions of the atoms, we also need information on how atoms interact with each other and how they act as a function of time as a result. The interactions are calculated through forces that atoms have on each other. The forces in turn are calculated from a potential energy function according to basic Newtonian mechanics. This potential energy function V and the derived mathematical equations describing how the atoms of a system interact with each other is known as the force field. The force field also includes other relevant parameters such as cut-off distances of interactions.

Equations of motion

The potential function $V(\vec{r}_1, \vec{r}_2, \dots, \vec{r}_N)$ represents the potential energy of a system of N interacting atoms as a function of their position $\vec{r}_i = (x_i, y_i, z_i)$. The force \vec{F}_i applied on a given particle i can be calculated from the potential function as

$$\vec{F}_i = -\frac{dV}{d\vec{r}_i}. \quad (5.1)$$

Once we have calculated the forces applied on all i particles of the system, we can use them to solve the Newton's equations of motion

$$m_i \frac{d^2 \vec{r}_i}{dt^2} = \vec{F}_i, \quad (5.2)$$

from which we can integrate the motions of the atoms with an algorithm of our choice [139]. By repeating the previous steps, we can see how the system evolves with time.

The most common algorithm for calculating the equations of motion is the leap-frog algorithm, which is a third-order numerical integration method [140]. It has

several major advantages in mechanics problems including time reversibility and subsequently the conservation of the equation of the system. Its equations can be written as

$$\vec{v}_i\left(t + \frac{1}{2}\Delta t\right) = \vec{v}_i\left(t - \frac{1}{2}\Delta t\right) + \frac{\vec{F}_i(t)}{m_i}\Delta t, \quad (5.3)$$

$$\vec{r}_i(t + \Delta t) = \vec{r}_i(t) + \vec{v}_i\left(t + \frac{1}{2}\Delta t\right)\Delta t, \quad (5.4)$$

where \vec{v}_i is the velocity of the particle, \vec{r}_i is its position, and Δt is the length of the time step.

The coordinates and velocities at each time step can be saved to a trajectory file, which can then be analyzed to give a detailed look on the behavior of the system over time. The time reversibility is a product of the fact that the positions and the velocities are calculated in a symmetrical way – one can always return to a previous time step by reversing the algorithm.

Potential function

The potential function is typically divided into two categories – bonded and non-bonded interactions – depending on whether the two atoms are connected by a chemical bond or if they only interact through long-range interactions [141].

The bonded interactions include the stretching of covalent bonds, the vibration of bond angles, and proper and improper dihedral angles, which describe the angles between adjacent planes and whether the molecules around the bond stay in their *cis*- or *trans*-configurations.

The potential function of a covalent bond is typically described by a harmonic potential

$$V_{\text{bond}}(r_{ij}) = \frac{1}{2}k_{ij}^r(r_{ij} - r_{ij}^0)^2, \quad (5.5)$$

where i and j are the two bonded atoms, k_{ij}^r the force constant of the bond, r_{ij} the distance between the two atoms, and r_{ij}^0 the reference distance, where the energy of the bond is the lowest. Small deviations from the reference distance increase the potential energy and cause harmonic stretching.

The angles between two covalent bonds are also susceptible to change and this is typically represented by another harmonic potential function. The harmonic potential for bond angle vibration on a triplet of connected atoms $i - j - k$ is described by

$$V_{\text{angle}}(\theta_{ijk}) = \frac{1}{2}k_{ijk}^{\theta} (\theta_{ijk} - \theta_{ijk}^0)^2, \quad (5.6)$$

where θ_{ijk} is the angle between the bonds $i - j$ and $j - k$, k_{ijk}^{θ} is the force constant of the angle, and θ_{ijk}^0 is the reference angle, where the potential energy is the lowest.

In order to define internal rotations, a function for torsional dihedral angle potential is also required. These are referred to as potential energy functions for dihedral angles. A typical way to define such a function for four connected atoms $i - j - k - l$ is by a periodical function

$$V_{\text{dihedral}}(\phi_{ijkl}) = k_{\phi} (1 + \cos(n\phi_{ijkl} - \phi_s)), \quad (5.7)$$

where n is an integer defining the periodicity, k_{ϕ} the force constant, ϕ_{ijkl} the angle between the two planes ijk and jkl , and ϕ_s the reference angle. If the atoms i and l are on the same side of the bond $j - k$, the dihedral angle is zero and it corresponds to a *cis* configuration. Likewise, if they are on the opposite sides of the bond, the dihedral angle is 180 degrees, which corresponds to a *trans* configuration.

In order to force planar atom groups to stay planar, or to prevent molecules from flipping to their mirror images, a group of improper dihedral functions can be defined. They can be periodic, in which case their form is identical to the proper periodic dihedral, or more usually of a harmonic type, where their potential function is defined by

$$V_{\text{id}}(\xi_{ijkl}) = \frac{1}{2}k_{\xi} (\xi_{ijkl} - \xi_{ijkl}^0)^2, \quad (5.8)$$

where ξ_{ijkl} corresponds to the angle between the planes ijk and jkl , ξ_{ijkl}^0 is the reference angle, and k_{ξ} is the force constant.

The non-bonded interactions of a force field are calculated as the sum of the electrostatic interactions and the van der Waals forces between two interacting atoms. They are long-range interactions and thus, unlike in bonded interactions, these atoms can interact with thousands of other atoms in the system.

The electrostatic term is depicted with the Coulombic potential

$$V_C(r_{ij}) = \frac{q_i q_j}{4\pi\epsilon_0\epsilon_r r_{ij}}, \quad (5.9)$$

where q_i and q_j are the charges of the two interacting atoms, ϵ_0 is the permittivity of the vacuum, ϵ_r is the relative permittivity of the medium, and r_{ij} is the distance between the two atoms.

The van der Waals forces are a sum of an attractive and repulsive term, usually depicted with the Lennard-Jones potential

$$V_{LJ}(r_{ij}) = 4\epsilon_{ij} \left(\left(\frac{\sigma_{ij}}{r_{ij}} \right)^{12} - \left(\frac{\sigma_{ij}}{r_{ij}} \right)^6 \right), \quad (5.10)$$

where ϵ_{ij} is the minimum energy of the potential well and σ_{ij} is the van der Waals distance, defining the point where the potential energy turns from repulsive to attractive.

Calculating all of the non-bonded interactions between every atom pair of the system at each time step would be computationally extremely heavy. However, as the strength of long-range interactions weakens as the distance r_{ij} between two atoms increases, it may be possible to use a certain cut-off radius to speed calculations up. The Lennard-Jones potential has an extremely fast decay rate, so short cut-off radii (of around 2 nm) can be used without creating unnecessary artifacts.

On the other hand, the Coulombic potential does not decay as rapidly, so a singular cut-off radius would produce inaccurate results. One typically used method for approximating long-range Coulombic interactions is the Particle Mesh Ewald method (PME), which greatly improves the calculation rates of these interactions [142]. There we employ a cut-off range after which the electrostatic energies are calculated in an efficient way with the Ewald method by utilizing Fourier transforms into reciprocal space and back with the help of periodic boundary conditions. PME is an improvement of the basic Ewald method, using a charge grid in the reciprocal space, improving both accuracy and computational speed.

Temperature and pressure coupling

After creating a system, it can be studied in the microcanonical ensemble, where the number of particles, the volume and the total energy are constant. While this ensemble is appealing, it can, however, be problematic since quite often the total energy of the system studied in experiments is not conserved. If one would like to compare the results of simulations to the results of experiments as directly as possible, then one obvious way is to carry out the simulations at constant temperature. In our simulations we used this approach, that is, the NpT ensemble with a set number of particles (N), pressure (p) and temperature (T). In order to keep these conditions close to the desired value, external barostats and thermostats are included. These are algorithms which control the pressure and temperature of the system preventing them from drifting due to external forces or computational errors.

The temperature coupling in this work was performed with the velocity rescale thermostat, which is a modified version of the Berendsen thermostat [143]. The Berendsen algorithm uses an external heat bath set at a reference temperature T_0 , and corrects the deviation of the system temperature as

$$\frac{dT}{dt} = \frac{T_0 - T}{\tau_T}, \quad (5.11)$$

where T is the temperature of the system and τ_T is the time constant for the exponential decay of the temperature deviation. The strength of the coupling can be adjusted by changing the time constant, which can be useful, for example, for a quick equilibration of the system.

The velocity rescale thermostat differs from the Berendsen thermostat only by an additional stochastic term in its algorithm for the kinetic energy of the system. The function of this additional term is to ensure correct kinetic energy distribution in the system in order to produce a correct canonical ensemble.

Several different methods also exist for controlling the pressure of the system. We used the popular Parrinello-Rahman barostat [144], which forces the box vectors (vectors determining the size of the simulation box) denoted by a matrix \mathbf{b} to follow an equation of motion

$$\frac{d\mathbf{b}^2}{dt^2} = V\mathbf{W}^{-1}\mathbf{b}'^{-1}(\mathbf{P} - \mathbf{P}_{\text{ref}}), \quad (5.12)$$

thus controlling the pressure matrix \mathbf{P} by changing the volume V of the box. The pressure is directed towards the reference pressure P_{ref} by the matrix parameter \mathbf{W} , which defines the strength of the coupling. The coupling parameter is defined as

$$(\mathbf{W}^{-1})_{ij} = \frac{4\pi^2\beta_{ij}}{3\tau_p^2L}, \quad (5.13)$$

where β_{ij} are the isothermal compressibilities, τ_p the pressure time constant, and L the largest box matrix element. The pressure is presented as a 3×3 tensor, which allows non-isotropic handling of the system pressure, which is desirable in the case of lipid bilayers. The Parrinello-Rahman barostat also produces a true NpT ensemble.

Periodic boundary conditions

To minimize the computational costs of a large system, molecular dynamic simulations are typically conducted in a finite box. In order to avoid artifacts caused by the sides of the box, periodic boundary conditions (PBCs) are often introduced in the simulations. Periodic boundary conditions place an infinite number of identical copies of the simulated system around itself. For bilayer systems, this basically extends a bilayer placed on the xy -plane to infinity. As a result, every particle in the simulated box can interact not only with the other particles placed in the same box, but also their images projected to adjacent boxes. In a similar fashion, when a particle crosses the box boundary, a replica of the same particle appears on the opposite side of the original box. As a result, the amount of particles N in the system remains constant.

Due to the nature of periodic boundary conditions, the simulation box has to be large enough to avoid artifacts that could arise from interactions with the images of particles. The size requirements are thus dependent on the employed cut-off values for non-bonded interactions. Even though the original box is copied numerous times, only the properties of the original simulation box need to be calculated. This makes PBCs a fast and reliable method for handling the boundaries of a simulation box.

5.3 Analysis methods

Root mean square deviations and fluctuations

During a simulation, a protein rarely keeps its original structure completely. During the crystallization process from which a protein structure is obtained, the conditions are extremely different compared to conditions where the protein is in its natural habitat inside a cell. Most simulations begin by inserting a structure of a crystallized protein into a system with cellular conditions which in turn induce changes in the protein structure.

When equilibrating a system with a protein, the compact crystallized structure will typically expand, causing the distances between the protein atoms to increase. Therefore, one important factor to follow during the equilibration process is the root mean square deviation of the atomic positions of the protein atoms. The root mean square deviation (RMSD) is defined as

$$\text{RMSD} = \sqrt{\frac{1}{N} \sum_{i=1}^N \sigma_i^2}, \quad (5.14)$$

where N is the total number of atoms and σ is the distance between atom i and its reference structure. The RMSD of a protein structure typically approaches a certain value and once it is adequately equilibrated, the RMSD value will remain approximately constant.

The root mean square deviations can also be used in order to analyze the behavior of different parts of a protein. For instance, by comparing the atomic position of each amino acid to its initial position over a long simulation period, we gain insight into protein dynamics during the simulation. These values are often referred to as root mean square fluctuations (RMSF) and are calculated as

$$\text{RMSF} = \sqrt{\frac{1}{N} \sum_{n=1}^N (x_n(t) - x_n(0))^2}, \quad (5.15)$$

where N is the number of atoms or residues we want to average, $x_n(t)$ is the current position of the residue and $x_n(0)$ its initial position. Calculating the root mean square fluctuations for each amino acid residue of the P2 protein played an

important role in the investigation of P2 dynamics in Papers I – III.

Dynamic cross-correlation maps

One method for investigating protein dynamics is through looking at how different parts of the protein move in relation to each other. This can be achieved through analysing the cross-correlation coefficients of atomic displacements which can be obtained from the trajectory data [145]. These cross-correlation coefficients can be displayed as a two-dimensional dynamical cross-correlation map (DCCM) which gives a clear visual indicator on how the dynamics of protein domains are connected to each other. For instance, the effects a point mutation has on protein dynamics can be easily seen by comparing the cross-correlation maps of wild type and a point mutant. The cross-correlation coefficients are calculated as

$$C_{ij} = \frac{\langle \Delta \vec{r}_i(t) \cdot \Delta \vec{r}_j(t) \rangle_t}{\sqrt{\langle \|\Delta \vec{r}_i(t)\|^2 \rangle_t} \cdot \sqrt{\langle \|\Delta \vec{r}_j(t)\|^2 \rangle_t}}, \quad (5.16)$$

where $\vec{r}_i(t)$ denotes the coordinate vector for atom i as a function of time, $\langle \cdot \rangle_t$ is the time ensemble average and the atomic displacements are calculated as $\Delta \vec{r}_i(t) = \vec{r}_i(t) - \langle \vec{r}_i(t) \rangle_t$ [146].

The cross-correlation coefficients can have values between -1 and 1, the positive values denoting correlation and the negative values anti-correlation between the movements of the two domains. For instance, a high positive value between two domains indicates that the movement of one domain causes similar movement in the other domain (same period and phase). For values close to zero, there is no correlation between the two domains. Anti-correlated movement occurs in the same period but within the opposite phase.

5.3.1 Free energy and umbrella sampling

On the concept of free energy

One important concept discussed in this Thesis are the free energy requirements for certain types of cellular events such as lipid flip-flop. Lipid flip-flop can be considered a diffusion-like reaction where the initial state involves the lipid in its starting

position, the transition state the headgroup in the hydrophobic membrane interior, and the final state has the lipid in the other leaflet [147]. Thermodynamic free energy is a useful quantity for measuring thermal and chemical processes as every chemical reaction involves a change in the free energy of the system. It is based on the principle that all chemical reactions strive towards equilibrium. The internal energy or the absolute free energy of the system is rarely of great interest in chemical reactions, so here when talking about free energies, we refer to the energy differences between the initial state and the final state [148].

Changes in the Gibbs free energy G are defined as $\Delta G = G_{\text{final}} - G_{\text{initial}}$. In other words, a reaction is spontaneous if ΔG is negative and some additional energy is required for the reaction to occur if ΔG is positive. Assuming constant pressure and temperature, the Gibbs free energy can be decomposed into measurable components, enthalpy H and entropy S by

$$\Delta G = \Delta H - T\Delta S, \quad (5.17)$$

where T is the temperature of the system. Temperature is important in free energy reactions – the entropic term plays a greater role at higher temperatures and is not as significant at lower temperatures. The enthalpic component can be associated with the heat of the system and is defined as

$$\Delta H = \Delta U + p\Delta V, \quad (5.18)$$

where U is the internal energy of the system, p the pressure, and V the volume. A positive enthalpic component means the absorption of heat and a negative enthalpic component means heat is transferred to the surroundings. The enthalpic and entropic components together can be used to assess the spontaneity of the reaction – when $\Delta S < 0$ and $\Delta H > 0$, $\Delta G > 0$ always, but in all other cases the spontaneity of the reaction is greatly affected by temperature.

One additional free energy concept is the Helmholtz free energy F , defined as

$$\Delta F = \Delta U - T\Delta S. \quad (5.19)$$

In other words it can be defined as the Gibbs free energy without the expansion term $\Delta F = \Delta G - p\Delta V$, basically meaning the amount of energy usable in the system once spontaneous expansion work has been performed. Helmholtz free energy

can be used for the calculation of the free energy profiles of lipid flip-flop through a method known as umbrella sampling as there is no driving enthalpic force facilitating the translocation of membrane lipids [147].

The free energy profiles of lipid flip-flop can further be decomposed into its entropic and enthalpic components. This can be performed with a centered difference method applied to the entropic portion of the free energy profile. Then the entropic contribution can be estimated as

$$-T\Delta S \approx \frac{T}{2\Delta T} [\Delta G(T + \Delta T) - \Delta G(T - \Delta T)], \quad (5.20)$$

where in order to obtain the entropic contribution on the free energy profile at temperature T , two additional free energy profiles for the same system must be obtained at temperatures $T + \Delta T$ and $T - \Delta T$ [149]. The enthalpic component of the reaction can then be calculated from Equation (5.17). For instance, past research has shown the activation free energy for lipid flip-flop to consist of large opposing enthalpic and entropic contributions [105, 150]. According to the basic laws of thermodynamics, entropy tends to spontaneously increase [148]. Therefore, in normal temperatures, when the entropic component plays a higher role, entropically driven chemical reactions are favorable and happen spontaneously. Enthalpically driven chemical reactions, in turn, generally require external energy to occur.

The energy requirements of lipid flip-flops can be associated with the rate with which lipid flip-flops occur. The rate constant k_f is dependent on the height of the energy barrier ΔG through an Arrhenius-like relation

$$k_f = \frac{k_B T}{h} \exp\left(-\frac{\Delta G}{RT}\right), \quad (5.21)$$

where k_B is the Boltzmann constant, h the Planck constant, and R the molar gas constant [151]. Through the equation, estimates of the effect a reduced free energy barrier has on the flip-flop rate can be made, and experimental measurements compared to simulated ones. However, obtaining accurate absolute values for the flip-flop rate or conversely on the free energy barrier through the equation is not as straightforward due to the fact that there are many unquantifiable factors such as transition probabilities related to the lipid position affecting lipid flip-flop.

Umbrella sampling – measuring the free energy profiles

Chemical processes are driven by free energy differences between two states. For example, certain proteins can be found in closed or open states. In order to move from one state to the other, the protein must overcome a free energy barrier. Another example can be found in lipid translocation, where in order to flip-flop across a bilayer, a lipid must cross an exceptionally high free energy barrier. One major challenge in molecular dynamics is the calculation of these free energy differences.

Due to the fact that free energies are thermal quantities, as kinetic energy is dependent on the temperature, free energy differences between two states can not be directly measured from the simulation data unlike work [152]. A main alternative method is the probability-based umbrella sampling, which uses bias potentials to help drive the system from one state to the other [153]. The basic concept of umbrella sampling is visualized in Figure 5.1.

The equations behind this method originate from the basic concepts of thermodynamics, according to which the amount of work W performed to the system is greater than the Helmholtz free energy difference ΔF when the system is transformed from one state to the other at a finite rate, so that $\langle W \rangle \geq \Delta F$ [154]. The inequality is related to dissipated work associated with entropy and can be replaced by an equality $\langle \exp(-\beta W) \rangle = \exp(-\beta \Delta F)$, which can be solved for the free energy

$$\Delta F = -1/\beta \ln \langle \exp(-\beta W) \rangle, \quad (5.22)$$

where $\beta = 1/(k_B T)$ is the inverse temperature and k_B the Boltzmann constant [154]. The amount of work can be directly measured from MD simulations and implemented into the equation. Such a direct calculation, however, can give very inaccurate results as in many cases an external force has to be applied to the system in order to facilitate transformation from one state to the other along a set reaction path.

A way to equilibrate these instabilities caused by the application of an external force is to divide the reaction path into windows and consider each of them as a separate simulation. External bias is applied to each window in order to keep the reaction close to its desired state inside the window and the windows are selected at such intervals that two neighboring windows may overlap at a small probability at any given time.

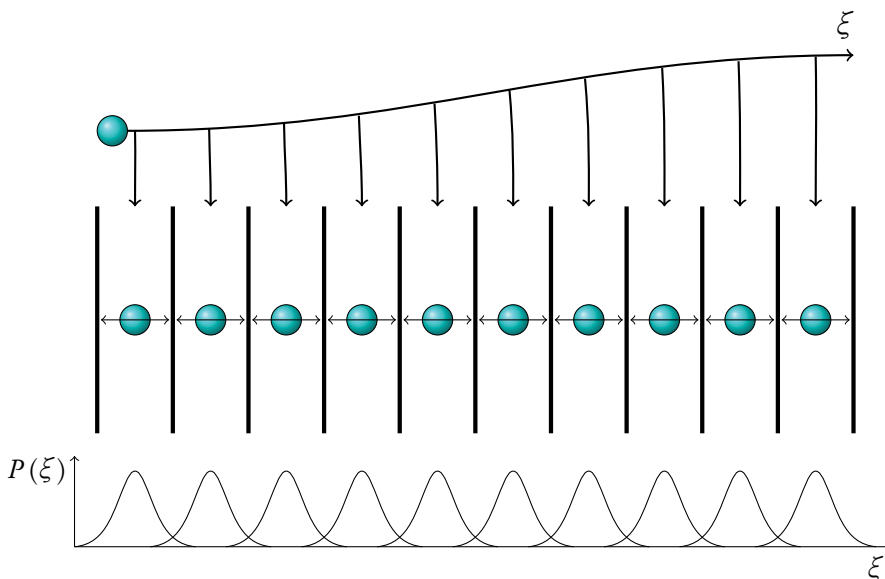


Figure 5.1 Illustration of the basic idea behind umbrella sampling. The reaction, represented by the cyan circle, propagates along the reaction coordinate ξ . The reaction path is divided into a number of sampling windows and each window is used as a starting point for a new independent simulation. In each window, the reaction is confined near its new starting point by using a bias potential. When the positions of the windows and the bias potentials are selected properly, there should be a small probability that the reaction will be found in the same phase in two adjacent windows. Therefore, the probability distributions of the reaction path for two adjacent windows will overlap. As a result, the continuous free energy can be integrated over the whole reaction path. Figure adapted from Ref. [123]

The total free energy A of a reaction path can then be integrated over the probabilities of finding the system at any given state along a reaction path over all i windows, as

$$A_i(\xi) = -\frac{1}{\beta} \ln P_i^b(\xi) - w_i(\xi) + F_i, \quad (5.23)$$

where P_i^b is the biased probability distribution, w_i are the bias potentials and F_i is the free energy obtained from the previous equation. The combined umbrella sampling simulations can then be analyzed, for instance, by the weighted histogram analysis method (WHAM), which aims to minimize the statistical errors and produces the free energy profile [155].

6 OVERVIEW OF THE SIMULATED SYSTEMS

Paper I

In the first paper, MD simulations were conducted on the P2 protein in a solvated box. Models for both the wild type protein and its P38G mutant were constructed. The plan was to investigate the dynamics of the wild type protein and see how a point mutation in the hinge of the lid of the barrel structure would affect the dynamics and structure of the protein especially around the lid area.

The simulations were conducted with the GROMACS 4.6 simulation package [156]. The model for the P2 wild type was obtained from the RCSB Protein Data Bank [137] under the PDB entry 4BVM [11], and the point mutant was constructed from the wild type by changing the amino acid at the point of the mutation. The modeling was done using the CHARMM36 force field [157] which gave an all-atom representation of the protein and the palmitate chain. All bonds were constrained with the LINCS algorithm [158]. Water was modeled with the TIP3P three-point model [159].

The simulations were carried out in NpT conditions with the Parrinello–Rahman barostat for pressure coupling [144] and the velocity-rescale method for temperature coupling [143]. The systems consisted of the wild type and P38G variants of the P2 protein both with and without the bound palmitate chain in a solvated box with added counter-ions to negate the charge of the protein. After an initial equilibration period of 500 ns, the systems were simulated for an additional 2.5 μ s in order to obtain enough data for reliable analysis.

For mean square deviation analysis of the protein hydrogens, we carried out additional simulations, selecting seven starting points from the original 3 μ s simulation, the first at 500 ns and the following ones taken at 200 ns intervals for sufficient sampling. These systems were simulated for a short period of 3 ns while saving the trajectories at every time step (2 fs) in order to capture the rapid motion of the hy-

drogen atoms. The first nanosecond of each simulation was then used to average the MSD of both CH₃ and CH₂ hydrogens of each protein system as it provided accurate enough data.

Paper II

In the second paper, we conducted MD simulations in a similar manner to the first paper while exploring the effect of the CMT1 associated point mutations on the dynamics of the P2 protein. The simulations were conducted with the GROMACS 4.6 simulation package and the three point mutants were obtained in the same fashion. The simulations were carried out in NpT conditions using the Parrinello–Rahman barostat and the velocity-rescale thermostat. All-atomistic representation of the system was done using the CHARMM36 force field.

A total of eight systems were investigated; the P2 wild type and its I43N, T51P and I52T mutants with and without the bound palmitate chain. These proteins were simulated in a solvated box with counter-ions to negate the total charge of the system. The total simulation time for each system was 2.5 μ s of which the first 500 ns was used for equilibration.

Paper III

In the third paper, we investigated another point mutant of the P2 protein, F57A through atomistic MD simulations. The F57 amino acid has a central role in regulating the opening of the barrel region of the P2 protein. The simulation parameters were exactly the same as in the previous publication.

The dynamic cross-correlation map (DCCM) analysis of the P2 mutants were performed with Bio3D, an R package for analysing trajectory data [160]. In addition to P2 wild type and the F57A mutant, DCCM analysis was performed on all previously (Paper I and II) simulated P2 mutants as well.

Paper IV

In the fourth paper, we performed molecular dynamics simulations on two different systems with the main goal of uncovering a protein-mediated mechanism for lipid

flip-flop. The free energy requirements for both rhodopsin-mediated flip-flop and that of a protein-free system were calculated. As the attached paper is a review article referencing mainly unpublished data from the author, the simulation details related to these results are described here in greater detail.

The main system consisted of a lipid bilayer with a composition of 50% POPC, 25% SSM and 25% cholesterol (162, 81 and 81 lipids respectively), mimicking a lipid raft system. Embedded in the bilayer was rhodopsin obtained from the RCSB Protein Data Bank [137] under the PDB entry 1U19 [17]. The ligands 11-*cis*-retinal and the two palmitoyl chains attached to rhodopsin were re-parametrized by calculating the partial charge values of the atoms using quantum mechanical derivation through the RESP ESP charge Derive (R.E.D.) package [161]. The system was then adequately solvated with approximately 28000 water molecules and the salt concentration was set to a physiological level of 150 mmol/l by addition of NaCl molecules. The protein-free system had the same lipid composition, but was smaller in size (64, 32 and 32 lipids). It was solvated with approximately 4000 water molecules and had the same salt concentration.

The simulations were conducted using the GROMACS 4.5.5 simulation package. The modeling was done at atomistic level using modified OPLS-AA representation [162, 163]. The water molecules were represented with the TIP3P model [159]. Simulations were mainly carried out in NpT conditions using a semi-isotropic Parrinello-Rahman barostat for pressure coupling and the velocity rescale method for temperature coupling. Energy minimization runs were performed with the steepest descent algorithm with LINCS constraints on all bonds and the molecular dynamics simulations were conducted with the leap-frog algorithm with time steps of 2 fs.

Steered molecular dynamics simulations were performed in order to move lipids from one place to the other. This was done by applying a force of $1000 \text{ kJ mol}^{-1} \text{ nm}^{-2}$ to the lipid head group, forcing the lipid to move into a certain direction. The rates of movement for the lipids varied from 0.1 to 1.0 nm/ns. This was especially useful for establishing a favorable path for the lipid to traverse across the bilayer interior in both systems. Snapshots were taken at 0.1-0.2 nm intervals along the flip-flop route, which were later used as the windows for umbrella sampling. These simulations were repeated for both POPC and cholesterol with and without the presence of rhodopsin.

A total of 33 umbrella sampling windows were used for POPC and 21 for cholesterol flip–flop in the system with rhodopsin. For the protein-free system, free energy profiles for both POPC and cholesterol flip–flops were calculated using 21 umbrella sampling windows. The free energy profiles involving lipid approach towards the protein had 30 umbrella sampling windows for POPC and 25 for cholesterol. The windows were equilibrated for 20 ns followed by a 50 ns data gathering period – the equilibration period long enough for the system to revert the effects caused by forced steering of the lipid, and the data period short enough for the system not to completely relax into its present state. During the umbrella simulations the lipids were held in place by a harmonic force constant of $4000 \text{ kJ mol}^{-1} \text{ nm}^{-2}$ during the equilibration period and $1000 \text{ kJ mol}^{-1} \text{ nm}^{-2}$ during the data gathering period. The lower harmonic force constant allowed the lipid to fluctuate more freely within the short time period resulting in a wider probability distribution ensuring continuity along the reaction path.

The obtained free energy profiles were later decomposed into their enthalpic and entropic components. The decomposition required repetition of the umbrella sampling simulations performed at two additional temperatures as per Eq. 5.20. We chose a temperature difference of 15 K, resulting in a set of umbrella sampling simulations at temperatures 295 K, 310 K and 325 K, for obtaining the enthalpic and entropic contribution at $T = 310 \text{ K}$.

7 RESULTS AND DISCUSSION

The key results obtained in the publications included in this Thesis are discussed in detail in this chapter. Even though the majority of the papers had experimental wet lab collaboration with additional insight into the results of the research, we mainly focus on the results obtained from the molecular dynamics simulations thereby focusing on the author's contribution.

7.1 Point mutation in P2 lid hinge increases protein dynamics

The myelin protein P2 is a main structural component of the myelin sheath in the peripheral nervous system. Its main role is to help stack lipid membranes together to form a functional myelin structure around an axon. *In vitro* studies of a P38G point mutation have shown that the P38G-variant of P2 increased its lipid stacking capacities while still remaining functional and not changing the overall structure of the protein [51]. The crystal structures of the two variants were found to be practically identical. The core reasons for functional differences were not reachable by conventional experimental means. Therefore, computational models were used to provide insight into the underlying dynamics of the P2 protein and its P38G mutant.

The proline residue 38 is found in the hinge region of P2, between the rigid barrel structure and the flexible lid. Previous assumptions have linked P38 with the opening of the helical lid of P2 during the binding and releasing processes of the protein ligand found inside the barrel [11]. The cyclic structure of the proline side chain has a significant effect on the rigidity of the protein structure around the residue. By mutating the proline into a glycine, we remove the cyclic structure which in turn weakens the protein structure in the hinge region, increasing the flexibility of the lid. Presumably, this should allow the lid to open more easily, facilitating the rate of

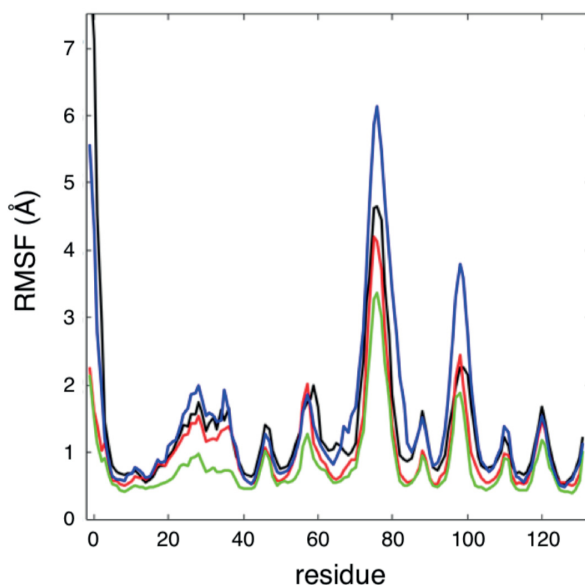


Figure 7.1 Root mean square fluctuation per residue for all four simulated systems. For the systems without a ligand, black corresponds to the wild type and red to the P38G mutant. For the systems with the bound palmitate, green corresponds to the wild type and blue to the P38G mutant. Larger RMSF values indicate a more mobile region. The lid region can be found between residues 16-36 and the two apposing loops at residues 74-78 and 97-99.

ligand transfer.

In Paper I, we constructed and simulated models of the P2 protein and its P38G mutant with and without a bound ligand that was found in the crystallized structure we used as a base model [11]. As the main focus of the publication was to observe the main dynamical differences of the two protein variants, the proteins were simulated in a simple solvated box without the presence of a lipid membrane.

The simulations provided insight into the dynamics of the P2 protein. By examining the root mean square fluctuations of every residue of the protein variants (Figures 7.1 and 7.2), we see which parts of the protein are the most flexible and how the dynamics of the protein variants compare to each other. The most mobile regions of P2 are found in the two loops (residues 74-78 and 97-99) apposing the lid region. The lid itself (residues 16-36) seems to be quite stable. This suggests that maybe the lid is not the opening part of the protein, but instead the two beta-strands on the opposite side give way for the ligand (a point further investigated in following publications).



Figure 7.2 A visualization of the RMS fluctuations in the P38G mutant with the palmitate chain inside the binding pocket. The yellow color corresponds to the mutated amino acid G38. The colorbar indicates the RMSF values, with bright magenta corresponding to the most flexible parts of the protein.

Comparing the protein variants to each other, we can see that the dynamics of the ligand-free P2 and its P38G mutant are quite similar, with maybe a slight decrease of flexibility upon mutation. However, when we add the palmitate ligand into the barrel, the dynamics change significantly. Firstly, the lid region is extremely stable in the wild type, likely due to strong interactions between the lid, the palmitate and the cyclic structure of proline. Upon changing the proline into glycine, we weaken these interactions, and the lid region and also the palmitate chain become more mobile. This can also be observed by examining the trajectory data. Secondly, the data shows that the wild type with the palmitate is considerably more stable than either of the two palmitate-free variants, especially in the loop regions. Conversely, the P38G mutant with the bound palmitate is the most mobile variant, especially in the aforementioned loop regions. The increased flexibility of the P38G mutant could explain the previously observed increase in membrane binding activity of the variant

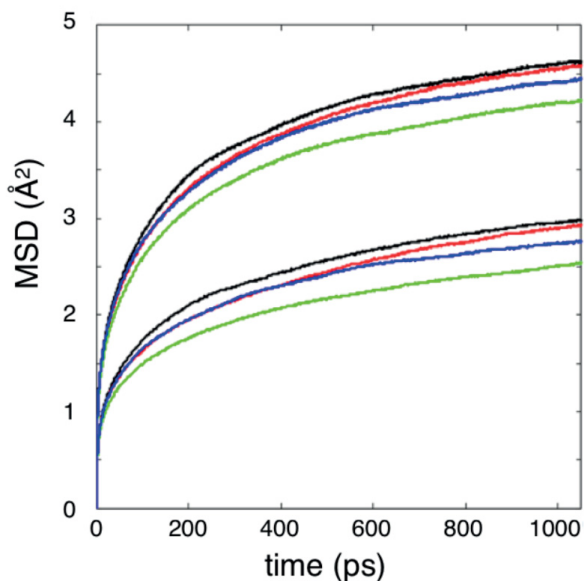


Figure 7.3 The averaged mean square deviations of CH_3 (top) and CH_2 (bottom) hydrogens. Proteins without palmitate are shown in black (wild type) and red (P38G mutant). Proteins with palmitate are shown in green (wild type) and blue (P38G mutant).

along with an enhanced ability to interact with lipids.

A secondary goal for the molecular dynamics simulations was to provide support for the use of elastic incoherent neutron scattering (EINS), which is a powerful experimental tool for investigating quantitative protein dynamics, for instance, as a function of temperature. For this reason, we performed additional simulations where the main focus was the dynamics of the protein hydrogens, separated into hydrogens of both CH_3 and CH_2 groups. The mean square deviations of both hydrogen groups depicted in Figure 7.3 show that the methyl hydrogens are much more mobile than the other hydrogens both in the travel distance (MSD values) and the rate of motion (tangents of curves). The mean square deviations also show that the hydrogens in the palmitated proteins are more constrained than in the palmitate-free protein confirming earlier observations that the bound fatty acid restricts P2 dynamics [11]. The results also support dividing P2 hydrogens into methyl and non-methyl groups for EINS analysis.

7.2 CMT1-associated point mutations affect P2 dynamics

As P2 is a major component of the peripheral myelin sheath, issues in its encoding may also lead to mutations which have harmful consequences. Often these mutations cause the protein to function in a different manner, which in turn affects its fatty acid binding capabilities leading to improper stacking of the myelin leaflets. One such case is the Charcot-Marie-Tooth neuropathy, which has been linked to certain point mutations found in P2 [75, 76]. The point mutations in question are I43N, T51P and I52T, all found near each other in the $\beta 2$ - and $\beta 3$ -strands of the barrel structure.

In Paper II, we performed molecular dynamics simulations on these three variants with and without the bound palmitate ligand found inside the crystallized structure of the protein. Included was the simulation data of the protein wild type from Paper I. The main goal of these simulations was to gain insight on how the point mutations affect the dynamics of P2 at an atomistic level. Coupled with experimental studies we were able to perform a detailed characterisation of the CMT1-linked P2 point mutations.

Root mean square fluctuations (shown in Figure 7.4) can again be used to compare the mobility of the different parts of the protein over the course of the simulation. By comparing the dynamics of the point mutants to the wild type, we can gain valuable information from their different behavior. From the data we can see that in the ligand-free protein, all point mutants are more stable than the wild type. I43N and T51P are extremely rigid, with the former showing slight movement around the lid area. On the other hand, I52T is quite mobile at the two loops opposite the lid. Upon introducing the bound palmitate ligand, there is significant change in the dynamics. T51P suddenly becomes the most dynamic of all the variants especially in the lid region and the following beta-sheets, contrary to its behavior in the absence of the ligand. I52T also shows larger fluctuations than the wild type in certain areas. Minimal differences can be seen in the I43N mutant. Generally in other areas, the protein is more stable in the palmitate-bound form. It seems that the presence of the palmitate destabilizes these certain areas while increasing stability elsewhere.

Differences in the point mutants can also be seen by observing the amount of water inside the beta-barrel of each variant. Over the course of the simulation, the average numbers of water molecules found inside the barrel were 27.7, 30.5, 23.7 and

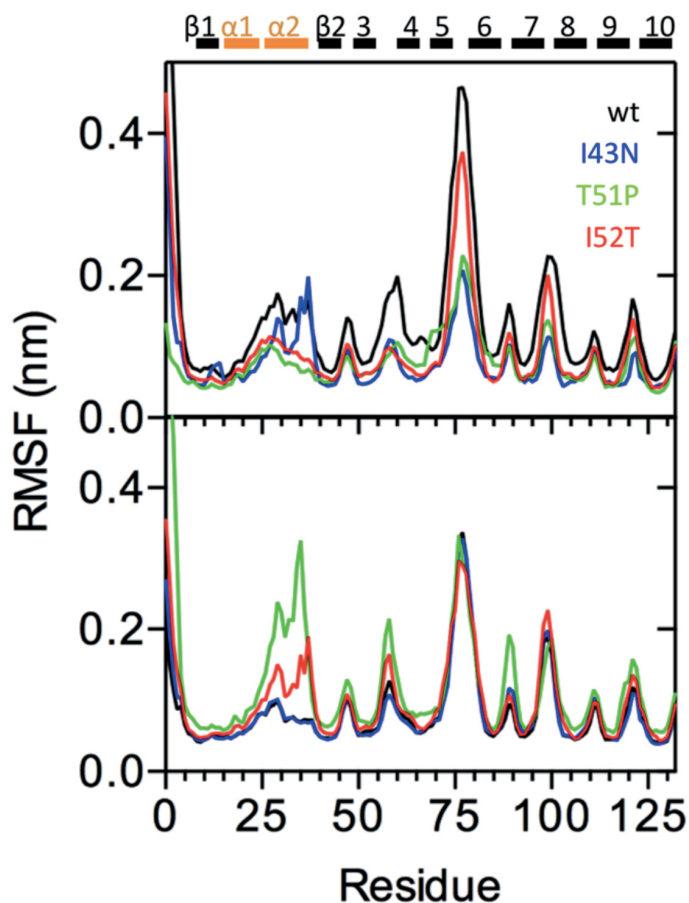


Figure 7.4 Root mean square fluctuation per residue for all eight simulated systems. The empty protein is shown in the top graph and the liganded P2 in the bottom. The corresponding point mutants are indicated by colorization.

30.4 for unliganded P2 wild type, I43N, T51P and I52T mutants respectively. For P2 with the bound palmitate, the respective numbers were 21.0, 22.1, 29.1 and 22.0. In general, the number of water molecules found inside the barrel was smaller in the presence of the ligand. The only exception was the T51P mutant, where the number of water molecules was much higher in the liganded form. This was explained by early opening of the T51P structure, allowing a larger number of water to enter the barrel (see Figure 7.5). Compared to the wild type, the Ile mutants I43N and I52T showed similar, higher amounts of water. These values are in accordance to previous FABP studies, where liganded proteins were found to have a higher water exchange

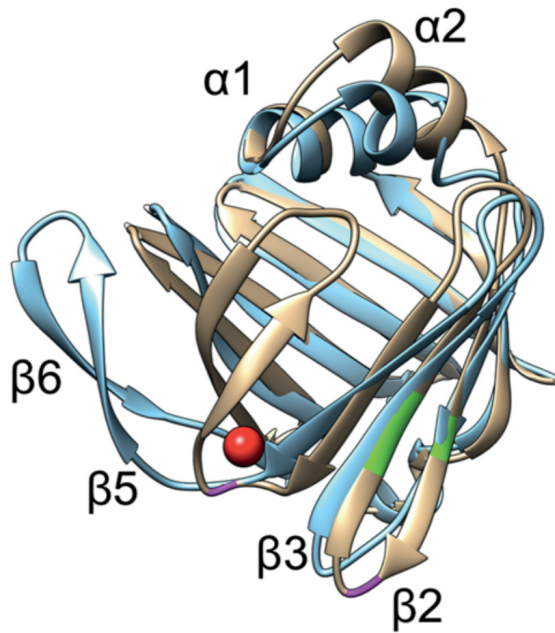


Figure 7.5 The structure of P2 wild type superimposed on the open conformation of the T51P mutant. The location of the three mutations are shown in green. The red dot indicates the hinge area of the barrel opening.

rate than their empty counterparts [164].

In addition to the T51P mutant, also the two other point mutants showed signs of opening during the simulation. The common factor in the barrel opening was the location. The β 5- and β 6-strands of the barrel flip away from the protein creating a large enough gap for a ligand to pass through. This movement can also be seen in the RMSF graphs at the area of highest fluctuations. At the root of these two beta-strands is a conserved glycine residue, a common theme in all human FABPs. It is therefore possible that the observed motion is a general mechanism for opening of all fatty acid binding proteins, a mechanism that has been suggested earlier, but not observed so far [165]. There may be several factors affecting the barrel opening, such as the presence of a ligand, mutations or a cell membrane. It is also possible that this increased instability may be a main factor in misfolding or deformation of the myelin sheath, a main cause behind the Charcot-Marie-Tooth neuropathy. It is worth noting that no spontaneous ligand transfer was observed in the simulations even though the palmitate chain drifted towards the gap on several occasions. External

influences such as a lipid membrane or other proteins may be required to facilitate the dissociation of the ligand.

7.3 P2 barrel opening is regulated by a conserved residue in the portal region

In the first two papers included in this Thesis, we observed an increase in protein dynamics of P2 upon introduction of certain point mutations, especially around the portal region. Opening of the beta barrel is critical for ligand transfer, which is thought to be a secondary function of P2. The barrel is large enough for a small lipid, such as cholesterol, one main component of the myelin sheath, and thus P2 might be able to function as a lipid transporter during the myelination process [166, 167]. However, the question of the opening mechanism has been elusive even when we know ligand transfer is an intrinsic property of FABPs.

In Paper III we delve deeper into the mechanisms behind the opening of the P2 portal region by investigating a conserved residue Phe57 located near the root of the barrel lid. The residue in question is prevalent in many FABPs and has been considered a gatekeeper for portal region opening during ligand transfer [168]. Phe57 has a ring structure that has been found to flip from inside the barrel towards the solvent and back in different FABP structures, and its position might play a central role in the opening of the portal region [168]. The point mutation considered in Paper III was simply to remove the ring structure, and mutating the residue to alanine in order to disrupt its central role in regulating the opening of the portal region, highlighting its importance in the opening process and giving us further insight on the opening mechanism.

We began by comparing the root mean square fluctuations for each residue of the F57A point mutant to the wild type protein. Again, we see higher dynamics for the mutant in the absence of the bound palmitate chain, while the differences are minimal in its presence (see Figure 7.6). It appears that the presence of the palmitate ligand stabilizes all lost contacts caused by the mutation due to the similarity of the RMSF curves of the liganded P2. The main differences in protein dynamics are again observed in the $\beta 5$ - $\beta 6$ -loop opposite the lid. Compared to the previously studied point mutants, the effects are even more profound, also denoted by clear and

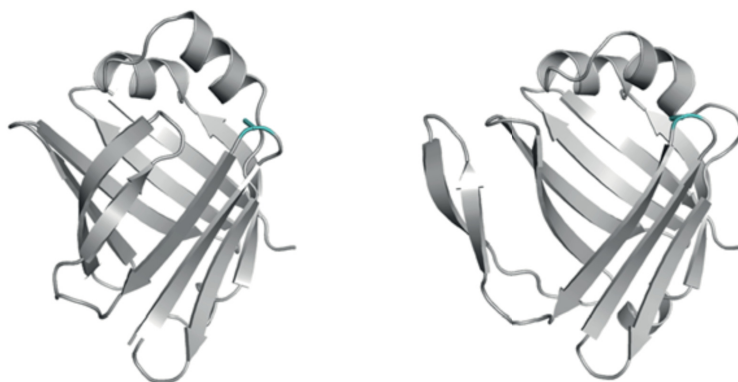
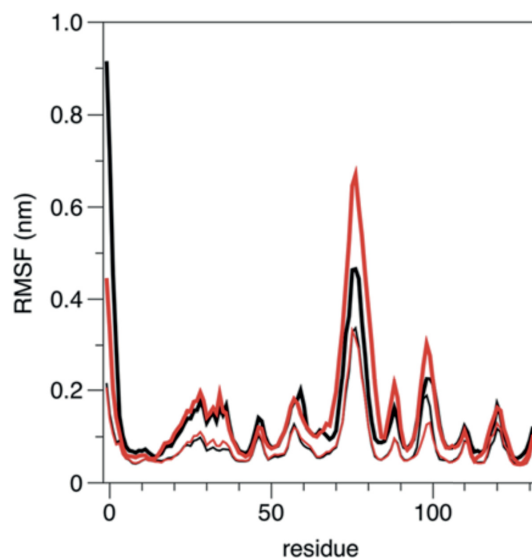


Figure 7.6 **Top:** Root mean square fluctuation per residue for the wild type P2 (black) and its F57A mutant (red). Thick lines indicate unliganded P2 and the thin lines P2 with a bound fatty acid. **Bottom:** The closed and open structures of the F57A mutant of P2 taken from the simulations. The location of the F57A mutation is shown in green.

prolonged opening of the protein between the $\beta 4$ - and $\beta 7$ -strands.

Here, we further investigated the causes and effects of the opening process. One way to analyze the simulation trajectories and look for intramolecular interactions within the protein is through dynamic cross-correlation networks. By comparing the dynamic cross-correlation matrices of the wild type P2 to its point mutants, we can see which interactions are disrupted by the point mutations. Specifically, the coordination of barrel opening may be observed.

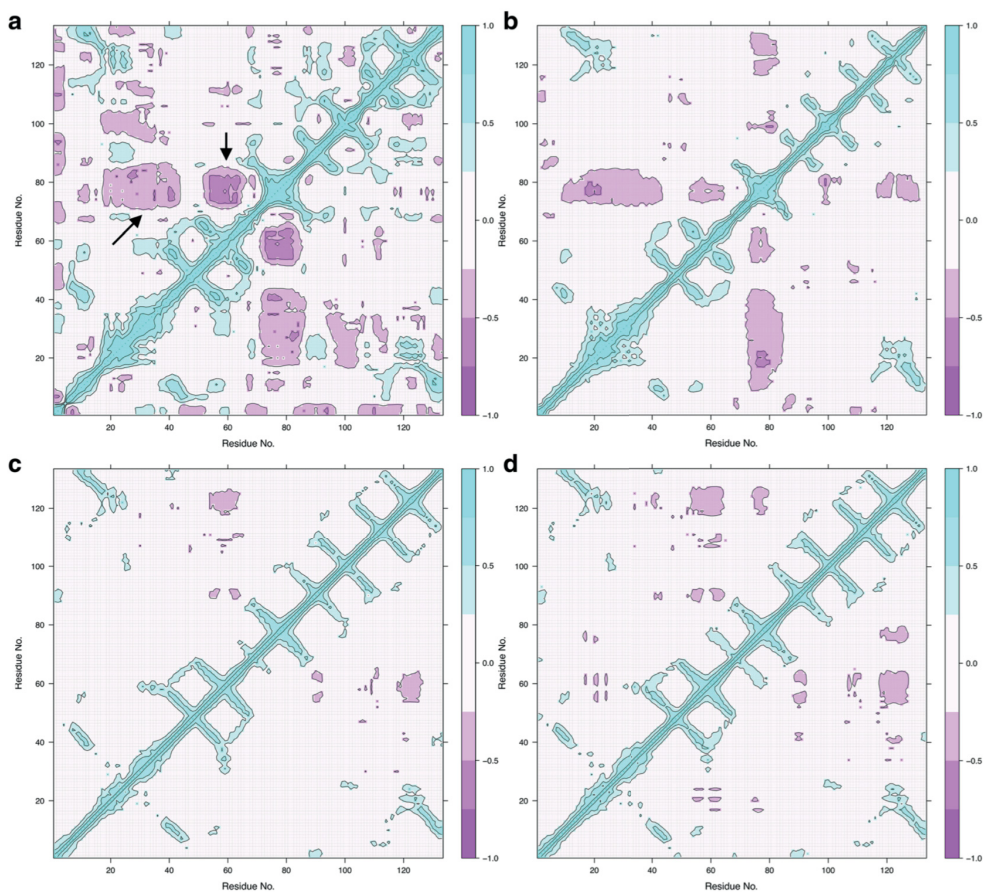


Figure 7.7 DCCM analysis of the simulations of the F57A point mutant. The maps for the unliganded wild type (a) and wild type with palmitate (b) show two main regions of anti-correlation denoted by the arrows. In the unliganded F57A (c) and the F57A with palmitate (d) this anti-correlation is absent.

The dynamic cross-correlation maps (Figure 7.7) for the wild type show areas of significant anti-correlation between the $\beta 5$ - $\beta 6$ -loop (residues 74-77) and the lid region (residues 16-36) and the adjacent $\beta 3$ - $\beta 4$ -loop (residues 55-58) denoted by the two arrows. This anti-correlation is also present in the wild type with the bound palmitate. We believe this anti-correlation to reflect the coordinated open-close movements of the $\beta 5$ - $\beta 6$ -flap upon ligand transfer. The DCCM analysis also shows that upon point mutation these areas of anti-correlation disappear, which indicates that the mutation removes the ability of the protein to regulate its opening. Upon further examination of the previously studied point mutants (P38G and the CMT-disease

mutants) with higher dynamics in the portal area, we also perceived similar changes through their dynamic cross-correlation maps. The common denominator for the increased protein dynamics seems to be the loss of regulated movement in the protein caused by a mutation.

With the results published in Paper III, combined with the re-analyzed data from the Papers I and II, we believe to have observed the general mechanism for P2 barrel opening. The barrel opening of FABPs through two adjacent β -strands has long since been suggested [169], but not shown at an atomistic level until now. Due to high structural similarities between all FABPs, we believe this mechanism to be likely to work for other FABPs as well.

7.4 Rhodopsin functions as a non-selective lipid scramblase

The fourth paper included in this Thesis is a review article discussing cell signaling and the roles lipids serve within the signaling processes. The approach taken to research this subject includes atomistic and multiscale molecular dynamics simulations. Several different studies are referenced in the review article including rhodopsin and β_2 -adrenergic receptor-mediated lipid flip-flop, the role of polyunsaturated fatty acids and cholesterol in oxidative stress, and how lipid messengers bind to receptors or target proteins and function in receptor activation. The author contributed to this review article by studying the scramblase properties of rhodopsin and the energetics of rhodopsin-mediated lipid flip-flop which allows lipids to translocate back and forth across the membrane at a relative ease. As a consequence of non-selective lipid scrambling, a large number of different types of lipids are able to reach the cell surface where they are recognized by target proteins and enzymes, resulting in a large variety of cellular processes. Therefore, lipids undergoing flip-flop are major contributors in cellular signaling, where information from within the cell has to be sent rapidly to the extracellular side. The main unpublished results related to the lipid flip-flop segments referenced in the review article, as well as the background behind the research, are discussed in depth within this subchapter.

Lipid flip-flop is an extremely slow process when no proteins, peptide chains or other membrane defects are present, with typical rates of one phospholipid flip-flop per day [170]. However, rapid lipid flip-flop is required for many physiological events such as sustaining cellular growth and maintaining lipid asymmetry in mem-

branes. During the past few decades, certain types of proteins – flippases and scramblases – have been identified, their function to greatly facilitate the flip–flop process in cellular membranes. One of the latest discoveries on the subject established a link between G protein-coupled receptors and non-selective lipid scrambling across the lipid bilayer [12]. Also, until now, the only existing x-ray structure of a verified scramblase is from a few years ago of transmembrane protein TMEM16 [16]. As a result, the molecular mechanisms behind protein-mediated lipid flip–flop are still relatively unknown. The main goal of our study was to utilize molecular dynamics simulations on lipid bilayer systems with an embedded rhodopsin – a well-known GPCR shown to exhibit scramblase activities – and to uncover the molecular mechanisms with which it facilitates lipid flip–flop.

Considering the central structures of all GPCRs – seven transmembrane helices crossing the membrane interior – three possible pathways seem likely candidates for lipid translocation and have been suggested by previous studies [12, 44, 128]. The first involves the lipid migrating across the membrane outside the protein and along the surface of the transmembrane helices. The second candidate mechanism has the lipid headgroup in a hydrophilic environment inside the transmembrane channel of the protein while the lipid tails remain outside in the hydrophobic membrane interior. The third possible mechanism has the lipid entering the transmembrane channel completely on one surface of the membrane and exiting only on the other side. However, the last one seems unlikely as lipid scrambling facilitated by GPCRs is nonselective, and especially lipids with larger headgroups may have trouble submerging into the transmembrane channel entirely.

Our studies focused on the first candidate with the lipid translocating along the protein surface. This was decided after many attempts of steered molecular dynamics where we tried to force the headgroup of a POPC molecule through the membrane along a large number of different pathways with the aforementioned mechanisms. From the initial results, POPC flip–flop along the surface of rhodopsin next to transmembrane helices II, III and IV seemed the easiest. This was also supported by multiple studies where even single peptide chains – with no hydrophilic transmembrane channels – were able to facilitate lipid flip–flop to an acceptable level [151, 171, 172], and that the flip–flop rates depend on the hydrophilicities of the central residues of the chain [173]. Also, the fact that the scrambling abilities of opsin remain in many of its holo-forms where the transmembrane channel is blocked by a ligand – such

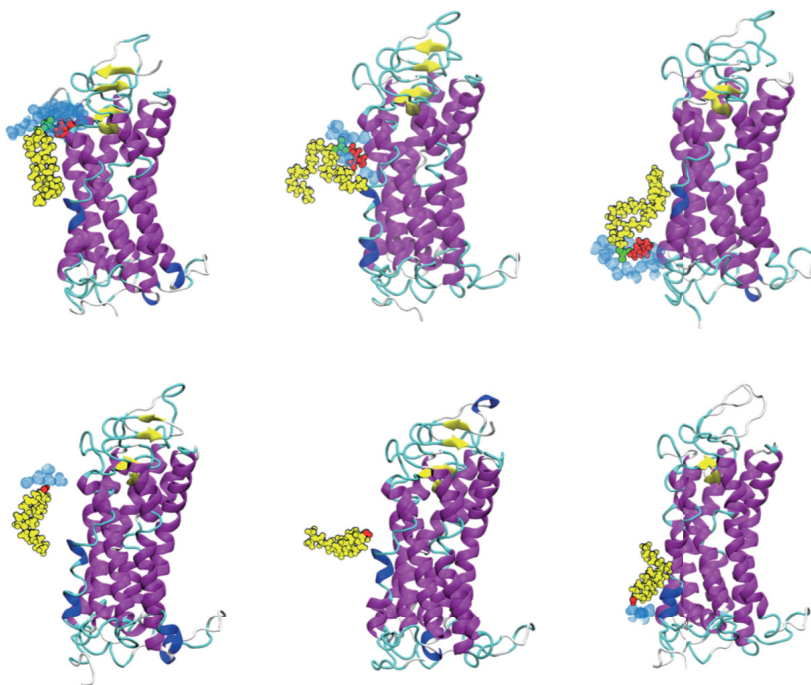


Figure 7.8 Snapshots from selected parts of the steered molecular dynamics simulations for POPC (above) and cholesterol (below) flip–flop. The figures are taken after a short equilibration period. The lipid bilayer and water are not shown for clarity with the exception of water molecules within 0.5 nm of the lipid undergoing flip–flop. The headgroup of POPC translocates across the membrane interior with a water pore that is formed during the flip–flop event.

as retinal in rhodopsin – imply that the main translocation path does not involve the central core of the protein [44]. However, it is worth noting that a recent simulation study successfully explored the second mechanism for opsin with the lipid headgroup migrating along a hydrophilic path between two adjacent transmembrane helices, insinuating that multiple translocation mechanisms do exist for a single protein [50].

The flip–flop mechanisms in the presence of rhodopsin for both POPC and cholesterol are illustrated in Figure 7.8. By applying a downward force to the lipid molecule headgroup, the lipid was steered from the upper leaflet of the bilayer to the lower leaflet along the protein surface. Interestingly, a water pore formed next to the protein surface during POPC flip–flop, giving the polar headgroup easier access to the hydrophobic membrane core. A similar water pore also formed during POPC flip–

flop in a protein-free membrane, the amount of water molecules in the vicinity of the lipid headgroup differing only by a few. However, no water molecules were present during the translocation process of cholesterol – likely due to the small size of the cholesterol headgroup. Cholesterol is known to spontaneously flip-flop at a rapid rate even in protein-free membranes, making their translocation process independent of flippases and other membrane defects such as water pores [105].

The free energy profiles for POPC and cholesterol flip-flop were calculated by umbrella sampling and are presented in Figure 7.9. The approximate height of the free energy barrier caused by the hydrophobic core of the membrane is 60 kJ/mol for POPC and 10 kJ/mol for cholesterol when flip-flop occurs along the surface of rhodopsin. In the protein-free system the respective values were 130 kJ/mol for POPC and 20 kJ/mol for cholesterol. Translocation from one leaflet to the other along the surface of rhodopsin reduced the height of the free energy barrier ΔG by a total of $\sim 60\%$ (or ~ 70 kJ/mol) for POPC and $\sim 50\%$ (or ~ 10 kJ/mol) for cholesterol when compared to a protein-free system. This is a significant reduction in free energy and is supported by previous experimental results where the presence of rhodopsin in large unilamellar vesicles greatly increases the scrambling rate of phospholipids [12]. The fact that the free energy barrier was also reduced for cholesterol further supports the suggestion that the scramblase properties of GPCRs are not lipid selective.

Umbrella sampling was also utilized in order to calculate the free energy profiles of both POPC and cholesterol approaching rhodopsin along the membrane surface (see Figures 7.10 and 7.11). The free energy profile for POPC was calculated at the initial stages of the study and thus only includes the approach towards the protein interface with helices VI-VII on the cytosolic side, containing the gap into which the lipid headgroup might enter as per our initial candidate mechanism for flip-flop. The free energy profiles for cholesterol were calculated later towards the interface with helices II-IV on both leaflets.

Both free energy profiles of POPC and cholesterol indicate a preferable position near rhodopsin towards which the free energy decreases. For POPC, near helices VI-VII, the free energy minimum occurs at approximately 2.5 nm from the protein center of mass. For cholesterol, the free energy minima can be found approximately at 1.5 – 2.0 nm from the protein center of mass on both leaflets. GPCRs such as rhodopsin or β_2 AR are also known to bind cholesterol at certain locations, where

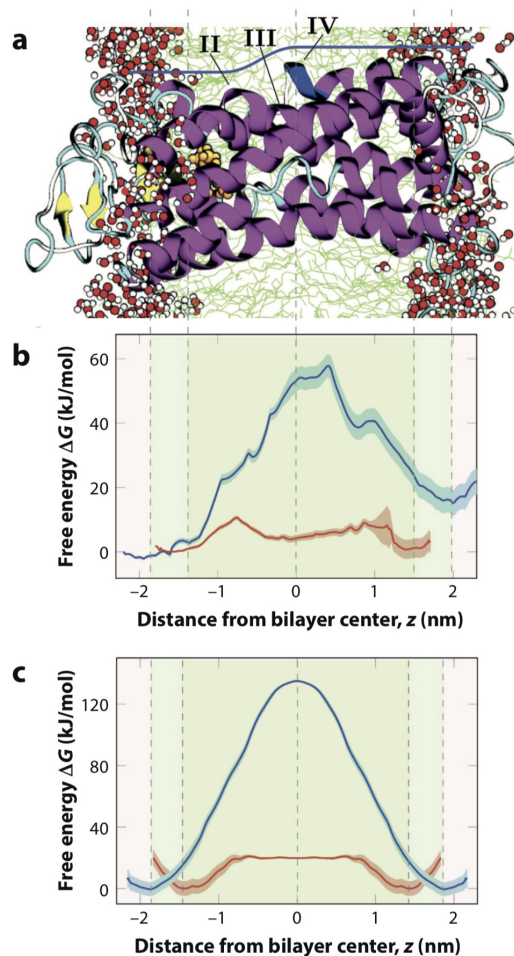


Figure 7.9 (a): Figure illustrating the lipid translocation path along the protein surface. Rhodopsin-mediated POPC flip-flop occurred along the transmembrane helices II, III and IV with the lipid headgroup following the blue line. Cholesterol translocation occurred along a similar path a little farther from the protein surface. (b): Free energy profiles of POPC (blue) and cholesterol (red) translocation along the rhodopsin-membrane interface. (c): Free energy profiles of POPC (blue) and cholesterol (red) in a protein-free membrane. The shaded areas represent statistical error. The reaction coordinate (z) refers to the distance between the lipid headgroup and the center of mass of the bilayer calculated along the membrane normal.

they induce packing of helices or modulate GPCR function [31], thus it is understandable that cholesterol is able to reach the protein surface with ease. The favorable distance for POPC may also be close enough to allow the protein to aid in the translocation process.

We analyzed the energetics behind the flip-flop process by calculating the inter-

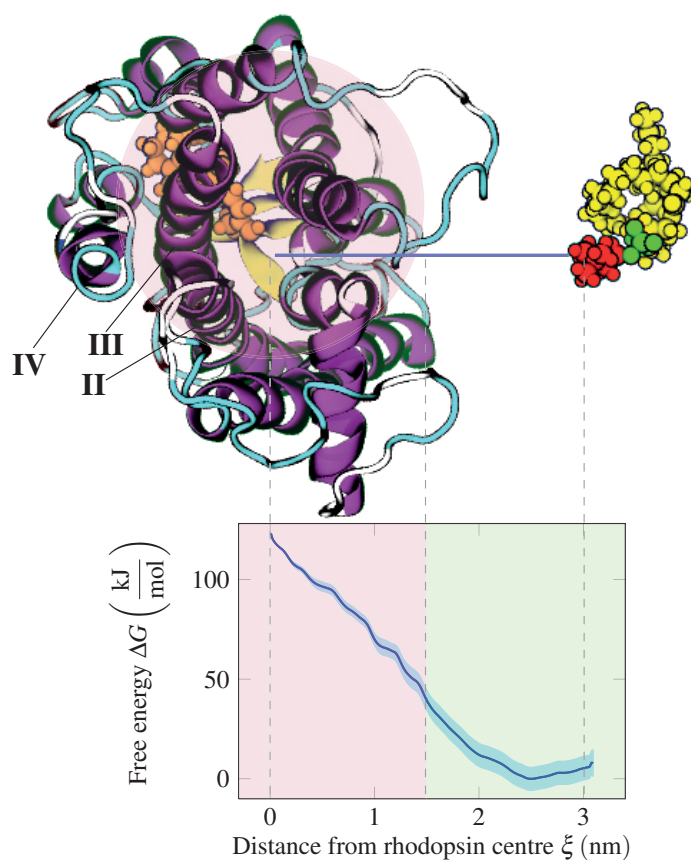


Figure 7.10 The free energy profile of POPC approaching rhodopsin on the cytosolic side of the bilayer. The green area indicates the area outside the protein surface and the red area the protein interior.

action energetics between the lipid headgroup and its surroundings. During cholesterol translocation, we observed high electrostatic interactions between the hydroxyl headgroup of cholesterol and certain charged amino acids of rhodopsin. During POPC translocation, these types of electrostatic interactions were heavily quenched by the surrounding water pore, but the interaction energies were still higher than for cholesterol. Both POPC and cholesterol showed the highest amount of electrostatic interaction energies with the rhodopsin upon entering and exiting the membrane interior. We also calculated the amount of hydrogen bonds the lipid undergoing flip-flop formed with its surroundings. POPC formed no hydrogen bonds with either the protein or the membrane in either system, but instead had an average of 4.63 and 5.16 hydrogen bonds with the surrounding water pore in the original and

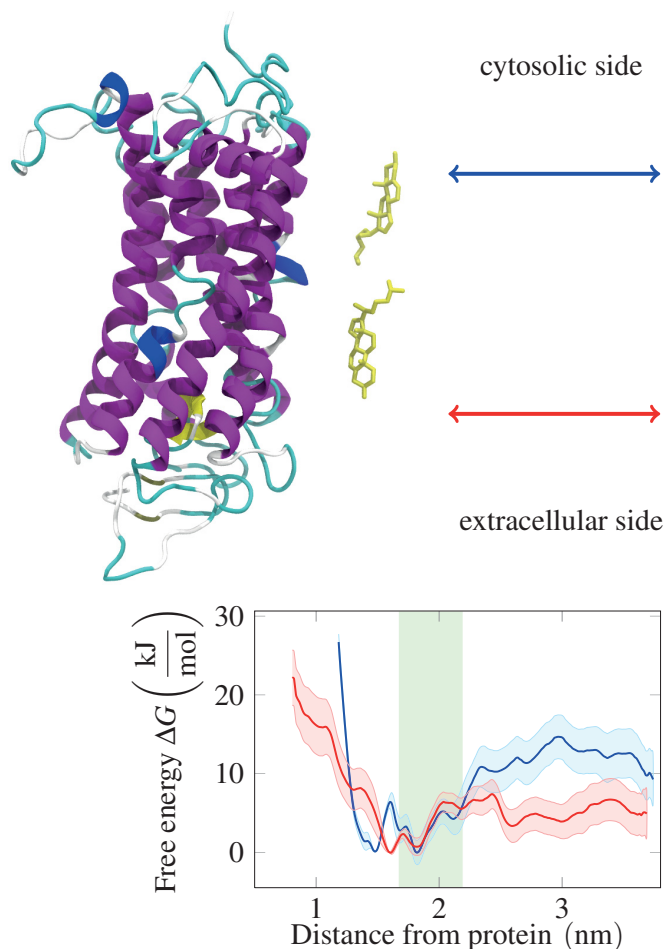


Figure 7.11 Free energy profiles of cholesterol approaching rhodopsin on the cytosolic side (blue) and on the extracellular side (red). The green area indicates the distance with the energy minima and the distance from protein when cholesterol flip-flop was initiated.

the protein-free system respectively. The hydroxyl group of cholesterol formed an average of 0.94 hydrogen bonds with the protein in the original system, and 0.50 hydrogen bonds with the membrane in the protein-free system. Again, we see the mitigating effect the water pore has on headgroup interactions with the surroundings.

We further analyzed the water pore by calculating the amount of water molecules in the vicinity of the POPC headgroup during flip-flop in both systems. Surprisingly, the number of water molecules was very similar with the protein-free system

having only a few more water molecules present in the pore. The difference is very small when compared to the free energy difference of the whole translocation process. It is clear that the presence of a water pore is necessary for flip–flop of lipids with larger headgroups, and its size is not significantly reduced in the presence of a scramblase. Therefore, it is likely that the protein disturbs the membrane in a way that a water pore can form more easily in the membrane interior. The protein may also stabilize the water pore enough that the translocating lipid has favorable conditions to flip–flop along the protein surface. This is one likely explanation for the large difference in the free energy profiles even though the flip–flop process is quite similar to when no protein is present. For lipids with small headgroups, such as cholesterol, when no water pore is formed, we believe membrane perturbations and electrostatic interactions with the protein surface to be the main facilitator of lipid translocation. Analysis was also performed on the membrane-perturbing effects of rhodopsin through examining the order parameters of nearby lipids and the thickness and the density of the membrane. However, the results showed no clear indication on how rhodopsin causes such effects.

We also performed further analysis on the free energy profiles of rhodopsin-mediated flip–flop by decomposing them into their enthalpic and entropic components according to the method described in Ref. [105], where similar analysis was done for cholesterol flip–flop in a DPPC bilayer. In order to achieve this, we performed two additional sets of umbrella sampling simulations for both POPC and cholesterol flip–flop at temperatures of 295 K and 325 K. The entropic contribution to the free energy profile at 310 K was calculated through Eq. (5.20) with $\Delta T = 15$ K, and the enthalpic contribution was then calculated through Eq. (5.17). The decomposed profiles are shown in Figure 7.12.

The decomposition of free energy for cholesterol flip–flop shows a clear separation into enthalpic and entropic components for the whole duration of the translocation process. The whole free energy profile consists of a positive enthalpic component ΔH increasing first to 50 kJ/mol and eventually to 120 kJ/mol upon entry into the membrane interior, and decreasing back to zero when exiting to the other leaflet. The entropic component $-T\Delta S$ mirrors the behavior of the enthalpic component remaining negative throughout the translocation process. A similar graph was obtained in a previous study for cholesterol flip–flop in a protein-free DPPC system in Ref. [105] and is another way of presenting why external energy needs to be given to

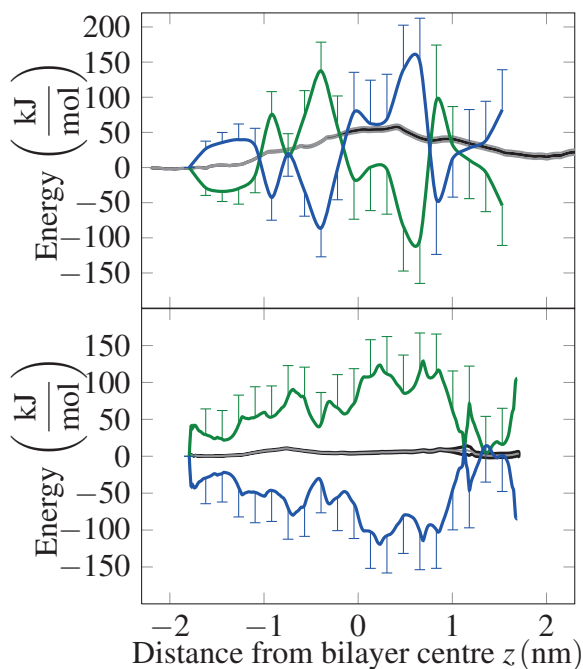


Figure 7.12 The enthalpic (green) and entropic (blue) contributions to the free energy profile of rhodopsin-mediated lipid flip-flop at $T = 310$ K (black). The profile for POPC (above) shows the flip-flop process being a sum of alternating enthalpic and entropic contributions. The translocation process for cholesterol (below) has a positive enthalpic contribution and a negative entropic contribution for the whole duration of the flip-flop.

a translocating cholesterol in the form of its internal energy ΔU (enthalpy increases), and why a lipid headgroup in the middle of a membrane will spontaneously exit into one leaflet (entropy increases).

The decomposed profile for POPC flip-flop consists of alternating enthalpic and entropic contributions increasing up to 200 kJ/mol near the middle of the membrane. It is difficult to discern a single reason behind this behavior, but there are many factors different between the translocation processes of both POPC and cholesterol, which had a clear separation in these two contributions. Firstly, the translocation of POPC headgroup is accompanied by a number of water molecules whereas no water was present during the flip-flop process of cholesterol (see Figure 7.8). Therefore, the cholesterol headgroup has to dissociate from water (in addition to the other polar headgroups) upon entry to the membrane interior, likely causing the initial increase in the enthalpic contribution, only interacting with water upon

entry into the other leaflet. For the POPC headgroup, no such dissociation is necessary and it is entirely possible that the initial entry into the membrane interior is entropy-driven requiring very little external energy due to the favorable hydrated environment created by the high number of interactions between the water pore and the protein. The free energy profile only clearly seems to increase near the 1.2 nm distance from the bilayer centre when the enthalpic and entropic contributions switch signs. It may be that the water pore that eventually follows the POPC headgroup dissociates with bulk water at this point causing the high enthalpic contribution. Secondly, the larger headgroup of POPC is more prone to interacting with its surroundings through electrostatics when compared to cholesterol. The transmembrane helices II-IV of rhodopsin host a number of charged amino acids and formation of new electrostatic interactions, along with breaking them, naturally has an effect on the entropic and enthalpic contributions. Even though the electrostatic interactions between POPC and rhodopsin were heavily quenched by the water pore, the water pore itself may orient itself towards these charged amino acids.

All in all, the scramblase research presented in this article treads on previously unexplored ground where the true mechanisms facilitating lipid flip-flop along a protein surface are not known. Therefore, some of the results obtained here still need more research including experimental collaboration in order to clarify the fundamental reasons for our observations. Multi-protein complexes or mutated amino acids along the translocation path could give deeper insight on the translocation mechanisms, but the computational costs often limit the research possibilities. For now, our results seem to indicate that rhodopsin-mediated flip-flop is non lipid-selective confirming earlier findings of rhodopsin acting as a potential scramblase. There seem to be multiple viable translocation paths, one of which is located on the protein surface near transmembrane helices II-IV. The exact translocation mechanisms are unknown, but they seem to involve a charge stabilized water pore on the protein surface giving polar lipid headgroups easy access into the membrane interior, and require no conformational changes in the protein.

8 CONCLUSIONS

In this Thesis, we presented new research on two proteins with vital functions in cellular life. Molecular dynamics simulations were shown to be a valuable companion to more traditional wet lab studies, giving additional insight on the phenomena occurring beyond visible range. Certain phenomena such as short-term fluctuations of the β barrel of P2 or the translocation paths of flip-flopping lipids can be extremely difficult to observe in real time, but are made relatively simple through computational modeling. Through our simulations, we produced atom-scale understanding on both the function of P2 and the scramblase properties of rhodopsin that can be expanded upon in later research.

On P2 and myelin sheath

In Papers I-III, we studied the myelin protein P2, one of the major components of peripheral myelin sheath. P2 is known to have a significant role in holding two apposing layers of myelin together along with its fatty acid binding properties. Past experiments have found the protein to have increased activity when certain amino acid residues are mutated, leading to changes in its lipid stacking abilities [11]. Mutated P2 has also been identified as a major contribuent in Charcot-Marie-Tooth disease, one of the main demyelinating diseases of the peripheral myelin sheath [74, 76]. However, structural information on the increased activity, namely on the mechanisms of the β -barrel opening has been lacking.

Our studies involved introducing a molecular dynamics approach on the properties of point mutated P2. To our knowledge, P2 had not been extensively studied with MD before. Also, complementing our simulation studies with the experimental research led by the Kursula group produced wide insight on the properties of various P2 point mutants. As the focal point of all three publications was the activity and function of the protein itself, the simulations were performed in a simple solvent

box in the absence of a lipid bilayer. However, simulations investigating P2 binding to a membrane with the lipid composition of a myelin bilayer, and its activity on the membrane surface are work in progress and should be published shortly. As the myelin sheath involves two lipid bilayers on both sides of the protein, molecular dynamics simulations on systems with two apposing bilayers could be performed to investigate the membrane stacking capabilities of P2 and its point mutated variants.

Through our research we discovered a mechanism by which the P2 barrel structure is opened through unflapping of two adjacent β -strands. This mechanism has long since been suggested [169], but has not been shown to occur before. The protein opened widely enough to allow a small ligand, such as the palmitate chain embedded in the crystal structure, or possibly a cholesterol molecule to fit through to the protein interior. Spontaneous escape of the bound ligand was not observed, and the presence of a membrane (or two) might be necessary for it to occur. The opened protein structures can be used later as starting points for a set of umbrella sampling simulations measuring the free energy barrier of ligand escape. Again, differences are likely to occur between the point mutated variants.

On rhodopsin and lipid flip–flop

Molecular dynamics simulations really excel in studies like the ones performed in Paper IV. Flippases and scramblases have been studied for many decades now, but the translocation mechanisms have remained elusive due to the fact that real-time tracking of the movement of single lipids in a bilayer is not possible through a microscope. Experimental studies have verified a number of potential lipid translocating proteins by using labeled lipids in artificially created vesicles. By inserting these marked lipids on only one leaflet of the bilayer, and observing their general progress to the other side, it has been shown that certain transmembrane proteins – such as opsins or β_1 AR – greatly increase the rate of lipid flip–flop [12, 174]. Recent improvements in the field of protein crystallization have also made increasing numbers of crystal structures of transmembrane proteins available, which naturally aids in their research.

Another factor relating to the slow progress in the study of the translocation mechanisms of potential scramblases are the computational resources required for such simulations. For a model of a studied system to be accurate enough – that is, to

represent real life as closely as possible – it must contain hundreds of lipids and be solvated with tens of thousands of water molecules, all of which is computationally extremely heavy to simulate at an atomistic detail. Coarse-grained models would lower the computational cost by quite a bit, but the loss of atomistic detail such as atom-atom interactions between lipid and protein can create significant artifacts in the simulation data. Still, lipid flip-flops in protein-free systems have been studied at great depth and have yielded accurate results even with coarse-grained models [105, 175]. Only in the last decade have computational capacities available to research groups increased and the computing algorithms evolved to such a level that over microsecond simulations are feasible for larger systems. As a related subject, the force fields used to describe molecular interactions have also evolved greatly, resulting in more accurate representations of systems containing proteins and lipids. Force field development has also allowed these interactions to be calculated in a more rapid fashion.

The aforementioned improvements in the field have resulted in several successful studies on the scrambling mechanisms of opsin and β_2 AR in the past few years. Our studies, published in Paper IV, showed that the surface of rhodopsin provides favorable conditions for non-selective lipid translocation across the membrane interior, greatly increasing the rate of flip-flop. Similar results were also observed for β_2 AR in our yet unpublished publication. Another simulation study by Morra et al. explored a different translocation path for opsin, where the lipid headgroup translocated between two transmembrane helices [50]. Their results, combined with ours, confirm that lipid translocation aided by opsins is not confined to a single path – a result that can possibly be generalized to other GPCRs as well.

As new crystal structures of GPCRs are obtained in the future, similar simulation studies can be performed on them in order to find out whether the scramblase activities truly are universal properties of GPCRs. The simplicity of creating models for molecular dynamics simulations when accurate structures for proteins and lipids are available, combined with the atomistic accuracy of the results, make simulations a highly desirable method for studying small-scale biological phenomena. Combined with constant improvements in computational methods, the next decades are definitely going to increase the viability and credibility of molecular simulation studies in biological sciences.

BIBLIOGRAPHY

- [1] **Spence, M. and Johnson, I.**, *The molecular probes handbook: a guide to fluorescent probes and labeling technologies*. Life Technologies Corporation, Paisley, UK. 2010, 1060 pp.
- [2] **Devaux, P.F.**, Static and dynamic lipid asymmetry in cell membranes. *Biochemistry*, 30(5): 1163–1173. 1991.
- [3] **Hengartner, M.O.**, The biochemistry of apoptosis. *Nature*, 407(6805): 770–776. 2000.
- [4] **Sanyal, S. and Menon, A.K.**, Flipping lipids: why an' what's the reason for? *ACS Chemical Biology*, 4(11): 895–909. 2009.
- [5] **Reggio, P.H.**, GPCRs moonlighting as scramblases: mechanism revealed. *Structure*, 26(2): 184–186. 2018.
- [6] **Majava, V., Polverini, E., Mazzini, A., Nanekar, R., Knoll, W., Peters, J., Natali, F., Baumgärtel, P., Kursula, I., and Kursula, P.**, Structural and functional characterization of human peripheral nervous system myelin protein P2. *PLoS One*, 5(4): e10300. 2010.
- [7] **Rossor, A.M., Tomaselli, P.J., and Reilly, M.M.**, Recent advances in the genetic neuropathies. *Current Opinion in Neurology*, 29(5): 537–548. 2016.
- [8] **Love, S.**, Demyelinating diseases. *Journal of Clinical Pathology*, 59(11): 1151–1159. 2006.
- [9] **Simons, M. and Trotter, J.**, Wrapping it up: the cell biology of myelination. *Current Opinion in Neurobiology*, 17(5): 533–540. 2007.

- [10] **Rossor, A.M., Polke, J.M., Houlden, H., and Reilly, M.M.**, Clinical implications of genetic advances in Charcot–Marie–Tooth disease. *Nature Reviews Neurology*, 9(10): 562–571. 2013.
- [11] **Ruskamo, S., Yadav, R.P., Sharma, S., Lehtimäki, M., Laulumaa, S., Aggarwal, S., Simons, M., Bürck, J., Ulrich, A.S., Juffer, A.H., et al.**, Atomic resolution view into the structure–function relationships of the human myelin peripheral membrane protein P2. *Acta Crystallographica Section D: Biological Crystallography*, 70(1): 165–176. 2014.
- [12] **Menon, I., Huber, T., Sanyal, S., Banerjee, S., Barré, P., Canis, S., Warren, J.D., Hwa, J., Sakmar, T.P., and Menon, A.K.**, Opsin is a phospholipid flippase. *Current Biology*, 21(2): 149–153. 2011.
- [13] **Sahu, S.K., Gummadi, S.N., Manoj, N., and Aradhyam, G.K.**, Phospholipid scramblases: an overview. *Archives of Biochemistry and Biophysics*, 462(1): 103–114. 2007.
- [14] **Phillips, R., Ursell, T., Wiggins, P., and Sens, P.**, Emerging roles for lipids in shaping membrane-protein function. *Nature*, 459(7245): 379–385. 2009.
- [15] **Suzuki, J., Denning, D.P., Imanishi, E., Horvitz, H.R., and Nagata, S.**, Xk-related protein 8 and CED-8 promote phosphatidylserine exposure in apoptotic cells. *Science*, 341(6144): 403–406. 2013.
- [16] **Brunner, J.D., Lim, N.K., Schenck, S., Duerst, A., and Dutzler, R.**, X-ray structure of a calcium-activated TMEM16 lipid scramblase. *Nature*, 516(7530): 207–212. 2014.
- [17] **Okada, T., Sugihara, M., Bondar, A.N., Elstner, M., Entel, P., and Buss, V.**, The retinal conformation and its environment in rhodopsin in light of a new 2.2 Å crystal structure. *Journal of Molecular Biology*, 342(2): 571–583. 2004.
- [18] **Hauser, A.S., Attwood, M.M., Rask-Andersen, M., Schiöth, H.B., and Gloriam, D.E.**, Trends in GPCR drug discovery: new agents, targets and indications. *Nature Reviews Drug Discovery*, 16(12): 829–842. 2017.

- [19] **Alberts, B., Bray, D., Lewis, J., Raff, M., Roberts, K., and Watson, J.,** *Molecular biology of the cell*. Garland Science. 2008, 1616 pp.
- [20] **Garrett, R. and Grisham, C.,** *Biochemistry*. Belmont, CA: Brooks/Cole Cengage Learning, p. 1169. 2010.
- [21] **Hart, H., Hadad, C.M., Craine, L.E., and Hart, D.J.,** *Organic chemistry: a short course*. Cengage Learning. 2011, 608 pp.
- [22] **Tymoczko, J.L., Berg, J.M., and Stryer, L.,** *Biochemistry: a short course*. Macmillan. 2011, 800 pp.
- [23] **OpenStax Content,** Structure and function of plasma membranes. <https://tophat.com/marketplace/science-&-math/biology/textbooks/oer-openstax-biology-openstax-content/79/4108>. 2016, [Online; accessed 13-May-2019].
- [24] **Fernandis, A.Z. and Wenk, M.R.,** Membrane lipids as signaling molecules. *Current Opinion in Lipidology*, 18(2): 121–128. 2007.
- [25] **University of California Davis,** Glycolipids. https://phys.libretexts.org/Courses/University_of_California_Davis/UCD%3A_Biophysics_241_-_Membrane_Biology/Lipids_Types/Glycolipids. 2018, [Online; accessed 16-March-2019].
- [26] **Humphrey, W., Dalke, A., and Schulten, K.,** VMD: visual molecular dynamics. *Journal of Molecular Graphics*, 14(1): 33–38. 1996.
- [27] **Stone, J.E.,** *An efficient library for parallel ray tracing and animation*. Citeseer. 1998, 79 pp.
- [28] **Stillwell, W.,** *An introduction to biological membranes: composition, structure and function*. Elsevier. 2016, 590 pp.
- [29] **De Almeida, R.F., Fedorov, A., and Prieto, M.,** Sphingomyelin/phosphatidylcholine/cholesterol phase diagram: boundaries and composition of lipid rafts. *Biophysical Journal*, 85(4): 2406–2416. 2003.
- [30] **Simons, K. and Ikonen, E.,** Functional rafts in cell membranes. *Nature*, 387(6633): 569–572. 1997.

- [31] **Hanson, M.A., Cherezov, V., Griffith, M.T., Roth, C.B., Jaakola, V.P., Chien, E.Y., Velasquez, J., Kuhn, P., and Stevens, R.C.,** A specific cholesterol binding site is established by the 2.8 Å structure of the human β 2-adrenergic receptor. *Structure*, 16(6): 897–905. 2008.
- [32] **Chini, B. and Parenti, M.,** G-protein-coupled receptors, cholesterol and palmitoylation: facts about fats. *Journal of Molecular Endocrinology*, 42(5): 371–379. 2009.
- [33] **Bruckner, R., Mansy, S., Ricardo, A., Mahadevan, L., and Szostak, J.,** Flip-flop-induced relaxation of bending energy: implications for membrane remodeling. *Biophysical Journal*, 97(12): 3113–3122. 2009.
- [34] **Cho, W. and Stahelin, R.V.,** Membrane-protein interactions in cell signaling and membrane trafficking. *Annual Review of Biophysics and Biomolecular Structures*, 34: 119–151. 2005.
- [35] **Vergara, C., Latorre, R., Marrion, N.V., and Adelman, J.P.,** Calcium-activated potassium channels. *Current Opinion in Neurobiology*, 8(3): 321–329. 1998.
- [36] **Xia, X.M., Fakler, B., Rivard, A., Wayman, G., Johnson-Pais, T., Keen, J., Ishii, T., Hirschberg, B., Bond, C., Lutsenko, S., et al.,** Mechanism of calcium gating in small-conductance calcium-activated potassium channels. *Nature*, 395(6701): 503–507. 1998.
- [37] **Rosenbaum, D.M., Rasmussen, S.G., and Kobilka, B.K.,** The structure and function of G-protein-coupled receptors. *Nature*, 459(7245): 356–363. 2009.
- [38] **Maurice, P., Guillaume, J.L., Benleulmi-Chaachoua, A., Daulat, A.M., Kamal, M., and Jockers, R.,** GPCR-interacting proteins, major players of GPCR function. *Advances in Pharmacology*, 62: 349–380. 2011.
- [39] **Litman, B.J. and Mitchell, D.C.,** Rhodopsin structure and function. *Biomembranes: a multi-volume treatise*, 2: 1–32. 1996.
- [40] **Betke, K.M., Wells, C.A., and Hamm, H.E.,** GPCR mediated regulation of synaptic transmission. *Progress in Neurobiology*, 96(3): 304–321. 2012.

- [41] Allen, J.A., Halverson-Tamboli, R.A., and Rasenick, M.M., Lipid raft microdomains and neurotransmitter signalling. *Nature Reviews Neuroscience*, 8(2): 128–140. 2007.
- [42] Missale, C., Nash, S.R., Robinson, S.W., Jaber, M., and Caron, M.G., Dopamine receptors: from structure to function. *Physiological Reviews*, 78(1): 189–225. 1998.
- [43] Overington, J.P., Al-Lazikani, B., and Hopkins, A.L., How many drug targets are there? *Nature Reviews Drug discovery*, 5(12): 993–996. 2006.
- [44] Goren, M.A., Morizumi, T., Menon, I., Joseph, J.S., Dittman, J.S., Cherezov, V., Stevens, R.C., Ernst, O.P., and Menon, A.K., Constitutive phospholipid scramblase activity of a G protein-coupled receptor. *Nature Communications*, 5: 5115. 2014.
- [45] Ségurel, L. and Bon, C., On the evolution of lactase persistence in humans. *Annual Review of Genomics and Human Genetics*, 18: 297–319. 2017.
- [46] Serjeant, G.R. and Serjeant, B.E., *Sickle cell disease*, volume 3. Oxford university press Oxford. 1992, 631 pp.
- [47] Williams, T.N., Mwangi, T.W., Roberts, D.J., Alexander, N.D., Weatherall, D.J., Wambua, S., Kortok, M., Snow, R.W., and Marsh, K., An immune basis for malaria protection by the sickle cell trait. *PLoS Medicine*, 2(5): e128. 2005.
- [48] Piel, F.B., Patil, A.P., Howes, R.E., Nyangiri, O.A., Gething, P.W., Williams, T.N., Weatherall, D.J., and Hay, S.I., Global distribution of the sickle cell gene and geographical confirmation of the malaria hypothesis. *Nature Communications*, 1: 104. 2010.
- [49] Hurley, D.M., Accili, D., Stratakis, C., Karl, M., Vamvakopoulos, N., Rorer, E., Constantine, K., Taylor, S., and Chrousos, G., Point mutation causing a single amino acid substitution in the hormone binding domain of the glucocorticoid receptor in familial glucocorticoid resistance. *The Journal of Clinical Investigation*, 87(2): 680–686. 1991.

- [50] Morra, G., Razavi, A.M., Pandey, K., Weinstein, H., Menon, A.K., and Khelashvili, G., Mechanisms of lipid scrambling by the G protein-coupled receptor opsin. *Structure*, 26(2): 356–367. 2018.
- [51] Laulumaa, S., Nieminen, T., Lehtimäki, M., Aggarwal, S., Simons, M., Koza, M.M., Vattulainen, I., Kursula, P., and Natali, F., Dynamics of the peripheral membrane protein P2 from human myelin measured by neutron scattering – A comparison between wild-type protein and a hinge mutant. *PLoS One*, 10(6): e0128954. 2015.
- [52] Marianayagam, N.J., Sunde, M., and Matthews, J.M., The power of two: protein dimerization in biology. *Trends in Biochemical Sciences*, 29(11): 618–625. 2004.
- [53] Pandey, K., Ploier, B., Goren, M.A., Levitz, J., Khelashvili, G., and Menon, A.K., An engineered opsin monomer scrambles phospholipids. *Scientific Reports*, 7(1): 16741. 2017.
- [54] Wong, R.S., Apoptosis in cancer: from pathogenesis to treatment. *Journal of Experimental & Clinical Cancer Research*, 30(1): 87. 2011.
- [55] Patestas, M.A. and Gartner, L.P., *A textbook of neuroanatomy*. John Wiley & Sons. 2016, 544 pp.
- [56] Amerman, E.C., *Human anatomy & physiology*. Pearson Boston. 2016, 1092 pp.
- [57] **Wikimedia Commons**, Neuron. <https://en.wikipedia.org/wiki/Neuron>. 2009, [Online; accessed 13-May-2019].
- [58] Hewstone, M.E., Fincham, F.D., Foster, J.E., Anderson, M., Augoustinos, M., Davila, J., Durkin, K., Fritz, C., Hall, G., Harris, J., et al., *Psychology*. Blackwell Publishing. 2005, 576 pp.
- [59] Snipes, G.J. and Suter, U., Molecular anatomy and genetics of myelin proteins in the peripheral nervous system. *Journal of Anatomy*, 186(3): 483–494. 1995.
- [60] Salzer, J. and Zalc, B., Myelination. *Current Biology*, 26(20): R971–R975. 2016.

- [61] **Snaidero, N. and Simons, M.**, Myelination at a glance. *Journal of Cell Science*, 127(14): 2999–3004. 2014.
- [62] **Snaidero, N., Möbius, W., Czopka, T., Hekking, L.H., Mathisen, C., Verkleij, D., Goebbels, S., Edgar, J., Merkler, D., Lyons, D.A., et al.**, Myelin membrane wrapping of CNS axons by PI (3, 4, 5) P3-dependent polarized growth at the inner tongue. *Cell*, 156(1): 277–290. 2014.
- [63] **Biology Dictionary**, Myelin sheath. <https://biologydictionary.net/myelin-sheath/>. 2015, [Online; accessed 13-May-2019].
- [64] **Waxman, S. and Bennett, M.V.**, Relative conduction velocities of small myelinated and non-myelinated fibres in the central nervous system. *Nature New Biology*, 238(85): 217–219. 1972.
- [65] **Jessen, K. and Mirsky, R.**, The repair Schwann cell and its function in regenerating nerves. *The Journal of Physiology*, 594(13): 3521–3531. 2016.
- [66] **Niemi, J.P., DeFrancesco-Lisowitz, A., Roldán-Hernández, L., Lindborg, J.A., Mandell, D., and Zigmond, R.E.**, A critical role for macrophages near axotomized neuronal cell bodies in stimulating nerve regeneration. *Journal of Neuroscience*, 33(41): 16236–16248. 2013.
- [67] **Gomez-Sanchez, J.A., Carty, L., Iruarrizaga-Lejarreta, M., Palomoirigoyen, M., Varela-Rey, M., Griffith, M., Hantke, J., Macias-Camara, N., Azkargorta, M., Aurrekoetxea, I., et al.**, Schwann cell autophagy, myelinophagy, initiates myelin clearance from injured nerves. *Journal of Cell Biology*, 210(1): 153–168. 2015.
- [68] **Greenfield, S., Brostoff, S., Eylar, E., and Morell, P.**, Protein composition of myelin of the peripheral nervous system. *Journal of Neurochemistry*, 20(4): 1207–1216. 1973.
- [69] **Trapp, B.D., Dubois-Dalcq, M., and Quarles, R.H.**, Ultrastructural localization of P2 protein in actively myelinating rat Schwann cells. *Journal of Neurochemistry*, 43(4): 944–948. 1984.
- [70] **Zenker, J., Stettner, M., Ruskamo, S., Domènech-Estévez, E., Baloui, H., Médard, J.J., Verheijen, M.H., Brouwers, J.F., Kursula, P., Kieseier,**

- B.C., et al.**, A role of peripheral myelin protein 2 in lipid homeostasis of myelinating Schwann cells. *Glia*, 62(9): 1502–1512. 2014.
- [71] **Friedman, R., Nachliel, E., and Gutman, M.**, Fatty acid binding proteins: same structure but different binding mechanisms? Molecular dynamics simulations of intestinal fatty acid binding protein. *Biophysical Journal*, 90(5): 1535–1545. 2006.
- [72] **Sedzik, J., Blaurock, A., and Hoechli, M.**, Reconstituted P2/myelin-lipid multilayers. *Journal of Neurochemistry*, 45(3): 844–852. 1985.
- [73] **Suresh, S., Wang, C., Nanekar, R., Kursula, P., and Edwardson, J.M.**, Myelin basic protein and myelin protein 2 act synergistically to cause stacking of lipid bilayers. *Biochemistry*, 49(16): 3456–3463. 2010.
- [74] **Gonzaga-Jauregui, C., Harel, T., Gambin, T., Kousi, M., Griffin, L.B., Francescato, L., Ozes, B., Karaca, E., Jhangiani, S.N., Bainbridge, M.N., et al.**, Exome sequence analysis suggests that genetic burden contributes to phenotypic variability and complex neuropathy. *Cell Reports*, 12(7): 1169–1183. 2015.
- [75] **Hong, Y.B., Joo, J., Hyun, Y.S., Kwak, G., Choi, Y.R., Yeo, H.K., Jwa, D.H., Kim, E.J., Mo, W.M., Nam, S.H., et al.**, A mutation in PMP2 causes dominant demyelinating charcot-marie-tooth neuropathy. *PLoS Genetics*, 12(2): e1005829. 2016.
- [76] **Motley, W.W., Palaima, P., Yum, S.W., Gonzalez, M.A., Tao, F., Wanschitz, J.V., Strickland, A.V., Löscher, W.N., De Vriendt, E., Koppi, S., et al.**, De novo PMP2 mutations in families with type 1 Charcot–Marie–Tooth disease. *Brain*, 139(6): 1649–1656. 2016.
- [77] **Lampert, P.W.**, Autoimmune and virus-induced demyelinating diseases. A review. *The American Journal of Pathology*, 91(1): 176. 1978.
- [78] **Ross, C.A. and Poirier, M.A.**, Protein aggregation and neurodegenerative disease. *Nature Medicine*, 10(7s): S10–S17. 2004.
- [79] **Mosby, I.**, *Mosby's dictionary of medicine, nursing and health professions*. Elsevier. 2013, 2064 pp.

- [80] **Compston, A. and Coles, A.**, Multiple sclerosis. *The Lancet*, 372(9648): 1502–1517. 2008.
- [81] **Goldenberg, M.M.**, Multiple sclerosis review. *Pharmacy and Therapeutics*, 37(3): 175–184. 2012.
- [82] **Tullman, M.J.**, Overview of the epidemiology, diagnosis, and disease progression associated with multiple sclerosis. *American Journal of Managed Care*, 19(2): S15–S20. 2013.
- [83] **Bartzokis, G.**, Age-related myelin breakdown: a developmental model of cognitive decline and Alzheimer’s disease. *Neurobiology of Aging*, 25(1): 5–18. 2004.
- [84] **Mudher, A. and Lovestone, S.**, Alzheimer’s disease—do tauists and baptists finally shake hands? *Trends in Neurosciences*, 25(1): 22–26. 2002.
- [85] **Goedert, M. and Spillantini, M.G.**, A century of Alzheimer’s disease. *Science*, 314(5800): 777–781. 2006.
- [86] **Solfrizzi, V., Panza, F., Frisardi, V., Seripa, D., Logroscino, G., Imbimbo, B.P., and Pilotto, A.**, Diet and Alzheimer’s disease risk factors or prevention: the current evidence. *Expert Review of Neurotherapeutics*, 11(5): 677–708. 2011.
- [87] **Barnard, N.D., Bush, A.I., Ceccarelli, A., Cooper, J., de Jager, C.A., Erickson, K.I., Fraser, G., Kesler, S., Levin, S.M., Lucey, B., et al.**, Dietary and lifestyle guidelines for the prevention of Alzheimer’s disease. *Neurobiology of Aging*, 35: S74–S78. 2014.
- [88] **Van Den Berg, B., Walgaard, C., Drenthen, J., Fokke, C., Jacobs, B.C., and Van Doorn, P.A.**, Guillain–Barré syndrome: pathogenesis, diagnosis, treatment and prognosis. *Nature Reviews Neurology*, 10(8): 469–482. 2014.
- [89] **National Institute of Neurological Disorders and Stroke**, Guillain–Barré syndrome fact sheet. <https://www.ninds.nih.gov/Disorders/Patient-Caregiver-Education/Fact-Sheets/Guillain-Barre-Syndrome-Fact-Sheet>. 2018, [Online; accessed 1-March-2019].

- [90] **Murphy, S.M., Laura, M., Fawcett, K., Pandraud, A., Liu, Y.T., Davidson, G.L., Rossor, A.M., Polke, J.M., Castleman, V., Manji, H., et al.**, Charcot–Marie–Tooth disease: frequency of genetic subtypes and guidelines for genetic testing. *Journal of Neurology, Neurosurgery, and Psychiatry*, 83(7): 706–710. 2012.
- [91] **Ruskamo, S., Nieminen, T., Kristiansen, C.K., Vatne, G.H., Baumann, A., Hallin, E.I., Raasakka, A., Joensuu, P., Bergmann, U., Vattulainen, I., et al.**, Molecular mechanisms of Charcot-Marie-Tooth neuropathy linked to mutations in human myelin protein P2. *Scientific Reports*, 7(1): 6510. 2017.
- [92] **Bird, T.D. and Kraft, G.H.**, Charcot-Marie-Tooth disease: Data for genetic counseling relating age to risk. *Clinical Genetics*, 14(1): 43–49. 1978.
- [93] **Pareyson, D. and Marchesi, C.**, Diagnosis, natural history, and management of Charcot–Marie–Tooth disease. *The Lancet Neurology*, 8(7): 654–667. 2009.
- [94] **Roa, B.B., Garcia, C.A., Suter, U., Kulpa, D.A., Wise, C.A., Mueller, J., Welcher, A.A., Snipes, G.J., Shooter, E.M., Patel, P.I., et al.**, Charcot-Marie-Tooth disease type 1A–Association with a spontaneous point mutation in the PMP22 gene. *New England Journal of Medicine*, 329(2): 96–101. 1993.
- [95] **Houlden, H. and Reilly, M.M.**, Molecular genetics of autosomal-dominant demyelinating Charcot-Marie-Tooth disease. *Neuromolecular Medicine*, 8(1-2): 43–62. 2006.
- [96] **Schröder, J.M.**, Neuropathology of Charcot-Marie-Tooth and related disorders. *Neuromolecular Medicine*, 8(1-2): 23–42. 2006.
- [97] **Fagone, P. and Jackowski, S.**, Membrane phospholipid synthesis and endoplasmic reticulum function. *Journal of Lipid Research*, 50: S311–S316. 2009.
- [98] **Van Meer, G., Voelker, D.R., and Feigenson, G.W.**, Membrane lipids: where they are and how they behave. *Nature Reviews Molecular Cell Biology*, 9(2): 112–124. 2008.
- [99] **van Meer, G.**, Dynamic transbilayer lipid asymmetry. *Cold Spring Harbor Perspectives in Biology*, 3(5): a004671. 2011.

- [100] **Kobayashi, T. and Menon, A.K.**, Transbilayer lipid asymmetry. *Current Biology*, 28(8): R386–R391. 2018.
- [101] **McMahon, H.T. and Boucrot, E.**, Membrane curvature at a glance. *Journal of Cell Science*, 128(6): 1065–1070. 2015.
- [102] **Bratton, D.L., Fadok, V.A., Richter, D.A., Kailey, J.M., Guthrie, L.A., and Henson, P.M.**, Appearance of phosphatidylserine on apoptotic cells requires calcium-mediated nonspecific flip-flop and is enhanced by loss of the aminophospholipid translocase. *Journal of Biological Chemistry*, 272(42): 26159–26165. 1997.
- [103] **Singer, S.J. and Nicolson, G.L.**, The fluid mosaic model of the structure of cell membranes. *Science*, 175(4023): 720–731. 1972.
- [104] **Sapay, N., Bennett, W.D., and Tieleman, D.P.**, Thermodynamics of flip-flop and desorption for a systematic series of phosphatidylcholine lipids. *Soft Matter*, 5(17): 3295–3302. 2009.
- [105] **Bennett, W.D., MacCallum, J.L., Hinner, M.J., Marrink, S.J., and Tieleman, D.P.**, Molecular view of cholesterol flip-flop and chemical potential in different membrane environments. *Journal of the American Chemical Society*, 131(35): 12714–12720. 2009.
- [106] **Homan, R. and Pownall, H.J.**, Transbilayer diffusion of phospholipids: dependence on headgroup structure and acyl chain length. *Biochimica et Biophysica Acta (BBA)-Biomembranes*, 938(2): 155–166. 1988.
- [107] **John, K., Schreiber, S., Kubelt, J., Herrmann, A., and Müller, P.**, Transbilayer movement of phospholipids at the main phase transition of lipid membranes: implications for rapid flip-flop in biological membranes. *Biophysical Journal*, 83(6): 3315–3323. 2002.
- [108] **Liu, J., Brown, K.L., and Conboy, J.C.**, The effect of cholesterol on the intrinsic rate of lipid flip-flop as measured by sum-frequency vibrational spectroscopy. *Faraday Discussions*, 161: 45–61. 2013.
- [109] **Bennett, W.D., Sapay, N., and Tieleman, D.P.**, Atomistic simulations of pore formation and closure in lipid bilayers. *Biophysical Journal*, 106(1): 210–219. 2014.

- [110] **Koshiyama, K., Yano, T., and Kodama, T.**, Self-organization of a stable pore structure in a phospholipid bilayer. *Physical Review Letters*, 105(1): 018105. 2010.
- [111] **Lee, M.T., Hung, W.C., Chen, F.Y., and Huang, H.W.**, Mechanism and kinetics of pore formation in membranes by water-soluble amphipathic peptides. *Proceedings of the National Academy of Sciences*, 105(13): 5087–5092. 2008.
- [112] **Tieleman, D.P., Leontiadou, H., Mark, A.E., and Marrink, S.J.**, Simulation of pore formation in lipid bilayers by mechanical stress and electric fields. *Journal of the American Chemical Society*, 125(21): 6382–6383. 2003.
- [113] **Betteridge, D.J.**, What is oxidative stress? *Metabolism*, 49(2): 3–8. 2000.
- [114] **Volinsky, R., Cwiklik, L., Jurkiewicz, P., Hof, M., Jungwirth, P., and Kinnunen, P.K.**, Oxidized phosphatidylcholines facilitate phospholipid flip-flop in liposomes. *Biophysical Journal*, 101(6): 1376–1384. 2011.
- [115] **Razzokov, J., Yusupov, M., Vanuytsel, S., Neyts, E.C., and Bogaerts, A.**, Phosphatidylserine flip-flop induced by oxidation of the plasma membrane: a better insight by atomic scale modeling. *Plasma Processes and Polymers*, 14(10): 1700013. 2017.
- [116] **Barnham, K.J., Masters, C.L., and Bush, A.I.**, Neurodegenerative diseases and oxidative stress. *Nature Reviews Drug discovery*, 3(3): 205–214. 2004.
- [117] **Kannan, K. and Jain, S.K.**, Oxidative stress and apoptosis. *Pathophysiology*, 7(3): 153–163. 2000.
- [118] **Devaux, P.F., Herrmann, A., Ohlwein, N., and Kozlov, M.M.**, How lipid flippases can modulate membrane structure. *Biochimica et Biophysica Acta (BBA)-Biomembranes*, 1778(7-8): 1591–1600. 2008.
- [119] **Palmgren, M.G. and Nissen, P.**, P-type ATPases. *Annual Review of Biophysics*, 40: 243–266. 2011.
- [120] **Tang, X., Halleck, M.S., Schlegel, R.A., and Williamson, P.**, A subfamily of P-type ATPases with aminophospholipid transporting activity. *Science*, 272(5267): 1495–1497. 1996.

- [121] **Folmer, D.E., Elferink, R.P.O., and Paulusma, C.C.**, P4 ATPases-lipid flippases and their role in disease. *Biochimica et Biophysica Acta (BBA)-Molecular and Cell Biology of Lipids*, 1791(7): 628–635. 2009.
- [122] **van Meer, G., Halter, D., Sprong, H., Somerharju, P., and Egmond, M.R.**, ABC lipid transporters: extruders, flippases, or floppless activators? *FEBS Letters*, 580(4): 1171–1177. 2006.
- [123] **Nieminen, T.**, *A study of rhodopsin as a potential phospholipid scramblase*. Master's thesis, Tampere University of Technology. 2012.
- [124] **Bevers, E.M. and Williamson, P.L.**, Phospholipid scramblase: an update. *FEBS Letters*, 584(13): 2724–2730. 2010.
- [125] **Orrenius, S., Zhivotovsky, B., and Nicotera, P.**, Calcium: Regulation of cell death: the calcium–apoptosis link. *Nature Reviews Molecular cell biology*, 4(7): 552–565. 2003.
- [126] **Williamson, P.**, Phospholipid scramblases. *Lipid Insights*, 8: 41–44. 2015.
- [127] **Malvezzi, M., Andra, K.K., Pandey, K., Lee, B.C., Falzone, M.E., Brown, A., Iqbal, R., Menon, A.K., and Accardi, A.**, Out-of-the-groove transport of lipids by TMEM16 and GPCR scramblases. *Proceedings of the National Academy of Sciences*, 115(30): E7033–E7042. 2018.
- [128] **Kol, M.A., de Kroon, A.I., Killian, J.A., and de Kruijff, B.**, Transbilayer movement of phospholipids in biogenic membranes. *Biochemistry*, 43(10): 2673–2681. 2004.
- [129] **Palczewski, K., Kumasaka, T., Hori, T., Behnke, C.A., Motoshima, H., Fox, B.A., Le Trong, I., Teller, D.C., Okada, T., Stenkamp, R.E., et al.**, Crystal structure of rhodopsin: a G protein-coupled receptor. *Science*, 289(5480): 739–745. 2000.
- [130] **Olausson, B.E., Grossfield, A., Pitman, M.C., Brown, M.F., Feller, S.E., and Vogel, A.**, Molecular dynamics simulations reveal specific interactions of post-translational palmitoyl modifications with rhodopsin in membranes. *Journal of the American Chemical Society*, 134(9): 4324–4331. 2012.

- [131] **Arandjelovic, S. and Ravichandran, K.S.**, Phagocytosis of apoptotic cells in homeostasis. *Nature Immunology*, 16(9): 907–917. 2015.
- [132] **Reed, J.C.**, Dysregulation of apoptosis in cancer. *Journal of Clinical Oncology*, 17(9): 2941–2941. 1999.
- [133] **Birge, R., Boeltz, S., Kumar, S., Carlson, J., Wanderley, J., Calianese, D., Barcinski, M., Brekken, R., Huang, X., Hutchins, J., et al.**, Phosphatidylserine is a global immunosuppressive signal in efferocytosis, infectious disease, and cancer. *Cell Death and Differentiation*, 23(6): 962–978. 2016.
- [134] **Shimohama, S.**, Apoptosis in Alzheimer’s disease – an update. *Apoptosis*, 5(1): 9–16. 2000.
- [135] **Barinaga, M.**, Is apoptosis key in Alzheimer’s disease? *Science*, 281(5381): 1303–1304. 1998.
- [136] **Thathiah, A. and De Strooper, B.**, The role of G protein-coupled receptors in the pathology of Alzheimer’s disease. *Nature Reviews Neuroscience*, 12(2): 73–87. 2011.
- [137] **Berman, H.M., Westbrook, J., Feng, Z., Gilliland, G., Bhat, T.N., Weissig, H., Shindyalov, I.N., and Bourne, P.E.**, The protein data bank. *Nucleic Acids Research*, 28(1): 235–242. 2000.
- [138] **Jo, S., Kim, T., Iyer, V.G., and Im, W.**, CHARMM-GUI: a web-based graphical user interface for CHARMM. *Journal of Computational Chemistry*, 29(11): 1859–1865. 2008.
- [139] **Marion, J.B.**, *Classical dynamics of particles and systems*. Academic Press. 2013, 592 pp.
- [140] **Verlet, L.**, Computer "experiments" on classical fluids. I. Thermodynamical properties of Lennard-Jones molecules. *Physical Review*, 159(1): 98. 1967.
- [141] **Schlick, T.**, *Molecular modeling and simulation: an interdisciplinary guide: an interdisciplinary guide*. Springer Science & Business Media. 2010, 723 pp.
- [142] **Darden, T., York, D., and Pedersen, L.**, Particle mesh Ewald: An N log (N) method for Ewald sums in large systems. *The Journal of Chemical Physics*, 98(12): 10089–10092. 1993.

- [143] **Bussi, G., Donadio, D., and Parrinello, M.**, Canonical sampling through velocity rescaling. *The Journal of Chemical Physics*, 126(1): 014101. 2007.
- [144] **Parrinello, M. and Rahman, A.**, Polymorphic transitions in single crystals: A new molecular dynamics method. *Journal of Applied Physics*, 52(12): 7182–7190. 1981.
- [145] **Swaminathan, S., Harte Jr, W., and Beveridge, D.L.**, Investigation of domain structure in proteins via molecular dynamics simulation: application to HIV-1 protease dimer. *Journal of the American Chemical Society*, 113(7): 2717–2721. 1991.
- [146] **Kasahara, K., Fukuda, I., and Nakamura, H.**, A novel approach of dynamic cross correlation analysis on molecular dynamics simulations and its application to Ets1 dimer–DNA complex. *PLoS One*, 9(11): e112419. 2014.
- [147] **Anglin, T.C. and Conboy, J.C.**, Lateral pressure dependence of the phospholipid transmembrane diffusion rate in planar-supported lipid bilayers. *Biophysical Journal*, 95(1): 186–193. 2008.
- [148] **Schroeder, D.V.**, *An introduction to thermal physics*. AAPT. 1999, 422 pp.
- [149] **MacCallum, J.L. and Tieleman, D.P.**, Computer simulation of the distribution of hexane in a lipid bilayer: spatially resolved free energy, entropy, and enthalpy profiles. *Journal of the American Chemical Society*, 128(1): 125–130. 2006.
- [150] **Anglin, T.C., Cooper, M.P., Li, H., Chandler, K., and Conboy, J.C.**, Free energy and entropy of activation for phospholipid flip-flop in planar supported lipid bilayers. *The Journal of Physical Chemistry B*, 114(5): 1903–1914. 2010.
- [151] **Anglin, T.C., Brown, K.L., and Conboy, J.C.**, Phospholipid flip-flop modulated by transmembrane peptides WALP and melittin. *Journal of Structural Biology*, 168(1): 37–52. 2009.
- [152] **Frenkel, D. and Smit, B.**, *Understanding molecular simulations: from algorithms to applications*. 2002, 664 pp.

- [153] **Kästner, J.**, Umbrella sampling. *Wiley Interdisciplinary Reviews: Computational Molecular Science*, 1(6): 932–942. 2011.
- [154] **Jarzynski, C.**, Nonequilibrium equality for free energy differences. *Physical Review Letters*, 78(14): 2690. 1997.
- [155] **Kumar, S., Rosenberg, J.M., Bouzida, D., Swendsen, R.H., and Kollman, P.A.**, The weighted histogram analysis method for free-energy calculations on biomolecules. I. The method. *Journal of Computational Chemistry*, 13(8): 1011–1021. 1992.
- [156] **Hess, B., Kutzner, C., Van Der Spoel, D., and Lindahl, E.**, GROMACS 4: algorithms for highly efficient, load-balanced, and scalable molecular simulation. *Journal of Chemical Theory and Computation*, 4(3): 435–447. 2008.
- [157] **Brooks, B.R., Brucoleri, R.E., Olafson, B.D., States, D.J., Swaminathan, S.a., and Karplus, M.**, CHARMM: a program for macromolecular energy, minimization, and dynamics calculations. *Journal of Computational Chemistry*, 4(2): 187–217. 1983.
- [158] **Hess, B., Bekker, H., Berendsen, H.J., and Fraaije, J.G.**, LINCS: a linear constraint solver for molecular simulations. *Journal of Computational Chemistry*, 18(12): 1463–1472. 1997.
- [159] **Jorgensen, W.L., Chandrasekhar, J., Madura, J.D., Impey, R.W., and Klein, M.L.**, Comparison of simple potential functions for simulating liquid water. *The Journal of Chemical Physics*, 79(2): 926–935. 1983.
- [160] **Grant, B.J., Rodrigues, A.P., ElSawy, K.M., McCammon, J.A., and Caves, L.S.**, Bio3d: an R package for the comparative analysis of protein structures. *Bioinformatics*, 22(21): 2695–2696. 2006.
- [161] **Dupradeau, F.Y., Pigache, A., Zaffran, T., Savineau, C., Lelong, R., Grivel, N., Lelong, D., Rosanski, W., and Cieplak, P.**, The REd. Tools: Advances in RESP and ESP charge derivation and force field library building. *Physical Chemistry Chemical Physics*, 12(28): 7821–7839. 2010.
- [162] **Jorgensen, W.L. and Tirado-Rives, J.**, The OPLS [optimized potentials for liquid simulations] potential functions for proteins, energy minimizations for

- crystals of cyclic peptides and crambin. *Journal of the American Chemical Society*, 110(6): 1657–1666. 1988.
- [163] **Kulig, W., Pasenkiewicz-Gierula, M., and Róg, T.**, Topologies, structures and parameter files for lipid simulations in GROMACS with the OPLS-aa force field: DPPC, POPC, DOPC, PEPC, and cholesterol. *Data In Brief*, 5: 333–336. 2015.
- [164] **Bakowies, D. and van Gunsteren, W.F.**, Simulations of apo and holo-fatty acid binding protein: structure and dynamics of protein, ligand and internal water1. *Journal of Molecular Biology*, 315(4): 713–736. 2002.
- [165] **Zanotti, G., Feltre, L., and Spadon, P.**, A possible route for the release of fatty acid from fatty acid-binding protein. *Biochemical Journal*, 301(2): 459–463. 1994.
- [166] **Garbay, B., Heape, A., Sargueil, F., and Cassagne, C.**, Myelin synthesis in the peripheral nervous system. *Progress in Neurobiology*, 61(3): 267–304. 2000.
- [167] **Saher, G. and Simons, M.**, Cholesterol and myelin biogenesis. pp. 489–508. 2010.
- [168] **Simpson, M.A. and Bernlohr, D.A.**, Analysis of a series of phenylalanine 57 mutants of the adipocyte lipid-binding protein. *Biochemistry*, 37(31): 10980–10986. 1998.
- [169] **Sacchettini, J., Gordon, J., and Banaszak, L.**, The structure of crystalline Escherichia coli-derived rat intestinal fatty acid-binding protein at 2.5-Å resolution. *Journal of Biological Chemistry*, 263(12): 5815–5819. 1988.
- [170] **Allhusen, J.S. and Conboy, J.C.**, The ins and outs of lipid flip-flop. *Accounts of Chemical Research*, 50(1): 58–65. 2016.
- [171] **Fattal, E., Nir, S., Parente, R.A., and Szoka Jr, F.C.**, Pore-forming peptides induce rapid phospholipid flip-flop in membranes. *Biochemistry*, 33(21): 6721–6731. 1994.
- [172] **Langer, M., Sah, R., Veser, A., Gütlich, M., and Langosch, D.**, Structural properties of model phosphatidylcholine flippases. *Chemistry & Biology*, 20(1): 63–72. 2013.

- [173] Nakao, H., Hayashi, C., Ikeda, K., Saito, H., Nagao, H., and Nakano, M., Effects of hydrophilic residues and hydrophobic length on flip-flop promotion by transmembrane peptides. *The Journal of Physical Chemistry B*, 122(15): 4318–4324. 2018.
- [174] Warne, T., Serrano-Vega, M.J., Baker, J.G., Moukhametzianov, R., Edwards, P.C., Henderson, R., Leslie, A.G., Tate, C.G., and Schertler, G.F., Structure of a β 1-adrenergic G-protein-coupled receptor. *Nature*, 454(7203): 486–491. 2008.
- [175] Tieleman, D.P. and Marrink, S.J., Lipids out of equilibrium: Energetics of desorption and pore mediated flip-flop. *Journal of the American Chemical Society*, 128(38): 12462–12467. 2006.

PUBLICATIONS

PUBLICATION

I

Dynamics of the Peripheral Membrane Protein P2 from Human Myelin Measured by Neutron Scattering – A Comparison between Wild-Type Protein and a Hinge Mutant

Saara Laulumaa, Tuomo Nieminen, Mari Lehtimäki, Shweta Aggarwal, Mikael Simons, Michael M. Koza, Ilpo Vattulainen, Petri Kursula & Francesca Natali

PLoS One 10(6) (2015)

DOI: 10.1371/journal.pone.0128954

Publication reprinted with the permission of the copyright holder

RESEARCH ARTICLE

Dynamics of the Peripheral Membrane Protein P2 from Human Myelin Measured by Neutron Scattering—A Comparison between Wild-Type Protein and a Hinge Mutant

Saara Laulumaa^{1,2,3}, Tuomo Nieminen⁴, Mari Lehtimäki¹, Shweta Aggarwal⁵, Mikael Simons⁵, Michael M. Koza⁶, Ilpo Vattulainen⁴, Petri Kursula^{1,2,7†*}, Francesca Natali^{6,8†*}

1 Biochemistry and Molecular Medicine & Biocenter Oulu, University of Oulu, Oulu, Finland, **2** German Electron Synchrotron (DESY), Hamburg, Germany, **3** European Spallation Source (ESS), Lund, Sweden, **4** Department of Physics, Tampere University of Technology, Tampere, Finland, **5** Max Planck Institute for Experimental Medicine, Göttingen, Germany, **6** Institut Laue-Langevin (ILL), Grenoble, France, **7** Department of Biomedicine, University of Bergen, Bergen, Norway, **8** CNR-IOM, OGG, Grenoble, France

† These authors are joint senior authors on this work.

* petri.kursula@biomed.uib.no (PK); natali@ill.fr (FN)



 OPEN ACCESS

Citation: Laulumaa S, Nieminen T, Lehtimäki M, Aggarwal S, Simons M, Koza MM, et al. (2015) Dynamics of the Peripheral Membrane Protein P2 from Human Myelin Measured by Neutron Scattering—A Comparison between Wild-Type Protein and a Hinge Mutant. PLoS ONE 10(6): e0128954. doi:10.1371/journal.pone.0128954

Academic Editor: Danilo Roccatano, Jacobs University Bremen, GERMANY

Received: January 22, 2015

Accepted: May 1, 2015

Published: June 11, 2015

Copyright: © 2015 Laulumaa et al. This is an open access article distributed under the terms of the [Creative Commons Attribution License](https://creativecommons.org/licenses/by/4.0/), which permits unrestricted use, distribution, and reproduction in any medium, provided the original author and source are credited.

Data Availability Statement: The structure factors and final refined coordinates were deposited at the Protein Data Bank, with entry codes 4D6A (wtP2 after neutron scattering experiments) and 4D6B (P2-P38G).

Funding: This study was supported by the Academy of Finland (www.aka.fi), the Sigrid Jusélius Foundation (www.sigridjuselius.fi), the Emil Aaltonen Foundation (www.emilaaltonen.fi), the European Spallation Source (www.europeanspallationssource.se), and the Research and Science Foundation of the

Abstract

Myelin protein P2 is a fatty acid-binding structural component of the myelin sheath in the peripheral nervous system, and its function is related to its membrane binding capacity. Here, the link between P2 protein dynamics and structure and function was studied using elastic incoherent neutron scattering (EINS). The P38G mutation, at the hinge between the β barrel and the α -helical lid, increased the lipid stacking capacity of human P2 *in vitro*, and the mutated protein was also functional in cultured cells. The P38G mutation did not change the overall structure of the protein. For a deeper insight into P2 structure-function relationships, information on protein dynamics in the 10 ps to 1 ns time scale was obtained using EINS. Values of mean square displacements mainly from protein H atoms were extracted for wild-type P2 and the P38G mutant and compared. Our results show that at physiological temperatures, the P38G mutant is more dynamic than the wild-type P2 protein, especially on a slow 1-ns time scale. Molecular dynamics simulations confirmed the enhanced dynamics of the mutant variant, especially within the portal region in the presence of bound fatty acid. The increased softness of the hinge mutant of human myelin P2 protein is likely related to an enhanced flexibility of the portal region of this fatty acid-binding protein, as well as to its interactions with the lipid bilayer surface requiring conformational adaptations.

Introduction

In the vertebrate central (CNS) and peripheral nervous systems (PNS), selected neuronal axons are covered by a protecting layer of myelin. The myelin sheath is a unique multilayered

City of Hamburg (<http://www.hamburg.de/bwf/forschungs-und-wissenschaftsstiftung-hamburg/>) (all to PK), as well as the Academy of Finland (Center of Excellence programme) and the European Research Council (Advanced Grant CROWDED-PRO-LIPIDS) (both to IV). The funders had no role in study design, data collection and analysis, decision to publish, or preparation of the manuscript.

Competing Interests: The authors have declared that no competing interests exist.

membrane, wrapped around PNS axons by Schwann cells. Myelin in the CNS is made by oligodendrocytes. Myelin enables the rapid saltatory conduction of nerve impulses along axons, which can be up to a meter long in the PNS [1]. The myelin membrane contains 75–80% lipids by dry weight, with a high, 30–40%, cholesterol content [2], and it is enriched in myelin-specific proteins that are expressed by myelinating cells [3,4]. The myelin proteome has been under investigation for decades [5,6], but the structure and function of several myelin proteins are still poorly understood [3].

Myelin protein P2 is one of the quantitatively major proteins of human peripheral nerve myelin. P2 has been reported to comprise up to 15% of total myelin protein [7]; however, it is only present in selected myelin sheaths [8,9]. The crystal structure of human P2 [10] has been solved at atomic (0.93 Å) resolution: 10 antiparallel β strands form a barrel, which is covered by a lid-like motif formed of two α helices (Fig 1) [11]. P2 belongs to the fatty acid binding

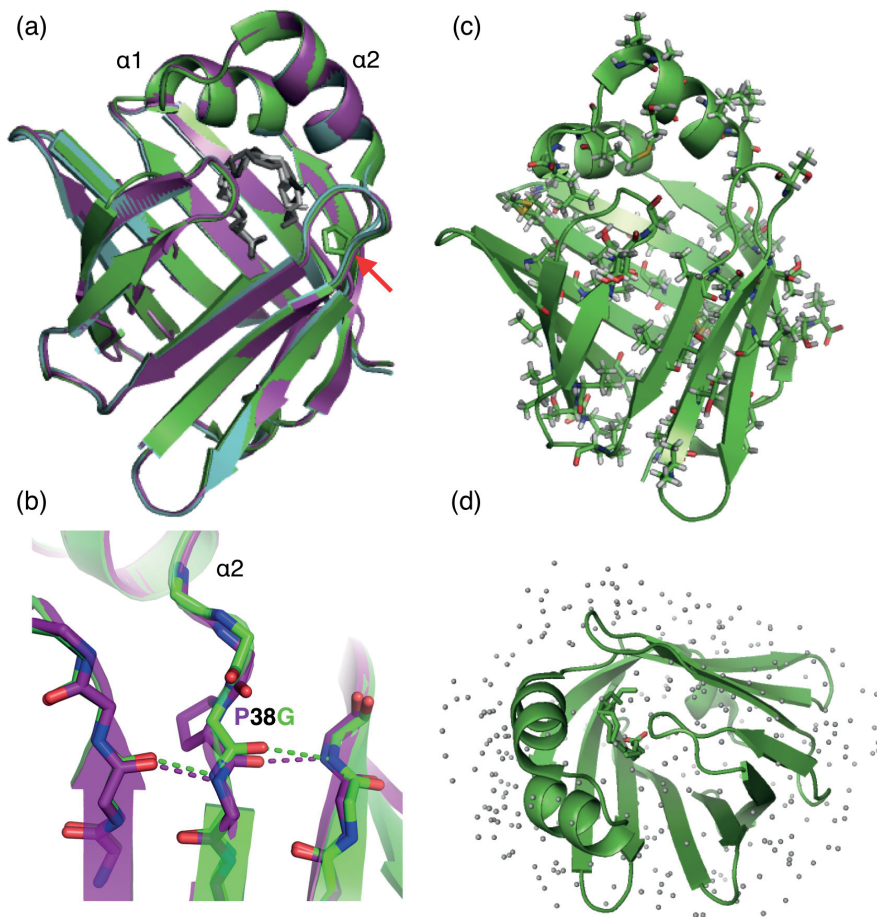


Fig 1. Crystal structure of human P2. (a) Superimposed structures of human wtP2 (cyan) and P2-P38G (green) before neutron scattering experiments and wtP2 after the experiment (magenta). Pro38 is indicated with the red arrow. (b) The P38G mutation site. Note how the main-chain hydrogen bonding (dashed lines) remains conserved at the edge of the β sheet also in the mutant. (c) Locations of the residues with side-chain methyl groups in P2 are shown as sticks. (d) A top view of the barrel-shaped P2 with bound fatty acid and stationary water molecules at cryo temperatures in the high-resolution crystal structure [11].

doi:10.1371/journal.pone.0128954.g001

protein (FABP) family; it has the ability to bind lipids and possibly plays a role in lipid transport and homeostasis in myelin, as indicated by the phenotype of P2-deficient mice [9]. While myelin appears normal in these animals, they have decreased nerve conduction velocity and an altered myelin lipid composition during development [9]. The β barrel of P2 contains a large (1000 \AA^3) ligand-binding pocket that is filled with a fatty acid and water molecules in the crystal structure [10]. Among myelin lipids, one natural ligand for P2 could be cholesterol, which is present in myelin at high concentrations and would fit into the cavity by size and by its electrostatic properties [10].

P2 binds phospholipids and stacks lipid bilayers together [11,12]. We previously reported decreased overall proton dynamics in liposomes in solution at physiological temperatures upon the addition of the P2 protein [13], as well as effects of bound P2 on multilayered lipid membrane structure [14]. P2 has been suggested to stack membrane layers together by binding to phospholipids through its positively charged surface residues, hydrophobic side chains from the α -helical lid partially penetrating the membrane [10,11]. Despite detailed mapping of the structural properties and physiological activity of the P2 protein, its role in healthy and diseased myelin remains unclear.

An insight into molecular motions and flexibility is important for understanding structure-function relationships in proteins [15,16]. Elastic incoherent neutron scattering (EINS) is a powerful tool for investigating quantitative protein dynamics [17–20]. EINS allows inspection of mean square displacements (MSD) of atoms as a function of external parameters, such as temperature, revealing information about eventual transitions occurring in proteins and the force constants required for protein motion activation. Using cold and thermal neutrons with energy resolutions from 70 to 0.9 μeV , atomic fluctuations on the time scale from 10 ps to 1 ns can be observed.

The effects of point mutations on protein dynamics have been studied using EINS before. When a mutation led to a nonfunctional enzyme or partial unfolding of the protein, the flexibility of the protein increased [21,22]. We previously reported an initial characterisation of the properties of human peripheral myelin protein P2 by studying protein dynamics on a fast dynamics scale (10 ps) using EINS [23]. We used wild-type P2 protein (wtP2) and its proline-38-to-glycine (P2-P38G) point mutant to investigate the dynamics of pure proteins as hydrated powders. P2-P38G showed increasing dynamics compared to wtP2 above 220 K [23]. Pro38 is a conserved residue located at a predicted hinge region, assumed to be involved in the opening of the helical lid of P2 upon ligand binding and release [11].

The aim of the present work was to extend earlier investigations on human P2 dynamics [23], expanding the time scale to 100 ps and 1 ns. We also carried out a thorough structural and functional characterisation of the samples to link the observed differences in dynamics to biomolecular function, and to confirm sample stability during the lengthy neutron scattering experiments. The results indicate that using EINS, we can obtain functionally relevant information on protein proton dynamics and the differences therein between the wild-type protein and a functional mutant.

Materials and Methods

Protein purification and EINS sample preparation

Human myelin wtP2 and P2-P38G [24] were expressed recombinantly in *E. coli* Rosetta (DE3) cells. The proteins were purified using Ni-ion affinity and size-exclusion chromatography, as previously described [10,24].

To get rid of buffer and salt traces in the protein sample, the purified protein was dialyzed three times against a large volume of H_2O . The protein was then lyophilised to remove all the

water and rehydrated with heavy water (D_2O) to $h = 0.28$ g/g (where h is defined as $g_{D_2O}/g_{\text{protein}}$) in a desiccator in a N_2/D_2O atmosphere. Due to the large excess of solvent deuterium atoms and the long equilibration time, this procedure guaranteed that most of the exchangeable hydrogen atoms in the protein sample were replaced by deuterium. The hydration level was controlled by weighing the sample during the hydration process. To obtain comparable wild-type and mutant protein samples, both samples were prepared in parallel.

Circular dichroism spectroscopy

Circular dichroism (CD) spectroscopy was used to study the folding and the secondary structure content of the sample proteins in solution. CD spectra were measured in H_2O at 0.25 mg/ml before and after the neutron scattering experiments using a Chirascan Plus spectropolarimeter (Applied Photophysics, United Kingdom) and a 0.5-mm quartz cuvette. Melting curves were measured from 293 to 363 K with a heating rate of 1 K/min at 0.25 mg/ml, in a buffer containing 0.8 mM HEPES (pH 7.5), 6 mM NaCl, and 0.4% glycerol.

Protein crystallography

P2-P38G was crystallised by vapour diffusion at 277 K using a well solution containing 3.15 M ammonium sulphate and 100 mM Tris (pH 8.5). X-ray diffraction data were collected at 100 K on beamline X12 at the DORIS storage ring, EMBL-Hamburg/DESY. wtP2 that had been used for neutron scattering experiments was resolubilised in protein buffer (0.8 mM HEPES (pH 7.5), 6 mM NaCl, 0.4% glycerol) and crystallised with vapour diffusion at 281 K, over a well solution of 28% PEG6000 and 0.1 M sodium citrate (pH 5.5). The diffraction experiment was done at 100 K on the I911-3 beamline, MAX-Lab (Lund, Sweden).

All data were processed with XDS [25], and the structures were solved with molecular replacement using wtP2 [10] as the search model. Refinement was carried out in phenix.refine [26] and model building in coot [27]. Molprobit [28] was used for structure validation. The structure factors and final refined coordinates were deposited at the Protein Data Bank with entry codes 4D6A (wtP2 after neutron scattering experiments) and 4D6B (P2-P38G).

Molecular dynamics simulations

The crystal structures of wtP2 and P2-P38G were subjected to atomistic molecular dynamics simulations, in order to pinpoint possible regions of differential dynamics linked to the mutation. Simulations were carried out in the presence and absence of bound fatty acid, and hydrogen dynamics were specifically addressed in the analysis.

The protein and the palmitate group were modeled by the CHARMM36 force field [29]. The protein model including palmitate was obtained from the PDB entry 4BVM [11] and converted to the CHARMM36 force field. The topology for wt-P2 was obtained directly from the conversion. P2-P38G was constructed from the wild type topology by changing the amino acid at the point of mutation. The three-point TIP3P model was used for water.

Four different protein systems were considered: wt-P2 and the P2-P38G, both with and without palmitate inside the binding pocket. The proteins were added to a solvated simulation box of approximately $(8 \times 8 \times 8) \text{ nm}^3$ with 16000 water molecules. Ten Cl^- ions were included to neutralise the total charge of the protein that had a palmitate in its pocket (in systems without palmitate, the number of Cl^- ions was 11 due to the charge of the palmitate).

The simulations were carried out under NpT conditions. Pressure coupling was done using the isothermal Parrinello-Rahman barostat [30] at a reference pressure of 1 bar, with a coupling time constant of 2.0 ps and isothermal compressibility of $4.5 \times 10^{-5} \text{ bar}^{-1}$. Temperature coupling was done with the velocity-rescale method [31], with separate temperature coupling

groups for the protein and the solvent. The reference temperatures were set as 300 K, with coupling time constants of 2.0 ps. Periodic boundary conditions were used. All bonds were constrained with the LINCS algorithm. The cut-off radii for the neighbor list, the Lennard-Jones interactions, and non-bonded interactions were set at 1.0 nm. For long-range electrostatics, we used the Particle-Mesh Ewald (PME) method with cubic interpolation (PME order 4) and a spacing of 0.16 nm for the Fourier grid.

The simulations were conducted using the GROMACS 4.6 simulation package [32]. The time increment used in integrating the equations of motion was 2 fs. The systems were first energy-minimised with the steepest descent algorithm and then simulated for a total of 3 μ s each. The systems were allowed to equilibrate for 500 ns, and the remaining part of the trajectory—over a period of 2.5 μ s—was used for analysis. The coordinate files for the trajectory were saved at a rate of $(50 \text{ ps})^{-1}$, except in simulations used for the calculation of the MSD, see below.

For analysis of MSDs of the protein hydrogens, we used additional simulations, since the dynamics of hydrogen movement are very rapid. As a starting point, we used the full 3- μ s trajectories discussed above. After the 500-ns equilibration period, seven different starting structures for each system were taken at 200-ns intervals, to obtain sufficient sampling over the whole simulation period. Each starting structure was then simulated for 3 ns, while saving the system coordinates every 2 fs to make sure that all the information of the rapid hydrogen movement would be accounted for in the analysis of MSDs. The root-mean square (RMS) fluctuation was calculated for each protein residue with the GROMACS tool `g_rmsf`.

MSDs of the protein hydrogen atoms were calculated to compare hydrogen mobility between the different systems. To this end, hydrogen mobility was explored for two different groups separately: i) hydrogens in CH_3 -groups, and ii) hydrogens in CH_2 - and CH -groups. For analysis (after the simulations had been completed), the protein was centered, and the rotation and translation of the protein backbone were fitted to the center of the simulation box, thus constraining protein movement during the analysis. The MSDs of the hydrogen atoms, compared to the initial starting structures, were then calculated from each of the 3-ns simulations with the GROMACS tool `g_msd`, using all the data in the trajectories. The final MSD curve for each case was obtained by averaging over the seven separate curves. In the results, we show the MSD behavior up to 1 ns, where the data are most accurate.

Functional assays

The lipid stacking properties of P2 were measured by following the turbidity resulting from vesicle aggregation, essentially as described [11]. 0–10 μ M P2 was mixed with 0.5 mM DMPC/DMPG (1,2-dimyristoyl-sn-glycero-3-phosphocholine/1,2-dimyristoyl-sn-glycero-3-phosphoglycerol) vesicles in 10 mM HEPES pH 7.4, 150 mM NaCl, and turbidity was measured at 600 nm using an Infinite M200 plate reader (Tecan, Switzerland).

In order to follow stacked membrane domain formation induced by P2 in living mammalian cells, a previously established method [11,33] was used. Briefly, wtP2 and P2-P38G were expressed in Ptk2 cells as fusions with green fluorescent protein and a transmembrane domain, and the cellular membrane organisation was followed by fluorescence microscopy. The formation of brightly fluorescent membrane domains is an indication of membrane stacking in this experimental system [33].

EINS data collection

To investigate protein dynamical properties, temperature-dependent EINS scans were performed on the thermal and cold neutron high resolution backscattering spectrometers IN13

and IN16, respectively, as well as on the time-focusing time-of-flight spectrometer IN6, all located at the Institut Laue-Langevin (ILL), Grenoble, France.

With a nearly Q -independent energy resolution of $\delta E = 8 \mu\text{eV}$ (full width at half maximum, FWHM) and an accessible momentum transfer range of $0.2 < Q < 4.9 \text{ \AA}^{-1}$, IN13 allows the investigation of molecular motions on a time scale up to 100 ps and with an amplitude from 1.3 \AA to $\sim 31 \text{ \AA}$ [34].

IN16 [35] is situated on a guide looking at one of the cold sources of the ILL. The Si(111) reflection of the monochromator is used to select a wavelength of $\lambda = 6.27 \text{ \AA}$ from the incoming neutrons. The instrumental setup results in a very narrow elastic energy resolution of $0.9 \mu\text{eV}$ (FWHM), corresponding to a time window of $\approx 1 \text{ ns}$ and a momentum transfer range of $0.19 < Q < 1.89 \text{ \AA}^{-1}$.

IN6 was used at an incident wavelength of $\lambda = 5.1 \text{ \AA}$, providing an energy resolution of $70 \mu\text{eV}$ (FWHM) and proton dynamics on the 10-ps time scale. The setting allows to access the momentum transfer range $0.3 < Q < 2 \text{ \AA}^{-1}$.

In all experiments, neutron scattering spectra were collected over a wide temperature range (20–310 K), with heating rates properly chosen to optimise the signal-to-noise ratio: 0.6 K/min from 20 K to 100 K, 0.4 K/min from 100 K to 220 K, and 0.15 K/min from 220 K to 310 K. Data were then binned using 5-K steps. As the same samples were used for data collection at all the instruments, the temperature scans were limited to 310 K to prevent the proteins from irreversible unfolding. To control sample integrity, protein structure was also analyzed after the neutron scattering experiments (see above).

The program LAMP [36] was used for data correction. The elastic scattered intensities were corrected for the empty cell contribution and normalised with respect to the lowest temperature scan ($T = 20 \text{ K}$) to compensate for differences in detector efficiency and geometry. In order to avoid corrections from multiple scattering events, cell thickness and geometry were properly chosen to minimise neutron absorption by the sample. A typical transmission of $\sim 95\%$ was guaranteed using standard flat aluminium sample holders with a thickness of 0.4 mm. No Bragg peaks from ice were detected in any of the spectra, which excludes the presence of free water in the samples.

EINS data analysis

Based on the atomic composition of P2, coherent scattering is estimated to correspond to less than 8% of the total scattering. Thus, in the following, it will be neglected, and we will focus exclusively on the behaviour of the incoherent scattering contribution.

The normalised incoherent elastic neutron scattering $S_{inc}(Q, \omega = 0)$ can be fitted using the Gaussian approximation within the region of its validity [17]:

$$S = I_0 e^{-\frac{\langle u^2 \rangle Q^2}{6}}, \quad (1)$$

where $\langle u^2 \rangle / 6$ is the normalised MSD, and $\langle u^2 \rangle$ is defined as

$$\langle u^2 \rangle = \langle u_r^2 - u_{20K}^2 \rangle. \quad (2)$$

In protein samples, incoherent scattering is dominated by hydrogen atoms, because hydrogen comprises approximately 50% of all protein atoms and the incoherent scattering cross section of hydrogen (80.27 barn) is significantly larger than that of other atoms in biological macromolecules (nitrogen 0.5 barn, carbon and oxygen 0.001 barn) [37]. With a hydration of $h = 0.28 \text{ g/g}$, the scattering contribution arising from the solvent (D_2O) is 1% of the total scattering (deuterium: 2.05 barn), which can be neglected.

Proteins are inhomogeneous macromolecules, each having a main chain of defined length and a unique side chain sequence and composition. Thus, one possibility is to describe protein dynamics using a bimodal distribution model [38,39]. In this model, hydrogen atoms are described as two different populations of homogeneously fluctuating atoms: methyl group hydrogen atoms and all other (non-methyl) non-exchangeable hydrogen atoms. Both populations can be described by a Gaussian function with a different width and the bimodal distribution of hydrogen atom MSD by

$$f(\langle u^2 \rangle) = a_1 \delta(\langle u^2 \rangle - \langle u^2 \rangle_1) + a_2 \delta(\langle u^2 \rangle - \langle u^2 \rangle_2), \quad (3)$$

where $\delta(x)$ is a delta function, a_1 and a_2 (with $a_2 = 1 - a_1$) represent the population fractions (temperature-independent), and $\langle u^2 \rangle_1$ and $\langle u^2 \rangle_2$ are the average MSDs of the hydrogen atoms in each fraction.

Using the Gaussian distribution function, the bimodal scattering function becomes

$$S(Q, \omega = 0) = I_0 \left[a_1 e^{-\frac{\langle u^2 \rangle_1 Q^2}{6}} + a_2 e^{-\frac{\langle u^2 \rangle_2 Q^2}{6}} \right]. \quad (4)$$

$\langle u^2 \rangle$ represents the full amplitude of atom dynamics in three dimensions, and atom displacement from the mean position is given by $\langle u^2 \rangle / 6$.

On the other hand, at low temperatures, protein dynamics are harmonic and can be described as a set of quantitated Einstein harmonic oscillators [40]:

$$\langle u^2 \rangle / 3 = \frac{h \langle \nu \rangle}{2k} \left[\coth \frac{h \langle \nu \rangle}{2k_B T} - 1 \right], \quad (5)$$

where k_B is the Boltzmann constant and h and $\langle \nu \rangle$ are the average frequency and the average force field constant of the oscillators, respectively.

Results and Discussion

Effects of the P38G mutation and neutron scattering experiments on protein structure

In order to enable the linking of experimentally measured protein dynamics to biomolecular structure and function, we carried out a characterisation of wtP2 and P2-P38G *in vitro*. These experiments were also aimed at studying any possible changes in protein structure or stability during and after the extensive neutron scattering experiments. Such a detailed sample characterisation allows to conclude, whether differences between samples are caused by large-scale structural re-arrangements, or if they can safely be assumed to result from real dynamical properties.

The human myelin protein P2 has a structure typical for FABPs, where β strands form a 10-stranded barrel covered by an α -helical lid [10,11]. Proline 38 lies at a putative hinge between the barrel and the lid (Fig 1a), and the P38G mutation would intuitively be expected to make the hinge more flexible, perhaps aiding lid opening motions or making the portal region less stable [11]. The crystal structure of P2-P38G (Table 1) indicates that the overall structure of P2 in the crystal state does not change due to the point mutation from an amino acid with the most rigid (Pro) to the one with the most flexible (Gly) backbone. The fatty acid palmitate is bound in the same mode in both forms of P2, and the flexible loops at both ends of the barrel are also in similar conformations. The helical lid is also closed in the mutant protein in the crystal state (Fig 1b).

Table 1. Crystallographic data collection and refinement statistics.

Dataset	wtP2 after EINS	P2-P38G
<i>Data collection</i>		
Beamline	I911-3 (MAX-Lab)	X12 (DESY)
Unit cell dimensions	a = b = 57.7 Å, c = 100.7 Å	a = b = 64.3 Å, c = 101.4 Å
Space group	P4 ₁ 2 ₁ 2	P4 ₁ 2 ₁ 2
Resolution (Å) ^a	20–1.45 (1.49–1.45)	20–2.12 (2.17–2.12)
R _{merge} (%)	4.9 (147.8)	5.1 (75.6)
<1/σ1>	21.9 (1.3)	23.5 (1.7)
Completeness (%)	99.8 (99.9)	97.8 (84.9)
Redundancy	7.0 (6.5)	7.7 (4.2)
CC _{1/2} (%) ^b	100 (40.4)	100 (70.8)
<i>Refinement</i>		
R _{work} /R _{free} (%)	14.7/18.4	21.9/27.3
RMSD		
Bond lengths (Å)	0.009	0.004
Bond angles (°)	1.3	0.7
Molprobability score (percentile) ^c	1.04 (99th)	0.77 (100th)
Ramachandran most favoured (%) ^c	100	100
Ramachandran outliers (%) ^c	0	0
PDB code	4D6A	4D6B

^a The numbers in parentheses refer to the highest-resolution shell.

^b CC_{1/2} is defined as the correlation coefficient between two random half-datasets [41]

^c Validation was carried out using Molprobability [28]

doi:10.1371/journal.pone.0128954.t001

wtP2 and P2-P38G have indistinguishable folding in solution as well, as shown by CD spectroscopy (Fig 2a). The melting curves for both proteins have similar trends: complete unfolding happens slowly between 310 and 350 K, the melting temperature being 331 K for wtP2 and 325 K for P2-P38G. This difference of 6 K in temperature stability is also likely to be reflected in the respective dynamics of wtP2 and P2-P38G, indirectly suggesting a more dynamic nature for the mutant protein.

To perform a neutron scattering experiment, the protein samples need to survive harsh conditions that are far from a physiological environment: dialysis to pure water, lyophilisation, rehydration with D₂O, time-consuming cycles of cooling and heating between 20 K and 310 K, and long neutron beam exposures. Therefore, the P2 protein quality before and after the neutron scattering experiment was analyzed. The P2 secondary structure content did not change, as seen in CD spectra (Fig 2a). To further check for the integrity of the sample during the experiments, wtP2 was resolubilised and crystallised after the neutron scattering experiments, and its crystal structure was refined at high resolution. The structure is essentially identical to that of fresh P2 (Fig 1a), proving that the P2 sample remains stable during the preparation of a hydrated powder and the neutron scattering measurements.

Simulation of P2 dynamics

As the crystal structures of wild-type and mutant P2 were essentially identical, we looked for differences in their dynamics with computer simulations. In addition to the expected increase in dynamics at the site of the mutation, the entire portal region—which must open, when a fatty acid enters—was expected to be more flexible in the mutant. This concerns especially the

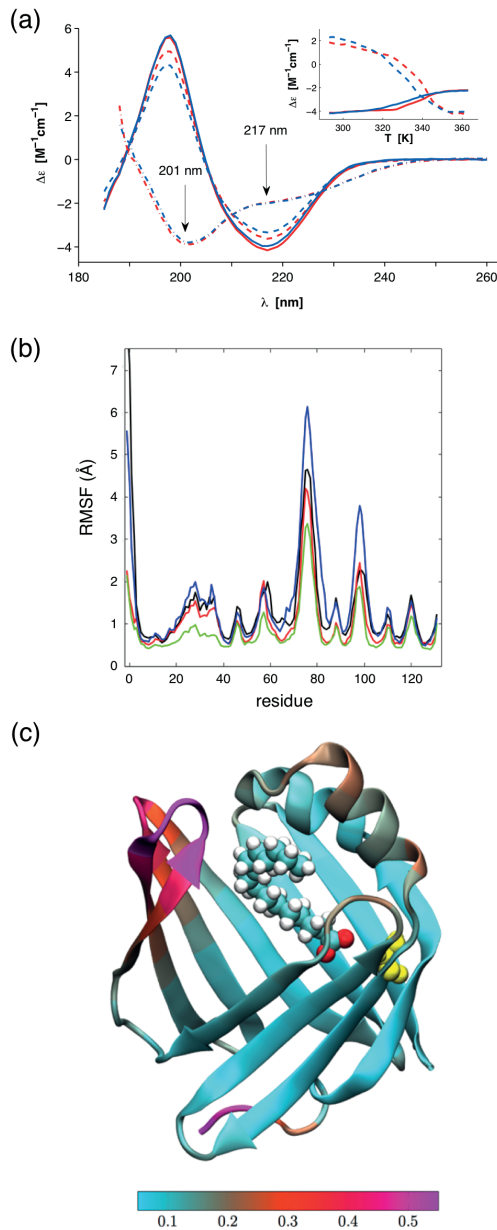


Fig 2. Folding and dynamics of P2. (a) CD spectra of wtP2 (red) and P2-P38G (blue) in solution. Solid lines represent the samples before neutron scattering experiments and dashed lines the samples after these experiments at 293 K. Dashed dotted lines are denatured samples at 363 K. The melting curves at 201 (dashed line) and 217 nm (solid line) as a function of temperature are shown in the inset. (b) Root-mean square fluctuation (RMSF) per residue analyzed for all the four simulated systems from the final 2500 ns of the simulation trajectory. Data for P2 without palmitate are shown in black (wild type) and red (P38G mutant). The results for P2 with palmitate are depicted in green (wild type) and blue (P38G). Large RMSF values

represent regions with high flexibility. The most flexible parts of the protein are found at the two loops opposing the lid. (c) A visualisation in VMD [42] of the RMS fluctuations in the P38G mutant with the palmitate chain inside the binding pocket. The yellow color corresponds to the mutated amino acid Gly38. The most flexible parts of the protein are pictured in bright magenta color. The colour bar at the bottom describes the range of RMSF values (light blue for low, violet for high).

doi:10.1371/journal.pone.0128954.g002

second helix of the helical lid, which we predicted to unfold upon lipid membrane binding [11]. Our earlier simulations, furthermore, suggested effects on the lid dynamics by the bound fatty acid [11]. The effect of the fatty acid was confirmed by the 2.5- μ s simulations here, as wtP2 was clearly stabilised by the bound fatty acid. On the other hand, bound ligand appeared to destabilise the portal region in the mutant protein.

The P2 protein is a β barrel with four loops at the top and at the bottom, and a lid consisting of two short α helices connected by a loop. The palmitate ligand resides inside the barrel, with its hydrophobic tail facing the lid. Pro38 lies in a short turn between the end of the second α helix and the subsequent β strand.

P2 crystal structure consists of a total of 132 amino acids. The lid consists of two α helices (16–23 and 27–36) and the loop between them. The loops on the lid side of the protein contain residues 55–58, 74–78, 97–99, and 119–122. The loops at the bottom of the protein are formed by residues 46–47, 65–68, 88–89, and 110–111. Apart from the N and C termini, the rest can be considered to be a β sheet structure, which forms a barrel.

RMS fluctuations characterise the dynamics of the protein (Fig 2b and 2c). The most flexible parts of P2 can be observed to reside on the side of the lid, *i.e.* within the portal region. The two loops apposing the lid (residues 74–78 and 97–99) are the most mobile parts of the protein (Fig 2c). Surprisingly, the lid itself does not move as much, as one might expect.

Comparing the different systems to each other, there do not seem to be significant differences in the dynamics of the palmitate-free proteins, though wt-P2 seems to be slightly more flexible than the P38G mutant. However, when palmitate is present, wt-P2 is considerably more stable than either of the palmitate-free proteins. Conversely, P2-P38G with bound palmitate is much more flexible, especially in the two loops apposing the lid. A point mutation at the root of the lid, therefore, renders the lid much more apt to open. This conclusion is supported by observations that the palmitate chain attempted multiple times to escape the barrel of the P38G mutant during the simulation (data not shown).

Functional assays

P2 is likely to stabilise the myelin structure and stack membrane layers together in compacted PNS myelin [43]. *In vitro*, membrane stacking and stabilisation by P2 have been observed earlier using different methods [11,13,43]. P2 was also shown to stack lipid bilayers in a vesicle aggregation assay, the hydrophobic Leu residue at the tip of the α -helical lid of P2 being crucial for membrane binding [11]. The latter experiment was also carried out for P2-P38G. The P38G mutation in the hinge region actually enhances the lipid stacking property of P2, which can be seen as increasing turbidity of a DMPC/DMPG vesicle solution at low P2 concentrations (Fig 3a).

In cultured Ptk2 cells, the overexpression of wtP2 causes the formation of stacked membrane domains, while the membrane binding-deficient mutant L27D failed to form such domains [11]. P2-P38G induces the formation of similar membrane domains as wtP2, also resulting in the extrusion of cell surface glycoproteins from the affected areas, proving the functionality of this variant also in a cellular environment (Fig 3b). Taking all the structural and functional characterisation together, P2-P38G is functional, and it is also stably folded in the

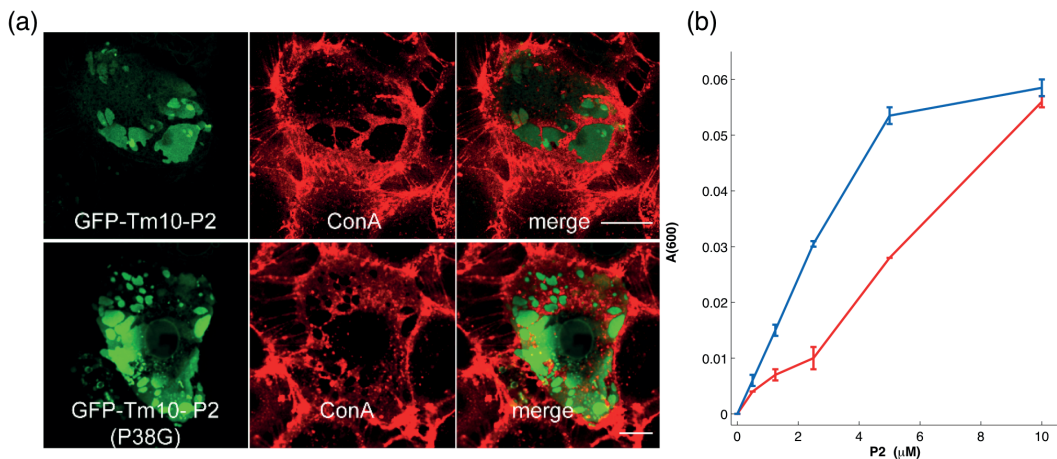


Fig 3. Functional assays. (a) Overexpressed wtP2 (top) and P2-P38G (bottom) both form stacked membrane domains in cell culture. The scale bar is 10 μm. Cell surface glycoproteins (visualised by concanavalin A; red) are depleted from the stacked membrane domains containing fluorescent P2 (green). (b) wtP2 (red) and P2-P38G (blue) both induce vesicle aggregation, which can be observed as increasing turbidity.

doi:10.1371/journal.pone.0128954.g003

crystal state and in solution, like the wild-type protein. Hence, any differences in mutant vs. wild-type protein dynamics will not be caused by large conformational differences between the samples or by misfolding of the mutant protein.

Elastic incoherent neutron scattering

Changes in P2 dynamics upon the introduction of the P38G point mutation were experimentally monitored as a function of sample temperature using EINS. The analysis of IN6 data in terms of a bimodal distribution was the subject of our earlier investigation, showing that the data, unlike those from IN13 and IN16, were best fitted using the Gaussian approximation [23]. The temperature dependence of the elastic scattering intensity, $S(Q, \omega = 0)$, of wtP2, normalised to 20 K temperature data, is reported in Fig 4 with fitting using the bimodal distribution model (Eq 4) and the Gaussian model (Eq 1).

The observed protein dynamics depend on the distance and time scales explored. Indeed, data at 200 K clearly show a deviation from a linear behaviour on IN16, which is less enhanced on IN13 in the low-Q region, but more evident at the fully explored Q-interval (Fig 4). This observation is more pronounced at higher temperatures. The deviation is absent in IN6 data, which is a sign of certain motions detectable in the 100 ps—1 ns time scale, indistinguishable within the 10-ps time window of IN6. These motions are likely to be fast methyl group rotations and slower amino acid side chain fluctuations [19,39].

A first insight into protein dynamics from EINS data was obtained from the sum of elastic incoherent scattering intensities over a Q-range as a function of temperature from 20 K to 305 K. The normalised summed elastic scattering intensities of P2 samples from data acquired on IN6, IN13, and IN16, grouped over the Q-range $0.2 < Q < 2 \text{ \AA}^{-1}$, as well as IN13 data binned over the whole accessible Q-range ($0.2 < Q < 4.9 \text{ \AA}^{-1}$), are shown Fig 5. IN13 data are binned in 10-K steps to improve the statistics.

A deviation from a linear decrease of the summed elastic intensities vs T, *i.e.* a change in the slope, is a clear sign of the activation of a motion falling within the time scale accessible through

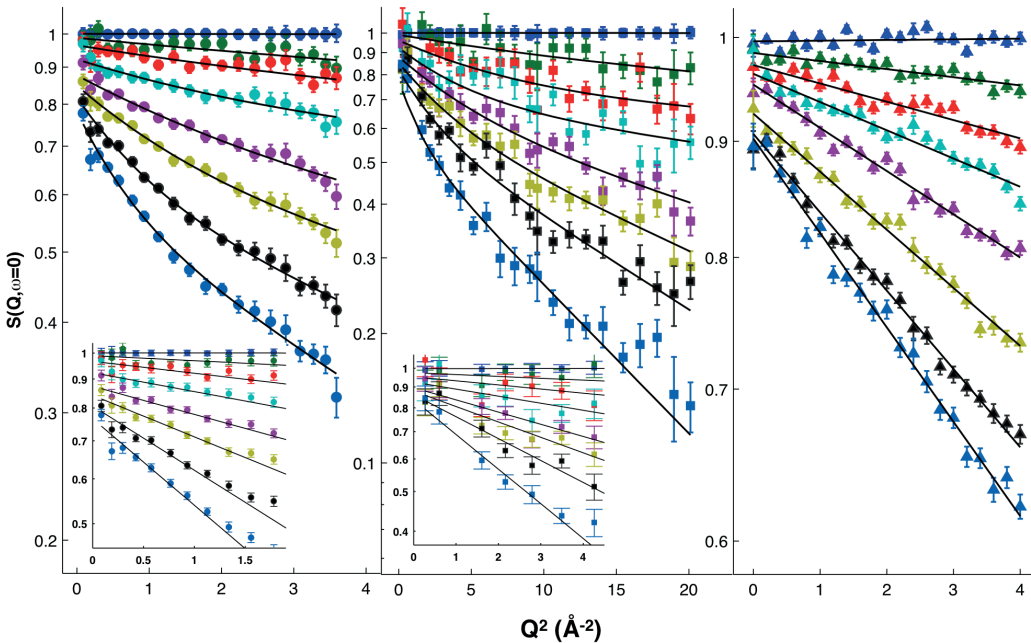


Fig 4. Temperature dependence of the normalised elastic scattering intensities. Data from wtP2 were acquired on IN16 (left), IN13 (middle), and IN6 (right). Data are shown for the temperatures 20, 100, 150, 200, 240, 260, 280, and 300 K (from top to bottom). Solid lines represent the best fitting to IN16 and IN13 data using Eq 4 and to IN6 data using Eq 1. Insets: magnification of the fitting region using Eq 1.

doi:10.1371/journal.pone.0128954.g004

the energy resolution of the used instrument. For wtP2, in IN6 data, the first change in the slope can be seen at 180 K, in IN13 data at 150 K, and in IN16 data at 130 K. A second, now instrument-independent, transition is seen at 240 K, above which the elastic signal is reduced for P2-P38G compared to wtP2 on all three instruments. In IN16 data, P2-P38G has a very rapid decrease in elastic signal at 240 K, but from 245 K on, the elastic signal continues with the same slope as wtP2. The same step can be seen on IN13, when the elastic signal over the full Q-range $0 < Q < 4.9 \text{ \AA}^{-1}$ is taken into account (Fig 5, right panel).

Gaussian approximation was used to estimate the total MSD of P2 samples on different time scales. IN6 data were fitted over the full Q-range to $Q^2 = 4 \text{ \AA}^{-2}$ (Fig 4, right panel), IN13 data to $Q^2 = 3.5 \text{ \AA}^{-2}$ (Fig 4, middle panel, inset), and IN16 data to $Q^2 = 0.77 \text{ \AA}^{-2}$ (Fig 4, left panel, inset) using Eq 1. The Q^2 region for Gaussian validity is instrument-dependent, being strictly linked to the MSD. Indeed, the Gaussian approximation is valid in the low-Q region, where $\log(S(Q, \omega = 0))$ is linear as a function of Q^2 , and, generally, when $Q^2 \langle u^2 \rangle \leq 2$ [17]. However, it depends heavily on the geometry of the motion. In a protein, the dynamics of an atom can be defined as localised motions within an ellipsoidal shape with axes 1:1:1.7 [44]. For elliptically moving atoms in proteins, the Gaussian approximation is valid to $\sqrt{Q^2 \langle u^2 \rangle} \approx 3$ [45]. The determined averaged MSDs are presented in Fig 6. The Gaussian approximation is valid up to the highest measured temperatures (305 K) on IN6, IN13, and IN16, where $\sqrt{Q^2 \langle u^2 \rangle}$ of P2-P38G reaches the maximum values 1.6, 2.3, and 2.0, respectively.

At low temperatures, proteins vibrate locally, and their dynamics can be described using the Einstein harmonic oscillator function [40]. The estimated MSDs of IN6 and IN13 data were

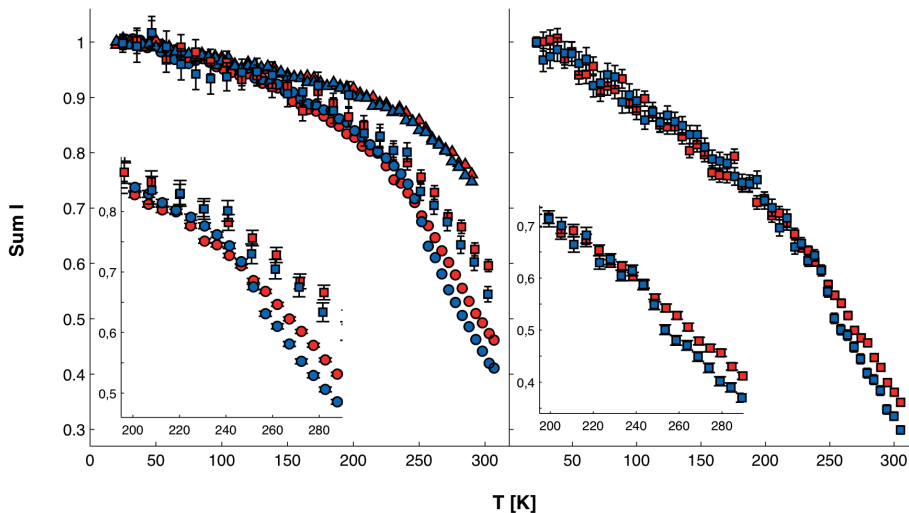


Fig 5. Normalised sums of intensities. Left: Normalised sum over $S(Q, \omega = 0)$ at $0 < Q < 2 \text{ \AA}^{-1}$ on IN6 (triangles), IN13 (squares), and IN16 (circles). Right: Sum over $S(Q, \omega = 0)$ at $0 < Q < 4.9 \text{ \AA}^{-1}$ on IN13. wtP2, red; P2-P38G, blue.

doi:10.1371/journal.pone.0128954.g005

fitted from 20 to 150 K, and the MSD of IN16 data to 130 K, using Eq 5 (Fig 6, Table 2). The average harmonic vibration for both wtP2 and P2-P38G varies within error bars, reaching $\langle u^2 \rangle = 0.05 \text{ \AA}^2$ at 300 K on all three instruments. The fitted average oscillation frequencies ν are around 2.5 ps^{-1} for IN6 and IN13 data, and approximately half of that for IN16 data. The estimated average force field constants (k) are 3–4 N/m. While the values of both k and ν are comparable to those estimated for artificial membranes [40], no significant difference can be observed between wtP2 and P2-P38G.

The first deviation of MSD from harmonic oscillation occurring at 120–180 K is thought to be the hydration-independent thermal activation of methyl proton rotations [46,47]. The methyl group activation (MGA) temperature has been shown to be instrument resolution-dependent [39]. The frequency of methyl group rotation depends on the amino acid side chain and its chemical environment [48] and increases as a function of temperature. Therefore, methyl rotations become observable at lower temperatures on instruments with the narrowest energy resolutions and longer time scales. In particular, the MGA temperatures of IN6, IN13, and IN16 have been determined as 180 K, 150 K, and 110 K, respectively, for a hydrated alanine polypeptide and albumin [39]. These temperatures are in good agreement with our P2 data, where MSD values deviate from the purely harmonic behavior fit at the MGA temperatures (Fig 6).

The transition at 240 K is generally called the protein dynamical transition (PDT). The origin of PDT has been under debate, but it is generally agreed that PDT is not dependent on instrument resolution but strongly depends on protein hydration [19,39,49]. In data from P2 samples, P2-P38G is systematically more dynamic than wtP2 above the PDT at all three measured energy resolutions (Fig 6). A steeper slope of MSD at high temperatures indicates increasing protein flexibility and softening of the protein [20].

Within a protein, atom dynamics do not correspond to free diffusion, but instead, all the atoms and their fluctuations are connected to their neighbouring atoms. The degree of freedom

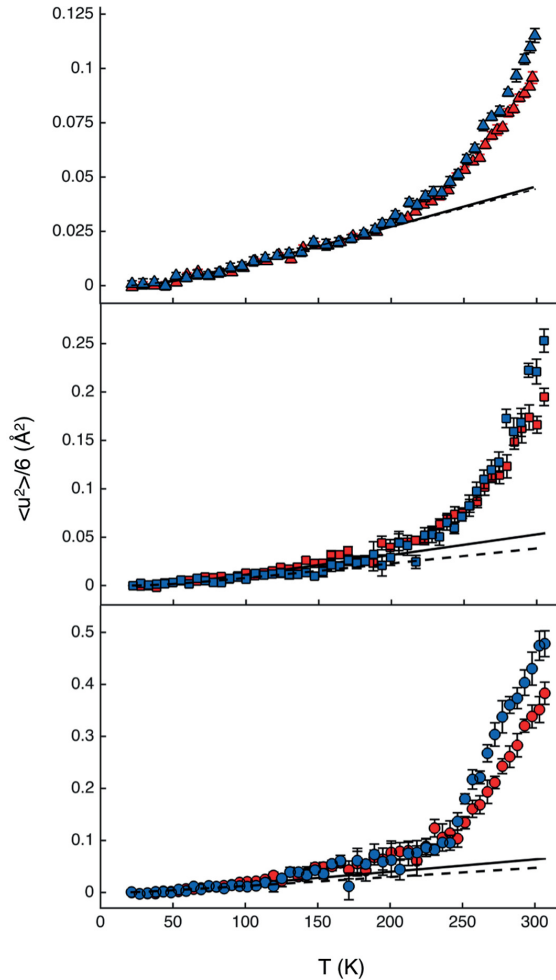


Fig 6. Temperature dependence of the MSD. Data from wtP2 (red) and P2-P38G (blue) were evaluated from the fit of data acquired on IN6 (top), IN13 (middle), and IN16 (bottom) using Eq 1. The low-temperature fits using the Einstein harmonic oscillator function (Eq 5) are shown as solid (wtP2) and dashed lines (P2-P38G).

doi:10.1371/journal.pone.0128954.g006

of hydrogen dynamics depends on the location of the hydrogen atom in the amino acid, such that the outermost side-chain hydrogen atoms are in general more mobile. The side chain dynamics depend on the length and polarity of the amino acid residue, as well as on the chemical environment of the side chain, which in turn is determined by the folding of the entire protein chain. Accordingly, an unfolded polypeptide chain is more flexible than a tightly folded globular protein [50,51].

A model that could univocally describe protein dynamics does not exist. Several different models have been introduced [39,52,53] to elucidate the main dynamical processes occurring in

Table 2. EINS data fitting parameters.

Instrument	Sample	wtP2		P2-P38G	
Gaussian approximation					
IN6	k [N/m]	3.7±0.3		3.7±0.2	
	v [ps ⁻¹]	2.5±0.4		2.5±0.3	
IN13	k [N/m]	3.2±0.4		4.3±0.8	
	v [ps ⁻¹]	2.5±0.4		2.7±0.6	
IN16	k [N/m]	2.9±0.4		3.9±0.6	
	v [ps ⁻¹]	1.5±0.4		1.3±0.4	
Bimodal distribution model					
		H _{methyl}	H _{non-methyl}	H _{methyl}	H _{non-methyl}
IN13	k [N/m]	2.0±0.5	5±1	2.1±0.8	6±2
	v [ps ⁻¹]	2±1	3±1	2±1	3±1
IN16	k [N/m]	0.6±0.1	20±2	0.6±0.1	25±4
	v [ps ⁻¹]	2.3±0.7	2.8±0.5	2.1±0.9	2.6±0.7

doi:10.1371/journal.pone.0128954.t002

a protein molecule. Here, in the bimodal model chosen by us, the hydrogen atoms of P2 were divided into methyl and non-methyl hydrogens, with the population fractions $a_1 = 0.26$ (methyl) and $a_2 = 0.74$ (non-methyl), corresponding to the calculated number of non-exchangeable hydrogen atoms in the P2 protein. It should be noted that these fractions are expected to be temperature-independent. We also tested the fitting procedure allowing the population fractions to vary (data not shown); a slight, negligible, effect on the observed methyl group fraction can be seen with increasing temperature, and the fractions converge to $a_1 = 0.26$ (wt-P2) and $a_1 = 0.32$ (P2-P38G) at room temperature (293 K)—very close to the values calculated based on chemical composition. In general, protein main-chain atoms are the most rigid, and the hydrogen atoms of long amino acid side chains furthest away from the main chain have the largest degree of freedom. Protein folding into secondary, tertiary, and quaternary structures, as well as protein interactions with binding partners, prohibits side chain rotations, reducing the possible side chain conformations [54,55]. Hydrogen atoms in methyl groups present an exception, as they have a high degree of freedom of rotation. Hydrogen atoms in a methyl group are chemically equivalent, and being uncharged, methyl groups do not form classical polar interactions [55]. Hence, methyl group dynamics are expected to provide the main contribution to global protein hydrogen dynamics.

Using a bimodal model for EINS data analysis, a distinction has previously been made between hydrogen atoms on the protein surface and in the core [21]. Unlike other proteins studied earlier by incoherent neutron scattering, P2 is a hollow barrel with a large cavity inside. Therefore, most of the side chains of P2 are in contact with solvent or the ligand inside the cavity (Fig 1c). The water molecules surrounding the P2 protein and within its internal cavity at cryo temperatures in the crystal state are shown in Fig 1d. According to protein dynamics simulations [56], the location of a residue—on the surface or in the core—has no remarkable effect on residue rigidity. Therefore, the distinction of hydrogen atoms between core and surface groups is not needed, and classification as methyl and non-methyl groups is justified in the current analysis.

Molecular dynamics trajectories were further analysed to validate the experimental model and data. MSDs were used to quantify the dynamics of the protein hydrogens separately for hydrogens in CH₃-groups, and for hydrogens in CH₂- and CH-groups. Fig 7a depicts that the methyl hydrogens are much more mobile than other hydrogens both in terms of the distance

they travel (magnitude of MSD), and in their rate of diffusive motion (tangents of the MSD curves). The hydrogens in the palmitated proteins are found to be more constrained than in their palmitate-free counterparts. In palmitate-free proteins, the hydrogens in wt-P2 are slightly more mobile than in P2-P38G. Conversely, in the proteins with bound palmitate, the hydrogens of the P38G mutant are more mobile than in wt-P2. The results confirm earlier indications of effects of bound fatty acid on P2 dynamics [11], and they justify the division of P2 hydrogens into methyl and non-methyl groups for the analysis of EINS data.

Similarly to the MSD defined by Gaussian approximation on IN13 and IN16, there is no visible difference between wtP2 and P2-P38G dynamics below 220 K in non-methyl hydrogen atoms, when the data are analyzed using the bimodal distribution model (Eq 4; Fig 7b, bottom). As expected, no MGA can be seen for non-methyl hydrogen atoms, and MSD follows the fitted harmonic oscillation contribution up to 200 K. The non-methyl hydrogen contribution seen on IN13 is close to the total dynamics seen on IN6 (Fig 6), with similar fitting parameters for low-temperature fluctuations (Table 2). On IN16, the non-methyl hydrogen contribution is very small below 200 K, resulting in force constant k values higher than 10 N/m. The short and fast fluctuations of non-methyl hydrogens occurring at low temperatures are probably out of the instrument resolution window and thus cannot be detected on IN16. Overall, there is no difference in the non-methyl hydrogen MSD values between wtP2 and P2-P38G samples obtained on IN13 and IN16 below 240 K, above which P2-P38G is more dynamic and its MSD higher.

The methyl proton contributions seen on IN13 and IN16 oscillate at low temperatures with frequencies ν of 2 ps^{-1} (Table 2), and estimated force constants k are 0.6 N/m for IN16 time scale vibrations and approximately three times higher for the dynamics seen on IN13. The MSD determined on IN13 faces MGA at 150 K, after which dynamics of the wild-type and mutant protein increase similarly up to the 240 K PDT temperature (Fig 7, left, top). On IN16, the MGA occurs at 130 K. Differently to IN13 data, at IN16 resolution, P2-P38G is more dynamic than wtP2 already between the MGA and PDT. In IN13 and IN16 data, the MSD of methyl

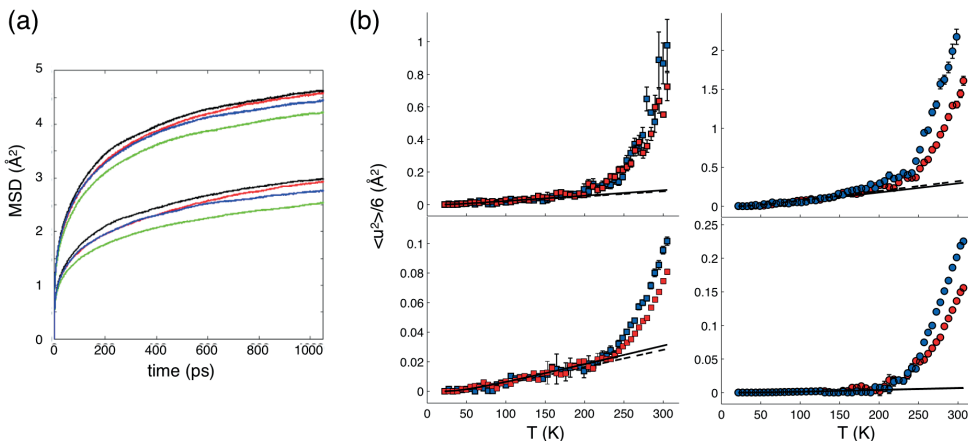


Fig 7. Simulated and experimental hydrogen MSDs. (a) The averaged MSD of i) hydrogens in CH₃-groups (top group of curves with higher MSD values) and ii) hydrogens in CH₂- and CH-groups (bottom group with lower MSD values) for all the four systems studied by MD simulations. Data for P2 without palmitate are shown in black (wild type) and red (P38G mutant). The results for P2 with palmitate are depicted in green (wild type) and blue (P38G). (b) Experimentally determined MSD contributions from methyl (upper panels) and non-methyl hydrogens (lower panels) for wtP2 (red) and P2-P38G (blue) using the bimodal model. Left: IN13; right: IN16. Solid (wtP2) and dashed (P2-P38G) lines represent the low-temperature harmonic vibrational contributions.

doi:10.1371/journal.pone.0128954.g007

hydrogens of P2-P38G increases more rapidly at PDT (240 K). This is in good agreement with the clear change in the slope of the sum of elastic intensities (Fig 5) at 240 K.

The total MSD of P2 is dominated by dynamics of the methyl hydrogens (Fig 7). Methyl groups are nonpolar moieties that are located outermost in amino acid residues, having less neighbouring atoms and more space to rotate freely. In P2, methyl groups are scattered throughout the protein (Fig 1c) and often have contact to the solvent.

The point mutation P38G in the hinge between the barrel and lid of P2 does not affect P2 folding (Fig 1a) or render it inactive (Fig 3a), but it increases the total flexibility of the protein (Fig 6). The dynamics experimentally observed above the PDT may be related to such functional dynamics of P2. Using EINS, only averaged total dynamics can be observed, and additional experiments and molecular dynamics simulations will be needed for understanding the results.

Inside the P2 β barrel, there is a bound fatty acid from the bacterial expression host. While P2, although being a folded protein, has no clearly defined hydrophobic core, the bound ligand could provide such a core, possibly playing a role in P2 stability. Could the differences between wild-type and mutated forms of P2 be partially related to the bound fatty acid? Firstly, the dynamics contributed by the fatty acid can be ignored from data analysis, because its hydrogens correspond to only 3% of the protein hydrogen atoms; the scattering from the fatty acid would be hidden by the much larger protein dynamics contribution. Secondly, an absence of bound fatty acid could increase the amount of water inside the barrel, which in turn could change the protein dynamics. In the crystal structures, though, the fatty acid is bound, and its interactions with the protein are similar. Possible differences in fatty acid binding between the two samples could lead to differential flexibility of the portal region. Thus, also in this situation, the observed increased dynamics of P2-P38G would be explained with an increasing flexibility of the hinge that allows the lid to move more freely in the mutant molecule. Intriguingly, our extended MD simulations revealed that while the wild-type protein was stabilised by bound fatty acid, the mutant actually became more dynamic, especially within the portal region. The P2-P38G simulation trajectory reveals that the tail of the fatty acid is extended throughout the portal region during the simulation, which would mimic eventual dissociation of the ligand; this is expected to happen, when P2 binds to a membrane surface [11]. The simulations, thus, both confirmed the increased dynamics of P2-P38G and justified the use of the bimodal model in EINS data analysis.

Conclusions

In order to fully understand structure-function relationships in proteins, an insight into protein dynamics is crucial. EINS allows the inspection of changes in total protein dynamics as a function of an external parameter, such as temperature. We used neutron scattering and complementary methods to study the link between P2 protein dynamics and its structure-function relationships. P2 is a structural component of myelin, and its function is most likely related to its membrane binding capacity. The P38G mutation increased the lipid membrane stacking capacity of P2 *in vitro*, and the mutated protein was also correctly folded and active in cells. However, neutron scattering indicated that the P38G mutant is more dynamic than the wild-type protein, especially on a slow 1-ns time scale. The fact that the mutation causes significantly increased dynamics of the portal area in P2 enabled us to use EINS in this study to experimentally observe differential dynamics of a wild-type and a mutant protein. Earlier, we have shown that binding to membranes induces changes in P2 structure, mainly partial unfolding of α -helices of the lid [11]. The increased membrane binding activity of P2-P38G could be explained by increasing protein flexibility and an enhanced ability to interact with lipids. While EINS allows the inspection of the total dynamics, it is limited with respect to analysis of the origin and type

of dynamics. Therefore, other methods, such as quasielastic neutron scattering and atomistic simulations on membrane binding, can be used in the future to provide more detailed information about functionally relevant protein dynamics in P2.

Acknowledgments

We would like to thank Tilo Seydel (ILL) for technical support during the experiment on IN16 and Miguel Gonzales (ILL) for help in data correction. Synchrotron beamtime at EMBL/DESY and MAX-Lab is gratefully acknowledged. CSC—IT Center for Science (Espoo, Finland) is thanked for computing resources.

Author Contributions

Conceived and designed the experiments: SL TN MS IV PK FN. Performed the experiments: SL TN ML SA MS MMK IV PK FN. Analyzed the data: SL TN ML SA MS MMK IV PK FN. Contributed reagents/materials/analysis tools: MS MMK IV FN. Wrote the paper: SL TN ML SA MS MMK IV PK FN.

References

- Pereira JA, Lebrun-Julien F, Suter U. Molecular mechanisms regulating myelination in the peripheral nervous system. *Trends Neurosci.* 2012; 35: 123–134. doi: [10.1016/j.tins.2011.11.006](https://doi.org/10.1016/j.tins.2011.11.006) PMID: [22192173](https://pubmed.ncbi.nlm.nih.gov/22192173/)
- O'Brien JS, Sampson EL. Lipid composition of the normal human brain: gray matter, white matter, and myelin. *J Lipid Res.* 1965; 6: 537–544. PMID: [5865382](https://pubmed.ncbi.nlm.nih.gov/5865382/)
- Han H, Myllykoski M, Ruskamo S, Wang C, Kursula P. Myelin-specific proteins: a structurally diverse group of membrane-interacting molecules. *Biofactors.* 2013; 39: 233–241. doi: [10.1002/biof.1076](https://doi.org/10.1002/biof.1076) PMID: [23780694](https://pubmed.ncbi.nlm.nih.gov/23780694/)
- Kursula P. Structural properties of proteins specific to the myelin sheath. *Amino Acids.* 2008; 34: 175–185. PMID: [17177074](https://pubmed.ncbi.nlm.nih.gov/17177074/)
- Buttermore ED, Thaxton CL, Bhat MA. Organization and maintenance of molecular domains in myelinated axons. *J Neurosci Res.* 2013; 91: 603–622. doi: [10.1002/jnr.23197](https://doi.org/10.1002/jnr.23197) PMID: [23404451](https://pubmed.ncbi.nlm.nih.gov/23404451/)
- Patzig J, Jahn O, Tenzer S, Wichert SP, de Monasterio-Schrader P et al. Quantitative and integrative proteome analysis of peripheral nerve myelin identifies novel myelin proteins and candidate neuropathy loci. *J Neurosci.* 2011; 31: 16369–16386. doi: [10.1523/JNEUROSCI.4016-11.2011](https://doi.org/10.1523/JNEUROSCI.4016-11.2011) PMID: [22072688](https://pubmed.ncbi.nlm.nih.gov/22072688/)
- Greenfield S, Brostoff S, Eylar EH, Morell P. Protein composition of myelin of the peripheral nervous system. *J Neurochem.* 1973; 20: 1207–1216. PMID: [4697881](https://pubmed.ncbi.nlm.nih.gov/4697881/)
- Trapp BD, McIntyre LJ, Quarles RH, Sternberger NH, Webster HD. Immunocytochemical localization of rat peripheral nervous system myelin proteins: P2 protein is not a component of all peripheral nervous system myelin sheaths. *Proc Natl Acad Sci U S A.* 1979; 76: 3552–3556. PMID: [291024](https://pubmed.ncbi.nlm.nih.gov/291024/)
- Zenker J, Stettner M, Ruskamo S, Domenech-Estevez E, Baloui H et al. A role of peripheral myelin protein 2 in lipid homeostasis of myelinating Schwann cells. *Glia.* 2014; 62: 1502–1512. doi: [10.1002/glia.22696](https://doi.org/10.1002/glia.22696) PMID: [24849898](https://pubmed.ncbi.nlm.nih.gov/24849898/)
- Majava V, Polverini E, Mazzini A, Nanekar R, Knoll W et al. Structural and functional characterization of human peripheral nervous system myelin protein P2. *PLoS One.* 2010; 5: e10300. doi: [10.1371/journal.pone.0010300](https://doi.org/10.1371/journal.pone.0010300) PMID: [20421974](https://pubmed.ncbi.nlm.nih.gov/20421974/)
- Ruskamo S, Yadav RP, Sharma S, Lehtimäki M, Laulumaa S et al. Atomic resolution view into the structure-function relationships of the human myelin peripheral membrane protein P2. *Acta Crystallogr D Biol Crystallogr.* 2014; 70: 165–176. doi: [10.1107/S1399004713027910](https://doi.org/10.1107/S1399004713027910) PMID: [24419389](https://pubmed.ncbi.nlm.nih.gov/24419389/)
- Sedzik J, Blaurock AE, Hoehli M. Reconstituted P2/myelin-lipid multilayers. *J Neurochem.* 1985; 45: 844–852. PMID: [2411857](https://pubmed.ncbi.nlm.nih.gov/2411857/)
- Knoll W, Natali F, Peters J, Nanekar R, Wang C et al. Dynamic properties of a reconstituted myelin sheath. *Spectroscopy.* 2010; 24: 585–592. PMID: [21037984](https://pubmed.ncbi.nlm.nih.gov/21037984/)
- Knoll W, Peters J, Kursula P, Gerelli Y, Ollivier J et al. Structural and dynamical properties of reconstituted myelin sheaths in the presence of myelin proteins MBP and P2 studied by neutron scattering. *Soft Matter.* 2014; 10: 519–529. doi: [10.1039/c3sm51393a](https://doi.org/10.1039/c3sm51393a) PMID: [24651633](https://pubmed.ncbi.nlm.nih.gov/24651633/)

15. Hensen U, Meyer T, Haas J, Rex R, Vriend G et al. Exploring protein dynamics space: the dynasome as the missing link between protein structure and function. *PLoS One*. 2012; 7: e33931. doi: [10.1371/journal.pone.0033931](https://doi.org/10.1371/journal.pone.0033931) PMID: [22606222](https://pubmed.ncbi.nlm.nih.gov/22606222/)
16. Micheletti C. Comparing proteins by their internal dynamics: exploring structure-function relationships beyond static structural alignments. *Phys Life Rev*. 2013; 10: 1–26. doi: [10.1016/j.plrev.2012.10.009](https://doi.org/10.1016/j.plrev.2012.10.009) PMID: [23199577](https://pubmed.ncbi.nlm.nih.gov/23199577/)
17. Gabel F. Protein dynamics in solution and powder measured by incoherent elastic neutron scattering: the influence of Q-range and energy resolution. *Eur Biophys J*. 2005; 34: 1–12. PMID: [15378211](https://pubmed.ncbi.nlm.nih.gov/15378211/)
18. Kneller GR, Chevrot G. Impact of anisotropic atomic motions in proteins on powder-averaged incoherent neutron scattering intensities. *J Chem Phys*. 2012; 137: 225101. doi: [10.1063/1.4769782](https://doi.org/10.1063/1.4769782) PMID: [23249033](https://pubmed.ncbi.nlm.nih.gov/23249033/)
19. Roh JH, Novikov VN, Gregory RB, Curtis JE, Chowdhuri Z et al. Onsets of anharmonicity in protein dynamics. *Phys Rev Lett*. 2005; 95: 038101. PMID: [16090773](https://pubmed.ncbi.nlm.nih.gov/16090773/)
20. Zaccai G. How soft is a protein? A protein dynamics force constant measured by neutron scattering. *Science*. 2000; 288: 1604–1607. PMID: [10834833](https://pubmed.ncbi.nlm.nih.gov/10834833/)
21. Nakagawa H, Kamikubo H, Kataoka M. Effect of conformational states on protein dynamical transition. *Biochim Biophys Acta*. 2010; 1804: 27–33. doi: [10.1016/j.bbapap.2009.06.025](https://doi.org/10.1016/j.bbapap.2009.06.025) PMID: [19595799](https://pubmed.ncbi.nlm.nih.gov/19595799/)
22. Sacquin-Mora S, Sebban P, Derrien V, Frick B, Lavery R et al. Probing the flexibility of the bacterial reaction center: the wild-type protein is more rigid than two site-specific mutants. *Biochemistry*. 2007; 46: 14960–14968. PMID: [18052234](https://pubmed.ncbi.nlm.nih.gov/18052234/)
23. Laulumaa S, Kursula P, Natali F. Neutron scattering studies on protein dynamics using the human myelin peripheral membrane protein P2. *Eur Phys J Web of Conferences*. 2015; 83: 02010
24. Lehtimäki M, Laulumaa S, Ruskamo S, Kursula P. Production and crystallization of a panel of structure-based mutants of the human myelin peripheral membrane protein P2. *Acta Crystallogr Sect F Struct Biol Cryst Commun*. 2012; 68: 1359–1362. doi: [10.1107/S1744309112039036](https://doi.org/10.1107/S1744309112039036) PMID: [23143249](https://pubmed.ncbi.nlm.nih.gov/23143249/)
25. Kabsch W. Automatic processing of rotation diffraction data from crystals of initially unknown symmetry and cell constants. *J Appl Cryst*. 1993; 26: 795–800.
26. Afonine PV, Grosse-Kunstleve RW, Echols N, Headd JJ, Moriarty NW et al. Towards automated crystallographic structure refinement with phenix.refine. *Acta Crystallogr D Biol Crystallogr*. 2012; 68: 352–367. doi: [10.1107/S0907444912001308](https://doi.org/10.1107/S0907444912001308) PMID: [22505256](https://pubmed.ncbi.nlm.nih.gov/22505256/)
27. Emsley P, Lohkamp B, Scott WG, Cowtan K. Features and development of Coot. *Acta Cryst D*. 2010; 66: 486–501.
28. Davis IW, Leaver-Fay A, Chen VB, Block JN, Kapral GJ et al. MolProbity: all-atom contacts and structure validation for proteins and nucleic acids. *Nucleic Acids Res*. 2007; 35: W375–83. PMID: [17452350](https://pubmed.ncbi.nlm.nih.gov/17452350/)
29. Brooks BR, Brooks CLR, Mackerell ADJ, Nilsson L, Petrella RJ et al. CHARMM: the biomolecular simulation program. *J Comput Chem*. 2009; 30: 1545–1614. doi: [10.1002/jcc.21287](https://doi.org/10.1002/jcc.21287) PMID: [19444816](https://pubmed.ncbi.nlm.nih.gov/19444816/)
30. Parrinello M, Rahman A. Polymorphic transitions in single crystals: A new molecular dynamics method. *J Appl Phys*. 1981; 52: 7182–7190.
31. Bussi G, Donadio D, Parrinello M. Canonical sampling through velocity rescaling. *J Chem Phys*. 2007; 126: 014101. PMID: [17212484](https://pubmed.ncbi.nlm.nih.gov/17212484/)
32. van der Spoel D, Lindahl E, Hess B, Groenhof G, Mark AE et al. GROMACS: fast, flexible, and free. *J Comput Chem*. 2005; 26: 1701–1718. PMID: [16211538](https://pubmed.ncbi.nlm.nih.gov/16211538/)
33. Aggarwal S, Snaidero N, Pahler G, Frey S, Sanchez P et al. Myelin membrane assembly is driven by a phase transition of myelin basic proteins into a cohesive protein meshwork. *PLoS Biol*. 2013; 11: e1001577. doi: [10.1371/journal.pbio.1001577](https://doi.org/10.1371/journal.pbio.1001577) PMID: [23762018](https://pubmed.ncbi.nlm.nih.gov/23762018/)
34. Natali F, Peters J, Russo D, Barbieri S, Chiapponi C et al. IN13 Backscattering spectrometer at ILL: looking for motions in biological macromolecules and organisms. *Neutron News*. 2008; 19: 14–18.
35. Frick B, Magerl A, Blanc Y, Rebesco R. The new backscattering spectrometer IN16 at the ILL. *Physica B*. 1997; 234: 1177–1179.
36. Richard D, Ferrand M, Kearley GJ. Analysis and visualisation of neutron-scattering data. *J Neutron Res*. 1996; 4: 33–39.
37. Sears VF. Neutron scattering lengths and cross sections. *Neutron news*. 1992; 3: 26–37.
38. Nakagawa H, Kamikubo H, Tsukushi I, Kanaya T, Kataoka M. Protein dynamical heterogeneity derived from neutron incoherent elastic scattering. *J Phys Soc Japan*. 2004; 73: 491–495.
39. Schiro G, Natali F, Cupane A. Physical origin of anharmonic dynamics in proteins: new insights from resolution-dependent neutron scattering on homomeric polypeptides. *Phys Rev Lett*. 2012; 109: 128102. PMID: [23005991](https://pubmed.ncbi.nlm.nih.gov/23005991/)

40. Natali F, Giliozzi A, Rolandi R, Cavatorta P, Deriu A et al. Myelin basic protein reduces molecular motions in DMPA, an elastic neutron scattering study. *Physica B: Condensed Matter*. 2001; 301: 145–149.
41. Karplus PA, Diederichs K. Linking crystallographic model and data quality. *Science*. 2012; 336: 1030–1033. doi: [10.1126/science.1218231](https://doi.org/10.1126/science.1218231) PMID: [22628654](https://pubmed.ncbi.nlm.nih.gov/22628654/)
42. Humphrey W, Dalke A, Schulten K. VMD: visual molecular dynamics. *J Mol Graph*. 1996; 14: 33–8, 27–8. PMID: [8744570](https://pubmed.ncbi.nlm.nih.gov/8744570/)
43. Suresh S, Wang C, Nanekar R, Kursula P, Edwardson JM. Myelin basic protein and myelin protein 2 act synergistically to cause stacking of lipid bilayers. *Biochemistry*. 2010; 49: 3456–3463. doi: [10.1021/bi100128h](https://doi.org/10.1021/bi100128h) PMID: [20334434](https://pubmed.ncbi.nlm.nih.gov/20334434/)
44. Kidera A, Go N. Refinement of protein dynamic structure: normal mode refinement. *Proc Natl Acad Sci U S A*. 1990; 87: 3718–3722. PMID: [2339115](https://pubmed.ncbi.nlm.nih.gov/2339115/)
45. Stadler AM, Pellegrini E, Johnson M, Fitter J, Zaccai G. Dynamics-stability relationships in apo- and holomyoglobin: a combined neutron scattering and molecular dynamics simulations study. *Biophys J*. 2012; 102: 351–359. doi: [10.1016/j.bpj.2011.12.031](https://doi.org/10.1016/j.bpj.2011.12.031) PMID: [22339872](https://pubmed.ncbi.nlm.nih.gov/22339872/)
46. Wood K, Tobias DJ, Kessler B, Gabel F, Oesterhelt D et al. The low-temperature inflection observed in neutron scattering measurements of proteins is due to methyl rotation: direct evidence using isotope labeling and molecular dynamics simulations. *J Am Chem Soc*. 2010; 132: 4990–4991. doi: [10.1021/ja910502g](https://doi.org/10.1021/ja910502g) PMID: [20302295](https://pubmed.ncbi.nlm.nih.gov/20302295/)
47. Schiro G, Caronna C, Natali F, Cupane A. Direct evidence of the amino acid side chain and backbone contributions to protein anharmonicity. *J Am Chem Soc*. 2010; 132: 1371–1376. doi: [10.1021/ja908611p](https://doi.org/10.1021/ja908611p) PMID: [20067251](https://pubmed.ncbi.nlm.nih.gov/20067251/)
48. Best RB, Clarke J, Karplus M. What contributions to protein side-chain dynamics are probed by NMR experiments? A molecular dynamics simulation analysis. *J Mol Biol*. 2005; 349: 185–203. PMID: [15876377](https://pubmed.ncbi.nlm.nih.gov/15876377/)
49. Doster W. The two-step scenario of the protein dynamical transition. *J Non-Cryst Solids*. 2011; 357: 622–628.
50. Dhindsa GK, Tyagi M, Chu XQ. Temperature-dependent dynamics of dry and hydrated beta-casein studied by quasielastic neutron scattering. *J Phys Chem B*. 2014; 118: 10821–10829. doi: [10.1021/jp504548w](https://doi.org/10.1021/jp504548w) PMID: [25144497](https://pubmed.ncbi.nlm.nih.gov/25144497/)
51. Perticaroli S, Nickels JD, Ehlers G, Mamontov E, Sokolov AP. Dynamics and rigidity in an intrinsically disordered protein, beta-casein. *J Phys Chem B*. 2014; 118: 7317–7326. doi: [10.1021/jp503788r](https://doi.org/10.1021/jp503788r) PMID: [24918971](https://pubmed.ncbi.nlm.nih.gov/24918971/)
52. Doster W, Cusack S, Petry W. Dynamical transition of myoglobin revealed by inelastic neutron scattering. *Nature*. 1989; 337: 754–756. PMID: [2918910](https://pubmed.ncbi.nlm.nih.gov/2918910/)
53. Meinhold L, Clement D, Tehei M, Daniel R, Finney JL et al. Protein dynamics and stability: the distribution of atomic fluctuations in thermophilic and mesophilic dihydrofolate reductase derived using elastic incoherent neutron scattering. *Biophys J*. 2008; 94: 4812–4818. doi: [10.1529/biophysj.107.121418](https://doi.org/10.1529/biophysj.107.121418) PMID: [18310248](https://pubmed.ncbi.nlm.nih.gov/18310248/)
54. Carbonell P, del Sol A. Methyl side-chain dynamics prediction based on protein structure. *Bioinformatics*. 2009; 25: 2552–2558. doi: [10.1093/bioinformatics/btp463](https://doi.org/10.1093/bioinformatics/btp463) PMID: [19648137](https://pubmed.ncbi.nlm.nih.gov/19648137/)
55. Liu W, Crocker E, Siminovitch DJ, Smith SO. Role of side-chain conformational entropy in transmembrane helix dimerization of glycophorin A. *Biophys J*. 2003; 84: 1263–1271. PMID: [12547806](https://pubmed.ncbi.nlm.nih.gov/12547806/)
56. Miao Y, Hong L, Yi Z, Smith JC, Zaccai neutron resilience and site-specific hydration dynamics in a globular protein. *Eur Phys J E Soft Matter*. 2013; 36: 72. doi: [10.1140/epje/i2013-13072-5](https://doi.org/10.1140/epje/i2013-13072-5) PMID: [23852576](https://pubmed.ncbi.nlm.nih.gov/23852576/)

PUBLICATION

II

Molecular mechanisms of Charcot-Marie-Tooth neuropathy linked to mutations in human myelin protein P2

Salla Ruskamo, Tuomo Nieminen, Cecilie K. Kristiansen, Guro H. Vatne, Anne Baumann, Erik I. Hallin, Arne Raasakka, Päivi Joensuu, Ulrich Bergmann, Ilpo Vattulainen & Petri Kursula

Scientific Reports 7:6510 (2017)


DOI: 10.1038/s41598-017-06781-0

Publication reprinted with the permission of the copyright holder

SCIENTIFIC REPORTS

OPEN

Molecular mechanisms of Charcot-Marie-Tooth neuropathy linked to mutations in human myelin protein P2

Salla Ruskamo¹, Tuomo Nieminen², Cecilie K. Kristiansen³, Guro H. Vatne³, Anne Baumann^{3,4}, Erik I. Hallin³, Arne Raasakka³, Päivi Joensuu⁵, Ulrich Bergmann^{1,6}, Ilpo Vattulainen^{2,7} & Petri Kursula ^{1,3}

Charcot-Marie-Tooth (CMT) disease is one of the most common inherited neuropathies. Recently, three CMT1-associated point mutations (I43N, T51P, and I52T) were discovered in the abundant peripheral myelin protein P2. These mutations trigger abnormal myelin structure, leading to reduced nerve conduction velocity, muscle weakness, and distal limb atrophy. P2 is a myelin-specific protein expressed by Schwann cells that binds to fatty acids and membranes, contributing to peripheral myelin lipid homeostasis. We studied the molecular basis of the P2 patient mutations. None of the CMT1-associated mutations alter the overall folding of P2 in the crystal state. P2 disease variants show increased aggregation tendency and remarkably reduced stability, T51P being most severe. In addition, P2 disease mutations affect protein dynamics. Both fatty acid binding by P2 and the kinetics of its membrane interactions are affected by the mutations. Experiments and simulations suggest opening of the β barrel in T51P, possibly representing a general mechanism in fatty acid-binding proteins. Our findings demonstrate that altered biophysical properties and functional dynamics of P2 may cause myelin defects in CMT1 patients. At the molecular level, a few malformed hydrogen bonds lead to structural instability and misregulation of conformational changes related to ligand exchange and membrane binding.

A multilamellar membrane structure, myelin, enwraps selected axons in the nervous system, enabling the prompt transmission of nerve impulses along the axonal membrane. Myelin contains a compact lipid-rich compartment with a unique set of membrane-associated proteins, such as myelin protein zero (MPZ), peripheral myelin protein of 22 kDa (PMP22), myelin basic protein (MBP), and myelin protein P2, and more loosely packed regions that also encompass cytoplasm. Close interplay between myelin proteins is important for the formation of cytoplasmic channels within myelin¹. In the peripheral nervous system (PNS), Schwann cells envelop axons and form insulating myelin sheaths. Defects in this fundamental structure result in chronic, severe neuropathological conditions, affecting nerve conduction velocity and neuron viability.

Charcot-Marie-Tooth disease (CMT) is one of the most common inherited human neuropathies (prevalence of 1:2500), affecting both motor and sensory nerve conduction in the PNS². Several types of CMT exist; the most common form, autosomal dominant CMT1, influences Schwann cells and myelin. In CMT1, motor and sensory nerve conduction velocities are remarkably reduced, leading to muscle weakness and atrophy in the feet and occasionally also in upper limbs. Demyelination and onion bulb formation are present in most CMT1 patients. Most commonly, CMT1a is caused by a duplication of or a point mutation in the *pmp22* gene, and 70–80% of all CMT1 cases are associated with *pmp22* mutations³. CMT1b results from mutations in the *mpz* gene and comprises 4% of all CMT1 cases. A number of other CMT1-associated genes have been described². Recently, three point mutations

¹Faculty of Biochemistry and Molecular Medicine, University of Oulu, 90220, Oulu, Finland. ²Department of Physics, Tampere University of Technology, 33720, Tampere, Finland. ³Department of Biomedicine, University of Bergen, 5020, Bergen, Norway. ⁴Division of Psychiatry, Haukeland University Hospital, 5021, Bergen, Norway. ⁵Department of Sustainable Chemistry, Technical Faculty, University of Oulu, 90570, Oulu, Finland. ⁶Biocenter Oulu, University of Oulu, 90220, Oulu, Finland. ⁷Department of Physics, University of Helsinki, 00560, Helsinki, Finland. Correspondence and requests for materials should be addressed to P.K. (email: petri.kursula@uib.no)

in the *pmp2* gene, coding for the myelin P2 protein, were linked to autosomal dominant CMT1. The I43N mutation was discovered in two families^{4,5} and T51P and I52T each in one family⁶. All patients with these mutations have reduced motor and sensory nerve conduction velocities, thinner myelin sheaths, and demyelinating axons with onion bulb formation. Symptoms also include progressive hand and foot muscle weakness and atrophy, as well as foot deformity and sensory loss in limbs^{4–6}. Although the pathological features of different CMT1 types are comparable, the molecular pathomechanisms are different⁷.

P2 is mainly expressed by Schwann cells in the PNS⁸. It is located in compact myelin, stabilizing the multilayered lipid membrane assembly. P2 is a small 15-kDa protein with a β barrel structure covered by an α -helical lid^{9,10}. It belongs to the conserved family of fatty acid-binding proteins (FABPs) and can transfer fatty acids from and to lipid membranes using a collision transfer mechanism, indicating a functional role in the lipid homeostasis of myelin¹¹. P2 may also bind cholesterol; a CRAC cholesterol binding motif is found at its C terminus^{9,12}.

Here, we show that the crystal structures of CMT1-associated P2 mutant forms remain nearly unaltered, but the stability of the mutant proteins is remarkably reduced. Mutant proteins show decreased solubility, T51P triggering the most significant effect. T51P has a reduced membrane stacking activity, while I43N and I52T maintain their ability to bind and stack lipid membranes. On the other hand, protein dynamics, as well as fatty acid and membrane binding kinetics, of all P2 mutants differ from those of wild-type P2 (P2wt). The mutations may cause defects in protein folding and the regulation of functional conformational changes, and they provide clues into ligand binding dynamics in the FABP family.

Results

In order to explore the functional and structural effects of CMT1-linked mutations in P2, we expressed and purified all three mutant proteins; I43N, T51P, and I52T. We used a range of experimental techniques together with atomistic simulations to study the effects of the mutations on P2 structure, function, and dynamics.

CMT mutations increase P2 aggregation but do not affect the overall crystal structure. In a prokaryotic expression system, all mutants showed a higher tendency to form insoluble aggregates than P2wt (Fig. 1A). Only ~5% of T51P was soluble, despite optimised cell lysis conditions. Also both I43N and I52T showed reduced solubility compared to P2wt. However, soluble forms of all mutants could be purified and eluted as a single monomeric peak in size exclusion chromatography (SEC). We used dynamic light scattering (DLS) to further investigate the aggregation tendency of P2. P2wt, I43N, and I52T remained 100% monomeric for 24 h after SEC, while T51P was 98.3% monomeric, and high-molecular-weight forms were already present (Fig. 1B). The hydrodynamic radius (R_h) of monomeric T51P was also larger compared to the other variants (Table 1).

Small-angle X-ray scattering (SAXS) data were collected to monitor possible variation in the solution structures of the patient mutants (Fig. 1C). Scattering patterns of all mutants resemble those of P2wt. Nevertheless, the radius of gyration (R_g) and maximum dimension (D_{max}) of I43N and T51P slightly deviate from P2wt, while I52T gave similar results (Table 1). The shape of the distance distribution function (Fig. 1D) differs between the variants, T51P and I52T being most divergent. This could be related to the position of the α -helical lid, the overall structure of the β barrel, and/or the level of saturation with fatty acid inside the barrel.

To address structural consequences of the mutations, we determined the respective crystal structures at high resolution (Table 2). All mutated residues are well defined in electron density. The mutations are located in the middle of the strands $\beta 2$ and $\beta 3$, in close proximity to the core of the β barrel (Fig. 1E,F). However, the overall fold of the structures is nearly identical to P2wt, with RMS deviations of 0.1–0.2 Å (C α atoms). Considering the differences in solution conformations, this is a reflection of the selection of a single low-energy conformer into the crystal lattice, closely resembling the wild-type crystal structure. All structures present a gap in the β barrel between the strands $\beta 4$ and $\beta 5$, with no hydrogen bonds formed between the strands. This is a common feature of the FABP family^{13–17}, and it is noteworthy that all the CMT1-linked P2 mutations lie close in space to this gap (Fig. 1E). The largest difference is triggered by the T51P mutation, which decreases the area of the β sheet $\beta 1$ – $\beta 4$ (Fig. 1G). The mutation hinders the carbonyl group of Ile50 from forming a hydrogen bond with the amino group of Phe65 in the $\beta 4$ strand; Pro51 also cannot form a hydrogen bond to Ser44 in the strand $\beta 2$ (Fig. 1H). Two water molecules in close proximity to the residue 51 and the $\beta 2$ and $\beta 3$ strands are not found in the crystal structure of T51P, but they exist in all other structures. I43N and I52T do not alter the main chain conformation, and neither side chain generates steric clashes. These changes from a non-polar to a polar residue do not induce large structural changes in the crystal structure. However, the amino group of the Asn43 side chain of I43N forms an extra hydrogen bond to the main chain carbonyl group of Phe5, located at the end of the short α helix at the N terminus of P2.

Mutated forms of P2 have reduced stability. Due to increased aggregation tendency, the folding of the P2 variants was examined using synchrotron radiation circular dichroism spectroscopy (SRCD). Spectra were recorded in water and in phosphate buffer (Fig. 2A). The intensity of both the positive (at 198 nm) and negative (at 218 nm) peaks varied, P2wt giving the highest and T51P the lowest signal, suggesting formation of soluble aggregates of the mutant proteins. Minor variations were also observed in the shape and x axis intersections of the spectra, mainly for T51P, indicative of lower secondary structure content or altered conformation.

In the presence of 1,2-dimyristoyl-*sn*-glycero-3-phosphocholine (DMPC): 1,2-dimyristoyl-*sn*-glycero-3-(phospho-*rac*-(1-glycerol)) (DMPG) or 1,2-dioleoyl-*sn*-glycero-3-phosphocholine (DOPC): 1,2-dioleoyl-*sn*-glycero-3-phosphatidyl-*rac*-glycerol (DOPG) vesicles, the spectra of P2 clearly changed (Fig. 2A). This phenomenon is more pronounced in water (Fig. 2A, right), where competition between lipid head groups and phosphate does not exist. In phosphate buffer (Fig. 2A, left), the positive peak at 198 nm decreased with P2wt and I52T, while I43N and T51P show opposite behavior. In water, the shape of the P2wt, I43N, and I52T spectra change considerably upon adding lipid vesicles, especially when DOPC:DOPG vesicles are introduced.

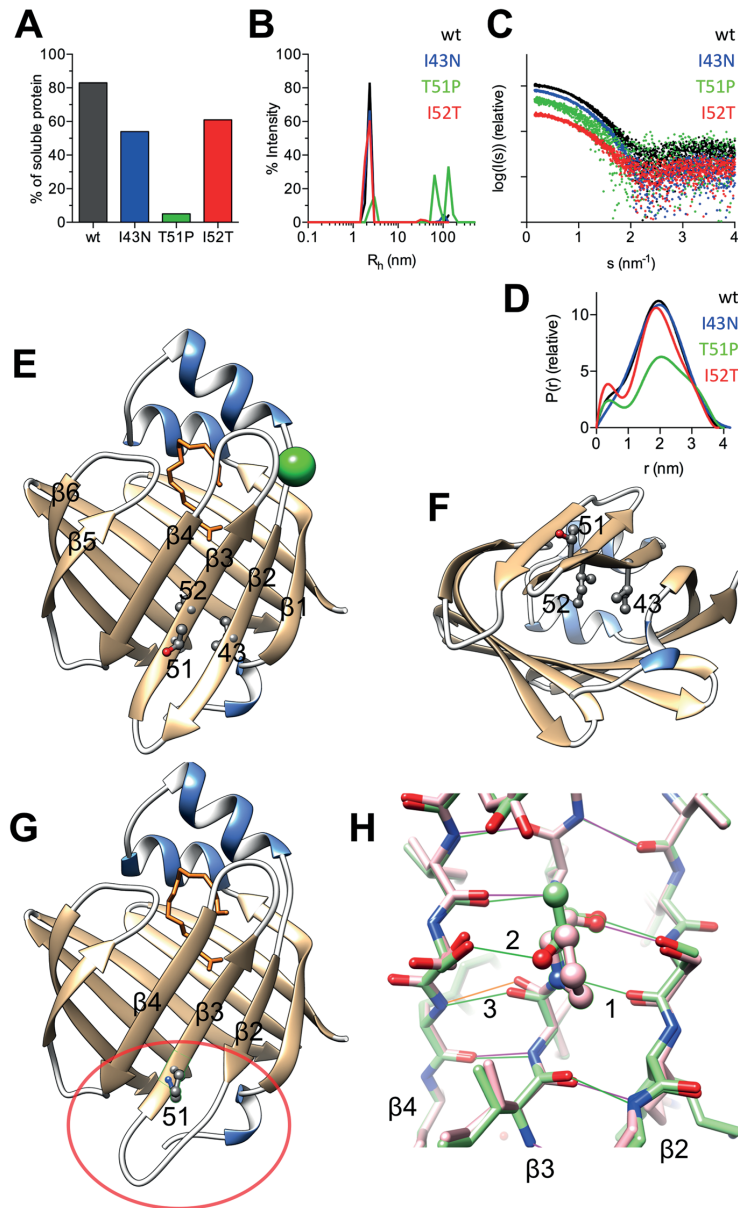


Figure 1. Structure and stability of P2. **(A)** Solubility analysis. **(B)** Dynamic light scattering indicates aggregation of T51P. Note that the curves for P2wt and I43N nearly overlap in panels B and D. **(C)** The SAXS scattering curve. **(D)** Distance distribution functions. **(E)** Crystal structure of P2 with the mutant positions labelled. The bound fatty acid is shown in orange and the anion binding site with a chloride ion (green). **(F)** The mutation hot spot viewed from the bottom. **(G)** The crystal structure of T51P. Note the decreased area of the β sheet close to the mutation; compare the circled area with the corresponding area in panel E. **(H)** Hydrogen bonds near residue 51 in wild-type (green) and T51P (pink); the shown region corresponds to the circled area in panel G. Three hydrogen bonds are labeled: 1) main-chain H bond that is lost in the mutant protein, 2) side-chain hydrogen bond lost in the mutant protein, 3) main-chain H bond that is in an unfavorable conformation in the mutant protein (orange).

Protein	DLS		SAXS			MD simulations	
	R_h (nm)	Monomeric (%)	R_g (nm)	D_{max} (nm)	V_{pore} (nm ³)	R_g apo (nm)	R_g holo (nm)
wt	2.11	100	1.45	3.9	14	1.45	1.44
I43N	2.18	100	1.55	4.0	18	1.43	1.44
T51P	2.40	98.3	1.56	4.2	13	1.50	1.45
I52T	2.22	100	1.45	3.9	12	1.43	1.45

Table 1. DLS, SAXS, and MD simulation parameters.

Mutant	I43N	T51P	I52T
<i>Data collection</i>			
Beamline	I04/Diamond	I03/Diamond	I04/Diamond
X-ray wavelength (Å)	0.9795	0.9762	0.9795
Space group	P41212	P41212	P41212
Unit cell dimensions a, b, c (Å)	65.0,65.0,101.1	66.0,66.0,100.9	64.8,64.8,101.1
α, β, γ (°)	90,90,90	90,90,90	90,90,90
Resolution range (Å)	46–1.59 (1.69–1.59)	46–1.72 (1.87–1.72)	46–1.53 (1.63–1.53)
No. unique reflections	29518 (2710)	44944 (7154)	33053 (3233)
Completeness (%)	98.7 (89.2)	99.6 (97.5)	99.6 (99.6)
Redundancy	6.6 (6.4)	6.1 (6.1)	6.0 (5.9)
R_{sym} (%)	6.7 (300)	7.4 (267)	5.1 (265)
R_{meas} (%)	7.0 (327)	8.1 (292)	5.3 (257)
$\langle I/\sigma I \rangle$	18.4 (0.7)	12.8 (0.8)	22.0 (0.7)
CC _{1/2} (%)	100 (73.4)	99.9 (67.8)	100 (72.8)
Wilson B (Å ²)	29.3	31.2	29.2
<i>Structure refinement</i>			
R_{cryst}/R_{free} (%)	18.4/21.4	16.9/19.1	17.0/20.1
RMSD bond lengths (Å)	0.007	0.006	0.007
RMSD bond angles (°)	1.0	1.0	1.1
Molprobrity score	1.24	1.57	1.97
Ramachandran favoured/outliers (%)	100/0	98.7/0	100/0

Table 2. Crystallographic data collection and structure refinement.

We further studied the thermal stability of P2 mutants using conventional CD spectroscopy (Fig. 2B). T_m analysis and CD spectra illustrate a drastic reduction of the stability of all patient mutants compared to P2wt ($T_m = +65$ °C); T51P has the lowest T_m , +41 °C, and already at +38 °C, the conformation of T51P changed and unfolding started. I43N has a T_m at +48 °C and I52T at +52 °C. Therefore, both of these mutants also have decreased thermal stability compared to P2wt.

Patient mutations modify the dynamics of all P2 mutants. Root mean square fluctuation (RMSF) analysis from atomistic molecular dynamics (MD) simulations was used to examine P2 dynamics with and without bound palmitate inside the β barrel. Palmitate-bound P2wt is generally more dynamic than its empty counterpart. The most mobile parts of P2wt are located in the loops and, to some extent, in the helical lid (Fig. 3A); these segments correspond to the portal region of FABPs. Similar behaviour was seen with palmitate-bound I43N. In MD simulations, palmitate-bound T51P is overall much more dynamic than the other P2 variants and shows strong fluctuations in the lid region as well as in the β sheets β 2-5 and the loops connecting them. The lid region and the β 3- β 4 loop of I52T also fluctuate more heavily than those of P2wt. However, when the fluctuations of ligand-free P2 are compared, P2wt seems to be the least dynamic variant. I52T shows some fluctuations at certain parts, while I43N and T51P are rather rigid. Surprisingly, T51P is the least dynamic of the apo forms (Fig. 3A). The apo form of T51P is overall less dynamic than palmitate-bound T51P. The lid region of I52T and the β 5- β 6 loop of I43N are also destabilised by palmitate, while other parts of the mutants show reduced fluctuation upon palmitate binding.

In simulations of P2, especially in the case of apo T51P, opening of the β barrel at the gap is observed (Fig. 3B). The hinge for this movement lies at Gly68 in the β 4- β 5 loop, which is one of the two absolutely conserved Gly residues across all human FABPs¹⁰. At the hinge also lies a buried water molecule, which is conserved in FABPs and was suggested to be relevant for correct folding¹⁸. It is possible that the conserved Gly residues and the water molecule also play roles in functional conformational changes in FABPs, including P2. R_g for all eight systems (four P2 forms, +/- palmitate) was estimated based on the MD simulations. The obtained values (Table 1) are in good agreement with those derived from SAXS. *Ab initio* modeling of T51P based on the SAXS data provides

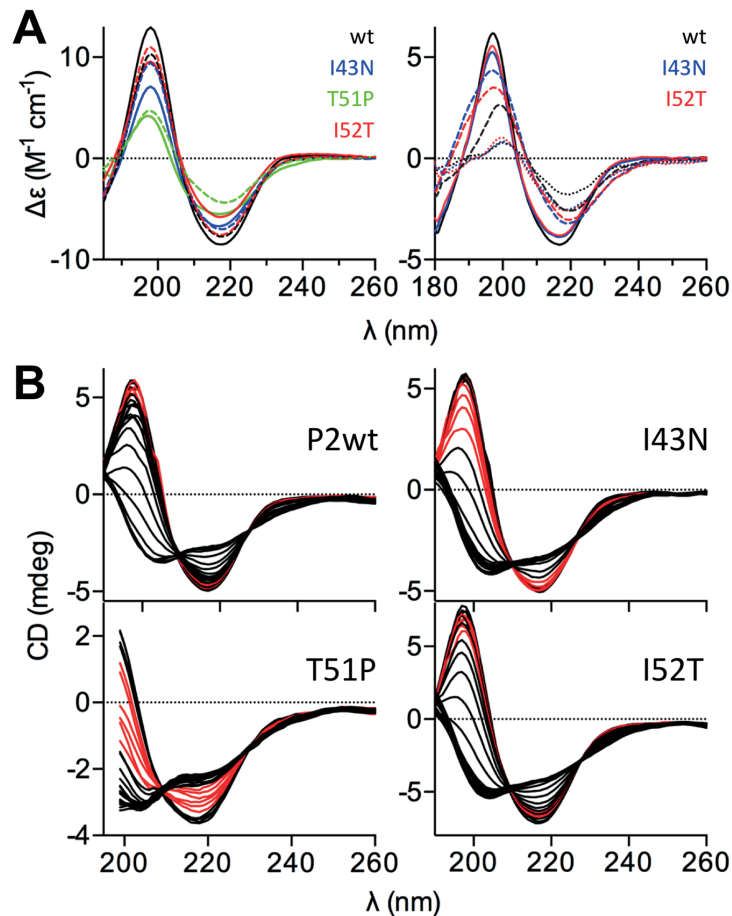


Figure 2. SRCD analysis of P2 folding and membrane interactions. (A) Left: SRCD in phosphate buffer with and without DMPC:DMPG vesicles. Right: SRCD in H₂O and with DMPC:DMPG (dashed lines) and DOPC:DOPG (dotted lines) vesicles. (B) Temperature scans of all variants. Temperatures between +40–50 °C are shown in red for clarity.

a shape very similar to that observed in the MD simulation (Fig. 3C), confirming the presence of an open, more extended conformation, of P2 in solution. In addition, multicomponent analysis of the SAXS data indicates a 7% fraction of open conformation of T51P in solution, while the other P2 forms exist in the closed conformation.

We also calculated the number of water molecules inside the P2 barrel during each simulation. The average number of water molecules inside unliganded P2 was 27.7, 30.5, 23.7, and 30.4 (for P2wt, I43N, T51P and I52T, respectively). For palmitate-bound P2 forms, the respective numbers of water molecules were 21.0, 22.1, 29.1, and 22.0. In both cases, T51P differs from the other variants, interestingly having less water molecules within the β barrel without than with palmitate inside. Here, the behaviour of the Ile mutants resemble each other but slightly differ from P2wt. These values are in accordance with studies on FABP, whereby faster exchange of water was observed for liganded FABP than for apo-FABP¹⁹ - a major route for water flow between bulk solvent and the internal cavity was suggested to be the gap between the strands β_4 and β_5 . Both the apparent lower water content of apo T51P as well as its low RMSF during the MD simulation can be explained by the observation that the unliganded T51P structure opens up early in the simulation and remains in the open conformation.

Fatty acid binding in P2 CMT mutants. P2 belongs to the family of FABPs, and in all crystal structures of human P2, there is a fatty acid inside the β barrel^{9,10,20,21}. Also in the crystal structures of all mutant proteins studied here, a fatty acid, modelled as palmitate, is visible inside the β barrel. P2 captures abundant fatty acids during expression in *E. coli*^{9,10}. With our earlier atomic-resolution crystallographic data, we modelled the fatty acid component as a mixture of palmitate and *cis*-vaccenate¹⁰.

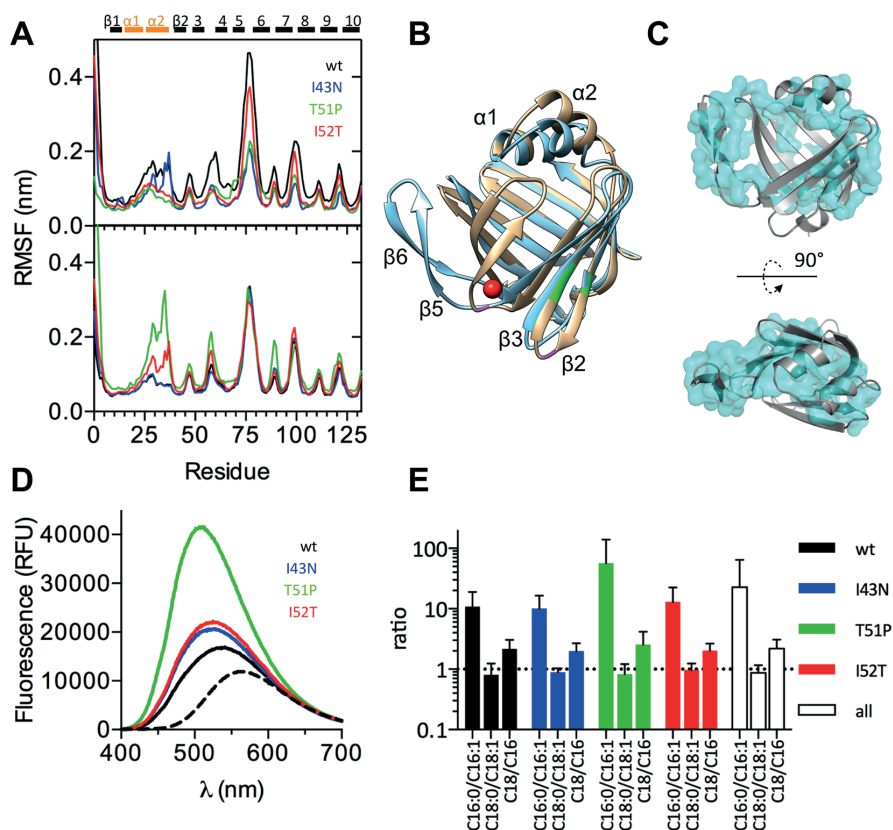


Figure 3. Dynamics, open conformation, and fatty acid binding. (A) RMS fluctuation of apo (top) and liganded (bottom) forms. Above the graphs, the secondary structure elements of P2 are shown (black, strand; orange, helix). (B) Structure of P2wt (light brown) superimposed on the open conformation of T51P seen in simulations (blue). The two conserved FABP Gly residues in the $\beta 2$ - $\beta 3$ and $\beta 4$ - $\beta 5$ loops are shown in magenta, the positions of the mutations in green, and the “structural” water molecule bound inside the $\beta 4$ - $\beta 5$ loop in FABPs in red. (C) Comparison of the open conformation (cartoon) and the SAXS envelope from T51P data (blue transparent surface) from two orientations. (D) Fluorescence spectra of DAUDA with $10\ \mu\text{M}$ proteins. (E) LC-MS fatty acid analysis. All P2 variants prefer either palmitate (C16:0) or 18-carbon fatty acids (C18:0 and C18:1) Recombinant P2 carries more C18 than C16 fatty acids.

To study fatty acid binding, we performed end-point binding assays with a fluorescent fatty acid derivative probe, 11-dansylaminoundecanoic acid (DAUDA)²². The peak maxima clearly increase and shift in the presence of P2, indicating an interaction involving a non-polar environment between DAUDA and all P2 variants (Fig. 3D). This phenomenon is most pronounced with T51P, but also I43N and I52T show higher fluorescence than P2wt. In this experimental setup, T51P seems to bind to DAUDA more effectively than the other mutants or P2wt, which might be related to its higher tendency to open.

Since the structure and dimensions of DAUDA diverge from natural fatty acids, we used liquid chromatography-mass spectrometry (LC-MS) to investigate the fatty acids bound to P2. Fatty acids with 16–20 carbons without or with a double bond were monitored. The total amount of bound fatty acids was similar between all the P2 variants, and C16 and C18 fatty acids together comprise nearly 100% of the total fatty acid content. We compared the amount of saturated and non-saturated C16 and C18 fatty acids, and noted the fatty acid content of all variants was nearly identical (Fig. 3E). P2 contains more C18 (60–70%) than C16 fatty acids (30–40%). Palmitate is the preferred C16 ligand, while for C18, nearly equal amounts of saturated and non-saturated fatty acid are observed. The result validates our high-resolution model¹⁰, in which we earlier built in palmitate (C16:0) and *cis*-vaccenate (C18:1) with partial occupancies.

P2 binding to immobilised lipid vesicles. The binding of P2 onto lipid membrane surfaces was studied using surface plasmon resonance (SPR) with two different lipid compositions, differing only in the identity of the hydrocarbon chains of the lipids (Fig. 4). SPR was not carried out with the T51P mutant due to its tendency

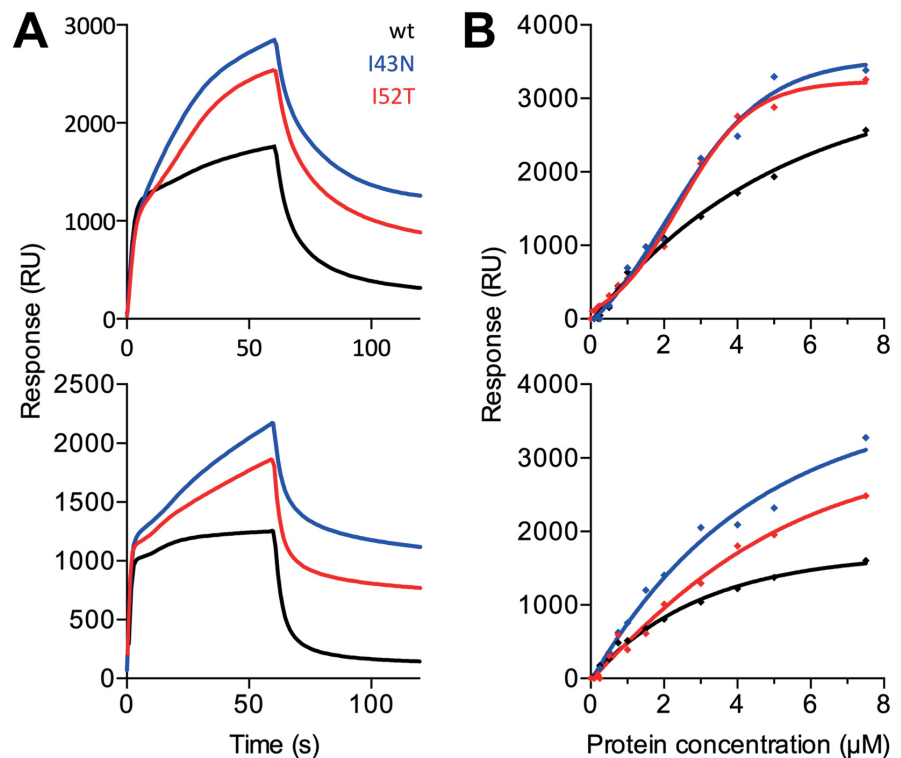


Figure 4. Membrane surface binding. (A) DMPC:DMPG (top) and DOPC:DOPG (bottom) sensorgrams with injection of 4 μM protein. (B) DMPC:DMPG (top) and DOPC:DOPG (bottom) fits for a protein titration.

P2 variant	P2wt		I43N		I52T	
	DMPC:DMPG	DOPC:DOPG	DMPC:DMPG	DOPC:DOPG	DMPC:DMPG	DOPC:DOPG
Two-state reaction	6.03 \pm 1.05	2.44 \pm 0.54	3.77 \pm 0.11	3.48 \pm 2.64	6.37 \pm 1.01	2.53 \pm 1.28
Sigmoidal model	4.78 \pm 0.45	2.59 \pm 0.62	3.25 \pm 2.69	5.24 \pm 1.22	0.95 \pm 0.06	3.12 \pm 0.65

Table 3. Membrane surface affinity of P2 deduced from SPR data. The values are apparent K_d in μM , based on two separate experiments.

to aggregate. P2wt and the I43N and I52T mutants all bound to membranes with affinities in the 2–6 μM range, irrespective of the lipid composition (Table 3). Despite similar apparent affinity, the kinetics of the wild-type and mutant proteins were different, and in fact, more of the mutant proteins eventually bound to the membrane, giving a continuous increase in response during the injection (Fig. 4A). This could be a sign of aggregation of the mutants onto the lipid bilayer after initial binding. P2wt, on the other hand, bound rapidly to the membrane, reaching a plateau by the end of the injection, and dissociated fast. All these features were similar between membranes made of DMPC:DMPG and DOPC:DOPG. The result is an indication of possible membrane-induced aggregation of mutant P2 forms. The behaviour of the P2 mutants resembles somewhat the kinetics shown by another major myelin protein, MBP, which folds onto the membrane surface, forming an amorphous phase of protein, and dissociates very slowly^{23,24}.

All mutants stack lipid membranes, but T51P is less active. In compact myelin, P2 is located in the cytoplasmic leaflet, interacting with two apposing membranes. An important feature of P2 is to bind lipid membranes and to stack them into multilayered systems. To test whether the mutant variants are able to attach lipid membranes together, we used a lipid vesicle aggregation assay and measured the increase in the turbidity of a lipid vesicle solution caused by P2. The results demonstrate that both Ile mutants can bind and stack lipid membranes as efficiently as P2wt (Fig. 5A). However, T51P showed a reduced capability to stack lipid membranes; the turbidity of the vesicle-T51P mixture was approximately half of that of the other samples (Fig. 5A). With

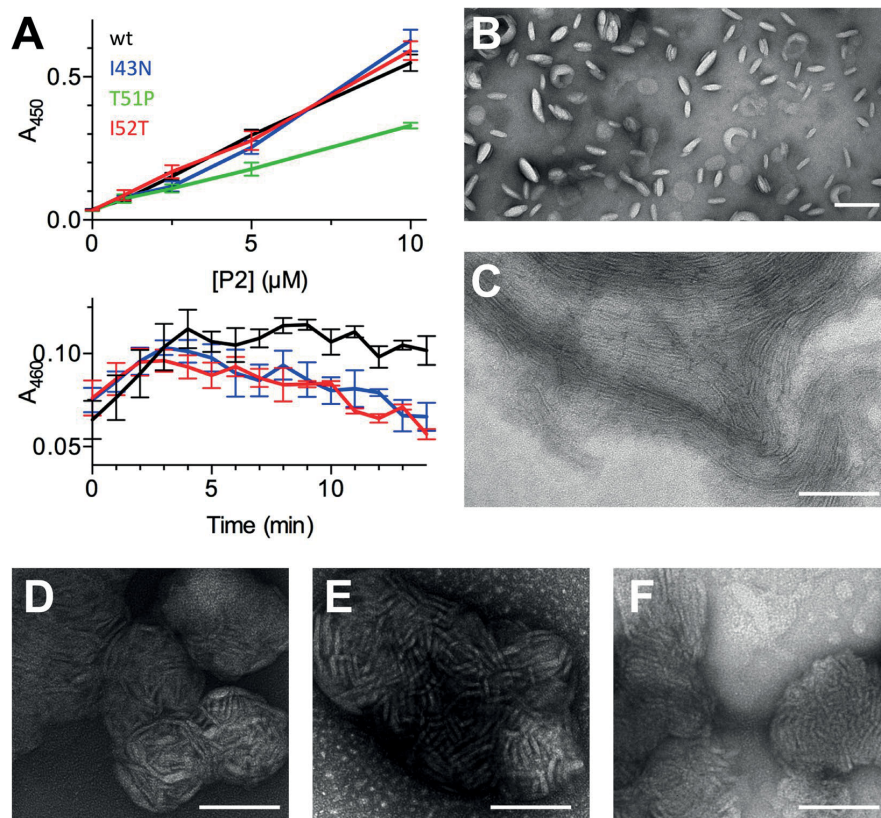


Figure 5. Membrane stacking by P2. (A) Top: end-point turbidity assay with all P2 variants. Bottom: time dependence of turbidity for P2wt and the Ile mutants. (B–F) Negatively stained TEM images of DMPC:DMPG vesicles (B) with P2wt (C) and mutants (D–I43N, E–T51P, F–I52T). Scale bar: 100 nm.

extended incubation, the Ile mutants slowly lost the turbidity, as opposed to P2wt, hinting at different stability of the proteolipid complex (Fig. 5B). We also visualised membrane stacks induced by P2 using transmission electron microscopy (TEM) and negative staining. In contrast to a control sample with only single unilamellar DMPC:DMPG vesicles (Fig. 5B), all P2 variants induced the formation of large clusters of multilamellar membrane stacks (Fig. 5C–F).

Discussion

Recently, three P2 point mutations were shown to result in the most common heritable human peripheral neuropathy, CMT. All P2 patient mutations trigger an autosomal dominant form of demyelinating CMT1^{4–6}. P2 mutations are located near each other in the structure, in close proximity to the fatty acid binding pocket and the gap between the strands β 4 and β 5. Comparing the sequences of all 12 human FABPs, it can be seen that the mutated residues are conserved in most human FABPs, especially those with a collision-type ligand transfer mechanism¹⁰. Based on our work, all CMT1-associated P2 mutant forms maintain their overall fold in the crystal state, but their stability is significantly reduced, and fatty acid and lipid membrane binding altered, compared to P2wt.

Most forms of CMT1 are caused by duplication or mutation of the *pmp22* gene, thought to lead to misfolding and aggregation of PMP22 in the ER of myelinating Schwann cells²⁵. The three P2 mutations (I43N, T51P, and I52T) studied here increase the tendency of P2 to form insoluble aggregates, when expressed in *E. coli*. Even though the prokaryotic expression system differs from the natural environment inside human Schwann cells, it can provide relevant information when comparing disease-associated forms of human proteins.

The secondary structure content of T51P in solution was lower than for the other variants. All forms of P2 showed conformational changes upon lipid vesicle binding. These changes, also seen before with P2wt¹⁰, may originate from the α -helical lid, which interacts with the head groups of lipids and may be partially buried inside the lipid membrane. The changes could also result from a membrane-induced opening of the β barrel, leading to possible ligand exchange with the membrane. The results indicate that all P2 variants interact with lipid membranes, but as seen with SPR, the mutants are different in their respective lipid binding dynamics.

Importantly, the thermal stability of all three CMT-linked P2 variants is dramatically reduced compared to P2wt. This finding supports the results from the solubility studies; reduced protein stability leads to partial or complete unfolding and the formation of protein aggregates. Overall, the T51P mutation has the most striking effect on the biophysical properties of P2. These results raise a question whether these mutants are able to fold properly in Schwann cells, or if the mutations lead to misfolding and protein accumulation.

The crystal structures of the disease-associated mutants are highly similar to P2wt, also regarding the fatty acid binding pocket^{9,10}, and differences are limited to 1–2 hydrogen bonds near the mutation site. Nevertheless, the fatty acid binding properties of all mutants differ from those of P2wt. Based on fluorescent probe assays, all three mutants bind fatty acids more effectively than P2wt, and T51P causes the highest change in DAUDA fluorescence. As DAUDA has a fairly large and rigid dansyl group at one end of the molecule, these results may suggest that T51P favours larger ligands than P2wt; the result can also reflect the increased open/close dynamics of the T51P variant. Different kinds of kinetics may come to play when the fatty acid ligand is replaced in this experiment, including affinities towards various ligands and different conformational dynamics.

RMSF analysis of MD simulations demonstrates altered dynamic properties for all disease mutants. Fatty acid-bound T51P is clearly more dynamic than P2wt and the other two mutants, and liganded T51P has more water molecules inside the β barrel than other palmitate-bound P2 variants. This is presumably the consequence of an increased flexibility of the α -helical lid and the β barrel structure of T51P, which at least to some extent arises from the lack of proper hydrogen bonds in the β sheet β 1–4 (Fig. 1). The opening of the β barrel observed in the MD simulations and in solution SAXS is expected to be thermodynamically realistic, since no main-chain hydrogen bonds of the barrel need to be broken for the opening to occur. It is likely that we are, indeed, observing a functional mechanism for FABP opening, in a process that is complementary with ligand exchange. Such a mechanism was suggested earlier²⁶, but to our knowledge, it has not been observed for FABPs. It is obvious that several factors may affect such conformational changes, including the bound ligand, contact to a membrane surface, and the presence of mutations. The opening of the β barrel could also be linked to misfolding and/or increased β aggregation, as observed for the T51P mutant.

A similar functional opening of a β barrel on the side has been observed for the bacterial outer membrane integral membrane protein BamA^{27,28}. The barrel opens into the membrane, and the opening is believed to facilitate ligand exchange, similarly to the mechanism proposed here for myelin P2 and the FABP family. In the case of BamA, hydrogen bonds exist between the β strands in the closed state²⁸, while in P2, no direct main-chain hydrogen bonds are observed even when the gap is closed. Lateral opening of the structure could present a general means of ligand exchange in β -barrel proteins.

The altered biochemical and dynamic properties of the α -helical lid, the β barrel, and the internal binding pocket of the P2 mutants may also affect the binding of other possible ligands, including cholesterol, which is bulkier than fatty acids. Cholesterol is highly abundant in myelin, and it has a rate-limiting role in myelin compaction and protein trafficking in Schwann cells²⁹. Schwann cells are sensitive towards changes in the stoichiometry of their membrane components; for proper myelin assembly and especially myelin maintenance, precise amounts of different lipids are required³⁰. Thus, altered fatty acid binding profiles and kinetics of membrane binding by the P2 mutants may lead to critical defects in Schwann cells and myelin stability.

P2 is localised in compact myelin, and it spontaneously stacks lipid membranes³¹. SPR showed that the mutant proteins bound to membrane surfaces, but had kinetics distinct from the wild-type protein, possibly indicating membrane-induced aggregation. Also all disease-associated forms of P2 induce the stacking of lipid membranes, as seen using TEM. A lower efficiency of the mutants to induce stable lipid membrane stacking could have severe effects on myelin compaction and stability.

Genetic knockout studies revealed changes in the lipid profile of PNS myelin in P2-deficient mice¹¹, which emphasises the contribution and importance of P2 to lipid homeostasis of PNS myelin. In addition, all three CMT1-linked patient mutations disrupt the multilayered structure of myelin^{4–6}. The altered stability, dynamics, and fatty acid/lipid membrane binding of the disease-associated P2 protein variants may be involved in CMT1 etiology and give rise to myelin defects, including abnormal myelin compaction and irregular myelin sheaths, in P2-linked CMT1 patients.

To conclude, we have carried out a detailed characterisation of CMT1-linked P2 mutant proteins and observed differences in their respective structures, functional properties, and dynamics. While the crystal structures of all variants are very similar, the mutant variants show clear structural changes in solution and simulations, as well as functional and stability deficits. The pathogenic point mutations drastically lower the stability of the mutant protein variants, which also have altered ligand- and membrane-binding properties. The mutations may also affect the functional dynamics of the FABP β barrel, whereby the observed opening of the gap between strands β 4 and β 5 may represent a general ligand entry mechanism in the protein family.

Methods

Mutagenesis, protein expression, and purification. Human P2 with an N-terminal His₆ tag followed by a Tobacco Etch virus (TEV) protease cleavage site in the pTH27 vector⁹ was used as a template in mutagenesis to produce expression constructs with the c.T128A (p.I43N), c.C151A (p.T51P), and c.T155C (p.I52T) mutations. Mutagenesis was carried out using the QuikChange Site-Directed Mutagenesis protocol, and all mutations were confirmed by DNA sequencing. Proteins were expressed in *E. coli* BL21 RIPL (DE3) cells in ZYM-5052 autoinduction medium³² with 100 μ g/ml carbenicillin and 34 μ g/ml chloramphenicol at +18 °C for 66 h. Cells were harvested and suspended in lysis buffer (0.3 M NaCl, 10 mM imidazole, 50 mM HEPES pH 7.5). Cells were lysed by sonication, and insoluble material was pelleted by centrifugation (30000 g, 40 min, at +4 °C). The soluble fraction was then mixed with the HisPur Ni-NTA Resin (Thermo Fisher Scientific) at +4 °C for 1 h. The resin was washed twice with washing buffer (0.3 M NaCl, 40 mM imidazole, 50 mM HEPES pH 7.5) using centrifugation (500 g, 5 min, at +4 °C) and then transferred into a gravity-flow column and further washed with 50 ml of washing

buffer. P2 was eluted with elution buffer (500 mM imidazole, 0.3 M NaCl, 50 mM HEPES pH 7.5). To cleave the His₆ tag, 33 nmol of recombinant TEV protease³³ were added. Imidazole was removed by dialysis through 6000–8000 MWCO dialysis tubing (SpectraPor) against 0.3 M NaCl, 1 mM DTT, 20 mM HEPES pH 7.5 at +4 °C for 16 h. Both TEV and the cleaved His₆ tag were removed with reverse chromatography using HisPur Ni-NTA. Finally, P2 was purified with SEC using the dialysis buffer and a Superdex 75 pg 16/600 column (GE Healthcare) and concentrated with an Amicon Ultra 15, MWCO 10 kDa concentrator (Millipore). In T51P purification, all buffers, excluding the SEC buffer, also contained 10% glycerol to maintain the protein soluble during purification.

Protein crystallisation, data collection, and structure determination. P2 mutants were crystallised at +4 or +20 °C using the sitting drop vapour diffusion method, while the concentrations of the I43N, T51P, and I52T mutants were 8.5, 6.2, and 5.5 mg/ml, respectively. 0.3 M NaCl, 10% glycerol, 20 mM HEPES pH 7.5 was used as the protein buffer and 100 µl of 2.1 M DL-malic acid pH 7.25–7.5 as the reservoir solution, with 600-nl drops containing an equal volume of reservoir and protein. Diffraction data were collected at 100 K on beamline I03 and I04 at the Diamond Light Source, Didcot, UK, and processed using XDS³⁴. The structures were solved by molecular replacement using the human P2 structure (PDB entry 4BVM¹⁰) as a search model in Phaser³⁵. The structures were refined and built using phenix.refine³⁶ and Coot³⁷. The refined coordinates and structure factors were deposited at the PDB with the entry codes 5N4M (I43N), 5N4P (I52T), and 5N4Q (T51P).

Small-angle X-ray scattering. Synchrotron SAXS data were collected on beamline P12 at the PETRAIII storage ring, DESY, Hamburg, Germany. 0.6–4.1 mg/ml P2wt, I43N, and I52T were studied in a buffer containing 0.3 M NaCl, 20 mM HEPES pH 7.5, and T51P in a buffer containing 0.3 M NaCl, 5% glycerol, 20 mM HEPES pH 7.5. Data were processed and further analysed using the ATSAS program package³⁸.

Protein aggregation analysis and dynamic light scattering. Samples from soluble and insoluble fractions were taken and run on SDS-PAGE. Intensities of the P2 protein bands were determined using ImageJ³⁹. Soluble fractions were then calculated (%). DLS measurements were conducted as triplicates at +25 °C with protein concentrations of 0.6–0.9 mg/ml in a buffer containing 0.3 M NaCl, 20 mM HEPES pH 7.5, using the DynaPro Plate Reader II (Wyatt). After SEC, the proteins were stored on ice for 24 h before DLS measurements.

Circular dichroism spectroscopy. SRCD was carried out on the DISCO (SOLEIL synchrotron, Paris) and UV-CD12 (ANKA synchrotron, Karlsruhe) beamlines. Proteins were first dialysed into 10 mM sodium phosphate pH 7.5 or dH₂O. SRCD spectra were measured at +30 °C using 0.2 mm pathlength quartz cuvettes with protein concentrations of 17–21 µM (~0.3 mg/ml). Spectra for the P2 variants were also recorded in the presence of unilamellar vesicles containing a 1:1 molar ratio of DMPC and DMPG, or DOPC and DOPG. The molar protein:lipid ratio was 1:100. Thermal stability measurements were carried out using a Chirascan Plus CD spectropolarimeter (Applied Photophysics). Proteins were first diluted into 10 mM sodium phosphate buffer (pH 7.5) to final concentrations of 3.4 µM (50 µg/ml). CD spectra were then recorded at 195–260 nm with a ramping rate of 1 °C/min between +22–90 °C. The melting temperatures (T_m) were calculated using Global 3 (Applied Photophysics).

Atomistic molecular dynamics simulations. The protein with bound palmitate was obtained from the PDB entry 4BVM¹⁰ and converted to the CHARMM36 force field⁴⁰. The topology for P2wt was directly obtained from the conversion. The point mutations (I43N, T51P, and I52T) were constructed from P2wt. Water molecules were modeled using the TIP3P model⁴¹.

Eight different systems were studied: P2wt and its point-mutated forms I43N, T51P, and I52T, all with and without a bound palmitate molecule inside the binding pocket. The proteins were simulated in solvated cubic simulation boxes with sizes of approximately $8 \times 8 \times 8 \text{ nm}^3$ and with 16000 water molecules, in accordance to our previous study⁴². Counter-ions (11 Cl⁻ in palmitate-free proteins and 10 Cl⁻ in proteins with palmitate) were included to neutralise the total charge of the system.

The MD simulations were carried out under NpT conditions. Temperatures were coupled using the velocity-rescale (v-rescale) method, with separate temperature coupling for protein and solvent. Reference temperatures of 300 K were used with coupling time constants of 2.0 ps. Pressure coupling was done isotropically with the isothermal Parrinello-Rahman barostat⁴³ at a reference pressure of 1 bar with a coupling time constant of 2.0 ps and isothermal compressibility of $4.5 \times 10^{-5} \text{ bar}^{-1}$. All bonds were constrained with the LINCS algorithm⁴⁴. Periodic boundary conditions were used. A cut-off radius of 1.0 nm was introduced for the neighbor list, the Lennard-Jones interactions, and the non-bonded interactions. The particle-mesh Ewald (PME) method⁴⁵ with cubic interpolation was used for calculating long-range electrostatics, using a spacing of 0.16 nm for the Fourier grid.

All simulations were conducted using GROMACS 4.6.7⁴⁶. A time step of 2 fs was used in integrating the equations of motion. All systems were first energy-minimised with the steepest descent algorithm and then simulated for a total of 2.5 µs each. An equilibration period of 500 ns was removed from the beginning of each trajectory, using the final 2 µs for analysis. The trajectory coordinates were saved every 50 ps.

The RMSF was calculated for each residue using the GROMACS tool `g_rmsf`. The RMSF of a residue shows its stability; the larger the value, the more mobile it is. Therefore, by calculating the RMSF, we can determine, which parts of the protein are most affected by the mutation and/or the presence of the ligand. Water analysis was done with the GROMACS tool `trjorder` by calculating the number of water molecules within 0.9 nm of the center of mass of the protein backbone (the radius of the P2 barrel is about 1.0 nm) at every time step over the course of the simulation.

Fatty acid binding assay. Fatty acid binding to P2 was studied with a fluorescent fatty acid analog, DAUDA. 10 μ M DAUDA and 10 μ M P2 were incubated for 1 h in 150 mM NaCl, 10 mM HEPES pH 7.5 at +23 °C. Fluorescence emission spectra were recorded with excitation at 345 nm and emission between 400–700 nm, using a Tecan Infinite M1000Pro plate reader.

Liquid chromatography-mass spectrometry for fatty acids. 20- μ l aliquots of protein solutions adjusted to the same concentration (30 μ M; 0.45 mg/ml) were acidified with 1 μ l formic acid and then precipitated with 20 μ l of acetone. Samples came from 2–3 separate production batches for each variant, and each sample was analysed 1–2 times. After centrifugation, fatty acids were extracted into 20 μ l of chloroform, the phases were separated by short centrifugation, and 5 μ l of the chloroform phase was subjected to LC-MS using an Acquity UPLC system coupled to a SynaptG1 Q-TOF type mass spectrometer. The chromatography column was a BEH C18, 2.1 \times 100, eluted with a gradient of acetonitrile (A: acetonitrile, B: 10 mM ammonium acetate 10% A to 100% A in 8 min, flow 0.3 ml/min). The mass spectrometer was operated in negative mode, collecting 0.2-s scans in centroid mode from m/z 50 to 1000. LC-MS was performed at the Proteomics and protein analysis core facility of Biocenter Oulu.

Surface plasmon resonance. SPR assays were performed using BiacoreT200 (GE Healthcare) for P2wt as well as the I43N and I52T mutants. Due to its low stability and tendency to aggregate, T51P was not used in SPR. 1 mM DOPC:DOPG (1:1) and DMPC:DMPG (1:1) vesicles in a buffer containing 150 mM NaCl and 10 mM HEPES pH 7.5 were immobilised on an L1 sensor chip (GE Healthcare) according to the manufacturer's instructions. The surface was then saturated with an injection of 1 μ M bovine serum albumin (BSA). Lipid immobilisation and BSA injection were done for each SPR cycle. Duplicate injections of P2wt and the mutants at 0.1–10 μ M, using 150 mM NaCl, 10 mM HEPES pH 7.5 as the running buffer, were carried out at +30 °C. Results were analysed with BiaEvaluation (GE Healthcare) using a kinetic two-state binding model as well as steady-state affinity. Due to the shape of the binding curves, fitting was also done using a sigmoidal 4-parameter model

$$f = y_0 + \frac{a}{(1 + \exp(-(x - x_0)/b))} \quad (1)$$

in SigmaPlot.

Vesicle binding assays. For a single-point assay, 0–10 μ M P2 was mixed with 0.5 mM unilamellar vesicles containing a 1:1 molar ratio of DMPC:DMPG in 150 mM NaCl, 10 mM HEPES pH 7.5, and the samples were incubated for 35 min at +30 °C. The turbidity of the vesicle-protein solutions was measured with a Tecan Infinite M1000 Pro plate reader using absorbance at 450 nm at +30 °C. The assay was repeated 3–5 times with all concentrations and P2 forms.

In order to study the time course of vesicle aggregation, 0.5 mM DMPC:DMPG vesicles were mixed with 5 μ M P2 in buffer containing 150 mM NaCl and 10 mM HEPES (pH 7.5). A VersaMax microplate reader (Molecular Devices) was used to measure the turbidity at 1-min intervals, shaking before each measurement. The temperature was set at +30 °C and the wavelength at 460 nm. The difference of 10 nm in the wavelength in the above two experiments was not considered to affect the outcome, as the measurement follows turbidity of the sample.

Transmission electron microscopy. 34 μ M (0.5 mg/ml) P2 was mixed with 740 μ M (0.5 mg/ml) DMPC:DMPG (1:1) unilamellar vesicles, and the samples were incubated at +22 °C for 1 h. 4- μ l samples were then pipetted onto glow-discharged carbon-coated copper grids, and after incubating for 1 min, excess solution was removed with filter paper. After 4 washes in droplets of dH₂O, samples were negatively stained with two drops of 2% uranyl acetate for 12 s in each drop and air-dried. TEM images were recorded using a Tecnai G2 Spirit 120 kV instrument equipped with a Quamesa CCD camera (Olympus Soft Imaging Solutions) at the EM core facility of Biocenter Oulu.

Data availability. The crystal structure coordinates and structure factors are available at the PDB with the entry codes 5N4M (I43N), 5N4P (I52T), and 5N4Q (T51P). Other datasets analysed during the current study are available from the corresponding author upon reasonable request.

References

1. Snaidero, N. *et al.* Antagonistic Functions of MBP and CNP Establish Cytosolic Channels in CNS Myelin. *Cell. Rep.* **18**, 314–323 (2017).
2. Rossor, A. M., Polke, J. M., Houlden, H. & Reilly, M. M. Clinical implications of genetic advances in Charcot-Marie-Tooth disease. *Nat. Rev. Neurol.* **9**, 562–571 (2013).
3. Rossor, A. M., Tomaselli, P. J. & Reilly, M. M. Recent advances in the genetic neuropathies. *Curr. Opin. Neurol.* **29**, 537–548 (2016).
4. Gonzaga-Jauregui, C. *et al.* Exome Sequence Analysis Suggests that Genetic Burden Contributes to Phenotypic Variability and Complex Neuropathy. *Cell. Rep.* **12**, 1169–1183 (2015).
5. Hong, Y. B. *et al.* A Mutation in PMP2 Causes Dominant Demyelinating Charcot-Marie-Tooth Neuropathy. *PLoS Genet.* **12**, e1005829 (2016).
6. Motley, W. W. *et al.* De novo PMP2 mutations in families with type 1 Charcot-Marie-Tooth disease. *Brain* **139**, 1649–1656 (2016).
7. Kamholz, J. *et al.* Charcot-Marie-Tooth disease type 1: molecular pathogenesis to gene therapy. *Brain* **123**, 222–233 (2000).
8. Trapp, B. D., Dubois-Dalq, M. & Quarles, R. H. Ultrastructural localization of P2 protein in actively myelinating rat Schwann cells. *J. Neurochem.* **43**, 944–948 (1984).
9. Majava, V. *et al.* Structural and functional characterization of human peripheral nervous system myelin protein P2. *PLoS One* **5**, e10300 (2010).
10. Ruskamo, S. *et al.* Atomic resolution view into the structure-function relationships of the human myelin peripheral membrane protein P2. *Acta Crystallogr. D Biol. Crystallogr.* **70**, 165–176 (2014).

11. Zenker, J. *et al.* A role of peripheral myelin protein 2 in lipid homeostasis of myelinating Schwann cells. *Glia* **62**, 1502–1512 (2014).
12. Sedzik, J. & Jastrzebski, J. P. High-resolution structural model of porcine P2 myelin membrane protein with associated fatty acid ligand: fact or artifact? *J. Neurosci. Res.* **89**, 909–920 (2011).
13. Armstrong, E. H., Goswami, D., Griffin, P. R., Noy, N. & Ortlund, E. A. Structural basis for ligand regulation of the fatty acid-binding protein 5, peroxisome proliferator-activated receptor beta/delta (FABP5-PPARbeta/delta) signaling pathway. *J. Biol. Chem.* **289**, 14941–14954 (2014).
14. Howard, E. I. *et al.* High-resolution neutron and X-ray diffraction room-temperature studies of an H-FABP-oleic acid complex: study of the internal water cluster and ligand binding by a transferred multipolar electron-density distribution. *IUCr* **3**, 115–126 (2016).
15. Sacchettini, J. C., Gordon, J. I. & Banaszak, L. J. Crystal structure of rat intestinal fatty-acid-binding protein. Refinement and analysis of the *Escherichia coli*-derived protein with bound palmitate. *J. Mol. Biol.* **208**, 327–339 (1989).
16. Sharma, A., Yogavel, M. & Sharma, A. Utility of anion and cation combinations for phasing of protein structures. *J. Struct. Funct. Genomics* **13**, 135–143 (2012).
17. Gonzalez, J. M. & Fisher, S. Z. Structural analysis of ibuprofen binding to human adipocyte fatty-acid binding protein (FABP4). *Acta Crystallogr. F Struct. Biol. Commun.* **71**, 163–170 (2015).
18. Lkic, V. A., Juranic, N., Macura, S. & Prendergast, F. G. A “structural” water molecule in the family of fatty acid binding proteins. *Protein Sci.* **9**, 497–504 (2000).
19. Bakowies, D. & van Gunsteren, W. F. Simulations of apo and holo-fatty acid binding protein: structure and dynamics of protein, ligand and internal water. *J. Mol. Biol.* **315**, 713–736 (2002).
20. Lehtimäki, M., Laulumaa, S., Ruskamo, S. & Kursula, P. Production and crystallization of a panel of structure-based mutants of the human myelin peripheral membrane protein P2. *Acta Crystallogr. Sect. F Struct. Biol. Commun.* **68**, 1359–1362 (2012).
21. Laulumaa, S. *et al.* Production, crystallization and neutron diffraction of fully deuterated human myelin peripheral membrane protein P2. *Acta Crystallogr. F Struct. Biol. Commun.* **71**, 1391–1395 (2015).
22. Wilkinson, T. C. & Wilton, D. C. Studies on fatty acid-binding proteins. *The binding properties of rat liver fatty acid-binding protein. Biochem. J.* **247**, 485–488 (1987).
23. Aggarwal, S. *et al.* Myelin membrane assembly is driven by a phase transition of myelin basic proteins into a cohesive protein meshwork. *PLoS Biol.* **11**, e1001577 (2013).
24. Wang, C. *et al.* Charge isomers of myelin basic protein: structure and interactions with membranes, nucleotide analogues, and calmodulin. *PLoS One* **6**, e19915 (2011).
25. Niemann, A., Berger, P. & Suter, U. Pathomechanisms of mutant proteins in Charcot-Marie-Tooth disease. *Neuromolecular Med.* **8**, 217–242 (2006).
26. Zanutti, G., Feltre, L. & Spadon, P. A possible route for the release of fatty acid from fatty acid-binding protein. *Biochem. J.* **301**, 459–463 (1994).
27. Noinaj, N. *et al.* Structural insight into the biogenesis of b-barrel membrane proteins. *Nature* **501**, 385–390 (2013).
28. Noinaj, N., Kuszak, A. J., Balusek, C., Gumbart, J. C. & Buchanan, S. K. Lateral opening and exit pore formation are required for BamA function. *Structure* **22**, 1055–1062 (2014).
29. Saher, G., Quintes, S. & Nave, K. A. Cholesterol: a novel regulatory role in myelin formation. *Neuroscientist* **17**, 79–93 (2011).
30. Schmitt, S., Castelvetri, L. C. & Simons, M. Metabolism and functions of lipids in myelin. *Biochim. Biophys. Acta* **1851**, 999–1005 (2015).
31. Suresh, S., Wang, C., Nanekar, R., Kursula, P. & Edwardson, J. M. Myelin basic protein and myelin protein 2 act synergistically to cause stacking of lipid bilayers. *Biochemistry* **49**, 3456–3463 (2010).
32. Studier, F. W. Protein production by auto-induction in high density shaking cultures. *Protein Expr. Purif.* **41**, 207–234 (2005).
33. van den Berg, S., Lofdahl, P. A., Hard, T. & Berglund, H. Improved solubility of TEV protease by directed evolution. *J. Biotechnol.* **121**, 291–298 (2006).
34. Kabsch, W. Automatic processing of rotation diffraction data from crystals of initially unknown symmetry and cell constants. *J. Appl. Crystallogr.* **26**, 795 (1993).
35. McCoy, A. J. *et al.* Phaser crystallographic software. *J. Appl. Crystallogr.* **40**, 658–674 (2007).
36. Afonine, P. V. *et al.* Towards automated crystallographic structure refinement with phenix.refine. *Acta Crystallogr. D Biol. Crystallogr.* **68**, 352–367 (2012).
37. Emsley, P., Lohkamp, B., Scott, W. G. & Cowtan, K. Features and development of Coot. *Acta Crystallogr. D Biol. Crystallogr.* **66**, 486–501 (2010).
38. Petoukhov, M. V. *et al.* New developments in the program package for small-angle scattering data analysis. *J. Appl. Crystallogr.* **45**, 342–350 (2012).
39. Schneider, C. A., Rasband, W. S. & Eliceiri, K. W. NIH Image to ImageJ: 25 years of image analysis. *Nat. Methods* **9**, 671–675 (2012).
40. Brooks, B. R. *et al.* CHARMM: the biomolecular simulation program. *J. Comput. Chem.* **30**, 1545–1614 (2009).
41. Jorgensen, W. L., Chandrasekhar, J. & Madura, J. D. Comparison of simple potential functions for simulating liquid water. *J. Chem Phys* **79**, 926 (1983).
42. Laulumaa, S. *et al.* Dynamics of the Peripheral Membrane Protein P2 from Human Myelin Measured by Neutron Scattering—A Comparison between Wild-Type Protein and a Hinge Mutant. *PLoS One* **10**, e0128954 (2015).
43. Parrinello, M. & Rahman, A. Polymorphic transitions in single crystals: A new molecular dynamics method. *J. Appl. Phys* **52**, 7182 (1998).
44. Hess, B., Bekker, H., Berendsen, H. J. C. & Fraaije, J. G. E. M. LINCS: A linear constraint solver for molecular simulations. *J. Comput. Chem* **18**, 1463 (1997).
45. Darden, T., York, D. & Pedersen, L. Particle mesh Ewald: An N^{-log(N)} method for Ewald sums in large systems. *J. Chem Phys* **98**, 10089 (1993).
46. van der Spoel, D. *et al.* GROMACS: fast, flexible, and free. *J. Comput. Chem.* **26**, 1701–1718 (2005).

Acknowledgements

This study was funded by the Academy of Finland grant 275225 (SR), the Academy of Finland Center of Excellence program (IV, TN), European Research Council (CROWDED-PRO-LIPIDS) (IV), Western Norway Regional Health Authority (AB), Sigrid Jusélius Foundation (PK), Emil Aaltonen Foundation (PK), and the Norwegian Research Council SYNKNØYT programme (PK). The use of the facilities and expertise of the Biocenter Oulu protein crystallography core facility, a member of Biocenter Finland and Instruct-FI, is gratefully acknowledged. We also thank Ilkka Miinalainen, Jarkko Koivunen, and Hongmin Tu for assistance and the Biocenter Oulu core facilities for Proteomics and protein analysis and Electron microscopy. We extend our special thanks to synchrotron beamline support at SOLEIL, ANKA, EMBL/DESY, and DIAMOND.

Author Contributions

The study was designed by S.R., U.B., I.V., and P.K. Samples were prepared and experiments performed by S.R., T.N., C.K.K., G.H.V., A.B., E.I.H., A.R., and P.J. Data were analysed by all authors. The manuscript was written by S.R., T.N., I.V., and P.K., with contributions from all authors. Funding was obtained by S.R., A.B., I.V., and P.K. All authors have given approval to the final version of the manuscript.

Additional Information

Competing Interests: The authors declare that they have no competing interests.

Change History: A correction to this article has been published and is linked from the HTML version of this paper. The error has been fixed in the paper.

Publisher's note: Springer Nature remains neutral with regard to jurisdictional claims in published maps and institutional affiliations.



Open Access This article is licensed under a Creative Commons Attribution 4.0 International License, which permits use, sharing, adaptation, distribution and reproduction in any medium or format, as long as you give appropriate credit to the original author(s) and the source, provide a link to the Creative Commons license, and indicate if changes were made. The images or other third party material in this article are included in the article's Creative Commons license, unless indicated otherwise in a credit line to the material. If material is not included in the article's Creative Commons license and your intended use is not permitted by statutory regulation or exceeds the permitted use, you will need to obtain permission directly from the copyright holder. To view a copy of this license, visit <http://creativecommons.org/licenses/by/4.0/>.

© The Author(s) 2017

PUBLICATION

III

Structure and dynamics of a human myelin protein P2 portal region mutant indicate opening of the β barrel in fatty acid binding proteins

Saara Laulumaa, Tuomo Nieminen, Arne Raasakka, Oda C. Krokengen, Anushik Safaryan, Erik I. Hallin, Guillaume Brysbaert, Marc F. Lensink, Salla Ruskamo, Ilpo Vattulainen & Petri Kursula

BMC Structural Biology 18:8 (2018)
DOI: 10.1186/s12900-018-0087-2


Publication reprinted with the permission of the copyright holder

RESEARCH ARTICLE

Open Access



Structure and dynamics of a human myelin protein P2 portal region mutant indicate opening of the β barrel in fatty acid binding proteins

Saara Laulumaa^{1,2}, Tuomo Nieminen³, Arne Raasakka⁴, Oda C. Krokengen⁴, Anushik Safaryan⁴, Erik I. Hallin⁴, Guillaume Brysbaert⁵, Marc F. Lensink⁵, Salla Ruskamo¹, Ilpo Vattulainen^{3,6} and Petri Kursula^{1,4*} 

Abstract

Background: Myelin is a multilayered proteolipid sheath wrapped around selected axons in the nervous system. Its constituent proteins play major roles in forming of the highly regular membrane structure. P2 is a myelin-specific protein of the fatty acid binding protein (FABP) superfamily, which is able to stack lipid bilayers together, and it is a target for mutations in the human inherited neuropathy Charcot-Marie-Tooth disease. A conserved residue that has been proposed to participate in membrane and fatty acid binding and conformational changes in FABPs is Phe57. This residue is thought to be a gatekeeper for the opening of the portal region upon ligand entry and egress.

Results: We performed a structural characterization of the F57A mutant of human P2. The mutant protein was crystallized in three crystal forms, all of which showed changes in the portal region and helix $\alpha 2$. In addition, the behaviour of the mutant protein upon lipid bilayer binding suggested more unfolding than previously observed for wild-type P2. On the other hand, membrane binding rendered F57A heat-stable, similarly to wild-type P2. Atomistic molecular dynamics simulations showed opening of the side of the discontinuous β barrel, giving important indications on the mechanism of portal region opening and ligand entry into FABPs. The results suggest a central role for Phe57 in regulating the opening of the portal region in human P2 and other FABPs, and the F57A mutation disturbs dynamic cross-correlation networks in the portal region of P2.

Conclusions: Overall, the F57A variant presents similar properties to the P2 patient mutations recently linked to Charcot-Marie-Tooth disease. Our results identify Phe57 as a residue regulating conformational changes that may accompany membrane surface binding and ligand exchange in P2 and other FABPs.

Keywords: Myelin, Crystal structure, Fatty acid-binding protein, Membrane binding, Molecular dynamics, Mutation, Protein stability

Background

A multitude of proteins interact with lipid membrane surfaces. These peripheral membrane proteins come from various protein families, and have generally little in common at the structural level. Both electrostatic and hydrophobic interactions are important for protein binding onto membranes. Conformational changes in the

protein are often observed upon membrane binding and embedding, and the dynamics of both the protein and lipid components may be altered upon proteolipid complex formation. The proteins of the myelin sheath are in intimate contact with lipid membranes, being either peripheral or integral membrane proteins [1]. Defects in myelin protein structure and/or function are linked to various chronic demyelinating conditions, such as multiple sclerosis and peripheral neuropathies.

Peripheral myelin protein P2 is one of the most abundant proteins in human peripheral nervous system

* Correspondence: petri.kursula@uib.no

¹Faculty of Biochemistry and Molecular Medicine, University of Oulu, Oulu, Finland

⁴Department of Biomedicine, University of Bergen, Bergen, Norway
Full list of author information is available at the end of the article



(PNS) myelin [2]. P2 is expressed inhomogeneously along myelinated axons: it can reach 15% of total myelin protein in selected areas in the PNS, and it is also expressed in the central nervous system in small amounts in the spinal cord and brain stem [2–4]. The physiological role of P2 remains unclear, even though it is expressed at such high levels in myelin. P2 is located in compact myelin, and it is expressed more in large axon myelin [3, 5]. P2 has the ability to stack membrane leaflets together [6, 7], and a dysfunction of P2 may lead to myelin degeneration. Recently, three point mutations in human P2 were linked to Charcot-Marie-Tooth disease (CMT), an inherited neuropathy [8–10]. We showed that these mutations all decrease the stability of P2, although they did not lead to major differences in the P2 fold in the crystal state [11]. The disease mutations also slightly altered membrane binding properties of P2 [11].

The structure of human P2 has been solved at 0.93-Å resolution using X-ray crystallography [12]. P2 belongs to the fatty acid binding protein (FABP) family, and the structure of P2 is typical for FABPs [13, 14]: the body of P2 is a barrel formed of 10 antiparallel β strands, and the loops that connect the β strands cover the open ends of the barrel. The loop between the first two strands is extended with two antiparallel α helices that form a lid-like cover for the open end of the barrel. Inside the barrel, there is a large ligand binding pocket, typical for FABPs [13, 14]. The β barrel is discontinuous, with no main-chain hydrogen bonds present between β strands 4 and 5. This feature is common to the entire FABP family, suggesting structural and/or functional importance.

During myelination, large-scale membrane synthesis takes place, and both protein and lipid components need to be transported to the correct location [15, 16]. P2 could, in addition to being a structural component of the myelin sheath, be important for transporting lipidic compounds into the myelin membrane. For example, myelin is rich in cholesterol [17], and P2 might function as a cholesterol transporter. Studies on P2-deficient mice showed a mild effect on nerve conduction velocity and an abnormal lipid composition during the period of most active myelination, although the ultrastructure of PNS myelin appeared visually normal [4]. A recent follow-up study identified a role for P2 in remyelination after nerve injury [18].

FABPs are small β barrel proteins that can function as lipid transporters [19]. They can roughly be divided into two groups based on their respective transport mechanisms [20, 21]. P2 is a member of the group employing collisional transfer upon interaction with a lipid membrane. The other group includes e.g. liver FABP, having a diffusive transfer mechanism, whereby the FABP spontaneously opens and closes to allow ligand exchange

[20]. P2 is unique in the FABP family, as it apparently has a stable contact to membranes, and it can stack lipid bilayers into highly ordered multilayers [6, 12]. Dynamics of the so-called portal region, consisting of helix $\alpha 2$ and the loops $\beta 3$ - $\beta 4$ and $\beta 5$ - $\beta 6$, have been identified as a key determinant of ligand binding-related conformational changes in the FABP family, although differences in this behaviour are apparent between family members [22, 23].

Here, we specifically focused on the conserved FABP family residue Phe57 in human P2. Phe57 is in a central position in the portal region, and it is believed to regulate ligand entry into the internal cavity in FABPs [24]. Mutagenesis of Phe57 into alanine (F57A) highlighted specific roles for Phe57 in ligand binding and structural integrity of the portal region. Stability and membrane binding of P2 were affected by the F57A mutation similarly to the CMT-linked point mutations. Furthermore, molecular dynamics (MD) simulations of the F57A mutant showed opening of the β barrel from the side, which is likely to be a general mechanism for FABP portal region opening. The regulation of this conformational change appears to be affected in mutant variants of P2.

Methods

Protein production and crystallisation

Wild-type P2 (wt-P2), as well as the F57A and P38G variants, were produced as earlier described [14, 25, 26]. Briefly, the proteins were expressed as His-tagged fusion proteins in *E. coli* using autoinduction [27], and they were purified with immobilized metal ion affinity chromatography (IMAC) and size exclusion chromatography (SEC). The His tag was cleaved with TEV protease, and IMAC and SEC were further used to obtain highly pure protein. Crystallization of the F57A mutant has been described [26]. Two additional crystal forms were obtained here; all crystallization conditions were similar, containing 40–42% PEG6000 at pH 6.0–7.0 (see results for details). Crystallization was done at +4 °C.

Crystallographic data collection and structure refinement

Diffraction data were collected on the EMBL beamline X12 at the DORIS synchrotron storage ring (DESY, Hamburg). 20% PEG200 was used for cryoprotection, prior to transferring the crystals to liquid nitrogen temperature. Data were collected at 100 K. The data were processed with XDS [28] and XDSi [29]. The structures were solved with molecular replacement using PHASER [30], using the wild-type P2 structure [14] as template, and refinement was carried out in phenix.refine [31]. Model building was done in coot [32] and validation in MolProbity [33]. The structures were deposited at the PDB with entry codes 6EW2, 6EW4, and 6EW5.

Lipid preparation

For stock solutions, dimyristoylphosphatidylcholine (DMPC) and dimyristoylphosphatidylglycerol (DMPG) (Larodan Fine Chemicals AB, Malmö, Sweden) were dissolved in chloroform:methanol (9:1 v/v) at 10–40 mg/ml final concentrations, and combined to reach an equimolar mixture (DMPC:DMPG (1:1)). Stock solutions and equimolar mixes of dioleoylphosphatidylcholine (DOPC) and dioleoylphosphatidylserine (DOPS) (Avanti Polar Lipids, Alabaster, Alabama) were prepared similarly, but without methanol. The mixtures were divided into aliquots, which were dried under a nitrogen stream at ambient temperature, followed by lyophilization overnight at $-52\text{ }^{\circ}\text{C}$ under vacuum. The dried lipids were stored at $-20\text{ }^{\circ}\text{C}$ until further use. To prepare lipid vesicles, 20 mM HEPES, 150 mM NaCl, pH 7.5 was added directly onto the dried lipids to obtain 5–7 mM concentration. Gentle agitation was applied overnight at ambient temperature. Large multilamellar vesicles (MLVs) were prepared from the suspensions by freeze-thawing 7 times using liquid nitrogen and a warm water bath, followed by vigorous vortexing. Large unilamellar vesicles (LUVs) were prepared by passing the MLVs through a 100-nm membrane 11 times, while heating to $+40\text{ }^{\circ}\text{C}$. All vesicle preparations were used immediately in downstream experiments.

Circular dichroism spectroscopy

A Chirascan Plus instrument (Applied Photophysics) was used for circular dichroism (CD) spectroscopy. CD spectra were measured at $+20\text{ }^{\circ}\text{C}$ in a 0.5-mm quartz cuvette. Protein concentration was 0.25 mg/ml (14 μM) in 0.8 mM HEPES pH 7.5, 6 mM NaCl, 0.4% glycerol. In mixtures with lipids, the lipids (DMPC/DMPG at 1:1 mixture) were in 100-fold molar excess (1.4 mM). Temperature scans, at a heating rate of $1\text{ }^{\circ}\text{C}/\text{min}$, were run for the same samples between $+20 - +90\text{ }^{\circ}\text{C}$. Full spectra were continuously measured as a function of temperature. Temperature scan data were analyzed using Global3™ (Applied Photophysics).

Atomistic molecular dynamics simulations

The crystal structure of P2-F57A was subjected to atomistic MD simulations exactly as previously described [11, 25] for wt-P2 and P2-P38G. Simulations were carried out in the presence and absence of bound palmitate, in a simulation box filled with TIP3P water molecules. Briefly, the system was energy-minimized with the steepest descent algorithm and then simulated for a total of 3 μs . MD simulations were run with GROMACS 4.6.7 [34]. The last 2.5 μs were used for analyses. Dynamic cross-correlation map (DCCM) analysis was performed using Bio3D [35].

Differential scanning calorimetry

Differential scanning calorimetry (DSC) was carried out essentially as earlier described for myelin basic protein (MBP) [36]. P2 and P2 F57A were mixed with MLVs of 350 μM DMPC:DMPG (1:1) in 20 mM HEPES, 150 mM NaCl, pH 7.5, at 1:100 and 1:200 protein-to-lipid (P/L) ratios. The samples were degassed for 10 min under vacuum with stirring at $+10\text{ }^{\circ}\text{C}$ before measurements. A control lipid sample without protein was also prepared.

DSC measurements were performed with a MicroCal VP-DSC instrument. Cell volume was 527.4 μl . The reference cell was filled with 20 mM HEPES, 150 mM NaCl, pH 7.5. Each sample was scanned from $+10$ to $+40\text{ }^{\circ}\text{C}$ and back to $+10\text{ }^{\circ}\text{C}$ in $1\text{ }^{\circ}\text{C}/\text{min}$ steps. Buffer baselines were subtracted from sample curves and zeroed between $+28-30\text{ }^{\circ}\text{C}$. All samples were prepared and measured twice and deemed reproducible.

Membrane surface binding

Surface plasmon resonance (SPR) was performed as described [11, 36]. Briefly, SPR measurements were performed using a Biacore T200 system (GE Healthcare) using 20 mM HEPES, 150 mM NaCl, pH 7.5 as running buffer at $+30\text{ }^{\circ}\text{C}$. LUVs of 1 mM DOPC:DOPS were immobilized on an L1 sensor chip (GE Healthcare), followed by a blocking injection of 0.2 mg/ml BSA, and a single injection of P2 or P2 F57A. Chip regeneration was performed using a 2:3 (v:v) mixture of isopropanol and 50 mM NaOH. The studied protein concentrations were 0.1–15 μM . A single concentration was analyzed per cycle, and all samples were measured in duplicate. Equilibrium binding responses were plotted against protein concentration and fitted using a one-site binding model ($Y = B_{\text{max}} * X / (K_d + X)$).

Lipid vesicle aggregation

Turbidimetry was used to follow vesicle aggregation, a sign of lipid membrane stacking by P2, as described before [11, 12, 37]. LUVs of 500 μM DMPC:DMPG (1:1) were mixed with 0.5–10 μM P2 or P2 F57A in 100- μl triplicate samples. Turbidity at 450 nm and 660 nm was recorded immediately after sample preparation and mixing at $+30\text{ }^{\circ}\text{C}$ using a Tecan SPARK 20 M plate reader for 15 min. The mixtures were stored overnight at $+4\text{ }^{\circ}\text{C}$ for further co-sedimentation analysis.

Protein-lipid co-sedimentation

To check for protein co-sedimentation with the lipid vesicles, samples were picked from the 10 μM vesicle aggregation samples, combined, and centrifuged at 16000 g, $+4\text{ }^{\circ}\text{C}$ for 10 min to separate the lipid-bound protein from soluble protein. The pellet was resuspended in 20 mM HEPES, 150 mM NaCl, pH 7.5. The

protein content of the supernatant and the pellet suspension was analyzed using SDS-PAGE.

In addition, co-sedimentation assays were separately carried out using 20 μ M wt-P2 mixed with 1 mM DMPC:DMPG (1:1) or DOPC:DOPS in 20 mM Tris-HCl (pH 7.5), 150 mM NaCl, 0.5 mM TCEP. After a 30-min incubation at ambient temperature, the samples were subjected to ultracentrifugation for 75 min at 435000 g at +20 °C. The supernatant and pellet were analyzed by SDS-PAGE.

Bioinformatics

Using the crystal structure of wt-P2 [14] and all the six independent F57A crystal structures described here, residue interaction networks (RINs) were generated with Chimera [38] through the structureViz [39] app for CytoScape [40], using default parameters without hydrogen bonds, and with own contact detection software (2.5–5 Å). RIN analyses were performed with the

RINspector [41] app for CytoScape. They included betweenness and residue centrality analysis. Only Z scores of ≥ 2 were considered relevant. The analyses were carried out with and without the bound palmitate ligand; the ligand dominated the networks when present. Sequence-based predictions of protein flexibility were done using DynaMine [42, 43]. Structure-based prediction of point mutation effects on P2 thermal stability was done with Cupsat [44] and MAESTRO [45].

Results

Myelin P2 folding and stability

The F57A and P38G mutants were compared to wt-P2 using CD spectroscopy (Fig. 1a). In solution, all three variants had similar CD spectra, indicating no large-scale structural effects by the mutations. This was earlier confirmed for the P38G mutant [25]. A large effect on the CD spectra of membrane-bound P2 was induced by both mutations (Fig. 1b), and difference

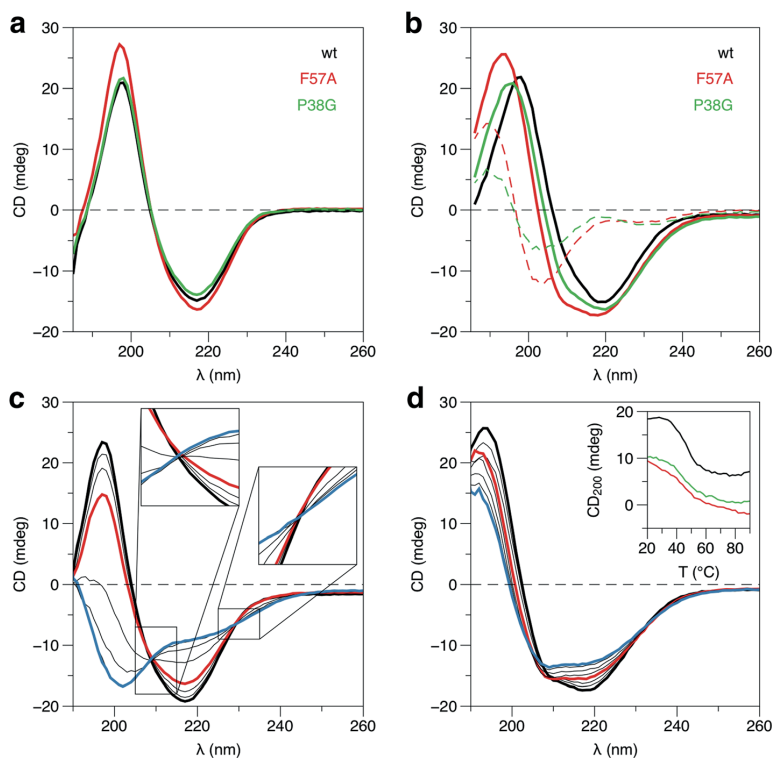


Fig. 1 Analysis of P2 folding by CD spectroscopy. **a** Comparison of CD spectra of wt-P2, P2-F57A, and P2-P38G. The spectra for wt-P2 and P2-P38G were presented earlier [25]. **b** Spectra for the same P2 variants in the presence of lipids. The dashed lines indicate difference spectra between wt-P2 and each mutant. **c** Stability analysis of P2-F57A by CD in solution. CD spectra are shown from +20 (black) to +90 °C (blue), at intervals of 10 °C for clarity. The spectrum at +50 °C is shown in red to aid in comparison between samples. **d** Stability of P2-F57A in the presence of lipids. Inset: CD signal at 200 nm of wt-P2 (black), F57A (red), and P38G (green) bound to lipids as a function of T

spectra indicate that the mutant variants contain less overall secondary structure than wt-P2.

Thermal CD scans were further employed to follow effects of the two mutations on P2 heat stability. In our previous study, we saw a decrease in stability for the P38G mutant [25]. Here, a lowered melting point of the P2-F57A protein was observed compared to wt-P2.

The secondary structure content of P2 changes once mixed with DMPC:DMPG vesicles (Fig. 1b). The temperature scans were repeated with proteins in a lipid environment: wtP2 did not get fully denatured even at + 90 °C, only a conformational shift to a more helical structure was observed [12]. The same behaviour, but including more unfolding, was observed for P2-F57A (Fig. 1c,d).

The different behaviour of wild-type and mutant P2 in solution and in the presence of lipid vesicles shows a strong effect on P2 stability and properties by lipid membrane binding. In solution, both wt-P2 and the mutants show very well-defined isobestic points (Fig. 1c), indicative of a simple two-state unfolding reaction; even though the melting temperatures are different. However, in the presence of membranes, the spectral changes are gradual, and isobestic points are not present at all (Fig. 1d). This is a sign of a complex stepwise conformational adaptation to the membrane environment by P2 as a function of temperature. A main change occurs in the range of + 50 °C, and actually at a lower temperature for wt-P2 (Fig. 1d, inset). After this transition, wt-P2 remains stable, while the mutants gradually change their structure even as temperatures approach + 90 °C; however, all the proteins remain in a folded state even at these high temperatures in the presence of lipids. Interestingly, the conformational changes start to be visible around physiological temperature.

Membrane binding and stacking by P2-F57A

When P2 is mixed with lipid vesicles, visible aggregation occurs, which can be quantified using turbidimetry [11, 12]. Turbidity can be used as a means to quantify the function of myelin proteins - binding lipid membranes together [36, 37]. At time point 0 of the vesicle aggregation experiments, there is only a marginal difference between P2 and the mutant, when the P/L ratio changes (Fig. 2a). As a function of time, it seems that the proteo-lipid aggregate stability is higher for wt-P2 (Fig. 2b). F57A reaches its maximum level quicker, but also decreases over time. This suggests differences in vesicle aggregation kinetics between wt-P2 and P2-F57A, which may be linked to effects on the P2 membrane binding mechanism by the mutation. The co-sedimentation of wt-P2 and F57A with lipids is similar (Fig. 2c). Electrophoretic analysis of the proteolipid pellet also occasionally reveals a ladder of different oligomeric forms of P2 in the protein-lipid pellet (Fig. 2d).

Using DSC, we followed the lipid tail phase transition of DMPC:DMPG vesicles in the presence and absence of P2 (Fig. 2e). The lipid phase transition behaviour is altered by P2, and upon addition of wt-P2, the main transition population decreases and a wide, fairly low-intensity population at + 25.5 °C is formed. The effect is dependent on P2 concentration. Earlier, we showed similar effects by MBP on negatively charged vesicles [36]. However, the F57A mutant does not show this behaviour, and the phase transition is not much affected.

We further studied the affinity of P2 towards DOPC:-DOPS membranes using SPR (Fig. 2f,g). The mutant seems to have a slightly lowered affinity for DOPC:-DOPS (1:1) LUVs (Table 1), while the maximum amount of protein bound to the surface is similar. In addition, as seen before for the CMT disease mutant variants [11], the binding kinetics for F57A are different from wt-P2; apparently both binding and dissociation occur more slowly with the mutant protein.

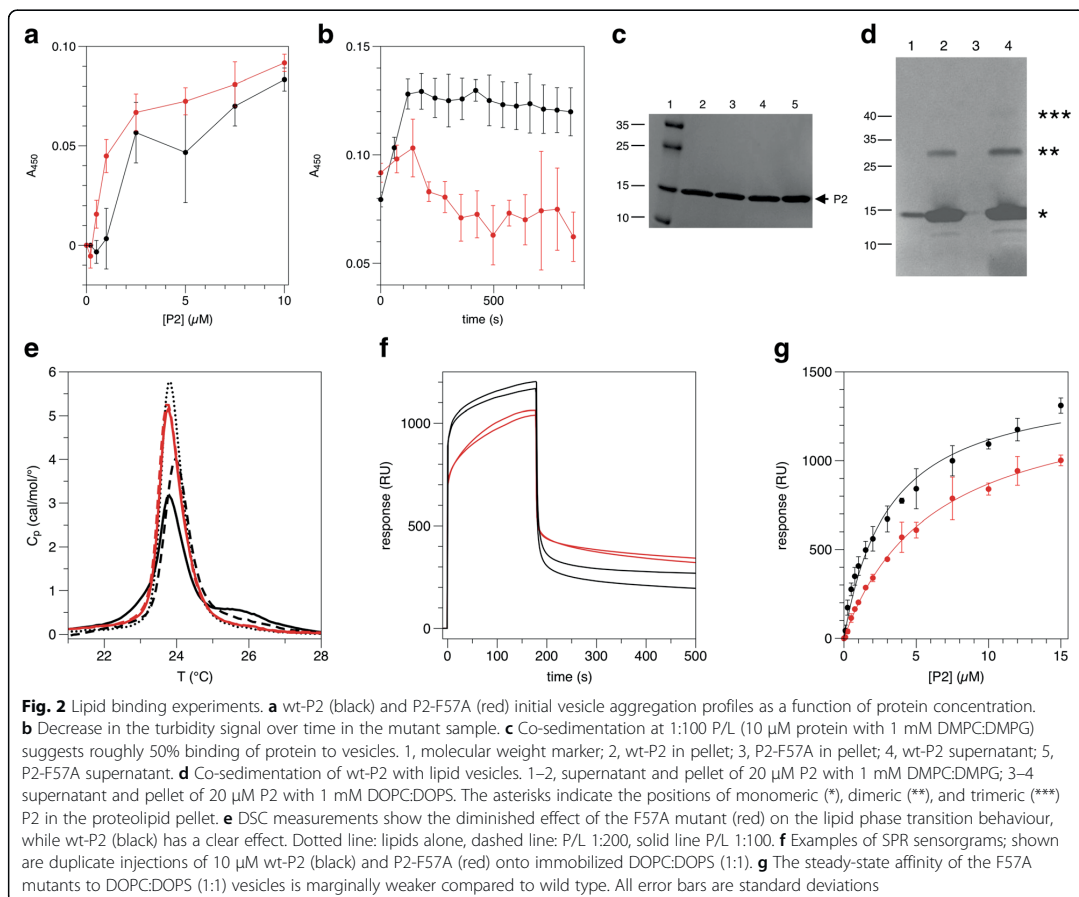
Structure of P2 F57A mutant in the crystal state

P2-F57A was crystallized in three different crystal forms under similar conditions (Table 2), and the crystal structure was solved from all of them. Phe57 lies at the tip of the β 3- β 4 loop, close to the bound fatty acid. The fatty acid, originating from the *E. coli* expression host, was modelled as palmitate. Phe57 forms C-H... π interactions with the nearby residues Lys58 and Leu32 that lie on opposite sides of the Phe ring (Fig. 3a).

In line with CD spectroscopy, no large-scale changes in P2 structure were induced by the mutation in the crystal state. Once the C-H... π interaction gets eliminated in P2-F57A, both helix α 2 and the β 3- β 4 loop alter their positions: helix α 2 turns inwards towards the palmitate bound in the cavity, and the β 3- β 4 loop bends outwards, slightly opening the portal region (Fig. 3b). In different crystal forms of P2-F57A, helix α 2 and loop β 3- β 4 are in slightly different conformations. The bound fatty acid adopts a more elongated conformation in F57A-P2 than in wild-type P2, correlating with the conformation of the β 3- β 4 loop (Fig. 3b). Strands β 4 and β 5 do not have any main-chain H bonds between them, and a line of water molecules mediates contacts between them (Fig. 3c).

Molecular dynamics simulations

In atomistic simulations of wt-P2 in solution, the Phe57 side chain alters its conformation occasionally, flipping outwards and pointing towards bulk solvent (Fig. 4a,b). Such conformations have been seen before in crystal structures of FABPs, including P2 [46]. Phe57 side chain flipping is apparently more frequent and lasts a longer time in the presence of bound fatty acid (Fig. 4a).



The F57A simulations presented here revealed a large-scale opening of the β barrel between strands $\beta 4$ and $\beta 5$ (Fig. 4c,d,e). Upon this opening, the ligand-binding cavity becomes accessible, as the hairpin unit formed by strands $\beta 5$ and $\beta 6$ flaps out. Based on the F57A simulation results, we re-analyzed our earlier simulations of WT and P38G P2 [25], and indeed, for both of them, an occasional opening of the β barrel at the same site is observed, with exposure of the bound ligand (Fig. 4d). This was especially prominent for the palmitate-bound P38G mutant, which we observed to have higher dynamics than the wild-type protein.

Table 1 SPR fitting parameters of P2 binding to DOPC:DOPS (1:1) vesicles

Protein	B_{max} (R.U.)	K_d (μ M)	R^2
P2	1466 \pm 54	3.1 \pm 0.3	0.9750
P2-F57A	1408 \pm 56	6.2 \pm 0.5	0.9884

An analysis of the root mean-square fluctuations in the MD trajectories reveals that F57A shows higher dynamics than wt-P2 in the absence of fatty acid (Fig. 4f), while dynamics are identical in the presence of bound ligand. Specifically, the site of the F57A mutation is not much affected, but the $\beta 5$ - $\beta 6$ and $\beta 7$ - $\beta 8$ loops are more mobile, indicating an increased flexibility of the portal region in the mutant.

For additional insight into concerted dynamics of P2, DCCM analyses were performed on the MD trajectories (Fig. 5). While wild-type P2 shows strong anti-correlation between the $\beta 5$ - $\beta 6$ loop and the rest of the portal region (helices $\alpha 1$ - $\alpha 2$ and the $\beta 3$ - $\beta 4$ loop), no such correlation exists in the F57A mutant. Similar results were obtained with and without bound palmitate (Fig. 5). In addition, we analyzed our earlier MD trajectories for the CMT disease mutations [11] as well as P38G [25]. All the mutations had similar effects to F57A, indicating loss of anti-correlations in portal region dynamics (Additional file 1: Figure S1).

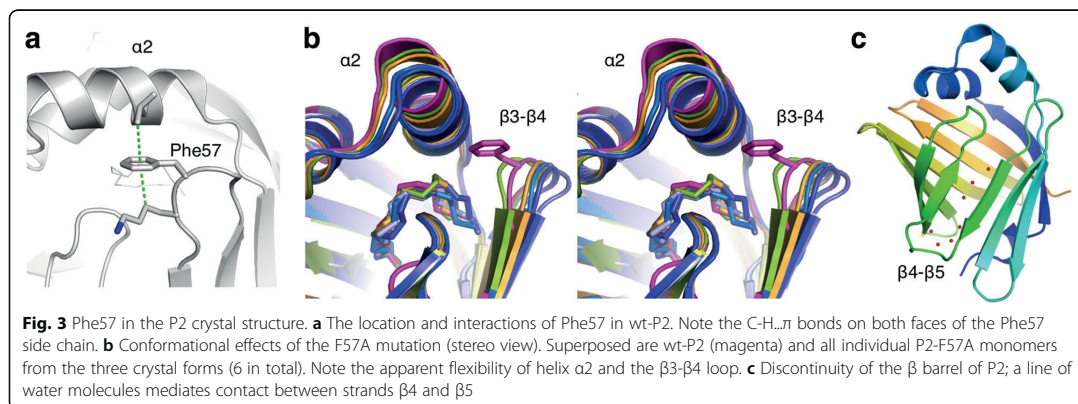
Table 2 Data processing and structure refinement statistics for P2-F57A

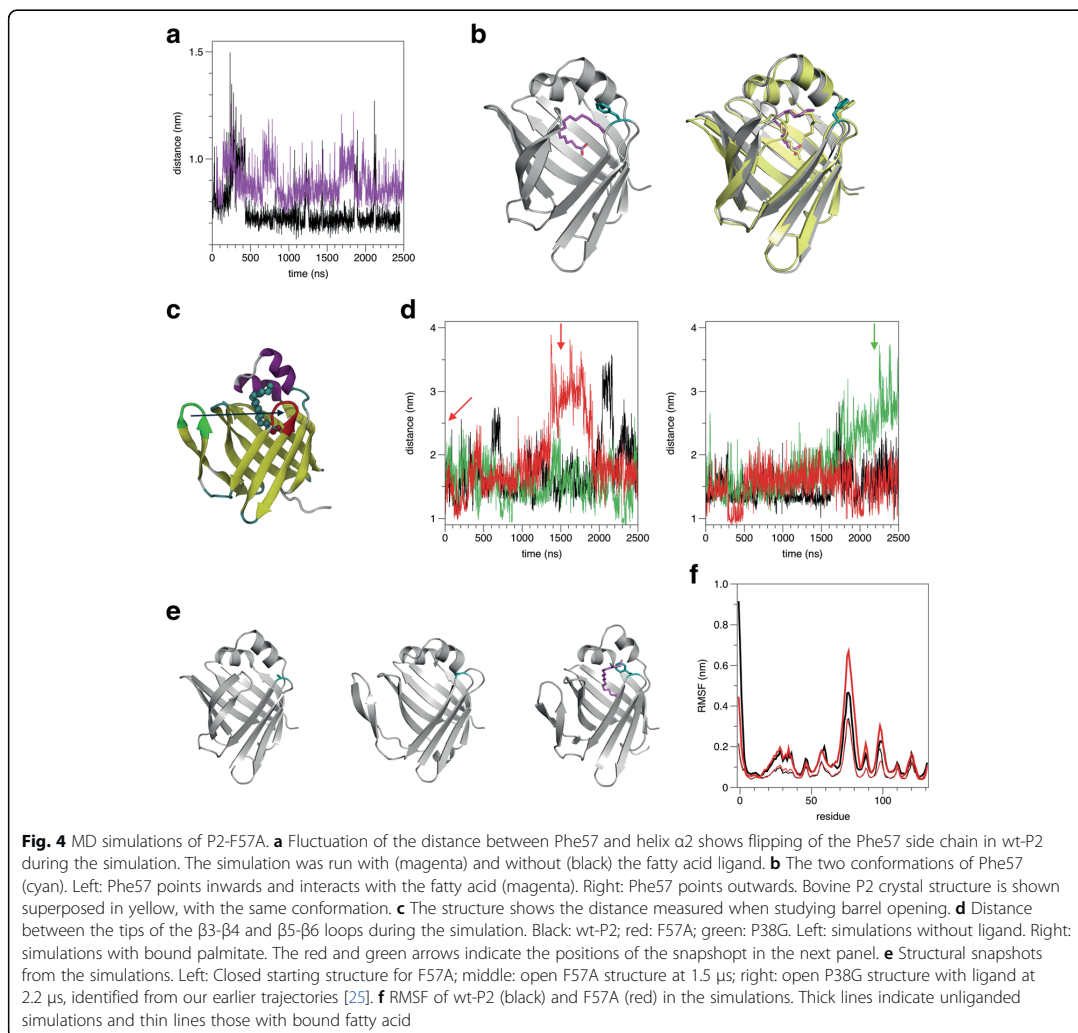
Space group	P4 ₃ 2 ₁ 2	C2 [26]	P2 ₁ 2 ₁ 2 ₁
Unit cell dimensions	a = b = 58.61 Å, c = 76.96 Å $\alpha = \beta = \gamma = 90^\circ$	a = 112.76 Å, b = 36.08 Å, c = 31.17 Å, $\alpha = \gamma = 90^\circ$, $\beta = 96.87^\circ$	a = 52.12 Å, b = 76.11 Å, c = 138.43 Å, $\alpha = \beta = \gamma = 90^\circ$
Wavelength (Å)	1.10	1.10	1.10
Resolution range (Å)	20–1.59 (1.63–1.59)	20–1.27 (1.30–1.27)	20–1.95 (2.00–1.95)
$\langle I/\sigma(I) \rangle$	19.1 (1.0)	8.2 (1.2)	11.6 (2.3)
R _{sym} (%)	6.5 (111.4)	7.6 (60.7)	15.8 (75.0)
R _{meas} (%)	7.2 (129.6)	9.2 (78.1)	17.3 (82.1)
Completeness (%)	98.7 (92.7)	96.8 (77.4)	99.1 (98.7)
Redundancy	5.7 (3.2)	2.9 (1.8)	6.0 (6.0)
CC _{1/2} (%)	99.9 (39.9)	99.6 (43.6)	99.4 (75.4)
Wilson B factor (Å ²)	27.2	16.9	20.2
R _{cryst} (%)	18.6	17.1	18.8
R _{free} (%)	21.6	22.4	23.6
rmsd bond lengths (Å)	0.012	0.009	0.005
rmsd bond angles (°)	1.3	1.2	0.9
Ramachandran favoured/allowed (%)	100/100	99.3/100	98.1/100
# molecules in asymmetric unit	1	1	4
MolProbity score (percentile)	1.25 (97 th)	1.48 (79 th)	1.32 (99 th)
PDB entry	6EW2	6EW4	6EWS

Predictions and network analyses

Flexibility predictions were carried out based on the P2 sequence, to compare the predicted effects of F57A and the CMT disease mutations. Each of the mutations is predicted to cause a local increase in flexibility (Fig. 6a,b). This is in line with the observed decrease in heat stability and the increased dynamics in simulations for the mutant variants. Based on the P2 crystal structure, we further predicted the effects of the mutations on protein stability (Table 3); overall, the predictions fit the measured decrease of T_m for the mutants. This result further shows that the F57A mutation behaves similarly to the disease mutations in structure-function assays.

For a deeper understanding of P2 folding and intramolecular interactions, residue interaction networks and centralities in the crystal structures were characterized and compared between wt-P2 and P2-F57A; all six independent F57A molecules in the three crystal structures with different space groups were included in the analysis. The analysis shows that Phe57 is structurally not a very central residue in the P2 structure, and its mutation to alanine has subtle effects on these networks (Additional file 2: Figure S2). This observation is slightly unexpected, having experimentally seen a drastic drop in thermal stability in the F57A mutant protein (see above). Interestingly, a group of residues, including the disease mutation sites, as well as residues on strand β_4 and in





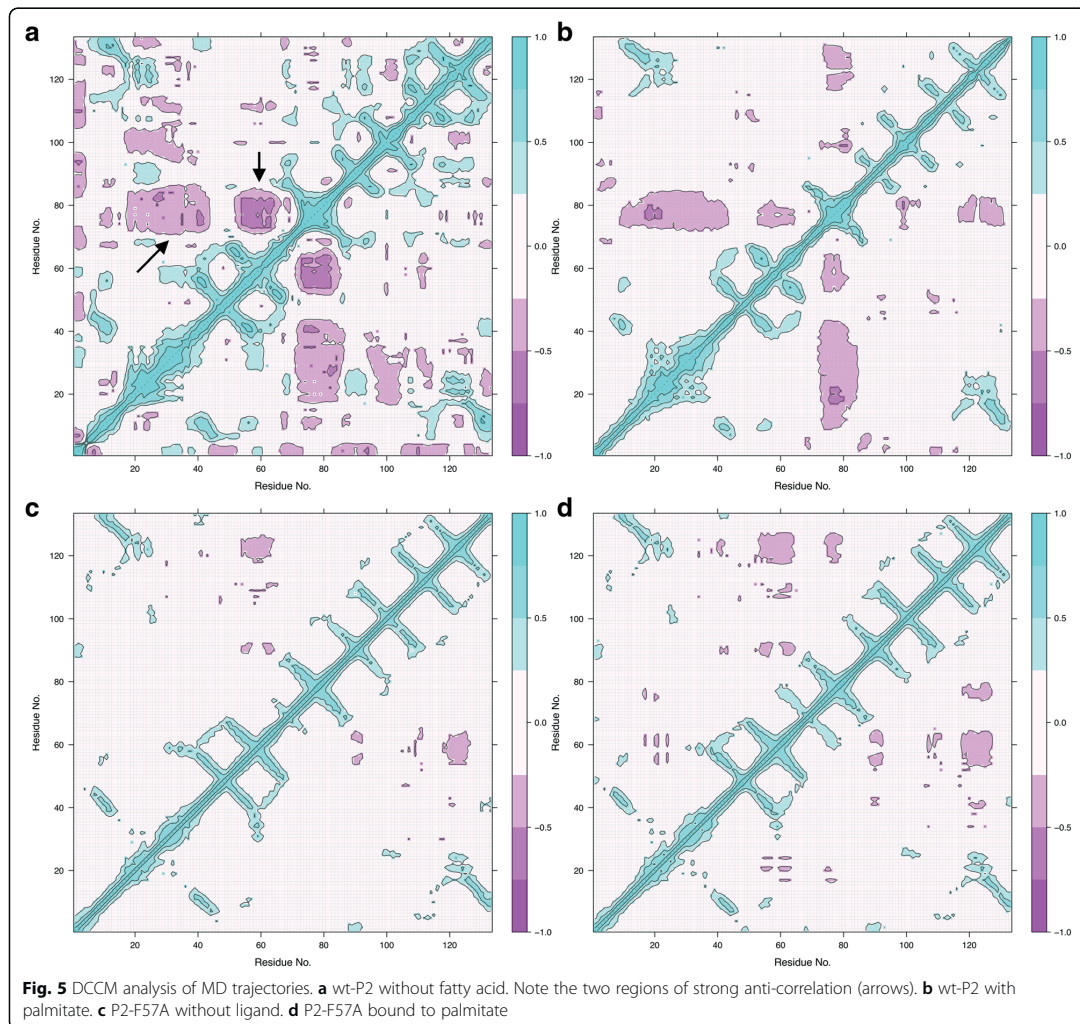
the $\beta 5$ - $\beta 6$ unit, become more central upon the F57A mutation (Fig. 6c and Additional file 2: Figure S2). Leu32 on helix $\alpha 2$ also belongs to this group. Also the interactions between P2 and the palmitate ligand are slightly altered through the mutation, in line with the subtle conformational changes observed in the respective crystal structures.

When the palmitate ligand is included in the analysis, it dominates the network, highlighting its multiple interactions and suggesting a stabilizing and therefore possible structural role in P2 and the FABP superfamily protein stability (data not shown). The two Arg residues coordinating the palmitate anionic group are central in P2 intramolecular networks, when the palmitate is not taken into

account. Additional central P2 residues can be observed. Some of them, especially Gln93 and Gln95, both pointing inwards on strand $\beta 7$ (Fig. 6c and Additional file 2: Figure S2), have not been of obvious importance in earlier analyses of P2 crystal structures. Gln93 is sandwiched between the charged side chains of Arg106 and Glu72 (close to the $\beta 5$ - $\beta 6$ loop) - both carrying buried charges inside the protein. Importantly, none of the central residues of wt-P2 lie in the $\beta 5$ - $\beta 6$ unit, which flips out during barrel opening (Fig. 6c).

Discussion

While the FABP family contains proteins with distinct functions, current evidence suggests that the FABPs

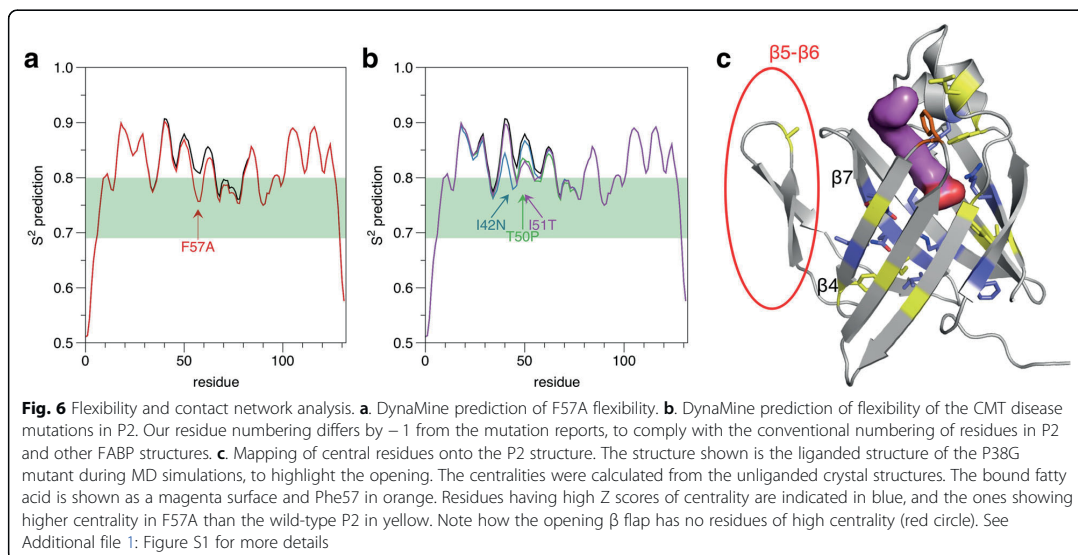


share not only structural, but also dynamical, properties. Phe57 is a highly conserved residue in the FABP family, thought to play an important role in the function of the portal region and ligand binding [24, 47, 48]. Its conformation varies between FABP crystal structures, being either swung in to interact with the hydrophobic ligand and helix $\alpha 2$ or pointing towards the solvent. In structures of P2, Phe57 is normally pointing inwards, making direct van der Waals contacts with the hydrocarbon tail of the bound fatty acid, although the first structure of bovine P2 had Phe57 pointing outwards [46]. We studied the importance of Phe57 in human myelin P2 protein through a variety of biophysical experiments.

P2 stability and folding

We showed before that binding of wt-P2 to lipid vesicles induced an apparent unfolding of helical structures, i.e. the lid of the β barrel [12]. Hence, we wanted to observe any potential effects on this unfolding by two mutations at the portal region, F57A and P38G. We showed that the P38G mutation renders the P2 protein more dynamic on different time scales [25]. The folding of both of the mutant proteins was affected by the presence of lipid vesicles more than that of the wild-type protein.

Thermal stability of both mutant P2 variants was decreased. For P38G, a flexibility increase in loop areas and helix $\alpha 2$ was also observed in computer simulations



[25], and for P2-F57A, the diversity in crystal structures indicates increased protein flexibility in the portal region.

Previously, for wt-P2 it appeared that binding to phospholipids would result in the unfolding of helices [12], whereas the P2 N-terminal peptide was shown to become helical when bound to lipids [14]. It is clear that binding to phospholipids increases P2 thermal stability drastically as a result of an interaction between the phospholipids and P2. This interaction can partially overcome the destabilizing effects of point mutations on the protein in solution. All in all, F57A behaves similarly to both P38G as well as the CMT-linked disease mutations [11, 25].

Membrane binding and stacking

Many FABPs have been shown to interact with lipid membranes [49–55]. For those FABPs employing a collisional transfer mechanism, such interactions are functionally crucial [49]. To our knowledge, however, P2 is

Table 3 Predicted and measured changes in heat stability for various P2 variants. T_m values for P38G and the disease mutations have been published [11, 25]

variant	Cupsat $\Delta\Delta G$ (kcal/mol)	MAESTRO $\Delta\Delta G$ (kcal/mol)	Experimental ΔT_m ($^{\circ}C$)
F57A	-1.91	1.16	-6
P38G	-5.38	1.64	-6
I43N	-7.63	3.92	-17
T51P	-1.51	1.43	-24
I52T	-5.17	2.89	-13

Note that Cupsat defines a destabilizing mutation with a negative $\Delta\Delta G$, while in MAESTRO, a destabilizing mutation has a positive $\Delta\Delta G$

the only member of the FABP family that stacks lipid membranes into multilayers; hence, one can expect its structure-function relationships to differ somewhat from other FABPs.

P2 bound to lipid membrane surfaces, and electrophoretic separation often resulted in a ladder of P2 in the membrane pellet. This reflects a very tight interaction of P2 with stacked membranes, not being dissociated by SDS and heating, and suggests the formation of supramolecular complexes by P2 molecules and two apposing lipid membranes. The structural details of this assembly are likely to be relevant for myelin formation, and further research will be required to elucidate the molecular architecture, also with respect to other myelin proteins present in the same compartment, such as MBP and P0.

Our DSC experiment indicated effects by P2 on lipid phase transition similar to those we observed with MBP [36]. The effect was, however not observed for P2-F57A here. This means that the insertion or hydrophobic effect of the protein – or the formation of lipid rafts or structures that have altered phase transition behavior – is not present with the mutant.

Crystal structures of P2-F57A

Phe57 is a conserved residue in most FABPs, and its stabilizing interactions may be a common feature of FABPs [12]. The conservation concerns especially FABPs thought to transfer ligands to membranes through the collisional mechanism. It is possible that upon membrane binding, these interactions are altered, allowing for conformational changes in the portal region of FABPs.

The possibility of crystallizing in different conformations indicates an increasing flexibility of the portal region, linked to the missing stabilizing C-H... π interactions of Phe57. The absence of Phe57 seems to both destabilize P2 as well as bring about small but clear conformational changes in the crystal state. These differences are likely to correspond to molecular motions upon extrusion of the ligand from the internal cavity. Phe57 lies close to the anion-binding pocket we observed previously [12]. In the structures of the F57A mutant, this pocket is usually occupied by an anionic group in the crystal. We believe this site can be relevant for membrane lipid headgroup binding and possible allosteric conformational changes induced thereby.

While fatty acid binding to FABPs in general causes only little changes in structure and dynamics [23], all experimental structures of P2 thus far have a bound fatty acid molecule inside the protein. Thus, comparisons between liganded and empty P2 cannot be yet done based on experimental data. MD simulations have shown, both in the current study and our earlier work [25], that bound palmitate decreases the overall dynamics of P2.

In all FABPs, the β barrel is in fact discontinuous, and water molecules between two strands interrupt the main-chain H-bonds one would expect for a perfect β barrel. Already since early FABP structures, it has been suggested that this could be a location of FABP flexibility and related to the opening of the portal region [56].

P2 dynamics and networks

In earlier coarse-grained simulations, Phe57 was found to be one of the residues possibly inserting into the hydrophobic interior of the lipid bilayer [12]. The flexibility of the large Phe57 residue observed in our simulations could be important in the dynamics of the portal region. Phe57 has been considered a gatekeeper of the portal region in FABPs [24, 47, 48].

In the F57A simulation, a large opening of the barrel between strands β 4 and β 5 was observed. Recently, we observed the same phenomenon in simulations as well as experimental SAXS solution studies for the CMT-linked variants of human P2 [11]. The increased dynamics of the F57A mutant correlate to the opening of the β 5- β 6 unit. We believe to have observed a general mechanism for opening of the FABP β barrel upon ligand exchange; the helical lid does not open in this process. Earlier studies on different FABPs have identified slightly varying mechanisms for fatty acid entry and egress [22, 57, 58]; while in general, opening of the portal region is considered most important, alternative routes for ligand entry and/or exit have been suggested at the bottom of the β barrel structure [58]. The significant opening of P2 at β 5- β 6 in our extended 3- μ s simulations,

which are at least an order of magnitude longer than most published FABP simulations, suggests this is the main ligand entry mechanism in the myelin P2 protein. How the conformational change is affected by binding to lipid membranes, remains currently unknown.

DCCM analyses indicated a clear loss of dynamic anti-correlations between the opening β 5- β 6 flap and the rest of the portal region in all analyzed mutants (Fig. 5, Additional file 1: Figure S1); similar results were obtained in both the presence and absence of bound fatty acid ligand. In wt-P2, this anti-correlation is likely to reflect coordinated open-close movements, and it appears that such coordination is lost in both the disease variants and the F57A and P38G mutants. These results further highlight the important role of Phe57 in regulating portal region structure and dynamics. While Phe57 does not directly interact with the β 5- β 6 loop, its close interaction with the α 2 helix is likely to be important for this indirect regulation; this mechanism may be applicable to also other members of the FABP family.

Similarly to fatty acid binding, also membrane binding mechanisms of various FABPs have been studied [49–55]. The binding was suggested to be heavily affected by macrodipoles present in the protein molecule [53]. The orientation of the FABP with respect to the membrane appears to not be conserved between different FABPs, and docking may occur both through the portal region or the opposite face [53, 59]. In this respect, it is important to remember that P2 is bound between two membrane surfaces, and it is likely that both of these modes are applicable to P2. Our earlier coarse-grained simulations suggested membrane interactions through both the portal region and the anti-portal bottom face of P2 [12].

Gln93 and Gln95, identified in our network analysis, could be crucial for correct folding and function-related conformational changes. Interestingly, alignment of all human FABPs [12] shows that whenever Glu72 is present, also Gln95 is conserved. Residue 93 is in these cases either Gln, His, or Cys; when it is a Cys, residue 106 is Gln instead of Arg. Thus, a residue at position 93 interacts with a buried charge on the β 5- β 6 unit, and the breaking of this interaction must take place upon β barrel opening. Earlier, it was shown that mutation of Glu72 to Ser caused destabilization of heart FABP [60].

Conclusions

Phe57 is a residue linking the β -turn loops β 3- β 4 and β 5- β 6 and helix α 2 in the portal region of P2, and in other FABPs. It interacts directly with the bound fatty acid, and it is likely to play a role in the regulation of portal region opening upon membrane contact. The opening of the β barrel observed in simulations of P2-F57A reveals a mechanism for FABP ligand exchange that has been long suggested [56], but was only recently

shown for the CMT disease mutants of P2 [11]. The discontinuity of the FABP β barrel is likely to be instrumental for its opening upon ligand binding - also highlighted by the fact that the hot spot for CMT mutations lies in close vicinity to the opening site in P2, on strands $\beta 3$ and $\beta 4$. Comparing all human FABPs, we earlier showed that only two Gly residues are fully conserved in all family members [12]; of these, Gly67 lies in the $\beta 4$ - $\beta 5$ loop (Fig. 3c), which may act as a functional hinge in the FABP superfamily during barrel opening.

Additional files

Additional file 1: Figure S1. DCCM analyses on earlier MD trajectories from P2 mutants. A. P38G. B. I42N. C. T50P. D. I51T. The empty structures are on the left and the palmitate-bound on the right. (PNG 3329 kb)

Additional file 2: Figure S2. Comparison of centrality analyses between wt-P2 and P2-F57A mutants. A residue interaction network (top) was generated from the crystal structures of P2 (bottom), and central residues were mapped onto them. A. Central residues globally conserved between wt-P2 and different P2-F57A mutant structures. Residues are considered central if their Z score ≥ 2 , and they are coloured in the network as a function of this Z score with a gradient from yellow (Z score = 2) to red (Z score ≥ 4). Z score values of the wt-P2 were chosen for these Figs. B. Central residues only identified in one or several F57A mutant structures and not in wt-P2. Yellow is indicative of Z score ≥ 2 . (PDF 1416 kb)

Abbreviations

CD: Circular dichroism; CMT: Charcot-Marie-Tooth disease; DCCM: Dynamic cross-correlation map; DMPC: Dimyristoylphosphatidylcholine; DMPG: Dimyristoylphosphatidylglycerol; DOPC: Dioleoylphosphatidylcholine; DOPS: Dioleoylphosphatidylserine; DSC: Differential scanning calorimetry; FABP: Fatty acid binding protein; IMAC: Immobilized metal ion affinity chromatography; LUV: Large unilamellar vesicle; MBP: Myelin basic protein; MD: Molecular dynamics; MLV: Multilamellar vesicle; PNS: Peripheral nervous system; RIN: Residue interaction network; SEC: Size exclusion chromatography; SPR: Surface plasmon resonance; wt-P2: Wild-type P2

Acknowledgements

The beamtime and beamline support on the EMBL/DESY beamline X12 is gratefully acknowledged. We thank CSC — IT Center for Science (Espoo, Finland) for computing resources and the BiSS facility (University of Bergen) for access to biophysical instrumentation.

Funding

This work was funded by grants from the Academy of Finland (#275225, SR), the Academy of Finland Center of Excellence program (#307415, IV), European Research Council (CROWDED-PRO-LIPIDS) (#290974, IV), Sigrid Jusélius Foundation (PK), and Emil Aaltonen Foundation (PK). TN thanks the graduate school of Tampere University of Technology for financial support.

Availability of data and materials

The crystallographic data and refined models are available at the Protein Data Bank (www.rcsb.org) under the entry codes 6EW2, 6EW4, and 6EW5. Other datasets used and/or analyzed during the current study are available from the corresponding author upon reasonable request.

Authors' contributions

SL conceived of the study, carried out crystallography and CD spectroscopy, and was a major contributor to writing the manuscript. TN carried out MD simulations and data analysis and participated in writing the manuscript. AR carried out and supervised membrane-binding assays and participated in writing the manuscript. OCK, AS, EI, and SR carried out membrane-binding assays. GB and MFL carried out network analyses and flexibility predictions and participated in writing the manuscript. IV conceived of the study, supervised MD simulations, and participated in manuscript writing. PK

conceived of the study, analyzed data, and was a major contributor to manuscript writing. All authors contributed to the analysis and interpretation of data and finalized and approved the manuscript.

Ethics approval and consent to participate

Not applicable.

Consent for publication

Not applicable.

Competing interests

The authors declare that they have no competing interests.

Publisher's Note

Springer Nature remains neutral with regard to jurisdictional claims in published maps and institutional affiliations.

Author details

¹Faculty of Biochemistry and Molecular Medicine, University of Oulu, Oulu, Finland. ²European Spallation Source (ESS), Lund, Sweden. ³Department of Physics, Tampere University of Technology, Tampere, Finland. ⁴Department of Biomedicine, University of Bergen, Bergen, Norway. ⁵Unité de Glycobiologie Structurale et Fonctionnelle, University of Lille, CNRS UMR8576 UGSF, F-59000 Lille, France. ⁶Department of Physics, University of Helsinki, Helsinki, Finland.

Received: 15 March 2018 Accepted: 13 June 2018

Published online: 25 June 2018

References

- Han H, Myllykoski M, Ruskamo S, Wang C, Kursula P. Myelin-specific proteins: a structurally diverse group of membrane-interacting molecules. *Biofactors*. 2013;39:233–41.
- Greenfield S, Brostoff S, Eylar EH, Morell P. Protein composition of myelin of the peripheral nervous system. *J Neurochem*. 1973;20:1207–16.
- Trapp BD, McIntyre LJ, Quarles RH, Sternberger NH, Webster HD. Immunocytochemical localization of rat peripheral nervous system myelin proteins: P2 protein is not a component of all peripheral nervous system myelin sheaths. *Proc Natl Acad Sci U S A*. 1979;76:3552–6.
- Zenker J, Stettner M, Ruskamo S, Domènech-Estévez E, Baloui H, Médard JJ, et al. A role of peripheral myelin protein 2 in lipid homeostasis of myelinating Schwann cells. *Glia*. 2014;62:1502–12.
- Hahn AF, Whitaker JN, Kachar B, Webster HD. P2, P1, and P0 myelin protein expression in developing rat sixth nerve: a quantitative immunocytochemical study. *J Comp Neurol*. 1987;260:501–12.
- Sedzik J, Blaurock AE, Hoehlich M. Reconstituted P2/myelin-lipid multilayers. *J Neurochem*. 1985;45:844–52.
- Suresh S, Wang C, Nanekar R, Kursula P, Edwardson JM. Myelin basic protein and myelin protein 2 act synergistically to cause stacking of lipid bilayers. *Biochemistry*. 2010;49:3456–63.
- Gonzaga-Jauregui C, Harel T, Gambin T, Kousi M, Griffin LB, Francescato L, et al. Exome sequence analysis suggests that genetic burden contributes to phenotypic variability and complex neuropathy. *Cell Rep*. 2015;12:1169–83.
- Hong YB, Joo J, Hyun YS, Kwak G, Choi YR, Yeo HK, et al. A mutation in PMP2 causes dominant demyelinating Charcot-Marie-tooth neuropathy. *PLoS Genet*. 2016;12:e1005829.
- Motley WW, Palaima P, Yum SW, Gonzalez MA, Tao F, Wanschitz JV, et al. De novo PMP2 mutations in families with type 1 Charcot-Marie-tooth disease. *Brain*. 2016;139:1649–56.
- Ruskamo S, Nieminen T, Kristiansen CK, Vatne GH, Baumann A, Hallin EI, et al. Molecular mechanisms of Charcot-Marie-tooth neuropathy linked to mutations in human myelin protein P2. *Sci Rep*. 2017;7:6510.
- Ruskamo S, Yadav RP, Sharma S, Lehtimäki M, Laulumaa S, Aggarwal S, et al. Atomic resolution view into the structure-function relationships of the human myelin peripheral membrane protein P2. *Acta Crystallogr D Biol Crystallogr*. 2014;70:165–76.
- Chmurzyńska A. The multigene family of fatty acid-binding proteins (FABPs): function, structure and polymorphism. *J Appl Genet*. 2006;47:39–48.
- Majava V, Polverini E, Mazzini A, Nanekar R, Knoll W, Peters J, et al. Structural and functional characterization of human peripheral nervous system myelin protein P2. *PLoS One*. 2010;5:e10300.

15. Garbay B, Heape AM, Sargueil F, Cassagne C. Myelin synthesis in the peripheral nervous system. *Prog Neurobiol*. 2000;61:267–304.
16. Simons M, Trotter J. Wrapping it up: the cell biology of myelination. *Curr Opin Neurobiol*. 2007;17:533–40.
17. Saher G, Simons M. Cholesterol and myelin biogenesis. *Subcell Biochem*. 2010;51:489–508.
18. Stettner M, Zenker J, Klingler F, Szezanowski F, Hartung HP, Mausberg AK, et al. The role of peripheral myelin protein 2 in Remyelination. *Cell Mol Neurobiol*. 2017;
19. Peeters RA, Veerkamp JH, Demel RA. Are fatty acid-binding proteins involved in fatty acid transfer. *Biochim Biophys Acta*. 1989;1002:8–13.
20. Hsu KV, Storch J. Fatty acid transfer from liver and intestinal fatty acid-binding proteins to membranes occurs by different mechanisms. *J Biol Chem*. 1996;271:13317–23.
21. Storch J. Diversity of fatty acid-binding protein structure and function: studies with fluorescent ligands. *Mol Cell Biochem*. 1993;123:45–53.
22. Friedman R, Nachliel E, Gutman M. Fatty acid binding proteins: same structure but different binding mechanisms? Molecular dynamics simulations of intestinal fatty acid binding protein. *Biophys J*. 2006;90:1535–45.
23. Ragona L, Pagano K, Tomaselli S, Favretto F, Ceccon A, Zanzoni S, et al. The role of dynamics in modulating ligand exchange in intracellular lipid binding proteins. *Biochim Biophys Acta*. 2014;1844:1268–78.
24. Simpson MA, Bernlohr DA. Analysis of a series of phenylalanine 57 mutants of the adipocyte lipid-binding protein. *Biochemistry*. 1998;37:10980–6.
25. Laulumaa S, Nieminen T, Lehtimäki M, Aggarwal S, Simons M, Koza MM, et al. Dynamics of the peripheral membrane protein P2 from human myelin measured by neutron scattering—a comparison between wild-type protein and a hinge mutant. *PLoS One*. 2015;10:e0128954.
26. Lehtimäki M, Laulumaa S, Ruskamo S, Kursula P. Production and crystallization of a panel of structure-based mutants of the human myelin peripheral membrane protein P2. *Acta Crystallogr Sect F Struct Biol Cryst Commun*. 2012;68:1359–62.
27. Studier FW. Protein production by auto-induction in high density shaking cultures. *Protein Expr Purif*. 2005;41:207–34.
28. Kabsch W. XDS. *Acta Crystallogr D Biol Crystallogr*. 2010;66:125–32.
29. Kursula P. XDSi: a graphical interface for the data processing program XDS. *J Appl Crystallogr*. 2004;
30. McCoy AJ, Grosse-Kunstleve RW, Adams PD, Winn MD, Storoni LC, Read RJ. Phaser crystallographic software. *J Appl Crystallogr*. 2007;40:658–74.
31. Afonine PV, Grosse-Kunstleve RW, Echols N, Headd JJ, Moriarty NW, Mustyakimov M, et al. Towards automated crystallographic structure refinement with phenix. *Refine*. *Acta Crystallogr D Biol Crystallogr*. 2012;68:352–67.
32. Emsley P, Lohkamp B, Scott WG, Cowtan K. Features and development of coot. *Acta Crystallogr D Biol Crystallogr*. 2010;66:486–501.
33. Chen VB, Arendall WB, Headd JJ, Keedy DA, Immormino RM, Kapral GJ, et al. MolProbity: all-atom structure validation for macromolecular crystallography. *Acta Crystallogr D Biol Crystallogr*. 2010;66:12–21.
34. Hess B, Kutzner C, van der Spoel D, Lindahl E. GROMACS 4: algorithms for highly efficient, load-balanced, and scalable molecular simulation. *Journal ChemTheory Comput*. 2008;4:435–47.
35. Skjærven L, Yao XQ, Scarabelli G, Grant BJ. Integrating protein structural dynamics and evolutionary analysis with Bio3D. *BMC Bioinformatics*. 2014;15:399.
36. Raasakka A, Ruskamo S, Kowal J, Barker R, Baumann A, Martel A, et al. Membrane association landscape of myelin basic protein portrays formation of the myelin major dense line. *Sci Rep*. 2017;7:4974.
37. Tuusa J, Raasakka A, Ruskamo S, Kursula P. Myelin-derived and putative molecular mimic peptides share structural properties in aqueous and membrane-like environments. *Mult Scler Demyelinating Disord*. 2017;24.
38. Pettersen EF, Goddard TD, Huang CC, Couch GS, Greenblatt DM, Meng EC, et al. UCSF chimera—a visualization system for exploratory research and analysis. *J Comput Chem*. 2004;25:1605–12.
39. Morris JH, Huang CC, Babbitt PC, Ferrin TE. structureViz: linking Cytoscape and UCSF chimera. *Bioinformatics*. 2007;23:2345–7.
40. Shannon P, Markiel A, Ozier O, Baliga NS, Wang JT, Ramage D, et al. Cytoscape: a software environment for integrated models of biomolecular interaction networks. *Genome Res*. 2003;13:2498–504.
41. Brysbaert G, Lorgouiloux K, Vranken W, Lensink MF. RINspecter: a Cytoscape app for centrality analyses and DynaMine flexibility prediction. *Bioinformatics*. 2017;
42. Cilia E, Pancsa R, Tompa P, Lenaerts T, Vranken WF. From protein sequence to dynamics and disorder with DynaMine. *Nat Commun*. 2013;4:2741.
43. Cilia E, Pancsa R, Tompa P, Lenaerts T, Vranken WF. The DynaMine webserver: predicting protein dynamics from sequence. *Nucleic Acids Res*. 2014;42:W264–70.
44. Parthiban V, Gromiha MM, Schomburg D. CUPSAT: prediction of protein stability upon point mutations. *Nucleic Acids Res*. 2006;34:W239–42.
45. Laimer J, Hofer H, Fritz M, Wegenkittl S, Lackner P. MAESTRO—multi agent stability prediction upon point mutations. *BMC Bioinformatics*. 2015;16:116.
46. Jones TA, Bergfors T, Sedzik J, Unge T. The three-dimensional structure of P2 myelin protein. *EMBO J*. 1988;7:1597–604.
47. Gillilan RE, Ayers SD, Noy N. Structural basis for activation of fatty acid-binding protein 4. *J Mol Biol*. 2007;372:1246–60.
48. Lücke C, Rademacher M, Zimmermann AW, van Moerkerk HT, Veerkamp JH, Rüterjans H. Spin-system heterogeneities indicate a selected-fit mechanism in fatty acid binding to heart-type fatty acid-binding protein (H-FABP). *Biochem J*. 2001;354:259–66.
49. Corsico B, Cistola DP, Frieden C, Storch J. The helical domain of intestinal fatty acid binding protein is critical for collisional transfer of fatty acids to phospholipid membranes. *Proc Natl Acad Sci U S A*. 1998;95:12174–8.
50. de Gerónimo E, Rodríguez Sawicki L, Bottasso Arias N, Franchini GR, Zamarreño F, Costabel MD, et al. IFABP portal region insertion during membrane interaction depends on phospholipid composition. *Biochim Biophys Acta*. 2014;1841:141–50.
51. Dyszy F, Pinto AP, Araújo AP, Costa-Filho AJ. Probing the interaction of brain fatty acid binding protein (B-FABP) with model membranes. *PLoS One*. 2013;8:e019198.
52. Falomir-Lockhart LJ, Franchini GR, Guerbi MX, Storch J, Córscico B. Interaction of enterocyte FABPs with phospholipid membranes: clues for specific physiological roles. *Biochim Biophys Acta*. 2011;1811:452–9.
53. Galassi W, Villarreal MA, Montich GG. Relevance of the protein macrodipole in the membrane-binding process. Interactions of fatty-acid binding proteins with cationic lipid membranes. *PLoS One*. 2018;13:e0194154.
54. Nolan V, Perduca M, Monaco HL, Maggio B, Montich GG. Interactions of chicken liver basic fatty acid-binding protein with lipid membranes. *Biochim Biophys Acta*. 2003;1611:98–106.
55. Zamarreño F, Herrera FE, Córscico B, Costabel MD. Similar structures but different mechanisms. Prediction of FABPs-membrane interaction by electrostatic calculation *Biochim Biophys Acta*. 2012;1818:1691–7.
56. Sacchettini JC, Gordon JJ, Banaszak LJ. The structure of crystalline *Escherichia coli*-derived rat intestinal fatty acid-binding protein at 2.5-Å resolution. *J Biol Chem*. 1988;263:5815–9.
57. Levin LB, Ganoth A, Amram S, Nachliel E, Gutman M, Tsfadia Y. Insight into the interaction sites between fatty acid binding proteins and their ligands. *J Mol Model*. 2010;16:929–38.
58. Long D, Mu Y, Yang D. Molecular dynamics simulation of ligand dissociation from liver fatty acid binding protein. *PLoS One*. 2009;4:e6081.
59. Villarreal MA, Perduca M, Monaco HL, Montich GG. Binding and interactions of L-BABP to lipid membranes studied by molecular dynamic simulations. *Biochim Biophys Acta*. 2008;1778:1390–7.
60. Zimmerman AW, Rademacher M, Rüterjans H, Lücke C, Veerkamp JH. Functional and conformational characterization of new mutants of heart fatty acid-binding protein. *Biochem J*. 1999;344(Pt 2):495–501.

Ready to submit your research? Choose BMC and benefit from:

- fast, convenient online submission
- thorough peer review by experienced researchers in your field
- rapid publication on acceptance
- support for research data, including large and complex data types
- gold Open Access which fosters wider collaboration and increased citations
- maximum visibility for your research: over 100M website views per year

At BMC, research is always in progress.

Learn more biomedcentral.com/submissions



PUBLICATION

IV

Understanding the Role of Lipids in Signaling Through Atomistic and Multiscale Simulations of Cell Membranes

Moutusi Manna, Tuomo Nieminen & Ilpo Vattulainen

Annual Review of Biophysics 48 (2019), 421–439

DOI: 10.1146/annurev-biophys-052118-115553

Publication reprinted with the permission of the copyright holder

Annual Review of Biophysics

Understanding the Role of Lipids in Signaling Through Atomistic and Multiscale Simulations of Cell Membranes

Moutusi Manna,¹ Tuomo Nieminen,²
and Ipo Vattulainen^{2,3}

¹Department of Chemistry, Indian Institute of Science Education and Research Bhopal, Bhopal, Madhya Pradesh 462 066, India

²Computational Physics Laboratory, Tampere University, FI-33014 Tampere, Finland

³Department of Physics, University of Helsinki, FI-00014 Helsinki, Finland;
email: Ipo.Vattulainen@helsinki.fi

Annu. Rev. Biophys. 2019. 48:421–39

The *Annual Review of Biophysics* is online at
biophys.annualreviews.org

<https://doi.org/10.1146/annurev-biophys-052118-115553>

Copyright © 2019 by Annual Reviews.
All rights reserved

ANNUAL
REVIEWS **CONNECT**

www.annualreviews.org

- Download figures
- Navigate cited references
- Keyword search
- Explore related articles
- Share via email or social media

Keywords

signaling, lipids, molecular dynamics, computer simulations, multiscale simulations

Abstract

Cell signaling controls essentially all cellular processes. While it is often assumed that proteins are the key architects coordinating cell signaling, recent studies have shown more and more clearly that lipids are also involved in signaling processes in a number of ways. Lipids do, for instance, act as messengers, modulate membrane receptor conformation and dynamics, and control membrane receptor partitioning. Further, through structural modifications such as oxidation, the functions of lipids as part of signaling processes can be modified. In this context, in this article we discuss the understanding recently revealed by atomistic and coarse-grained computer simulations of nanoscale processes and underlying physicochemical principles related to lipids' functions in cellular signaling.

Contents

INTRODUCTION	422
LIPID FLIP-FLOPS AS PROCESSES DELIVERING INFORMATION ACROSS MEMBRANES	422
LIPID TRANSLOCATION MEDIATED BY MEMBRANE DEFECTS	425
PHOSPHATIDYLSERINE AS A MESSENGER OF DEATH—AND THE ROLE OF OXIDATIVE STRESS	426
POLYUNSATURATED FATTY ACIDS INVOLVED IN STRESS RESPONSE UNDER OXIDATIVE STRESS	427
CHOLESTEROL AND OXIDATIVE STRESS	428
MEMBRANE REGISTRATION AND INTERDIGITATION—MEANS FOR CROSS TALK BETWEEN BILAYER LEAFLETS	429
LIPID MESSENGERS BIND TO RECEPTORS AND TARGET PROTEINS AS ORTHOSTERIC LIGANDS	431
LIPIDS IN ALLOSTERIC MODULATION OF RECEPTOR ACTIVATION	432
LIPIDS MODULATING LIPID RECEPTORS	434
CONCLUDING REMARKS	434

INTRODUCTION

Life is based on communication. Even individual cells communicate as they receive messages from the outside of the cell that guide their activity and functions. This information is received at the cell membrane surface from which it is directed to the correct destination inside the cell. If anything in this process goes wrong, the consequences are often unpleasant—in the most severe cases, a disease. In essence, communication is crucial for survival.

The information arriving to the cell is primarily recognized by receptors embedded in cell membranes. Given that cell membranes are mostly composed of lipids, a number of intriguing questions emerge about the role of lipids in cellular signaling. How do lipids modulate receptor activation and function? Is it possible that lipids could act as messages, or messengers, such that their transport would also be a means of communication? Is it possible that the function of lipids could be reprogrammed by chemical modification?

Quite surprisingly, there are major gaps in our understanding regarding the role of lipids in cellular communication. This largely stems from the tiny scales in space and time that are typical for molecular-scale signaling processes. However, this is exactly the region where molecular simulation techniques are often the method of choice.

Here in this review, we discuss how atomistic and coarse-grained molecular simulations can be used to unravel how lipids contribute to cellular signaling. Given the conciseness of this article, the aim of this review is not to be exhaustive—rather, we discuss selected examples of recent work where computer simulations have shown the added value that they can provide to complement experiments. Other review articles discussing related topics, largely from an experimental point of view, are available in the literature (23, 98).

LIPID FLIP-FLOPS AS PROCESSES DELIVERING INFORMATION ACROSS MEMBRANES

Lipid translocation across biological membranes (flip-flop) is of profound importance in cell physiology. Phospholipids are mainly synthesized on the cytoplasmic face of the endoplasmic

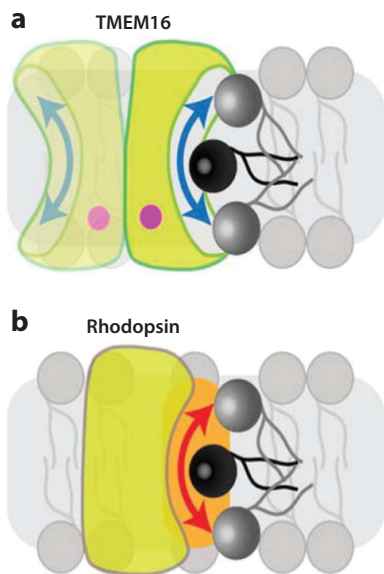


Figure 1

(a) Homodimeric transmembrane protein 16 (TMEM16) scramblase (containing bound Ca^{2+} indicated by pink dots) capable of scrambling a lipid along a hydrophilic groove facing the membrane, similar to swiping a credit card through a card reader. (b) Rhodopsin-mediated lipid scrambling taking place along the rhodopsin–membrane interface (orange zone). Figure adapted from Reference 21.

reticulum (ER) and must be scrambled between the two leaflets for uniform expansion of ER during cell growth (98). In plasma membranes, flip-flops are needed to establish and also dissipate the characteristic transmembrane lipid asymmetry, where the asymmetry is crucial for activating blood coagulation and apoptosis (38, 97). Specialized transporter enzymes such as ATP-dependent flippases and floppases use metabolic energy to translocate specific lipids across the membrane. Scramblases in turn promote rapid, nonspecific, and bidirectional movement of lipids without consuming ATP. It is intriguing that despite decades of active research, the molecular identities of scramblases and the understanding of their function are only beginning to emerge.

The first X-ray crystal structure of a scramblase [transmembrane protein 16 (TMEM16)] was reported in 2014 (12). The homodimeric structure of TMEM16 contains a membrane-faced, transbilayer hydrophilic groove on each of the subunits, through which the polar headgroup of a lipid can slide across the membrane, keeping the acyl chains in a favorable hydrophobic environment in a fashion that is analogous to swiping a credit card through a card reader (8, 12) (Figure 1). Earlier, Menon et al. (61) had discovered unexpected and robust scrambling activity for rhodopsin [a G protein–coupled receptor (GPCR)], which is structurally very different from TMEM16. Upon reconstitution into vesicles, different conformational states of rhodopsin were observed to facilitate rapid scrambling of phospholipids ($>10^4$ lipids per rhodopsin per second), speeding translocation up by a factor of $\sim 1,000$ and implying that conformational changes in the scramblase protein are not required for scrambling (27). Similar scrambling ability for the apo and the holo forms suggests that the lipid translocation path does not involve the water-containing

central core of the protein (27), which was also proposed earlier (61). These results suggest that the transverse diffusion of lipids along the rhodopsin–membrane interface could be a possible scrambling mechanism (21, 27) (**Figure 1**).

Computer simulations can provide precise atom-scale understanding of how the GPCR-facilitated scramblase function takes place. This is highlighted in recent simulation studies. T. Nieminen, M. Manna, T. Róg & I. Vattulainen (unpublished manuscript) used extensive atomistic molecular dynamics (MD) simulations to provide intriguing insight into the lipid scrambling mechanism of opsin—the apoprotein of rhodopsin. The study assessed the feasibility of various lipid transport routes and showed that opsin provides favorable conditions for the flip-flop of phospholipids along the protein surface. By fostering the hydration of the lipid headgroup as it glided next to helices II, III, and IV on the opsin surface, the free energy barrier of phospholipid flip-flop was reduced by ~50% compared to a protein-free membrane (**Figure 2**). This likely explains the high scrambling rate found in experiments. The study also concluded that the free energy barrier associated with the translocation of phospholipids through the central water core of opsin is very high, thus supporting the prediction previously made based on experiments (61). The simulation results (T. Nieminen, M. Manna, T. Róg & I. Vattulainen, unpublished manuscript) further suggested that the scramblase activity of opsin is not lipid selective, since the study showed opsin to lower the free energy barrier of cholesterol translocation by ~60% compared to a protein-free membrane with the same lipid composition (**Figure 2**). Similar conclusions were drawn for another receptor in the class-A GPCR family [β_2 -adrenergic receptor (β_2 AR)], which was also found to reduce the free energy barrier of cholesterol translocation, in agreement with experiments. Overall, these simulations (T. Nieminen, M. Manna, T. Róg & I. Vattulainen, unpublished manuscript) provide mechanistic insight into how selected proteins in the GPCR family function as ATP-independent nonselective lipid scramblases.

The molecular mechanism by which opsin facilitates rapid phospholipid scrambling has also been explored in another recent simulation study (63). The study reported that translocation took place in a manner where the lipid headgroup migrates along a hydrophilic path between the transmembrane helices VI and VII of opsin, while the lipid chains remained in the hydrophobic membrane region—similar to what is referred to as the credit card model proposed by experiment. The Markov state model analysis discussed in this study suggests that the rate-limiting step of the scrambling process is the opening of the hydrophilic path triggered by the conformational changes in opsin structure, where the internal hydration of opsin plays a key role in the scrambling mechanism (63).

Recent studies have shown that lipid flip-flops can be facilitated by synthetic transmembrane (TM) peptides characterized by low complexity (47). TM peptides can induce packing defects in the bilayer due to movement of the helices, local bilayer thinning, and transient penetration of water into the bilayer (39). Facilitated by defects at the lipid–helix interface, a lipid may “slip” into the membrane hydrophobic core with its headgroup in a solvated state and then “pop out” on the other side of the membrane (21). A recent study (67), which combined experiments and MD simulations, showed that the lipid scrambling activity of a single TM model peptide depends on the hydrophobic length of the peptide and the hydrophilicity of its central residues. Short peptides were observed to cause membrane thinning under negative mismatch, and the presence of a hydrophilic residue in the membrane core region fostered the penetration of water to the membrane interior. Together, these factors promote peptide-induced phospholipid flip-flop. An example highlighting this in practice is discussed in Reference 90, which demonstrated through atomistic simulations that the transmembrane WALP₂₃ peptide facilitates phospholipid flip-flop by lowering the free energy barrier of lipid translocation.

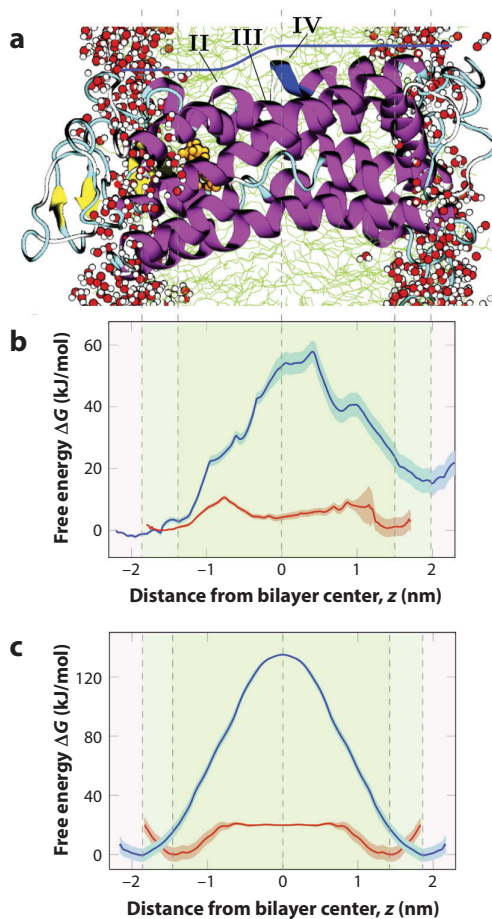


Figure 2

(*a*) Translocation path next to helices II, III, and IV of opsin. (*b*) Free energy profiles for POPC (1-palmitoyl-2-oleoyl-*m*-glycero-3-phosphocholine) (*blue*) and cholesterol (*red*) translocation along the opsin-membrane interface. Statistical errors are depicted by the shaded area. The reaction coordinate (z) is the difference between the lipid headgroup's center of mass and the bilayer center along the bilayer normal. (*c*) Free energy profiles for POPC (*blue*) and cholesterol (*red*) translocation in a protein-free membrane.

LIPID TRANSLOCATION MEDIATED BY MEMBRANE DEFECTS

In defect-free lipid membranes without proteins, passive lipid flip-flop is a very slow process—typical rates per lipid being of the order of one per day (1). However, this does not mean that flip-flops would not take place and the asymmetric lipid distributions in cell membrane structure would last forever even without ATP-driven nonequilibrium transport. Simulations have revealed that the slow rate is due to the energetically costly transport of the polar lipid headgroups through the hydrophobic membrane interior. As demonstrated by simulations, this can be speeded up by defects, such as membrane pores (29). Then the rate-limiting step in translocation is the formation of pores (defects) that can be induced by, for example, an applied external electric field, transmembrane ion imbalance, or the presence of surface-active molecules or antimicrobial peptides

(6, 30, 49, 99). The kinetics and thermodynamics of passive lipid translocation thereby strongly depend on membrane properties, such as lipid acyl chain length, headgroup chemistry, bilayer phase behavior (lipid packing), and the concentration of cholesterol that quite strongly modulates membrane packing (1, 7, 17, 52, 89).

PHOSPHATIDYLSERINE AS A MESSENGER OF DEATH—AND THE ROLE OF OXIDATIVE STRESS

The most prominent loss of transmembrane lipid asymmetry occurs during programmed cell death (apoptosis)—a coordinated process controlling the removal of damaged cells (4, 9, 22). In healthy cells, phosphatidylserine (PS) is confined to the cytoplasmic leaflet of the plasma membrane, while in cells undergoing apoptosis, PS is exposed to the exoplasmic leaflet. PS exposure therefore serves as a so-called eat-me signal that ensures effective recognition and engulfment of the dying cell by phagocytes. Given this, PS is a highly effective marker of apoptosis and has clinical applications in, for example, cancer therapy and infections. Scramblases such as proteins belonging to the TMEM16 family and Xk-related family are known to randomize the transmembrane PS distribution, while flippases such as P4-ATPase restore PS to the cytosolic leaflet (66). Intriguingly, despite extensive research, the precise role of these specific enzymes in apoptosis and their differential lipid translocation mechanisms remain obscure.

Another hallmark of apoptosis is oxidative stress. It takes place when the compensatory antioxidant defense of a cell is overwhelmed by excessive production of reactive oxygen species (ROS), which can oxidize membrane lipids and damage cell membranes. Recent studies (83, 100) have demonstrated that the oxidative damage of the plasma membrane can effectively catalyze PS scrambling in a nonenzymatic fashion.

Using MD simulations, Volinsky et al. (100) estimated the free energy of POPS (1-palmitoyl-2-oleyl-*sn*-glycero-3-phospho-L-serine) translocation in the presence and absence of oxidized POPC (1-palmitoyl-2-oleoyl-*sn*-glycero-3-phosphocholine) (100). The oxidized POPC simulated in this study had a truncated *sn*-2 hydrocarbon chain linked to an aldehyde group at the chain end (PoxnoPC), which is one of the major oxidation products in polyunsaturated phosphatidylcholines (PCs). In a membrane with 20 mol% of PoxnoPC, Volinsky et al. observed a 20-kJ/mol reduction in the free energy barrier of PS translocation, which can enhance the flip-flop rate by a factor of $\sim 10^3$ – 10^4 . To validate the simulation predictions, the authors also measured the transmembrane lipid diffusion using fluorescence techniques (100). They observed a profound enhancement of PS flip-flop in liposomes containing oxidized PC; for example, the half-time was found to be ~ 2 h in membranes with 16 mol% of PoxnoPC, while in intact membranes, the half-time was several weeks. These findings are supported by another simulation study, which showed the free energy barrier of PS translocation to decrease linearly with increasing concentration of peroxidized PC (83) (**Figure 3**). For 50 mol% peroxidized PC, the free energy barrier of POPS translocation was found to drop $\sim 30\%$ compared to an intact membrane. Interestingly, both of the abovementioned computational studies indicate that the translocation of PS is accompanied by the formation of a membrane defect, which facilitates the crossing of the polar lipid headgroup through the hydrophobic core of the membrane. In membranes rich in oxidized lipids, the polar oxidized group most obviously lowers the energy cost of formation of membrane defects/pores, thus reducing the free energy barrier of PS translocation.

PS externalization in response to high-field nanosecond-long electric pulses was demonstrated in Reference 99 using a combination of simulations and fluorescence microscopy imaging. In simulations of asymmetric bilayers (with PS located in one of the leaflets) subjected to a high transmembrane voltage (>450 mV/nm), Vernier et al. observed fast intrusion of water on the

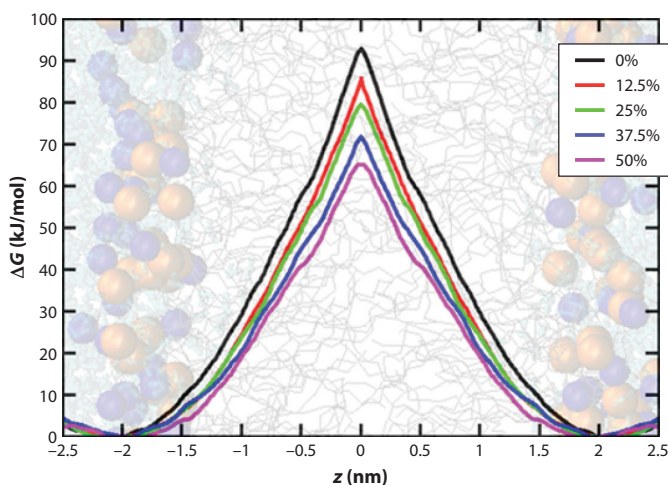


Figure 3

Free energy profiles for phosphatidylserine translocation through phospholipid bilayers with different levels of peroxidation (see legend). Figure adapted from Reference 83.

cathode side of the membrane, leading to pore formation. The anionic PS headgroup was then electrophoretically dragged along the pore wall. The authors showed that PS translocates only after pore formation and always to the anode side of the membrane, in line with the experimental observations made on live cells (99). Similar electroporation and PS externalization were reported earlier based on coarse-grained simulations (35). The field-driven alignments of water and lipid headgroup dipoles are critical for electroporation and anode-directed PS translocation.

POLYUNSATURATED FATTY ACIDS INVOLVED IN STRESS RESPONSE UNDER OXIDATIVE STRESS

As described above, an excessive amount of ROS causes cellular damage and contributes to aging and age-related disorders. The significance of the problem is illustrated by the fact that nearly 5% of the total energy used by the body is spent for maintaining and repairing cell membranes damaged by oxidation (11). In this context, the primary targets of ROS are polyunsaturated fatty acids (PUFAs) because of the numerous double bonds in their hydrocarbon chains. In phospholipids, two major oxidized lipid products of the PUFA chain in the *m*-2 position typically include either a hydroperoxide group or a truncated chain containing an aldehyde or a carboxylic group at the terminus (102). When a hydrophilic group is attached to the *m*-2 chain, the acyl chain is expected to change its orientation in order to contact water (acyl chain reversal), unlike intact PUFA chains that adopt a typical orientation toward the hydrophobic core of a bilayer. The reorientation of the acyl chain depends on the chemical structure of the oxidative modification. For example, an oxidized chain with a terminal carboxyl group in the deprotonated state flips toward water along the bilayer normal, whereas the protonated form of the chain adopts a parallel orientation along the lipid-water interfacial plane (60). In the same context, it was found that while the hydroperoxide group of an oxidized lipid rises to the membrane surface, the peroxy radical intermediate is instead positioned in the innermost region of a membrane like a nonoxidized lipid (24). The acyl chain reversal increases the area per lipid, leads to bilayer thinning, and decreases lipid chain conformational order, thus promoting water permeability and membrane deformation. The effects of

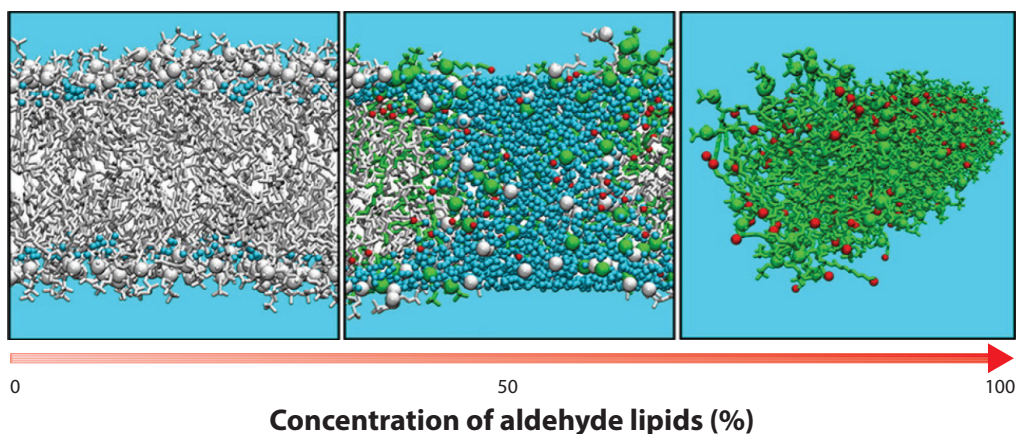


Figure 4

Pore formation and micellation in a lipid bilayer for an increasing concentration of aldehyde lipids (*green*) mixed with nonoxidized phospholipids (*white*). Green and white spheres represent the phosphorus atoms of the lipids. Red spheres depict the oxygen atom of the aldehyde group of the oxidized lipid tails. Blue spheres represent oxygen of water. Figure adapted from Reference 10.

oxidized lipids on the structure and permeation properties of lipid bilayers have been studied by simulations (10, 51, 69, 75, 93, 101) and experiments (37, 87) quite extensively.

A recent computational study demonstrated how the polar groups of oxidized lipids perturb the bilayer, induce formation of pores and other membrane defects, and also induce micellation (10). In a binary mixture of polyunsaturated PCs and their peroxide and aldehyde products, Boonnoy et al. observed formation of membrane defects with both peroxide and aldehyde lipids, but full pores were found only with aldehyde at medium concentrations (~50 mol%). With aldehyde lipids, the hydrophilic tips of the oxidized chains were highly mobile inside the bilayer and got into contact with lipids of the opposing leaflet. Consequently, the aldehyde groups pulled water into the bilayer interior, leading to the formation of a water pore stabilized by the flipping of lipid headgroups along the pore wall (**Figure 4**) (10). At higher aldehyde concentrations (>75 mol%), the membrane pores were unstable and the bilayer deformed into a micelle (**Figure 4**). Meanwhile, no pores or micelles were formed with peroxidized lipids (10), suggesting that the highly polar peroxidized groups prefer the membrane–water interface to the bilayer interior.

CHOLESTEROL AND OXIDATIVE STRESS

The role of cholesterol in oxidative stress and the related signaling phenomena is twofold. First, results for intact (nonoxidized) cholesterol demonstrate that cholesterol has a protecting effect against mechanical instability arising from lipid oxidation. Recent computational studies showed that cholesterol forms hydrogen bonds with the oxidized lipids and thereby prevents pore formation and micellation (75). The condensing and ordering effects of the sterol backbone were found to be significant even in a massively peroxidized membrane with all phospholipids and cholesterol peroxidized (69).

Second, cholesterol itself can also be oxidized through the double bond in the ring of cholesterol or H-atom transfer from the allylic position (102). ROS generate ring-oxidized sterols, whereas tail-oxidized sterols are produced by enzymatic oxidation. Despite their relatively low concentrations at physiological conditions, oxysterols are primary players in many biological processes, including signaling, given that there are quite a few oxysterol-binding membrane receptors

(40). As shown by MD simulations for a wide range of ring- and tail-oxidized sterols, the ordering and condensing effects of oxysterols correlate with their orientation in a lipid bilayer (42, 74). While ring-oxidized sterols behave more or less similar to cholesterol, tail-oxidized sterols can orient themselves either parallel or perpendicular to the bilayer normal because of an additional polar group at the hydrocarbon chain. Oxysterols with rather weak headgroup polarity (e.g., the 3β -OH group replaced by the ketone group in 4-cholesten-3-one) undergo frequent interleaflet movements or flip-flop motion (70, 86). Also, this oxidized derivative has a lower free energy barrier for desorption from the membrane to the water phase than cholesterol, and it can be readily transferred to its extracellular acceptors (70), which has a direct consequence for the cellular trafficking of cholesterol.

As discussed above, lipid flip-flops in the absence of scramblases are usually very slow; however, sterols seem to be an exception to this rule. A variety of simulation studies have determined free energy barriers associated with cholesterol translocation (7, 17, 70) and identified the flip-flop mechanism, which is based on cholesterol turning around in the middle of the bilayer. For oxysterols, the flip-flop mechanism can be distinctly different, as highlighted by a recent computational study, which revealed a novel translocation mechanism for tail-oxidized sterols (41): 27-OH-cholesterol was shown to move back and forth along the membrane normal with either its 3β -OH group (in the head) exposed to water with the 27-OH group (in the tail) buried inside the membrane, or vice-versa. This so-called bobbing mechanism does not require the energetically costly change in sterol orientation during the flip-flop process and thereby renders the translocation process extremely fast (41). For a related oxysterol (25-OH-cholesterol), it has been demonstrated that it transfers from the plasma membrane to the ER with a rate that is 100 times faster than that of cholesterol (45, 46). For 24S-OH-cholesterol and 27-OH-cholesterol, the transport from erythrocytes to the plasma membrane is fast, while the transport of cholesterol is almost negligible (59). While the reasons for the distinctly different transport rates are not known, it is quite possible that the rapid translocation in terms of the bobbing mechanism plays a role in the rapid signaling mediated by selected oxysterols.

MEMBRANE REGISTRATION AND INTERDIGITATION—MEANS FOR CROSS TALK BETWEEN BILAYER LEAFLETS

Plasma membranes of eukaryotic cells are characterized by considerable transbilayer lipid asymmetry. Sphingomyelin (SM) is more concentrated in the extracellular leaflet, whereas PS and phosphatidylethanolamine (PE) are more confined to the cytosolic leaflet (38, 98). The distribution of cholesterol is a matter of debate, but it is inferred to be concentrated more in the extracellular leaflet by virtue of its predicted association with SM (38). If the two leaflets were uncoupled, then only the extracellular leaflet would be expected to form raft-like domains. Such transbilayer compositional asymmetry may lead to phase asymmetry or antiregistration, meaning that the two opposing leaflets have different fluidity. Alternatively, a domain in one leaflet can induce the formation of a similar domain in the opposite leaflet, leading to phase symmetry or registration (58, 71). This paradigm may explain why certain proteins that are exclusively associated with the cytosolic leaflet of the plasma membrane are colocalized with raft components (103). But then, how do the two leaflets of a biological membrane modulate each other's physical properties? While several plausible mechanisms have been proposed (18, 58), the idea of dynamic chain interdigitation is one of the most promising ways to understand the cross talk between the membrane leaflets.

A recent study employed atomistic simulations to assess how the extracellular and cytosolic leaflets of membranes interact through interdigitation (85). The study used realistic model

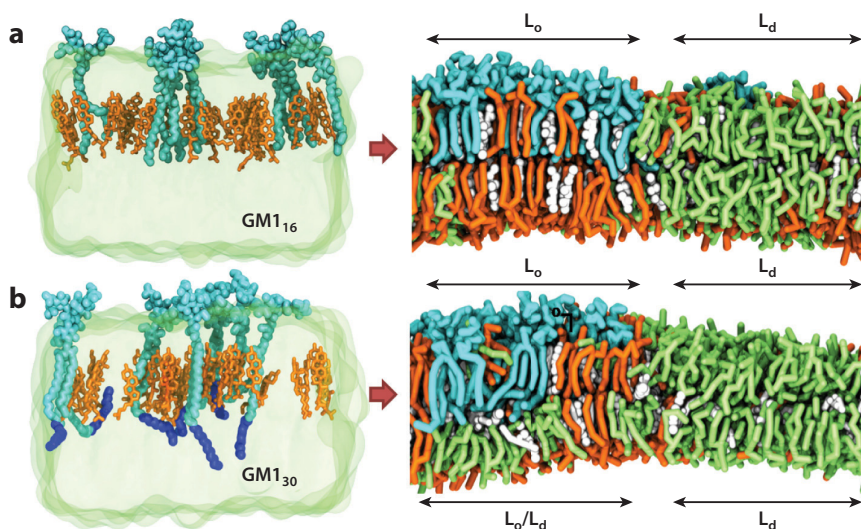


Figure 5

(a) Transmembrane domain registration in a bilayer containing short-chain GM1. L_o stands for the liquid-ordered phase (domain) and L_d for the liquid-disordered phase. (b) Mixing of saturated and unsaturated lipids in the inner leaflet induced by interdigitation of GM1 with long acyl chains. Figure adapted from Reference 53.

membrane systems, which closely mimicked the composition of eukaryotic plasma membranes. The results revealed that SM with a long saturated acyl chain (SM 18:1–24:0) protruded deep into the opposing bilayer leaflet, and the penetration was particularly strong when the bilayer was asymmetric. The interdigitation affected the conformational order of the penetrating SM acyl chain as well as the order of the opposing membrane leaflet, thereby strengthening the interaction and the coupling across the membrane (85). A similar mechanism was reported in another atom-scale simulation study, where a long-chain ganglioside (GM1) was observed to promote transbilayer coupling through interdigitation (53). To unravel how the acyl chain length of GM1 contributes to membrane registration, the study also used coarse-grained simulations probing longer timescales in large membrane systems. The results showed that with short-chain GM1 lipids (with ~18 carbons) in the extracellular leaflet, both bilayer leaflets readily underwent complete phase separation leading to a phase-symmetric bilayer with strong membrane registration (**Figure 5**). In contrast, GM1 with an extended acyl chain (~30 carbons) was found to perturb the phase of the GM1-free cytosolic leaflet. The significant interdigitation of the long acyl chain of GM1 into the opposite leaflet was observed to induce the mixing of saturated and unsaturated lipids, thus preventing or at least slowing down the phase separation in the cytosolic leaflet and weakening the overall membrane registration process (**Figure 5**) (53).

An earlier study using extensive coarse-grained simulations showed a transition from the registered to antiregistered bilayer configurations when the length of the saturated lipids was increased from ~16 to ~20 carbons, increasing the height mismatch between ordered and disordered domains by ~0.4 nm (80). The results showed that in compositionally symmetric phase-separated bilayers composed of cholesterol, saturated lipids, and unsaturated lipids, the transbilayer phase asymmetry results from the mismatched acyl chain lengths. Theoretical models have suggested that domain registration is directed by the balance between two tensions (58): the interleaflet

tension at the bilayer midplane, which is minimized by transbilayer registration, and the intraleaflet tension at domain boundaries due to height mismatch, which can be relieved by mixing saturated and unsaturated lipids at domain boundaries (80).

In conclusion, the simulation studies suggest that the physical interactions between the two leaflets in the form of interdigitation provide a means to mediate transmembrane communication associated with signal transduction.

LIPID MESSENGERS BIND TO RECEPTORS AND TARGET PROTEINS AS ORTHOSTERIC LIGANDS

Lipids are not just passive constituents of cell membranes or a source of stored energy; they can also act as signaling molecules (23). Extracellular stimuli can elicit cellular responses through generation of intracellular second messengers. Agonists of cellular receptors, such as GPCRs and tyrosine kinases, activate enzymes such as phospholipases, sphingomyelinases, and phosphatidylinositol-3-kinase, which catalyze the cleavage of lipids (73). Lipid metabolites such as sphingosine-1-phosphate (S1P), diacylglycerol, or ceramide are important examples of lipid messengers, which serve as intracellular signals and bind target proteins to mediate specific cellular responses.

The mechanisms of lipid signal transduction are poorly understood but often involve GPCRs. As reviewed recently (96), over 50 GPCRs have been implicated in signaling lipids that include lysophospholipids, phospholipids, fatty acids, and eicosanoids. Dysregulation of these lipid GPCRs contributes to diverse cancer-related processes and may be therapeutically exploited (96). Most lipid GPCRs belong to class-A (rhodopsin-like) GPCRs. However, unlike prototypical GPCRs that recognize small hydrophilic ligands, lipid GPCRs are activated by lipid mediators, which possess a polar headgroup and long hydrophobic moieties, thus implying significantly different activation mechanisms. Sphingosine-1-phosphate receptors (S1PR₁₋₅) and lysophosphatidic acid receptors belong to this receptor superfamily. In the past few years, crystal structures of several lipid GPCRs have been resolved, including the structure of antagonist-bound S1PR₁ (33). S1P activates five cell-surface GPCRs (S1PR₁₋₅). By combining MD simulations and functional assays using S1P analogs with different alkyl chain lengths, a recent study demonstrated that the alkyl chain length of the lipidic agonist is the key structural feature in the activation of S1P receptors (95). The data suggest that the headgroup of S1P is required for high-affinity binding, but the alkyl chain is responsible for triggering the activation. S1P stabilizes the active state of S1PR₁ by inserting its lipid chain into the small hydrophobic cavity of the receptor between TM domains 3, 5, and 6. The ligand efficacy was observed to be directly related to the alkyl chain length and to vary within receptor subtypes owing to different volumes of binding cavities (95). Another recent work by the McCammon group (15) investigated the activation mechanism of ligand-free S1PR₁. The simulations captured four independent activation events and correlated helix movement during activation. During the simulations, a lipid molecule was repeatedly found to enter the receptor between the extracellular ends of TM1 and TM7.

Cholesterol is known for its modulatory role on GPCRs. Cholesterol and its derivatives are even speculated to modulate functions of certain class-A GPCRs from the orthosteric binding pocket, similar to conventional class-A ligands (5, 92). A recent crystal structure shows a cholesterol molecule at the binding site of the extracellular domain of a class-F GPCR (14). The rather surprising orthosteric mode of action of cholesterol is less explored. It has been postulated that cholesterol can allosterically regulate GPCRs by directly interacting with them at specific sites on the receptor surface or by indirectly changing the physical properties of the membrane (25, 76). In certain cases, however, the impact of cholesterol on GPCRs can go beyond pure allosteric

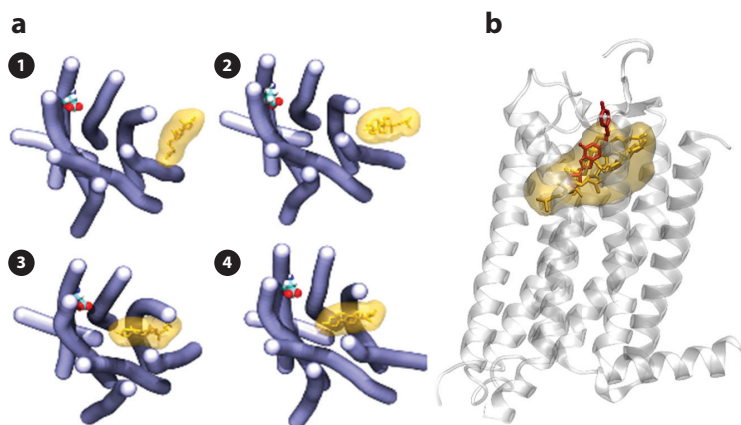


Figure 6

(a, 1–4) Entrance of cholesterol (yellow) into the orthosteric ligand-binding site of the adenosine A_{2A} receptor (blue). (b) The average position of cholesterol in the binding site calculated from simulations (yellow transparent region) and superimposed on the crystal structure of the agonist-bound receptor (red sticks). Also shown is the final simulation snapshot of cholesterol at the binding site (yellow sticks). Figure adapted from Reference 28.

modulation. By combining experimental and computational approaches, a recent study showed that membrane cholesterol can spontaneously invade into the orthosteric ligand-binding pocket of the adenosine A_{2A} receptor (Figure 6) and compete with specific ligand binding (28). In addition to several interaction sites on the receptor surface, simulations demonstrated high cholesterol densities to populate a significant area of the orthosteric ligand-binding site of the receptor, overlapping with the position of the ligand found in the crystal structure (Figure 6). Cholesterol entered the binding pocket through the extracellular side of TM5–6 using the same portal gate that was previously suggested for the entry of a ligand into opsin. Confirming the simulations, experiments showed specific ligand binding to increase for decreasing cholesterol content. Further, the authors confirmed the presence of cholesterol inside the receptor by chemical modification of the receptor interior in a biotinylation assay. The study (28) strongly suggests a new regulatory mechanism of cholesterol and also provides an example of how simulations can bring added value to experiments.

LIPIDS IN ALLOSTERIC MODULATION OF RECEPTOR ACTIVATION

Lipids are progressively emerging as essential modulators of membrane protein functions, including major families of cellular receptors such as GPCRs (19, 25, 82), receptor tyrosine kinases (36, 62), T-cell receptors (94), and ligand-/voltage-gated ion channels (3, 31, 43, 78). These receptors are signaling machines embedded in cell membranes, which convert extracellular stimuli into cellular responses. Biological membranes host dynamic lipid–protein assemblies, where a protein with selected lipids may create its own functional lipid microenvironment (44, 78). Several studies have identified and characterized lipid interaction sites in a variety of membrane proteins (34, 44, 78). A lipid specifically bound to a protein at a site that is not an orthosteric site may also regulate protein structure and function, a process referred to as allosteric modulation. Despite substantial instances of lipid modulation, the mechanisms of allosteric modulation remain unclear. MD simulations could offer detailed insight into specific lipid–protein interactions and their effects (2, 91),

but so far, only limited computational studies have been able to link these physical interactions to functional consequences of receptor activation/function. These studies have mostly focused on GPCRs owing to their involvement in a multitude of physical processes, the acknowledged lipid dependency of GPCRs, and also the availability of several crystal structures, which make GPCRs viable for computational investigations.

Biologically relevant phospholipids can act as allosteric regulators of GPCR function. A recent experimental study showed that lipids with the phosphatidylglycerol (PG) headgroup strongly favor agonist binding and receptor activation of the β_2 AR, whereas the PE headgroup favors antagonist binding and stabilizes the inactive state of the receptor (19). A recent computational study (13) provided mechanistic insight into positive and negative allosteric modulation and showed that the effect is attributed to the chemical differences between and charges of these lipid headgroups, which modify the lipid–receptor interactions and alter membrane properties. Simulations also showed that the negatively charged 1,2-dioleoyl-*sn*-glycero-3-phosphoglycerol (DOPG) lipid preferentially interacts with the positively charged residues of the intercellular loop 3 and the intercellular end of TM6, which give rise to an outward pull on TM6 and stabilize receptor conformation with an open G protein–binding interface that is characteristic of the active state of the receptor. Further, this study, and also an earlier computational investigation, showed that PG from the cytosolic leaflet intrudes into the empty G protein–binding site between TM6 and TM7 of β_2 AR that is in the active state (13, 68). The negatively charged PG headgroup specifically interacts with R131^{3,50} on TM3 and inhibits the formation of a conserved R131^{3,50}–E268^{6,30} ionic lock, which characterizes the inactive state of the receptor. These studies suggest that the binding of anionic PG stabilizes the active state of the receptor via conformational selection. Meanwhile, the neutral 1,2-dioleoyl-*sn*-glycero-3-phosphoethanolamine (DOPE) lipids (with a positively charged ethanol amine moiety in the headgroup) create unfavorable interactions with the positively charged residues of TM6, thereby destabilizing the active state and strongly favoring complete deactivation of β_2 AR (13).

Another recent computational study (88) showed that the PE headgroup and the polyunsaturated docosahexaenoic acid chains preferentially bind to the inactive conformation of rhodopsin, suggesting that the lipid modulation arises from both solvent-like (membrane mediated) and ligand-like (direct lipid–protein) interactions that depend on the state/conformation of the receptor. Reference 13 further showed that another neutral lipid [1,2-dioleoyl-*sn*-glycero-3-phosphocholine (DOPC)] can induce partial deactivation of β_2 AR, in agreement with computational results by Dror and colleagues (20, 48) that showed gradual inactivation of β_2 AR in a POPC membrane. Unlike PE, the PC headgroup is more hydrophobic and unable to form interlipid hydrogen bonds, resulting in a lower membrane density. In a less dense DOPC membrane, β_2 AR exhibits greater conformational freedom and inactivates slower than in a DOPE bilayer, in agreement with experimental results (19).

Cholesterol is frequently invoked as a modulator of protein structure (16, 55, 65), stability (32, 104), oligomerization (reviewed in Reference 79), and ligand binding of several GPCRs (25, 26, 72, 76, 77, 81, 82). The literature reporting the functional role of cholesterol as a positive or negative modulator of GPCR activity is extensive. It has been a matter of intense debate whether the modulation is due to cholesterol-induced changes in membrane properties, specific and direct cholesterol–GPCR interactions, or both. Crystal structures have revealed the binding of cholesterol to the surface of several GPCRs (25, 32, 34), suggesting specific allosteric sites for cholesterol. However, the functional relevance of these physical interactions and the atomic-scale mechanism of cholesterol modulation have remained unknown. A recent computational study clarified this issue to a large degree, however. It provided atomistic insight into the mechanism of allosteric regulation of β_2 AR by cholesterol (56). The study showed that under cholesterol-rich conditions,

cholesterol has a large impact on the conformational dynamics of β_2 AR, as cholesterol limits the receptor conformation predominantly to one state. Under cholesterol-poor conditions, the conformational distribution was found to be very broad (54, 56). The mechanism of action was revealed to be based on binding of cholesterol at two specific interaction sites located near the TM5, TM6, and TM7 domains, which are evolutionally conserved among β_2 AR orthologs. Cholesterols bound at these sites significantly impeded the mobility of the respective helices, thereby reducing the overall conformational flexibility of the receptor. The effect was found to depend on the strength of cholesterol binding and not on the physical state of the surrounding bilayer (56). The study also showed that cholesterol bound between TM5 and TM6 on the intracellular side exerts the strongest effect by preventing the outward movement of TM6 required for activation of β_2 AR. However, cholesterol also stabilizes the active state of the receptor by preventing the inward movement of TM6. Altogether, the study shows that cholesterol reduces the conformational flexibility of β_2 AR, weakening chances to switch between different functional states (56).

LIPIDS MODULATING LIPID RECEPTORS

Not all receptors are proteins. There are also quite a few lipids acting as receptors, with glycosphingolipids being perhaps the primary example of this class. Glycolipids are challenging to consider through computer simulations, since in these lipids, the carbohydrate headgroup carries out the recognition that is highly dependent on the chemical details of the headgroup. Instead of coarse-grained models, the most appropriate approach is to use atomistic simulations (57). Lingwood et al. (50) used this strategy to reveal the mechanism used by cholesterol to modulate the receptor function of GM1. By inducing a tilt in the GM1 headgroup, cholesterol was able to induce a loss of access for ligand binding. Recent simulations by Rissanen et al. (84) support this picture. Exploring this issue more broadly would be exceptionally justified.

CONCLUDING REMARKS

Cell signaling coordinates cell actions and controls a variety of cellular processes. Errors in signaling often lead to diseases such as cancer and diabetes. By understanding the underlying physical and chemical bases of signaling, the chances of clarifying why and how these diseases emerge would be significantly improved.

Even though membrane proteins are the main contributor to cellular communication taking place in or through cell membranes, there is reason to keep in mind that membrane proteins are modulated by a number of factors, particularly lipids. Further, since it is quite possible that membrane lipid compositions are altered in certain diseases (64), the modulation of membrane proteins by lipids is also dependent on whether the subject is healthy or exposed to a disease.

In this article, we have discussed how lipids contribute to and take part in cell signaling. Among many other ways, lipids modulate protein conformations and act as messengers, and they are subject to structural modifications that can change the lipids' functions in the context of signaling. Further, even though there is not enough space to discuss this topic more broadly, it is worth mentioning that lipids can also control protein activation by, for example, modulating the partitioning of membrane proteins by varying membrane physical properties and altering the intramembrane pressure profile exerted on transmembrane proteins. There are many ways in which lipids can take part in signaling, but the very essence of the matter remains the same: The role of lipids in cellular signaling is significant. And the added value given by simulations to reveal how lipids are involved in cellular signaling is impressive.

DISCLOSURE STATEMENT

The authors are not aware of any affiliations, memberships, funding, or financial holdings that might be perceived as affecting the objectivity of this review.

ACKNOWLEDGMENTS

We thank the Department of Biotechnology, government of India, for financial support under the Bio-CARe for Women Scientists 2016 program (no. BT/PR17981/BIC/101/576/2016) (M.M.). We also acknowledge financial support granted by the Sigrid Jusélius Foundation, HiLIFE (University of Helsinki), Academy of Finland [Centre of Excellence project (grant no. 307415)], and the European Research Council [Advanced Grant project CROWDED-PRO-LIPIDS (grant no. 290974)]. CSC-IT Center for Science (Espoo, Finland) is acknowledged for computing resources.

LITERATURE CITED

1. Allhusen JS, Conboy JC. 2016. The ins and outs of lipid flip-flop. *Acc. Chem. Res.* 50:58–65
2. Aponte-Santamaría C, Briones R, Schenk AD, Walz T, de Groot BL. 2012. Molecular driving forces defining lipid positions around aquaporin-0. *PNAS* 109:9887–92
3. Baenziger JE, Morris ML, Darsaut TE, Ryan SE. 2000. Effect of membrane lipid composition on the conformational equilibria of the nicotinic acetylcholine receptor. *J. Biol. Chem.* 275:777–84
4. Balasubramanian K, Schroit AJ. 2003. Amino phospholipid asymmetry: a matter of life and death. *Annu. Rev. Physiol.* 65:701–34
5. Benned-Jensen T, Norn C, Laurent S, Madsen CM, Larsen HM, et al. 2012. Molecular characterization of oxysterol binding to the Epstein-Barr virus-induced gene 2 (GPR183). *J. Biol. Chem.* 287:35470–83
6. Bennett WFD, Hong CK, Wang Y, Tieleman DP. 2016. Antimicrobial peptide simulations and the influence of force field on the free energy for pore formation in lipid bilayers. *J. Chem. Theory Comput.* 12:4524–33
7. Bennett WFD, MacCallum JL, Hinner MJ, Marrink SJ, Tieleman DP. 2009. Molecular view of cholesterol flip-flop and chemical potential in different membrane environments. *J. Am. Chem. Soc.* 131:12714–20
8. Bethel NP, Grabe M. 2016. Atomistic insight into lipid translocation by a TMEM16 scramblase. *PNAS* 113:14049–54
9. Bevers EM, Williamson PL. 2016. Getting to the outer leaflet: physiology of phosphatidylserine exposure at the plasma membrane. *Physiol. Rev.* 96:605–45
10. Boonnoy P, Jarerattanachai V, Karttunen M, Wong-ekkabut J. 2015. Bilayer deformation, pores, and micellation induced by oxidized lipids. *J. Phys. Chem. Lett.* 6:48844–48
11. Brenna JT, Carlson SE. 2014. Docosahexaenoic acid and human brain development: evidence that a dietary supply is needed for optimal development. *J. Hum. Evol.* 77:99–106
12. Brunner JD, Lim NK, Schenck S, Duerst A, Dutzler R. 2014. X-ray structure of a calcium-activated TMEM16 lipid scramblase. *Nature* 516:207
13. Bruzzese A, Gil C, Dalton JA, Giraldo J. 2018. Structural insights into positive and negative allosteric regulation of a G protein-coupled receptor through protein-lipid interactions. *Sci. Rep.* 8:4456
14. Byrne EF, Sircar R, Miller PS, Hedger G, Luchetti G, et al. 2016. Structural basis of Smoothed regulation by its extracellular domains. *Nature* 535:517–22
15. Caliman AD, Miao Y, McCammon JA. 2017. Activation mechanisms of the first sphingosine-1-phosphate receptor. *Protein Sci.* 26:1150–60
16. Casiraghi M, Damian M, Lescop E, Point E, Moncoq K, et al. 2016. Functional modulation of a G protein-coupled receptor conformational landscape in a lipid bilayer. *J. Am. Chem. Soc.* 138:11170–75
17. Choubey A, Kalia RK, Malmstadt N, Nakano A, Vashishta P. 2013. Cholesterol translocation in a phospholipid membrane. *Biophys. J.* 104:2429–36

18. Collins MD, Keller SL. 2008. Tuning lipid mixtures to induce or suppress domain formation across leaflets of unsupported asymmetric bilayers. *PNAS* 105:124–28
19. Dawaliby R, Trubbia C, Delporte C, Masureel M, van Antwerpen P, et al. 2016. Allosteric regulation of G protein-coupled receptor activity by phospholipids. *Nat. Chem. Biol.* 12:35–39
20. Dror RO, Arlow DH, Maragakis P, Mildorf TJ, Pan AC, et al. 2011. Activation mechanism of the β_2 -adrenergic receptor. *PNAS* 108:18684–89
21. Ernst OP, Menon AK. 2015. Phospholipid scrambling by rhodopsin. *Photochem. Photobiol. Sci.* 14:1922–31
22. Fadeel B, Xue D. 2009. The ins and outs of phospholipid asymmetry in the plasma membrane: roles in health and disease. *Crit. Rev. Biochem. Mol. Biol.* 44:264–77
23. Fernandis AZ, Wenk MR. 2007. Membrane lipids as signaling molecules. *Curr. Opin. Lipidol.* 18:121–28
24. Garrec J, Monari A, Assfeld X, Mir LM, Tarek M. 2014. Lipid peroxidation in membranes: The peroxy radical does not “float.” *J. Phys. Chem. Lett.* 5:1653–58
25. Gimpl G. 2016. Interaction of G protein coupled receptors and cholesterol. *Chem. Phys. Lipids* 199:61–73
26. Gimpl G, Burger K, Fahrenholz F. 1997. Cholesterol as modulator of receptor function. *Biochemistry* 36:10959–74
27. Goren MA, Morizumi T, Menon I, Joseph JS, Dittman JS. 2014. Constitutive phospholipid scramblase activity of a G protein-coupled receptor. *Nat. Commun.* 5:5115
28. Guixà-González R, Albasanz JL, Rodríguez-Espigares I, Pastor M, Sanz F, et al. 2017. Membrane cholesterol access into a G-protein-coupled receptor. *Nat. Commun.* 8:14505
29. Gurtovenko AA, Anwar J, Vattulainen I. 2010. Defect-mediated trafficking across cell membranes: insights from in silico modeling. *Chem. Rev.* 110:6077–103
30. Gurtovenko AA, Vattulainen I. 2007. Molecular mechanism for lipid flip-flops. *J. Phys. Chem. B* 111:13554–59
31. Hansen SB, Tao X, MacKinnon R. 2011. Structural basis of PIP₂ activation of the classical inward rectifier K⁺ channel Kir2.2. *Nature* 477:495–98
32. Hanson MA, Cherezov V, Griffith MT, Roth CB, Jaakola V-P, et al. 2008. A specific cholesterol binding site is established by the 2.8 Å structure of the human β_2 -adrenergic receptor. *Structure* 16:897–905
33. Hanson MA, Roth CB, Jo E, Griffith MT, Scott FL, et al. 2012. Crystal structure of a lipid G protein-coupled receptor. *Science* 335:851–55
34. Hedger G, Sansom MS. 2016. Lipid interaction sites on channels, transporters and receptors: recent insights from molecular dynamics simulations. *Biochem. Biophys. Acta* 1858:2390–400
35. Hu Q, Joshi RP, Schoenbach KH. 2005. Simulations of nanopore formation and phosphatidylserine externalization in lipid membranes subjected to a high-intensity, ultrashort electric pulse. *Phys. Rev. E* 72:031902
36. Kaszuba K, Grzybek M, Orłowski A, Danne R, Róg T, et al. 2015. N-glycosylation as determinant of epidermal growth factor receptor conformation in membranes. *PNAS* 112:4334–39
37. Knobloch JJ, Nelson AR, Köper I, James M, McGillivray DJ. 2015. Oxidative damage to biomimetic membrane systems: in situ Fe (II)/ascorbate initiated oxidation and incorporation of synthetic oxidized phospholipids. *Langmuir* 31:12679–87
38. Kobayashi T, Menon AK. 2018. Transbilayer lipid asymmetry. *Curr. Biol.* 28:R386–91
39. Kol MA, van Laak AN, Rijkers DT, Killian JA, de Kroon AI, de Kuijff B. 2003. Phospholipid flop induced by transmembrane peptides in model membranes is modulated by lipid composition. *Biochemistry* 42:231–37
40. Kulig W, Cwiklik L, Jurkiewicz P, Rog T, Vattulainen I. 2016. Cholesterol oxidation products and their biological importance. *Chem. Phys. Lipids* 199:144–60
41. Kulig W, Mikkolainen H, Olżyńska A, Jurkiewicz P, Cwiklik L, et al. 2018. Bobbing of oxysterols: molecular mechanism for translocation of tail-oxidized sterols through biological membranes. *J. Phys. Chem. Lett.* 9:1118–23
42. Kulig W, Olżyńska A, Jurkiewicz P, Kantola AM, Komulainen S, et al. 2015. Cholesterol under oxidative stress—how lipid membranes sense oxidation as cholesterol is being replaced by oxysterols. *Free Radic. Biol. Med.* 84:30–41

43. Laganowsky A, Reading E, Allison TM, Ulmschneider MB, Degiacomi MT, et al. 2014. Membrane proteins bind lipids selectively to modulate their structure and function. *Nature* 510:172–75
44. Landreh M, Marty MT, Gault J, Robinson CV. 2016. A sliding selectivity scale for lipid binding to membrane proteins. *Curr. Opin. Struct. Biol.* 39:54–60
45. Lange Y, Ye J, Rigney M, Steck TL. 1999. Regulation of endoplasmic reticulum cholesterol by plasma membrane cholesterol. *J. Lipid Res.* 40:2264–70
46. Lange Y, Ye J, Strebel F. 1995. Movement of 25-hydroxycholesterol from the plasma membrane to the rough endoplasmic reticulum in cultured hepatoma cells. *J. Lipid Res.* 36:1092–97
47. Langer M, Sah R, Veser A, Gülich M, Langosch D. 2013. Structural properties of model phosphatidylcholine flippases. *Chem. Biol.* 20:63–72
48. Latorraca NR, Venkatakrisnan AJ, Dror RO. 2016. GPCR dynamics: structures in motion. *Chem. Rev.* 117:139–55
49. Leontiadou H, Mark AE, Marrink SJ. 2006. Antimicrobial peptides in action. *J. Am. Chem. Soc.* 128:12156–61
50. Lingwood D, Binnington B, Rog T, Vattulainen I, Grzybek M, et al. 2011. Cholesterol modulates glycolipid conformation and receptor activity. *Nat. Chem. Biol.* 7:260–62
51. Lis M, Wizert A, Przybyło M, Langner M, Swiatek J, et al. 2011. The effect of lipid oxidation on the water permeability of phospholipids bilayers. *Phys. Chem. Chem. Phys.* 13:17555–63
52. Liu J, Brown KL, Conboy JC. 2013. The effect of cholesterol on the intrinsic rate of lipid flip-flop as measured by sum-frequency vibrational spectroscopy. *Faraday Disc.* 161:45–61
53. Manna M, Javanainen M, Monne HM-S, Gabius H-J, Rog T, Vattulainen I. 2017. Long-chain GM1 gangliosides alter transmembrane domain registration through interdigitation. *Biochim. Biophys. Acta* 1859:870–78
54. Manna M, Kulig W, Javanainen M, Tynkkynen J, Hensen U, et al. 2015. How to minimize artifacts in atomistic simulations of membrane proteins, whose crystal structure is heavily engineered: β_2 -adrenergic receptor in the spotlight. *J. Chem. Theory Comput.* 11:3432–45
55. Manna M, Mukhopadhyay C. 2011. Cholesterol driven alteration of the conformation and dynamics of phospholamban in model membranes. *Phys. Chem. Chem. Phys.* 13:20188–98
56. Manna M, Niemelä M, Tynkkynen J, Javanainen M, Kulig W, et al. 2016. Mechanism of allosteric regulation of β_2 -adrenergic receptor by cholesterol. *eLife* 5:e18432
57. Manna M, Róg T, Vattulainen I. 2014. The challenges of understanding glycolipid functions: An open outlook based on molecular simulations. *Biochim. Biophys. Acta* 1841:1130–45
58. May S. 2009. Trans-monolayer coupling of fluid domains in lipid bilayers. *Soft Matter* 5:3148–56
59. Meaney S, Bodin K, Diczfalusy U, Bjorkhem I. 2002. On the rate of translocation in vitro and kinetics in vivo of the major oxysterols in human circulation: critical importance of the position of the oxygen function. *J. Lipid Res.* 43:2130–35
60. Mendes Ferreira T, Sood R, Bärenwald R, Carlström G, Topgaard D, et al. 2016. Acyl chain disorder and azelaoyl orientation in lipid membranes containing oxidized lipids. *Langmuir* 32:6524–33
61. Menon I, Huber T, Sanyal S, Banerjee S, Barré P, et al. 2011. Opsin is a phospholipid flippase. *Curr. Biol.* 21:149–53
62. Michailidis IE, Rusinova R, Georgakopoulos A, Chen Y, Iyengar R, et al. 2011. Phosphatidylinositol-4,5-bisphosphate regulates epidermal growth factor receptor activation. *Pflügers Arch.* 461:387–97
63. Morra G, Razavi AM, Pandey K, Weinstein H, Menon AK, Khelashvili G. 2018. Mechanisms of lipid scrambling by the G protein-coupled receptor opsin. *Structure* 26:356–67
64. Muller CP, Reichel M, Muhle C, Rhein C, Gulbins E, Komhuber J. 2015. Brain membrane lipids in major depression and anxiety disorders. *Biochim. Biophys. Acta* 1851:1051–65
65. Muth S, Fries A, Gimpl G. 2011. Cholesterol-induced conformational changes in the oxytocin receptor. *Biochem. J.* 437:541–53
66. Nagata S, Suzuki J, Segawa K, Fujii T. 2016. Exposure of phosphatidylserine on the cell surface. *Cell Death Differ.* 23:952–61
67. Nakao H, Hayashi C, Ikeda K, Saito H, Nagao H, Nakano M. 2018. Effect of hydrophilic residues and hydrophobic length on flip-flop promotion by transmembrane peptides. *J. Phys. Chem. B* 122:4318–24

68. Neale C, Herce HD, Pomès R, García AE. 2015. Can specific protein-lipid interactions stabilize an active state of the beta 2 adrenergic receptor? *Biophys. J.* 109:1652–62
69. Neto AJ, Cordeiro RM. 2016. Molecular simulations of the effects of phospholipid and cholesterol peroxidation on lipid membrane properties. *Biochim. Biophys. Acta* 1858:2191–98
70. Neuvonen M, Manna M, Mokka S, Javanainen M, Rog T, et al. 2014. Enzymatic oxidation of cholesterol: properties and functional effects of cholestenone in cell membranes. *PLoS ONE* 9:e103743
71. Nickels JD, Smith JC, Cheng X. 2015. Lateral organization, bilayer asymmetry, and inter-leaflet coupling of biological membranes. *Chem. Phys. Lipids* 192:87–99
72. Oates J, Watts A. 2011. Uncovering the intimate relationship between lipids, cholesterol and GPCR activation. *Curr. Opin. Struct. Biol.* 21:802–7
73. Okazaki Y, Saito K. 2014. Roles of lipids as signaling molecules and mitigators during stress response in plants. *Plant J.* 79:584–96
74. Olsen BN, Schlesinger PH, Baker NA. 2009. Perturbations of membrane structure by cholesterol and cholesterol derivatives are determined by sterol orientation. *J. Am. Chem. Soc.* 131:4854–65
75. Owen MC, Kulig W, Rog T, Vattulainen I, Strodel B. 2018. Cholesterol protects the oxidized lipid bilayer from water injury: an all-atom molecular dynamics study. *J. Membr. Biol.* 17:1–4
76. Paila YD, Chattopadhyay A. 2009. The function of G-protein coupled receptors and membrane cholesterol: specific or general interaction? *Glycoconj. J.* 26:711–20
77. Paila YD, Jindal E, Goswami SK, Chattopadhyay A. 2011. Cholesterol depletion enhances adrenergic signaling in cardiac myocytes. *Biochem. Biophys. Acta* 1808:461–65
78. Patrickj W, Boone CD, Liu W, Conover GM, Liu Y, et al. 2018. Allostery revealed within lipid binding events to membrane proteins. *PNAS* 115:2976–81
79. Periole X. 2016. Interplay of G protein-coupled receptors with the membrane: insights from supra-atomic coarse grain molecular dynamics simulations. *Chem. Rev.* 117:156–85
80. Perlmutter JD, Sachs JN. 2011. Interleaflet interaction and asymmetry in phase separated lipid bilayers: molecular dynamics simulations. *J. Am. Chem. Soc.* 133:6563–77
81. Pontier SM, Percherancier Y, Galandrin S, Breit A, Galés C, Bouvier M. 2008. Cholesterol-dependent separation of the β_2 -adrenergic receptor from its partners determines signaling efficacy: insight into nanoscale organization of signal transduction. *J. Biol. Chem.* 283:24659–72
82. Pucadyil TJ, Chattopadhyay A. 2006. Role of cholesterol in the function and organization of G-protein coupled receptors. *Prog. Lipid Res.* 45:295–333
83. Razzokov J, Yusupov M, Vanuytsel S, Neyts EC, Bogaerts A. 2017. Phosphatidylserine flip-flop induced by oxidation of the plasma membrane: a better insight by atomic scale modeling. *Plasma Processes Polym.* 14:e1700013
84. Rissanen S, Grzybek M, Orłowski A, Rog T, Cramariuc O, et al. 2017. Phase partitioning of GM1 and its bodipy-labeled analog determine their different binding to Cholera Toxin. *Front. Physiol.* 8:252
85. Róg T, Orłowski A, Llorente A, Skotland T, Sylvänne T, et al. 2016. Interdigitation of long-chain sphingomyelin induces coupling of membrane leaflets in a cholesterol dependent manner. *Biochim. Biophys. Acta* 1858:281–88
86. Róg T, Stimson LM, Pasenkiewicz-Gierula M, Vattulainen I, Karttunen M. 2008. Replacing the cholesterol hydroxyl group with the ketone group facilitates sterol flip-flop and promotes membrane fluidity. *J. Phys. Chem. B* 112:1946–52
87. Runas KA, Malmstadt N. 2015. Low levels of lipid oxidation radically increase the passive permeability of lipid bilayers. *Soft Matter* 11:499–505
88. Salas-Estrada LA, Leioatts N, Romo TD, Grossfield A. 2018. Lipids alter rhodopsin function via ligand-like and solvent-like interactions. *Biophys. J.* 114:355–67
89. Sapay N, Bennett WD, Tieleman DP. 2009. Thermodynamics of flip-flop and desorption for a systematic series of phosphatidylcholine lipids. *Soft Matter* 5:3295–302
90. Sapay N, Bennett WD, Tieleman DP. 2010. Molecular simulations of lipid flip-flop in the presence of model transmembrane helices. *Biochemistry* 49:7665–73

91. Sengupta D, Prasanna X, Mohole M, Chattopadhyay A. 2018. Exploring GPCR–lipid interactions by molecular dynamics simulations: excitements, challenges and the way forward. *J. Phys. Chem. B* 122:5727–37
92. Sensi C, Daniele S, Parravicini C, Zappelli E, Russo V, et al. 2014. Oxysterols act as promiscuous ligands of class-A GPCRs: in silico molecular modeling and in vitro validation. *Cell. Signal.* 26:2614–20
93. Siani P, de Souza RM, Dias LG, Itri R, Khandelia H. 2016. An overview of molecular dynamics simulations of oxidized lipid systems, with a comparison of ELBA and MARTINI force fields for coarse grained lipid simulations. *Biochim. Biophys. Acta* 1858:2498–511
94. Swamy M, Beck-Garcia K, Beck-Garcia E, Hartl FA, Morath A, et al. 2016. A cholesterol-based allosteric model of T cell receptor phosphorylation. *Immunity* 44:1091–101
95. Troupiotis-Tsailaki A, Zachmann J, González-Gil I, Gonzalez A, Ortega-Gutiérrez S, et al. 2017. Ligand chain length drives activation of lipid G protein-coupled receptors. *Sci. Rep.* 7:2020
96. van Jaarsveld MT, Houthuijzen JM, Voest EE. 2016. Molecular mechanisms of target recognition by lipid GPCRs: relevance for cancer. *Oncogene* 35:4021–35
97. van Meer G. 2011. Dynamic transbilayer lipid asymmetry. *Cold Spring Harb. Perspect. Biol.* 3:a004671
98. van Meer G, Voelker DR, Feigenson GW. 2008. Membrane lipids: where they are and how they behave. *Nat. Rev. Mol. Cell Biol.* 9:112–24
99. Vernier PT, Ziegler MJ, Sun Y, Chang WV, Gundersen MA, Tieleman DP. 2006. Nanopore formation and phosphatidylserine externalization in a phospholipid bilayer at high transmembrane potential. *J. Am. Chem. Soc.* 128:6288–89
100. Volinsky R, Cwiklik L, Jurkiewicz P, Hof M, Jungwirth P, Kinnunen PK. 2011. Oxidized phosphatidylcholines facilitate phospholipid flip-flop in liposomes. *Biophys. J.* 101:1376–84
101. Wong-Ekkabut J, Xu Z, Triampo W, Tang IM, Tieleman DP, Monticelli L. 2007. Effect of lipid peroxidation on the properties of lipid bilayers: a molecular dynamics study. *Biophys. J.* 93:4225–36
102. Yin H, Xu L, Porter NA. 2011. Free radical lipid peroxidation: mechanisms and analysis. *Chem. Rev.* 111:5944–72
103. Zacharias DA, Violin JD, Newton AC, Tsien RY. 2002. Partitioning of lipid-modified monomeric GFPs into membrane microdomains of live cells. *Science* 296:913–16
104. Zocher M, Zhang C, Rasmussen SGF, Kobilka BK, Müller DJ. 2012. Cholesterol increases kinetic, energetic, and mechanical stability of the human β_2 -adrenergic receptor. *PNAS* 109:E3463–72

